# TRANSPORT OF ELECTROLYTES THROUGH CERAMIC NANOFILTRATION MEMBRANES

Leden van de promotie-commissie:

prof. dr. -ing. M. Wessling, Universiteit Twente (promotor)
dr. ir. N.E. Benes, Universiteit Twente (assistent promotor)
dr. ir. P.M. Biesheuvel, Universiteit Wageningen
prof. dr. W.R. Bowen, University of Wales
prof. dr. ir. J.T.F. Keurentjes, Technische Universiteit Eindhoven
prof. dr. ir. J.A.M. Kuipers, Universiteit Twente
prof. dr. ir. L. Lefferts, Universiteit Twente
prof. dr. J. Lyklema, Universiteit Wageningen

Twente University Press

Publisher: Twente University Press, P.O. Box 217, 7500 AE Enschede, the Netherlands, www.tup.utwente.nl.

Front cover: Liquid permeation set-up (top) and comparison of model and experimental retention for a ternary electrolyte solution (bottom).
Back cover: Approach adopted in this thesis for comparing the model and experimental retention and flux of an electrolyte solution.

Print: Océ Facility Services, Enschede.



ISBN: 90-365-1868-7

# TRANSPORT OF ELECTROLYTES THROUGH CERAMIC NANOFILTRATION MEMBRANES

## PROEFSCHRIFT

ter verkrijging van
de graad van doctor aan de Universiteit Twente,
op gezag van de rector magnificus,
prof. dr. F.A. van Vught,
volgens besluit van het College voor Promoties
in het openbaar te verdedigen
op vrijdag 7 februari 2003 te 16.45 uur

door

Willem Bernhard Samuel de Lint
geboren op 10 februari 1974
te Alkmaar

Dit proefschrift is goedgekeurd door de promotor:

prof. dr. -ing. M. Wessling

en de assistent promotor:

dr. ir. N.E. Benes

# Table of Contents

This is not a book, a lump of lifeless paper,
but a mind alive on the shelve.
*Adapted from Gilbert Highet (1906-1978)*

# Chapter 1

## General Introduction


### Abstract

In this thesis, the separation properties of inorganic nanofiltration (NF) membranes are discussed for dilute aqueous electrolyte solutions ($1<c_{salt}<100$ mol/m$^3$) at pressure differences below 2 MPa and at ambient temperature (25 °C). Because their separation mechanisms are not known in detail, the aim of this work is to improve the understanding of transport through nanofiltration (NF) membranes by the development of a model that is able to predict their separation characteristics without any adjustable parameters.

This chapter gives a general introduction into the field of NF. The state-of-the-art in NF materials is discussed and a review is given on separation descriptions currently available. The basic concepts used throughout the thesis are introduced and linked to the content of the different chapters in the thesis.

# 1. Introduction

Membranes act as selective barriers between two phases that are not in thermodynamic equilibrium. By influencing the movement of different species to a different extent a membrane can promote transport of one (or more) particular species relative to other species, and thus induce separation.

The majority of membrane separation processes is based on a difference in size between species. A natural ordering of membranes can therefore be either based on the size of species they retain or their pore size (Perry and Green, 1997; Mulder, 1998). Reverse osmosis (RO) is employed for the desalination of aqueous solutions, the production of ultrapure water, and applications in the food and dairy industry. Since very small species have to be retained in RO, very small pore sizes (hydrated ion size <1 nm) and consequently high pressures (> 4 MPa) are required. To separate species from 1 up to 100 nm (e.g., polymers, proteins, viruses), ultrafiltration (UF) is conventionally applied. In UF membranes much larger pores than in RO can be used and also lower pressure differences are required (<1 MPa).

The last two decades, considerable effort has been invested into the development of membranes that combine the high retention of RO with the lower pressures of UF. This has resulted in the development of nanofiltration (NF) membranes. To date, NF is becoming increasingly important, filling the niche between UF and RO. The pore size of NF membranes is in between that of UF and RO (~2 nm or smaller) and therefore species in an intermediate range can be retained as a result of their size. Additionally, NF materials are charged, and by means of electrostatic effects they can partly retain charged species that are about one order of magnitude smaller than their pore size. By controlling these electrostatic effects, the *effective* pore size of NF membranes can, to some degree, be regulated and therefore the

separation of charged species can be performed without having to resort to smaller pore sizes and, consequently, higher pressures (such as in RO).

In this thesis the separation of aqueous electrolyte solutions by ceramic NF membranes is studied, and consequently the electrostatic effects, in particular the membrane charging behaviour, will be the primary focus in the following chapters. In the thesis NF separation is discussed using an alumina membrane (see Figure 1) as a reference.

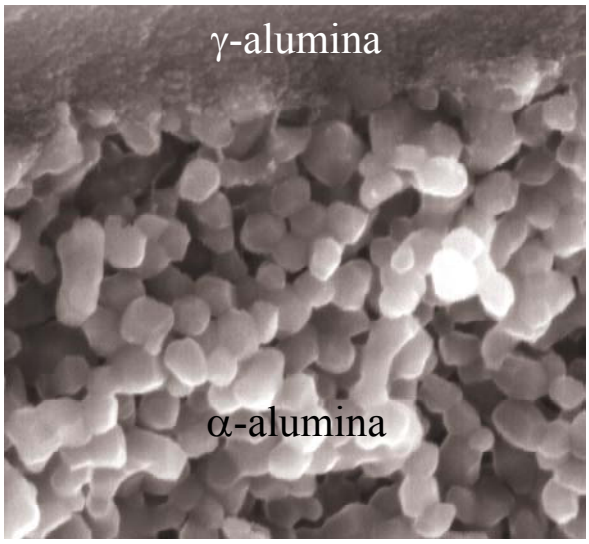


Figure 1: SEM-micrograph of a supported alumina membrane.

## 2. Nanofiltration

### 2.1 Introduction

According to the IUPAC recommendations (Koros, Ma and Shimidzu, 1996) nanofiltration is a "pressure-driven membrane-based separation process in which particles and dissolved molecules smaller than about 2 nm are retained." The number of applications in which NF is used is growing rapidly. Currently the reduction of hardness (removal of divalent ions like $Ca^{2+}$, $Mg^{2+}$, $SO_4^{2-}$) and dissolved organics from water is the most important application (Lakshminarayan, Cheryan and Rajagopalan, 1994). Examples of

other NF applications are the cleaning of water streams from metalworking plants by the removal of heavy metals (Ni, Fe, Cu, Zn) and the cleaning up of organics, like the reportedly carcinogenic halogen compounds thrihalomethanes, from contaminated groundwater. In the food industry, NF is used for the recovery of organic acids from fermentation broths, and the desalting of whey.

## 2.2 NF materials

Most NF membranes are thin-film composites of organic (polymeric) or inorganic (ceramic) nature. A membrane top layer is responsible for the separation while the support layer provides mechanical strength (see Figure 1). There is a large diversity of polymeric NF membranes, but mainly cellulose esters, aromatic polyamides (PA) and polyethersulfones (PES) are used (Rautenbach and Gröschl, 1990; Lakshminarayan, Cheryan and Rajagopalan, 1994; Mulder, 1998). Cellulose esters like cellulose acetate (CA) are very suitable for desalination because of their high permeability for water in combination with a very low solubility in salts (Mulder, 1998). However, the chemical and thermal stability of these membranes is quite poor and therefore cleaning of the membrane modules is difficult. Typical operating conditions are in the pH range of 4 to 6 (Kucera, 1997) and around 30 °C. The chemical stability of PA and PES membranes is much better than for CA (e.g., pH stability ≈3-10), but they are degraded by oxidizers and the feed water must therefore be dechlorinated (Kucera, 1997). The PA and PES materials have a high selectivity, but their water flux is generally lower than for the CA membranes.

Inorganic NF membranes are (mixed) oxides, generally of aluminium, zirconium or titanium. Due to their material properties they all have good mechanical strength and feature very good thermal and chemical stability. Because of the latter they can withstand high temperature cleaning treatments like sterilisation. The pH stability of alumina membranes is

similar to that of polyamides and polyethersulfones, that is, between 4-10 (chapter 8 of this thesis). By substituting titania or zirconia for alumina, inorganic membranes with a superior pH stability can be obtained. Titania is reported to be stable for pH values between 2-12 (Hofman-Züter, 1995; Van Gestel, 2002) and similar numbers have been found for zirconia (Hofman-Züter, 1995; Shojai and Mäntylä, 2001), significantly better than for most polymeric membranes. Vacassy *et al.* (1997) reported that doping zirconia with magnesium oxide can even result in stable membranes through the whole pH range (i.e., 1<pH<14).

Because they have larger pores, typically the fluxes for inorganic membranes are higher than for polymeric membranes and the retention of ceramic membranes is lower, especially for more concentrated (> 1 mol/$m^3$) electrolyte solutions.

## 2.3 NF separation mechanisms

The separation of NF membranes is mainly governed by electrostatic exclusion. The membranes contain ionisable groups that can charge their surface, leading to the rejection of charged solutes. The sign and magnitude of a solute's charge determines its degree of electrostatic exclusion. For polymeric membranes separation by size is also of considerable importance. Recently another separation mechanism called dielectric exclusion has been proposed to be of importance (e.g., Bontha and Pintauro, 1994; Yaroshchuk, 2000). According to the theory of dielectric exclusion, the permittivity (of a liquid) in NF pores will be lower than the bulk permittivity, creating an additional energy barrier for solutes to enter the membrane.

The growing interest in NF membranes has also lead to a tremendous increase in the development of models that describe their separation behaviour. These models consist of two parts:

1. A description of membrane charging,

2. A mass transport description.

Since the charging behaviour of a NF membrane mainly controls its separation for charged solutes, a correct description of membrane charging is of paramount importance to properly model NF retention. A mass transport description links the charge characteristics of the membrane to the movement of species though it. Depending on the type of separation behaviour a NF membrane exhibits, different exclusion mechanisms can be incorporated in the transport model.

## 2.4 State-of-the-art

### 2.4.1 Membrane charging

In NF, mass transport and charging effects are interrelated. Therefore any transport model has to be supplemented by a proper description of the membrane charging properties (i.e., its charge and potential) and the variation of the latter with the membrane pore size (charge regulation).

In the early NF models, the charge is considered constant and independent of the solution properties. In the field of colloid chemistry it is, however, already known for more than thirty years that the charge and potential may change as a function of the type of electrolyte, the electrolyte concentration and the pH (e.g., Ninham and Parsegian, 1971; Chan *et al.*, 1975; Healy and White, 1978; Healy, Chan and White, 1980). Currently, the most sophisticated NF models describe the adsorption mechanism of the charge-determining ions in terms of a Langmuir or Freundlich isotherm (Takagi and Nakagaki, 1990; Bowen and Mukthar, 1996; Schaep *et al.*, 1999), assuming a linear logarithmic dependence between the membrane charge density [mol/m$^3$], the electrolyte bulk concentration (Takagi and Nakagaki, 1990; Bowen and Mukthar, 1996) and the type of electrolyte (Schaep *et al.*, 1999). In these approaches, the influence of the charge on the

pH is not taken into account, nor is the variation of the charge and potential with pore size.

There is, however, an approach that in a self-contained way describes the variation of the membrane charging properties as a function of all the solution properties, including the pH and the pore size. This concept, termed charge regulation (Ninham and Parsegian, 1971; Chan *et al.*, 1975), is more basic than the Langmuir and Freundlich adsorption approaches because it directly considers the ion-material surface chemistry, which is the underlying behaviour that determines the membrane charging properties. The charge regulation (CR) approach facilitates in the determination of the ion adsorption parameters. Several authors have applied this approach (Basu and Sharma, 1997; Hall, Starov and Lloyd, 1997; Hall, Lloyd and Starov, 1997) for NF separation and this concept will also be adopted in this thesis.

### 2.4.2 Transport descriptions

To date, a vast amount of papers dealing with mass transport in NF systems can be found in literature. Though in these articles several different approaches are used to describe transport, they all assume that there is a linear relationship between the fluxes and the driving forces as is stated by the theory of linear irreversible thermodynamics. Two general approaches can be distinguished:

- Classical linear thermodynamic descriptions,
- Maxwell-Stefan (MS) type models.

Both concepts are essentially derived from the theory of linear irreversible thermodynamics. The basic difference between both approaches is that they define the fluxes and driving forces in an apposite manner. In the classical thermodynamic descriptions the diffusion vectors are chosen as forces (i.e.,

the flux of a species is assumed to be a linear function of the diffusion vectors of all species present), while the opposite approach yields the Maxwell-Stefan concept (see chapter 2 of this thesis).

In the MS theory, the total force acting on a species is counterbalanced by the friction of this species with the different components, including the membrane, in a system. Because friction between different species is explicitly accounted for, the MS approach is especially suited for the description of multi-component mass transport. Currently the MS theory is most widely used in NF literature, including this thesis. Therefore only a brief overview will be given of transport descriptions employing this approach.

Generally all MS derived descriptions are similar in the sense that they model the membrane as a collection of cylindrical pores of uniform diameter and length and assume thermodynamic equilibrium between the pore interfaces and the connecting bulk electrolyte solutions. The convective velocity profile within the pores is assumed fully developed and parabolic (Poiseuille-type). There are different descriptions for transport within the pores. Two approaches can be roughly distinguished:

- The uniform potential model (one-dimensional),
- The space-charge model (two-dimensional).

Since NF membranes contain pores with a size in the order of the double layer thickness, potential and concentration gradients in the radial direction can often be neglected, leading to a one-dimensional transport description in the direction of the flow. This uniform potential (UP) approach has been used with good results by many authors (e.g., Sonin, 1976; Bowen and Mukhtar, 1996; Bowen, Mohammad and Hildal, 1997; Hall, Starov and Lloyd, 1997; Schaep *et al.*, 1999). The UP concept is also explored in this thesis.

Osterle and co-workers (Morrison jr. and Osterle, 1965; Gross and Osterle, 1968; Fair and Osterle, 1971) developed a more complex theory. In their Space-Charge (SC) model they take radial variations of the potential and concentration into account, resulting in a two-dimensional transport description.

### 2.4.3 Input parameters for transport

In order to describe transport, apart from the driving forces, the diffusion coefficients, membrane pore size and thickness are required as input parameters. The diffusion coefficients at infinite dilution can be used, but in more sophisticated descriptions, they are corrected for the structure of the porous matrix (i.e., porosity and tortuosity) and the distribution of a species within a pore, which is a result of the interaction of species with the membrane pore wall.

Unless the membrane top layer and the support are mixed (as with some polymers), the membrane thickness can be easily determined. It is much more difficult to accurately obtain the pore size of membrane. Therefore this parameter is often determined by fitting a model to separation data.

## 3. Problem definition and chosen experimental methods

In the current state-of-the-art models, the membrane charge characteristics are either determined by fitting a model to membrane separation (i.e., retention) data (e.g., Bowen and Mukhtar, 1996; Hall, Starov and Lloyd, 1997; Hall, Lloyd and Starov, 1997; Schaep *et al.*, 1999) or they are measured independently (Hagmeyer and Gimbel, 1998; Palmeri *et al.*, 2000; Yang and Pintauro, 2000). In most of these models the variation of charge and potential is directly related to the solution properties, that is, they do not consider the underlying surface adsorption chemistry that directs the charging behaviour. Furthermore, the charging properties are measured

directly on the membrane. The direct application of charge and potential data strongly complicates the prediction of the separation behaviour in multi-component electrolyte solutions because the approach does not discriminate between the adsorption properties of individual ions. Furthermore, if the charging properties are measured directly on the membrane, the degree of double layer overlap will influence the charge and potential in a membrane pore. If this double layer overlap is not accounted for in the determination of the charging properties, the charging properties for membranes of the same material but with a different pore size have to be determined again.

The objective of this thesis is to develop a predictive NF separation model without adjustable parameters. In such a model, the charging behaviour should be characterised unambiguously and furthermore a detailed transport description with solution-material input parameters is required.

For a proper characterisation of the charging properties of a NF membrane and a prediction of its separation behaviour, a method has to be used that determines the individual charging (adsorption) properties of ions and that either eliminates or accounts for double layer overlap. In this thesis, ion-material specific adsorption parameters are derived, combining electrophoretic mobility measurements with a site-binding model for the surface adsorption chemistry. The adsorption parameters for single ions can be used directly in a transport model to calculate the retention in a multi-component electrolyte solution. Because dilute suspensions of membrane particles are used in the mobility experiments, particle double layer overlap is eliminated.

A detailed Maxwell-Stefan description with input data related to the membrane (i.e., top layer and support) structure (i.e., porosity, tortuosity, pore size, thickness) is employed to predict transport within the membrane. Several independent measurement techniques are used to determine the

structural membrane parameters, but gas and liquid permeation experiments are the most important since both the porosity/tortuosity ratio and the pore size can be obtained with these techniques. Permeation experiments are considered the best approach to access the structural parameters because they are non-equilibrium analysis techniques just as the separation experiments. The data obtained via permeation will therefore best reflect the membrane structure during a separation experiment.

## 4. Basic concepts and tools

To describe membrane charging, in this thesis a site-binding model for the surface chemistry is combined with an electrostatic approach for the double layer at the surface. The concept of charge regulation (CR) is employed to determine the change of these charge properties with respect to the variation of the membrane pore size. Both approaches are integrated into the Maxwell-Stefan (MS) transport relations or derivative expressions thereof.

### 4.1 Membrane charging

CR describes the variation of the charge and the potential when two charged surfaces approach each other and their double layers begin to overlap. In order to do this, CR has to integrate a description of the material's surface chemistry with a model for the electrostatic double layer.

In a wet state, hydroxyl groups (sites) develop at the surface of inorganic oxide materials. Competitive adsorption of protons, cations and anions takes place on these surface hydroxyl sites, resulting in a certain surface charge. The cause for ion adsorption can be electrostatic, chemical or a combination of both. Although the surface of an oxide is usually heterogeneous, in this thesis the surface is assumed effectively homogeneous, containing only a single type of averaged surface site at a fixed total concentration.

The adsorption of electrolyte ions screens the charge present at the immediate oxide surface. To relate this screening effect of the surface charge to the potential decrease away from the surface, an electrostatic double layer model has to be adopted. There exist many varieties of these electrostatic double layer descriptions some of which will be used in this thesis.

### 4.2 Mass transport

In a system with mobile charged species, the driving force for mass transport consists of diffusion, migration (transport resulting from an electric field) and convection. All of these transport mechanisms play an important role in NF. The MS theory and derivations thereof offer a good intuitive framework to describe NF mass transport.

In this thesis two types of transport approaches can be distinguished, the Nernst-Planck (NP) and the complete MS relations. The NP description is a simplification of the MS approach, valid for transport in dilute electrolyte solutions where the interactions with the porous matrix are negligible.

## 5. Thesis outline

This thesis describes the separation of aqueous electrolyte solutions with inorganic membranes. The central themes in each chapter are ion-material interactions, integrated in the CR concept and mass transport (NP or MS). In each chapter these concepts will be elaborated step by step.

*Chapter 2* gives a short introduction into the charging properties of inorganic NF membranes and discusses the derivation of the Maxwell-Stefan and Nernst-Planck mass transport relations from the theory of irreversible processes.

*Chapter 3* is the first attempt to describe NF separation behaviour by the use of charge regulation. The retention is directly related to the electrostatic exclusion of coions at the membrane interface, which is at thermodynamic equilibrium with the feed bulk solution.

In *chapter 4* the concept of thermodynamic equilibrium is replaced by a Nernst-Planck description for mass transport. The CR concept from chapter 3 is maintained.

The dependence of the ion-material adsorption parameters, the input parameters for the CR description, on the charging behaviour of a membrane is studied in *chapter 5*. Furthermore, the extraction of adsorption parameters from literature charging data is investigated.

In *chapter 6* the adsorption parameters for NaCl, $CaCl_2$ and $Na_2SO_4$ on an unsupported γ-alumina membrane material are determined using electrophoretic mobility measurements and a combination of a surface chemistry approach (1-pK site-binding) with an electrostatic double layer description, a triple-layer model.

The charging model and the adsorption parameters derived in chapter 6 are combined with a Maxwell-Stefan transport description in *chapter 7*. The retention predictions for this model are discussed in detail.

In *chapter 8* the retention predictions of the transport model discussed in chapter 7 are compared to experimental retention data for two binary electrolytes (NaCl and $CaCl_2$) and a ternary electrolyte mixture of NaCl with $CaCl_2$.

*Chapter 9* summarises the major achievements of the thesis and proposes some recommendations for future work.

## References


1. Basu S., and Sharma M.M., "An Improved Space-Charge Model for Flow Through Charged Microporous Membranes," *J. Membrane Sci.*, **124**, 77 (1997).
2. Bontha J.R., and Pintauro P.N., "Water Orientation and Ion Solvation Effects During Multicomponent Salt Partitioning in a Nafion Cation Exchange Membrane," *Chem. Eng. Sci.*, **49**, 3835 (1994).
3. Bowen W.R., and Mukhtar H., "Characterisation and Prediction of Separation Performance of Nanofiltration Membranes," *J. Membrane Sci.*, **112**, 263 (1996).
4. Bowen W.R., Mohammad A.W., and Hildal N., "Characterisation of Nanofiltration Membranes for Predictive Purposes – Use of Salts, Uncharged Solutes and Atomic Force Microscopy," *J. Membrane Sci.*, **126**, 91 (1997).
5. Chan D.Y.C., Perram J.W., White L.R., and Healy T.W., "Regulation of Surface Potential at Amphoteric Surfaces During Particle-Particle Interaction," *J. Chem. Soc. Faraday Trans. I*, **71**, 1046 (1975).
6. Fair J.C., and Osterle J.F., "Reverse Electrodialysis in Charged Capillary Membranes," *J. Chem. Phys.*, **54**, 3307 (1971).
7. Gross R.J., and Osterle J.F., "Membrane Transport Characteristics of Ultrafine Capillaries," *J. Chem. Phys.*, **49**, 228 (1968).
8. Hagmeyer G., and Gimbel R., "Modelling the Salt Rejection of Nanofiltration Membranes for Ternary Ion Mixtures and for Single Salts at Different pH Values," *Desalination*, **117**, 247 (1998).
9. Hall M.S., Starov V.M., and Lloyd D.R., "Reverse Osmosis of Multicomponent Electrolyte Solutions. Part I. Theoretical Development," *J. Membrane Sci.*, **128**, 23 (1997).
10. Hall M.S., Lloyd D.R., and Starov V.M., "Reverse Osmosis of Multicomponent Electrolyte Solutions. Part II. Experimental Verification," *J. Membrane Sci.*, **128**, 39 (1997).
11. Healy T.W., and White L.R., "Ionizable Surface Group Models of Aqueous Interfaces," *J. Colloid Interface Sci.*, **9**, 303 (1978).
12. Healy T.W., Chan D., and White L.R., "Colloidal Behaviour of Materials with Ionizable Group Surfaces," *Pure & Appl. Chem.*, **52**, 1207 (1980).
13. Hofman-Züter J.M., "Chemical and Thermal Stability of (Modified) Mesoporous Ceramic Membranes," Ph.D. Thesis, 1995, University of Twente, The Netherlands, chapter 4.
14. Koros W. J., Ma Y. H., and Shimidzu T., "Terminology for Membranes and Membrane Processes IUPAC Recommendations 1996," *J. Membrane Sci.*, **120**, 149 (1996).
15. Kucera J., "Properly Apply Reverse Osmosis," *Chem. Eng. Prog.*, **93**, 54 (1997).
16. Lakshminarayan P.R., Cheryan M., and Rajagopalan N., "Consider Nanofiltration for Membrane Separation," *Chem. Eng. Proc.*, 68-74 (1994).

17. Morrison Jr. F.A., and Osterle J.F., "Electrokinetic Energy Conversion in Ultrafine Capillaries," *J. Chem. Phys.*, **43**, 2111 (1965).
18. Mulder M., "Basic Principles of Membrane Technology," 2nd edition, Kluwer, Dordrecht, 1998, chapters II and VI.
19. Ninham B.W., and Parsegian V.A., "Electrostatic Potential Between Surfaces Bearing Ionizable Groups in Ionic Equilibrium with Physiologic Saline Solution," *J. Theor. Biol.*, **31**, 405 (1971).
20. Palmeri J., Blanc P., Larbot A., and David P., "Hafnia Ceramic Nanofiltration Membranes. Part II. Modeling of Pressure-Driven Transport of Neutral Solutes and Ions," *J. Membrane Sci.*, **179**, 243 (2000).
21. Perry R.H., and Green D.W., "Perry's Chemical Engineers' Handbook," 7th edition, McGraw-Hill, New York, 1997, pp. **22**-37 – **22**-69.
22. Rautenbach R., and Gröschl A., "Separation Potential of Nanofiltration Membranes," *Desalination*, **77**, 73 (1990).
23. Schaep J., Vandecasteele C., Mohammad A.W., and Bowen W.R., "Analysis of the Salt Retention of Nanofiltration Membranes Using the Donnan-Steric Partitioning Pore Model," *Sep. Sci. Technol.*, **34**, 3009 (1999).
24. Shojai F., and Mäntylä T.A., "Chemical Stability of Yttria Doped Zirconia Membranes in Acid and Basic Aqueous Solutions: Chemical Properties, Effect of Annealing and Ageing Time," *Ceram. Int.*, **27**, 299 (2001).
25. Sonin A.A., "Osmosis and Ion Transport in Charged Porous Membranes: a Macroscopic, Mechanistic Model," in "Charged Gels and Membranes I", pp. 255-265, Reidel, Dordrecht, 1976.
26. Takagi R., and Nakagaki M., "Theoretical Study of the Effect of Ion Adsorption on Membrane Potential and its Application to Collodion Membranes," *J. Membrane Sci.*, **53**, 19 (1990).
27. Vacassy R., Guizard C., Thoraval V., and Cot L., "Synthesis and Characterization of Microporous Zirconia Powders: Application in Nanofilters and Nanofiltration Characteristics," *J. Membrane Sci.*, **132**, 109 (1997).
28. Van Gestel T., Vandecasteele C., Buekenhoudt A., Dotremont C., Luyten J., Leysen R., Van der Bruggen B., and Maes G., "Alumina and Titania Multilayer Membranes for Nanofiltration: Preparation, Characterization and Chemical Stability," *J. Membrane Sci.*, **207**, 73 (2002).
29. Yang Y., and Pintauro P.N., "Multicomponent Space-Charge Transport Model for Ion-Exchange Membranes," *AIChE J.*, **46**, 1177 (2000).
30. Yaroshchuk A.E., "Dielectric Exclusion of Ions from Membranes," *Adv. Colloid Interface Sci.*, **85**, 193 (2000).

Computers are useless. They can only give you answers.

*Pablo Picasso (1881-1973)*

# Chapter 2

## Nanofiltration Charging Characteristics and Mass Transport


### Abstract

A general discussion on the charging and charge regulation of ceramic oxides is presented, followed by a derivation of the Maxwell-Stefan and Nernst-Planck expressions for mass transport. Both transport concepts originate from the theory of irreversible processes. Therefore, a discussion is presented on this theory, and the assumptions involved in its application to multi-component transport of simple electrolytes in nanofiltration membranes are explained.

# 1. Introduction

The charging properties and transport behaviour of a nanofiltration (NF) membrane determine to a large degree its separation performance for charged species. Since in NF systems these two mechanisms are interrelated, any description for mass transport has to be supplemented by a proper description of the membrane charging behaviour. In this thesis, the charging characteristics of ceramic oxide NF membranes are described by the concept of charge regulation, while the Maxwell-Stefan (MS) relations, or the more simple Nernst-Planck (NP) expressions are used to study mass transport. In this chapter both concepts are discussed.

# 2. Theory

## 2.1 Charge regulation

The theory of charge regulation (CR) describes the variation of charge and potential on two charged surfaces as they approach each other and their double layers begin to overlap (Ninham and Parsegian, 1971; Chan *et al.*, 1975). At increased double layer interaction the potential increases (Biesheuvel and Lange, 2001). When the species at the surface are mobile, this potential effect is counterbalanced by a decrease in the surface charge (Chan *et al.*, 1975). The charging of the surface is strongly influenced by the amount and type of ions present in the electrolyte solution, and the pH (Randon *et al.*, 1991a; Randon *et al.*, 1991b; Vacassy *et al.*, 1997; chapter 6 of this thesis). CR effects occur in the pores of NF membranes, as their size is in the order of the Debye length and are therefore important to take into account when studying NF transport behaviour.

CR models generally consist of a kinetic interpretation of the ion-surface reactions and an electrostatic description for the double layer.

### 2.1.1 Surface chemistry

Inorganic NF membranes consist of (mixed) oxides (e.g., $Al_2O_3$, $TiO_2$, $ZrO_2$), which form surface hydroxyl groups in aqueous solutions. The surface of an oxide is usually heterogeneous, *i.e.*, the surface hydroxyl groups it contains are neither identical nor energetically independent (Morterra and Magnacca, 1996; Sohlberg, Pennycook and Pantelides, 2000). Because adequate information about the heterogeneity is generally missing, in this thesis the surface will be assumed homogeneous, containing only a single type of averaged surface site [-$OH^q$] ($q$ being the initial charge of the hydroxyl groups, if any). On these surface sites competitive adsorption of protons, cations ($C^{m+}$) and anions ($A^{n-}$) takes place. Many different surface reactions have been proposed in literature (e.g., Healy and White, 1978). An example of a set of possible surface reactions for adsorption on one site is given in Eq. [1].

$$\begin{aligned} \text{Al-OH}^q + \text{H}^+(\text{s}) &\overset{K^+}{\rightleftharpoons} \text{Al-OH}_2^{q+1} \\ \text{Al-OH}^q + \text{C}^{m+}(\text{s}) &\overset{K_\text{C}}{\rightleftharpoons} \text{Al-OH}^q\text{C}^{m+} \\ \text{Al-OH}_2^{q+1} + \text{A}^{n-}(\text{s}) &\overset{K_\text{A}}{\rightleftharpoons} \text{Al-OH}_2^{q+1}\text{A}^{n-} \end{aligned} \quad . \qquad [1]$$

The reactions in Eq. [1] are thought to occur in an equipotential plane and the addition (s) denotes non-adsorbed ions that are virtual in this plane. The Boltzmann expression relates the concentration of these non-adsorbed species to that in the bulk of the electrolyte. The surface complexes, e.g., Al-$OH^qC^{m+}$, in Eq. [1] are species that apart from electrostatic interactions exhibit a chemical interaction with the surface. This chemical interaction with the surface is referred to as specific adsorption.

Generally, the charge σ on an oxide is related to the concentration of its surface complexes $c_i^{sc}$,

$$\sigma = F\sum_{\ell=1}^{n} z_\ell c_\ell^{sc} \,, \qquad [2]$$

with $F$ the Farraday constant, $n$ the total number of mobile species, and $z_i$ the charge number of a species $i$.

### 2.1.2 Electrostatic double layer description

Apart from the surface chemistry, a double layer model has to be adopted to describe the variation of the potential and charge at the surface. The background and structure of several double layer models have been well described by Westall and Hohl (1980) and Lyklema (1995) and only the most important features are mentioned here.

In the double layer models, the surface charge can be compensated by counter charge located on one or more Helmholtz planes, in a diffuse layer, or several combinations of both. Adsorbed ions are assumed to be present at the surface or on Helmholtz planes located at discrete distances from the surface. In the diffuse double layer no discrete effects are present and this layer only contains ions that are weakly electrostatically adsorbed.

For any Helmholtz plane $p$ the charge $\sigma_p$ is related to a difference in potential $\phi$ by

$$\sigma_p = C_{p+1}\left(\phi_p - \phi_{p+1}\right) - \sigma_{p-1} \qquad \text{for } p=0..np \text{ and } \sigma_{-1}=0, \qquad [3]$$

where $C_{p+1}$ is the double layer capacitance and $np$ is the total number of planes. The charge in the diffuse layer $\sigma_d$ is (Lyklema, 1995)

$$\sigma_d = -\text{sign}\left(\phi_d\right)\sqrt{2\varepsilon_0\varepsilon_r RT\sum_{\ell=1}^{n} c_\ell^b\left[\exp\left(\frac{-z_\ell F}{RT}\phi_d\right)-1\right]}\,, \qquad [4]$$

with $\varepsilon_0\varepsilon_r$ the permittivity of the solvent, $R$ the ideal gas constant, $T$ the temperature, and $c^b_i$ the bulk concentration of species $i$. In writing Eq. [4] a planar geometry is assumed. Furthermore, any position in the diffuse double layer should be in thermodynamic equilibrium with the bulk solution (Boltzmann relation), the bulk is thermodynamically ideal, and the solvent permittivity is assumed independent of the electric field. Also, the electrostatic potential in the bulk solution is set equal to zero.

## 2.2 Theory of irreversible processes

The occurrence of irreversible processes requires that a system is not at thermodynamic equilibrium. However, intuitively local thermodynamic equilibrium may be assumed, especially when following a small mass element along its centre of gravity motion or barycentric velocity **v** (De Groot and Mazur, 1962). Assuming local equilibrium, concepts such as pressure and temperature may still be used intelligibly and can be considered continuously differentiable functions. For some systems other choices than the velocity **v** are more appropriate for assuming local equilibrium (Kuiken, 1994).

Transport with respect to the barycentric velocity is due to local deviations from equilibrium and is referred to as diffusion. The transport due to the barycentric velocity is referred to as convection. Hence, in our assumption of local equilibrium we have assumed the convective and diffusive transport to be additive.

Diffusion is related to production of entropy. For an isothermal system without chemical reactions the production of entropy $\pi_s$ in molar units is (De Groot and Mazur, 1962)

$$\Phi = T\pi_s = -\sum_{\ell=1}^{n} c_\ell \left(\mathbf{u}_\ell - \mathbf{v}\right)\cdot\left(\nabla_T \mu_\ell - \mathbf{F}_\ell\right) - \boldsymbol{\Pi} : \nabla\mathbf{v} \qquad [5]$$

with $c_i$ the concentration and $\mathbf{u}_i$ the velocity of species *i*. Eq. [5] is referred to as the dissipation function. It contains the viscous pressure tensor $\boldsymbol{\Pi}$ that represents thermal effects resulting from shear. These thermal effects are generally negligible in separation applications (Bird, Stewart and Lightfoot, 1960), and $\Phi$ becomes

$$\Phi = -\sum_{\ell=1}^{n} c_\ell \left(\mathbf{u}_\ell - \mathbf{v}\right)\cdot \mathbf{d}_\ell \,, \qquad [6]$$

The diffusion vector $\mathbf{d}_i$ in Eq. [6] depends on the chemical potential gradient $\mu_i$ and the body force acting on the species, $\mathbf{F}_i$,

$$\mathbf{d}_i \equiv \frac{x_i}{RT}\left(\nabla_T \mu_i - \mathbf{F}_i\right), \qquad [7]$$

with $x_i$ the molar fraction of species *i*. Summation of Eq. [7] over all species *i* yields:

$$RT\sum_{\ell=1}^{n} \mathbf{d}_\ell = \bar{V}\nabla p - \mathbf{F} \qquad [8]$$

Where $\bar{V}$ is the total molar volume and we have used the Gibbs-Duhem equation $\sum_{\ell=1}^{n} x_\ell \nabla_T \mu_\ell = \bar{V}\nabla p$. The right hand side of equation [8] is a measure of the deviation from mechanical equilibrium. Often a so-called mechanical diffusion vector is defined, (e.g., Bird, Stewart and Lightfoot, 1960; De Groot and Mazur, 1962; Taylor and Krishna, 1993), which accounts for this deviation. For all problems studied in this work, it can be assumed that mechanical equilibrium is established much faster than diffusion equilibrium (De Groot and Mazur, 1962) so that the right hand side of [8] vanishes. Furthermore, for liquids the mechanical diffusion vector is difficult to calculate and its use may also be rather confusing in the case of gases. Therefore, from Eq. [8] onwards $\sum_{\ell=1}^{n} \mathbf{d}_\ell = \mathbf{0}$ is used. Given that $\sum_{\ell=1}^{n} \mathbf{d}_\ell = \mathbf{0}$ it is

clear that the reference velocity can be chosen arbitrarily, since $\sum_{\ell=1}^{n}\mathbf{d}_\ell\cdot(\mathbf{u}_\ell-\mathbf{v})=\sum_{\ell=1}^{n}\mathbf{d}_\ell\cdot(\mathbf{u}_\ell-\mathbf{v}\pm\mathbf{V})$ where $\mathbf{V}$ is an arbitrarily chosen velocity (Prigogine, 1947).

### 2.2.1 Maxwell-Stefan

The dissipation function, Eq. [5], describes irreversible processes in terms of fluxes and forces (Kuiken, 1994). The theory of linear irreversible processes assumes a linear relation between fluxes and forces, where the words 'flux' and 'force' are interchangeable. Historically, the diffusion vectors are chosen as forces, i.e., the flux of a species is assumed to be a linear function of the diffusion vectors of all species present. The opposite approach yields the following expression (Kuiken, 1994),

$$\mathbf{d}_i=-cRT\sum_{\ell=1}^{n}\mathbf{R}_{i\ell}\cdot\mathbf{u}_\ell\ , \qquad [9]$$

where we have set the reference velocity equal to zero. This can be rewritten to the well-known Maxwell-Stefan (MS) expressions (Kuiken, 1994)

$$-\mathbf{d}_i=\sum_{\ell=1}^{n}f_{i\ell}x_ix_\ell(\mathbf{u}_i-\mathbf{u}_\ell) \qquad [10]$$

With $f_{ij}$ the friction coefficient between the species *i* and *j*. Equation [10] states that the driving force on a species, **d**, is opposed by the total transfer of momentum between species *i* and all other species (Taylor and Krishna, 1993). Because friction between different species is explicitly accounted for by the Maxwell-Stefan (MS) theory, it is especially suited for describing multi-component mass transport.

## 2.3 Nanofiltration

### 2.3.1 Fluxes

In this work the MS expressions are applied to transport of aqueous electrolyte solutions through porous nanofiltration membrane. In a membrane momentum transfer occurs not only between the various mobile species (including the solvent), but also between species and the membrane material M. This can be accounted for by treating the membrane as an additional species. For this case the MS expressions are

$$-\boldsymbol{\delta}_i = \sum_{\ell=1}^{n} \zeta_{i\ell}^{\mathrm{eff}} y_i y_\ell \left(\mathbf{u}_i - \mathbf{u}_\ell\right) + \zeta_{i\mathrm{M}}^{\mathrm{eff}} y_i \left(\mathbf{u}_i - \mathbf{u}_\mathrm{M}\right), \qquad [11]$$

where the membrane material is included in the diffusion vector $\boldsymbol{\delta}$ and molar fractions $y$.

The structure of the porous membrane should be accounted for by correcting the friction factors for porosity $\varphi$ and tortuosity $\tau$. For a membrane with pore sizes in the order of the (hydrated) solute size (as for electrolytes and NF pores) species will exhibit an interaction with the wall and be radially distributed due to their size and the (radial) electrical pore potential (Deen, 1987). The contribution of this effect to diffusion of a species is represented by the parameter $H^{\mathrm{d}}{}_i$, and has to be considered concurrently with the structural effects, resulting in an effective friction coefficient, $\zeta_{ij}^{\mathrm{eff}} = \tau \Big/ \left(\varphi H_i^{\mathrm{d}}\right) \zeta_{ij}$ (see Eq. [11]). Obviously, for the solvent $H^{\mathrm{d}}{}_i$=1.

Expressed in terms of the mobile components only, expression [11] becomes

$$-\mathbf{d}_i = \sum_{\ell=1}^{n} f_{i\ell}^{\mathrm{eff}} x_i x_\ell \left(\mathbf{u}_i - \mathbf{u}_\ell\right) + f_{i\mathrm{M}}^{\mathrm{eff}} x_i \mathbf{u}_i \qquad [12]$$

where we used $y_i\zeta_{ij} = x_i f_{ij}$ (Mason and Viehland, 1978), and $\mathbf{u}_M = \mathbf{0}$. This expression is identical to the one proposed by Present and DeBethune (1948) for gaseous diffusion in a capillary. The velocity $\mathbf{u}_i$ corresponds to the diffusive flux $\mathbf{J}_i$, but it is preferable to rewrite the equation in terms of the molar fluxes $\mathbf{N}_i$, i.e., the fluxes with respect to a fixed coordinate system. Substituting $\mathbf{J}_i = \mathbf{N}_i - c_i\mathbf{v}$ in Eq. [12] yields

$$-\mathbf{d}_i = \sum_{\ell=1}^{n} f_{i\ell}^{\text{eff}} \frac{\left(x_\ell \mathbf{N}_i - x_i \mathbf{N}_\ell\right)}{c} + f_{i\text{M}}^{\text{eff}} \frac{\mathbf{N}_i}{c} - f_{i\text{M}}^{\text{eff}} x_i \mathbf{v} \,. \qquad [13]$$

Although this treatment has been generally accepted in literature (Present and DeBethune, 1948; Stewart and Prober, 1964; Mason and Viehland, 1978; Lightfoot, 1974; Lorimer, 1983; Mason and Del Castillo, 1985; Wesslingh and Krishna, 1990; Krishna and Wesslingh, 1997), it seems inconsistent as the $\mathbf{u}_i$ are already defined with respect to the membrane. In other words, by choosing $\mathbf{u}_M = \mathbf{0}$ we have already used Prigogine's theorem (1947) on the independence of the dissipation function on the reference velocity. However, experimental evidence suggests that it is a valid approach and Eq. [13] will be utilised as the starting point for the transport descriptions presented in this thesis.

If the solute size and pore size are similar, convection (just as diffusion) will be influenced by the radial distribution of solute species. To account for this, the convective velocity in Eq. [13] should be multiplied by a convective correction, $H^c_i$ (Deen, 1987).

### 2.3.2 Driving forces

In nanofiltration mass transport and surface charge effects are interrelated. The driving force $\mathbf{d}_i$ for transport contains two contributions; one related to the gradient in chemical potential and one related to the presence of an

electric field (see Eq. [7]). Charged species may experience an external body force imposed by an electric field,

$$\mathbf{F}_i = -z_i F \nabla \phi \,. \qquad [14]$$

The chemical potential gradient in Eq. [7] is decomposed as

$$\nabla_T \mu_i = RT \nabla \ln\left(\gamma_i x_i\right) + \bar{V}_i \nabla p \,, \qquad [15]$$

with $\bar{V}_i$ the molar volume, and $\gamma_i$ the activity coefficient. After substitution in Eq. [7] the driving force becomes

$$-\mathbf{d}_i = -x_i \nabla \ln\left(\gamma_i x_i\right) - \frac{\bar{V}_i}{RT} x_i \nabla p - \frac{F}{RT} x_i z_i \nabla \phi \,. \qquad [16]$$

Combination of [13] and [16] yields the final form of the MS equations

$$-x_i \nabla \ln\left(\gamma_i x_i\right) - \frac{\bar{V}_i}{RT} x_i \nabla p - \frac{F}{RT} x_i z_i \nabla \phi - H_i^{\mathrm{c}} \frac{x_i}{Đ_{i\mathrm{M}}^{\mathrm{eff}}} \mathbf{v} = \sum_{\ell=1}^{n} \frac{x_\ell \mathbf{N}_i - x_i \mathbf{N}_\ell}{c Đ_{i\ell}^{\mathrm{eff}}} + \frac{\mathbf{N}_i}{c Đ_{i\mathrm{M}}^{\mathrm{eff}}} \,. \qquad [17]$$

The effective Maxwell-Stefan diffusion coefficients *Đ* are simply the inverse of the friction coefficients *f*.

For mathematical convenience, Eq. [17], is often expressed in matrix notation as

$$-c\mathbf{d} = \mathbf{A}\mathbf{N} \,, \qquad [18]$$

with the diffusion matrix **A** defined by

$$\begin{aligned} A_{ii} &= \frac{1}{Đ_{i\mathrm{M}}^{\mathrm{eff}}} + \sum_{\ell=1}^{n} \frac{x_\ell}{Đ_{i\ell}^{\mathrm{eff}}} \\ A_{ij} &= -\frac{x_i}{Đ_{ij}^{\mathrm{eff}}} \end{aligned} \,. \qquad [19]$$

## 2.4 Nernst-Planck

The Nernst-Planck (NP) relations are a simplification of the MS expressions that are often used in NF systems. In the NP approach an infinitely dilute system is assumed and all effects from the porous matrix are neglected (i.e., a free solution). Because the membrane is omitted as a component, there are only $n$-1 independent relations of Eq. [17] (due to the Gibbs-Duhem relation) and they are generally solved for the electrolyte species in the system.

### 2.4.1 Driving forces

For an infinitely dilute system the activity coefficients equal unity. Although not directly connected to the assumption of infinite dilution, the $-\bar{V}_i x_i \nabla p/RT$ term is generally small in NF applications (low pressure differences) and therefore often neglected in the driving force. Furthermore, in a solution without membrane interactions, convection does not have to be corrected for pore effects and hence, $H_t^c$=1.

With these assumptions, the driving force at infinite dilution reduces to

$$\mathbf{d}_i = -\nabla x_i - \frac{F}{RT} x_i z_i \nabla\phi - \frac{x_i}{Đ_{i\mathrm{w}}^{\circ}} \mathbf{v} \,. \qquad [20]$$

### 2.4.2 Fluxes

Infinite dilution implies for the solvent and electrolyte fractions $x_\mathrm{w}$ and $x_i$ ($i$≠w) that $x_\mathrm{w} \cong 1,\ x_i \cong 0$. Applying this concept and neglecting membrane contributions, reduces the diffusion matrix in Eq. [19] to $n$-1 diagonal elements (Taylor and Krishna, 1993)

$$\begin{aligned} A_{ii} &= \frac{1}{Đ_{i\mathrm{w}}^{\circ}} \,. \\ A_{ij} &= 0 \end{aligned} \qquad [21]$$

Often the Maxwell-Stefan diffusion coefficients at infinite dilution $Đ_{i\mathrm{w}}^{\circ}$ are set equal to the binary diffusion coefficients $D_{i\mathrm{w}}$.

Substituting Eqs. [20] and [21] in Eq. [17], the well-known Nernst-Planck expressions are obtained.

$$\mathbf{N}_i = -cD_{i\mathrm{w}}\nabla x_i - D_{i\mathrm{w}}\frac{F}{RT}c_i z_i \nabla\phi - c_i\mathbf{v}\,. \qquad [22]$$

## 3. Conclusion

Since the charging properties and transport behaviour of NF membranes are interrelated, both mechanisms have to be taken into account when devising an adequate theory for NF separation. Therefore, in this chapter a general description is given for the charging of ceramic oxides. Such descriptions consist of a model for the ion-adsorption reactions at the oxide surface and some kind of double layer model that accounts for the variation in the potential in the vicinity of the surface. Throughout this thesis, ion adsorption on the oxide is thought to occur on homogeneous surface sites.

Furthermore a discussion is presented on the background of the Maxwell-Stefan theory. In the MS approach the diffusion vectors of all species are assumed to be a linear function of the flux. Though the MS relations are generally used, there seems to be a remarkable inconsistency in its derivation as two different reference velocities are used. This inconsistency, however, does not hamper the applicability of the MS approach in mass transport descriptions as experimental evidence suggests that it is a valid approach. Since the MS theory is especially suited to describe multi-component mass transport it will be used to study NF transport in this thesis.

## Nomenclature

| | | |
|---|---|---|
| $c$ | total concentration | [mol m$^{-3}$] |
| $c_i$ | concentration of species $i$ | [mol m$^{-3}$] |
| $c_i^{sc}$ | concentration of surface complexes $i$ | [mol m$^{-2}$] |
| $Đ_{i\ell}$ | Maxwell-Stefan diffusion coefficient | [m$^2$ s$^{-1}$] |
| $\mathbf{d}_i$ | driving force for mass diffusion of species $i$ | [m$^{-1}$] |
| $F$ | constant of Faraday | [C mol$^{-1}$] |
| $\mathbf{F}_i$ | external force on species $i$ | [N mol$^{-1}$] |
| $f_{i\ell}$ | friction coefficient between species $i$ and $\ell$ | [s m$^{-2}$] |
| $G$ | structure parameter | [m] |
| $H^c{}_i$ | hydrodynamic parameter for convection | [-] |
| $H^d{}_i$ | hydrodynamic parameter for diffusion | [-] |
| $I$ | ionic strength | [mol m$^{-3}$] |
| $\mathbf{J}_i$ | diffusive molar flux | [mol m$^{-2}$ s$^{-1}$] |
| $\mathbf{N}_i$ | molar flux at stationary coordinates | [mol m$^{-2}$ s$^{-1}$] |
| $n$ | number of species | [-] |
| $p$ | pressure | [N m$^{-2}$] |
| $R$ | ideal gas constant | [J mol$^{-1}$ K$^{-1}$] |
| $\mathbf{R}_{i\ell}$ | phenomenological coefficients | [m s J$^{-1}$] |
| $T$ | temperature | [K] |
| $\mathbf{u}_i$ | velocity of species $i$ | [m s$^{-1}$] |
| $\mathbf{v}$ | barycentric velocity | [m s$^{-1}$] |
| $\mathbf{V}$ | arbitrary reference velocity | [m s$^{-1}$] |
| $\bar{V}$ | total molar volume | [m$^3$ mol$^{-1}$] |
| $\bar{V}_i$ | molar volume of species $i$ | [m$^3$ mol$^{-1}$] |
| $x_i$ | molar fraction of species $i$ | [-] |
| $y_i$ | molar fraction of species $i$ including the porous matrix | [-] |
| $z_i$ | charge number of species $i$ | [-] |

Greek

| | | |
|---|---|---|
| $\gamma_i$ | activity coefficients of species $i$ | [-] |
| $\boldsymbol{\delta}_i$ | driving force for diffusion of species $i$ including the porous matrix | [m$^{-1}$] |
| $\zeta_{i\ell}$ | friction coefficient between species $i$ and $\ell$ including the porous matrix | [s m$^{-2}$] |
| $\lambda_i$ | ratio of solute radius over the pore radius | [-] |
| $\mu$ | Newtonian viscosity | [N s m$^{-2}$] |
| $\mu_i$ | chemical potential of species $i$ | [J mol$^{-1}$] |
| $\mu^0$ | chemical potential at a reference state | [J mol$^{-1}$] |
| $\boldsymbol{\Pi}$ | viscous pressure tensor | [J m$^{-3}$] |
| $\pi_s$ | entropy production | [J m$^{-3}$ s$^{-1}$ K$^{-1}$] |
| $\tau$ | tortuosity | [-] |
| $\Phi$ | entropy dissipation | [J m$^{-3}$ s$^{-1}$] |
| $\phi$ | potential | [V] |
| $\varphi$ | porosity | [-] |

Super- and subscripts

| | |
|---|---|
| eff | effective: corrected for the matrix |
| M | membrane |

## References


1. Biesheuvel P.M., and Lange F.F., "Application of the Charge Regulation Model to the Colloidal Processing of Ceramics," *Langmuir*, **17**, 3557 (2001).
2. Bird R.B., Stewart W.E., and Lightfoot E.N., "Transport Phenomena," Wiley, 1960, chapters 3 and 18.
3. Chan D.Y.C., Perram J.W., White L.R., and Healy T.W., "Regulation of Surface Potential at Amphoteric Surfaces During Particle-Particle Interaction," *J. Chem. Soc. Faraday Trans. I*, **71**, 1046 (1975).
4. De Groot S.R., and Mazur P., "Non-Equilibrium Thermodynamics," Interscience, New York, 1962, chapters 3 and 5.
5. Deen W.M., "Hindered Transport of Large Molecules in Liquid-Filled Pores," *AIChE J.*, **33**, 1409 (1987).
6. Healy T.W., and White L.R., "Ionizable Surface Group Models of Aqueous Interfaces," *Adv. Colloid Interface Sci.*, **9**, 303 (1978).
7. Krishna R., and Wesselingh J.A., "The Maxwell-Stefan Approach to Mass Transfer," *Chem. Eng. Sci.*, **52**, 861 (1997).
8. Kuiken D.G.C., "Thermodynamics of Irreversible Processes," Wiley, Chichester, 1994, chapter 1.
9. Lightfoot E.N., "Transport Phenomena and Living Systems: Biomedical Aspects of Momentum and Mass Transport," Wiley, New York, 1974, part III.
10. Lorimer J.W., "Phenomenological Coefficients and Frames of Reference for Transport Processes in Liquids and Membranes. Part 3 – Theory of Convective Contribution to Isothermal and Non-Isothermal Transport in Ionic Membranes," *J. Membrane Sci.* **14**, 275 (1983).
11. Lyklema J., "Fundamentals of Interface and Colloid Science. Volume II: Solid-Liquid Interfaces," Academic Press, London, 1995, chapter 3.
12. Mason E.A., and del Castillo L.F., "The Role of Viscous Flow in Theories of Membrane Transport," *J. Membrane Sci.*, **23**, 199 (1985).
13. Mason E.A., and Viehland L.A., "Statistical-Mechanical Theory of Membrane Transport for Multicomponent Systems: Passive Transport through Open Membranes," *J. Chem. Phys.*, **68**, 3562 (1978).
14. Morterra C., and Magnacca G., "A Case Study: Surface Chemistry and Surface Structure of Catalytic Aluminas, as studied by Vibrational Spectroscopy of Adsorbed Species," *Catal. Today*, **27**, 497 (1996).

15. Ninham B.W., and Parsegian V.A., "Electrostatic Potential Between Surfaces Bearing Ionizable Groups in Ionic Equilibrium with Physiologic Saline Solution," *J. Theor. Biol.*, **31**, 405 (1971).
16. Present R. D., and DeBethune A. J., "Separation of a Gas Mixture Flowing through a Long Tube at Low Pressure," *Phys. Rev.*, **75**, 15 (1948).
17. Prigogine I., "Etude Thermodynamique des Phénomènes Irréversibles," Desoer, Liège, 1947.
18. Randon J., Larbot A., Cot L., Lindheimer M., and Partyka S., "Sulfate Adsorption on Zirconium Dioxide," *Langmuir*, **7**, 2654 (1991).
19. Randon J., Larbot A., Guizard C., Cot L., Lindheimer M., and Partyka S., "Interfacial Properties of Zirconium Dioxide Prepared by the Sol-Gel Process," *Colloids and Surfaces*, **52**, 241 (1991).
20. Sohlberg K., Pennycook S.J., and Pantelides S.T., "The Bulk and Surface Structure of γ-Alumina," *Chem. Eng. Comm.*, **181**, 107 (2000).
21. Stewart W.E., and Prober R., "Matrix Calculation of Multicomponent Mass Transfer in Isothermal Systems," *Ind. Eng. Chem. Fundam.*, **3**, 224 (1964).
22. Taylor R., and Krishna R., "Multicomponent Mass Transfer," Wiley, New York, 1993, chapter 2.
23. Vacassy R., Guizard C., Thoraval V., and Cot L., "Synthesis and Characterization of Microporous Zirconia Powders: Application in Nanofilters and Nanofiltration Characteristics," *J. Membrane Sci.*, **132**, 109 (1997).
24. Wesselingh J.A. and Krishna R., "Mass Transfer," Ellis Horwood, Chichester, 1990.
25. Westall J., and Hohl H., "A Comparison of Electrostatic Models for the Oxide/Solution Interface," *Adv. Colloid Interface Sci.*, **12**, 265 (1980).

# Chapter 3

## Application of the Charge Regulation Model to the Separation of Ions by Hydrophilic Membranes


### Abstract

Equation Section (Next)Separation of ions from aqueous solutions by the use of hydrophilic membranes can be described by the charge regulation (CR) model. This is an approach in which the Poisson-Boltzmann equation is combined with a boundary condition at the surface that relates the local ion concentrations in the solution next to the surface to the concentration of each of the adsorbed species. Here, we use the CR model in a simple calculation in which we assume thermodynamic equilibrium and calculate the ion concentrations across the radius of a cylindrical pore slice that is far enough from either of the membrane surfaces for axial concentration gradients to be zero. We use an expression for the ion retention that is based on the equilibrium ion profiles in that slice. For a pure, monovalent salt, this expression qualitatively describes the change of ion retention with pore radius, ion concentrations and pH. The present calculation does not yet incorporate ion transport expressions; hence, it cannot account for the influence of pressure and flux on retention or describe the retention for mixtures of salts.


---


Published with minor modifications as: P.M. Biesheuvel, and W.B.S. de Lint, "Application of the Charge Regulation Model to the Separation of Ions by Hydrophilic Membranes," *J. Colloid Interface Sci.*, **241**, 422 (2001).

## 1. Introduction

The separation of mixtures of ions in aqueous solutions using hydrophilic membranes is very important in biological, environmental and industrial systems. Understanding this transport problem in terms of the fundamental equations of mass transfer (Maxwell-Stefan), momentum transfer (Navier-Stokes) and electrostatics (Poisson) is complicated for the multidimensional geometry of a membrane. Simplifications (one-dimensional geometry, thermodynamically ideal systems in equilibrium) are helpful as well as less complicated transport models like the Nernst-Planck equation (Taylor and Krishna, 1993) or the Teorell-Meyer-Sievers model (Meyer and Sievers, 1936; Teorell, 1936, 1951). In many efforts, a certain constant and homogeneous surface charge (on the outer surface of the membrane, as well as in the pores) is assumed, and its value is obtained by fitting the transport model to the results of electrolyte permeation experiments (Tsuru *et al.*, 1991; Wang *et al.*, 1995; Bowen and Mukhtar, 1996; Bowen, Mohammad and Hildal, 1997). In other cases the electrokinetic or surface charge of the membrane was derived from electrophoretic mobility measurements using small particles of the membrane material, by the streaming potential technique or by titration (Westermann-Clark and Anderson, 1983; Alami-Younssi *et al.*, 1995). In these cases, the potential and charge are determined for an isolated surface. However, to obtain good separation behaviour for hydrophilic membranes the electrostatic double layers have to overlap. In this case the surface potential and charge are decisively different from an isolated surface (i.e., the closer two opposing hydrophilic surfaces, the lower the surface charge and the higher the surface potential). The changing surface conditions with changing pore geometry and pore size decisively influence the concentration of ions in the pore and therefore the retention behaviour of the membrane system.

To describe the ion separation behaviour of hydrophilic membranes we use the charge regulation (CR) model (Ninham and Parsegian, 1971; Chan *et al.*, 1975). This model combines the Poisson-Boltzmann equation for the ionic concentrations in the diffuse part of the double layer with a surface boundary condition that relates concentrations of adsorbed species with local concentrations of ions in solution. The CR model was used to describe the forces between opposing hydrophilic surfaces (Basu and Sharma, 1994; Zhmud, Meurk and Bergström, 1998; Biesheuvel, 2001b; Biesheuvel and Lange, 2001) and transport through membranes (Basu and Sharma, 1997). In the CR model first the equilibrium constants for the adsorption of the different ions onto the surface must be determined (measured, e.g., by one the aforementioned techniques, or derived from thermodynamic arguments). We will show that when the equilibrium constants are known, the CR model can predict in a straightforward manner physical phenomena such as the increase of retention with decreasing pore size or the decrease of retention when the pH approaches on the point of zero charge. A further advantage of the CR boundary condition is that the model distinguishes between all different ionic species. Finally, the CR model implements material properties such as the point of zero charge and the number of available surface sites into the equations that describe the surface charge and the retention, in agreement with observations, e.g., that different materials have different separation properties.

In this chapter we use the charge regulation model to describe the ion retention behaviour of a hydrophilic membrane. We will make a simple introductory calculation in which the ion profiles in a cylindrical pore are determined at thermodynamic equilibrium, from which ion retentions are derived. By nature, this equilibrium calculation does not relate retention to the driving forces for transport such as trans-membrane pressure and gradients in the chemical potential. A transport model combining electrolyte transport and charge regulation will be developed in chapter 4.

We consider a cylindrical pore that is long enough for a pore slice in the middle part of the membrane not to be influenced by entrance and exit effects on either side of the pore (pore radius / pore length << 1). We use an aqueous electrolyte solution of a certain monovalent salt CA – with C the cation (e.g. $Na^+$) and A the anion (e.g. $Cl^-$) – which is either acidified with a strong acid HA or alkalised by the addition of a strong base COH. We show how the CR model qualitatively describes the influence of pore size, ion concentration and pH in the solution outside the membrane on the retention of ions. In this paper only cylindrical pores are considered but the theory can be reworked to describe slit-shaped pores.

In this paper surface adsorption is based on a 2-pK model. The cations, anions and protons compete for the fixed number of hydroxyl surface sites. The adsorption isotherm is based on ideal Langmuir adsorption behaviour, but other charging reactions can be used without changing the essential idea of charge regulation as the boundary condition for the Poisson-Boltzmann equation in porous media.

## 2. Theory

### 2.1 Poisson equation

The charge regulation model for a cylindrical pore starts with the Poisson equation, which is a simplification of Maxwell's first law for a constant permittivity,

$$\frac{1}{r}\frac{\partial}{\partial r}\left(r\frac{\partial \phi}{\partial r}\right)+\frac{\partial^2 \phi}{\partial z^2}=\frac{-F}{\varepsilon_r \varepsilon_0}\sum_{\ell=1}^{n} z_\ell c_\ell \,. \qquad [1]$$

In Eq. [1] $\phi$ is the electrostatic potential [V], $\varepsilon_r$ the relative permittivity (for water, $\varepsilon_r$=78), $\varepsilon_0$ the permittivity of vacuum ($8.854\cdot10^{-12}$ C/(V·m)), $F$ Faraday's constant (96,485 C/mol), $z_i$ the charge number of ionic species $i$, $c_i$ the

concentration of ions [mol/m$^3$], $r$ the radial coordinate [m], $z$ the axial coordinate [m] and $n$ the total number of mobile species. The permittivity $\varepsilon_r$ is independent of the electric field for $E$ below ≈20 MV/m (Basu and Sharma, 1994), which corresponds to a surface charge $\sigma_0$ below ≈14 mC/m$^2$ and holds for our base case, Table 1. It will be assumed that except for the pore entrance and exit, $\partial^2\phi/\partial z^2$ is negligibly small and can be neglected. This simplifies Eq. [1] to

$$\frac{1}{r}\frac{\mathrm{d}}{\mathrm{d}r}\left(r\frac{\mathrm{d}\phi}{\mathrm{d}r}\right)=\frac{-F}{\varepsilon_r\varepsilon_0}\sum_{\ell=1}^{n}z_\ell c_\ell \ . \qquad [2]$$

## 2.2 Thermodynamic equilibrium

For thermodynamically ideal systems at equilibrium, the Boltzmann distribution relates the ion concentration $c_i$ to the ion concentration in the bulk phase and the electrostatic potential $\phi$,

$$c_i = c_i^{\mathrm{b}}\exp\left(\frac{-z_i F\phi}{RT}\right), \qquad [3]$$

where the subscript 'b' refers to the (neutral) bulk solution (where $\phi$ is set to zero), $R$ is the gas constant (8.3144 J/(mol·K)) and $T$ temperature (we use 298 K). Combining Eqs. [2] and [3] the Poisson-Boltzmann (PB) equation can be obtained. The PB relation has been used in transport calculations of the potential and concentration across a cylindrical pore by combining it with the Navier-Stokes and the Nernst-Planck relation (e.g., Sasidhar and Ruckenstein, 1981; Koh and Silverman, 1983; Westermann-Clark and Anderson, 1983; Westermann-Clark and Christoforou, 1986; Hawkins Cwirko and Carbonell, 1989; Guzmán-Garcia *et al.*, 1990; Basu and Sharma, 1994; Wang *et al.*, 1995). This approach was first proposed by Osterle and co-workers (Morrison and Osterle, 1965; Gross and Osterle, 1968; Fair and Osterle, 1971) and is known as the Space-Charge model.

Here we will not use the Space-Charge model but focus on the equilibrium situation.

## 2.3 Charge neutrality

Overall charge neutrality over a cross-section of a cylinder results with Eq. [2] in

$$\sigma = -\frac{1}{2\pi a}\int_0^a F\sum_{\ell=1}^{n} z_\ell c_\ell 2\pi r \,\mathrm{d}r = \varepsilon_r\varepsilon_0 \left.\frac{\mathrm{d}\phi}{\mathrm{d}r}\right|_s , \qquad [4]$$

where $a$ is the pore radius [m], $\sigma$ is the surface charge [C/m$^2$] and the subscript $s$ refers to the surface, where $r$=$a$; the subscript '0' refers to the pore centre axis at $r$=0.

## 2.4 Charge regulation

To solve this set of equations, the constant potential model can be used assuming a certain surface potential $\phi_s$. Another option is to use the constant surface charge model, where the surface charge $\sigma$ is fixed. However, in a real system neither the surface potential nor the surface charge are constant, but change as function of pore size, pH and salt concentration (Healy, Chan and White, 1980). These effects are considered in the CR model which uses an expression for $\sigma$, additional to Eq. [4], set up in terms of the concentrations of ions near the surface $c^s_i$ [mol/m$^3$]; thus being a direct function of $\phi_s$ via Eq. [3]. Here we consider a layer of hydroxyl surface sites $[OH]^s$ that may dissociate in either $[O^-]^s$ sites or react with the $H^+$ ions in solution (formally $H_3O^+$, symbol H) to form positive $[OH_2^+]^s$ sites. In that case, the surface charge is given by

$$\sigma = F\left([OH_2^+]^s - [O^-]^s\right), \qquad [5]$$

where $[...]^s$ denote surface concentrations [mol/m$^2$]. Competitive adsorption by monovalent ions (one type of cation and one type of anion) is implemented by assuming that the $[O^-]^s$ sites may react with cations ($C^+$) to form $[OC]^s$ sites and that the $[OH_2^+]^s$ sites may react with anions ($A^-$) to form $[OH_2A]^s$ sites. All four reactions are governed by equilibrium constants, being $K^-$, $K^+$, $K_C$ and $K_A$, respectively (Basu and Sharma, 1994; Basu and Sharma, 1997; Biesheuvel, 2001a, 2001b; Biesheuvel and Lange, 2001). With the assumption that protons, cations and anions adsorb directly at the surface (i.e., no Stern layer) the resulting expression for the surface charge is

$$\sigma = F c_{\mathrm{tot}}^{//} \frac{\left(c_{\mathrm{H}}^{\mathrm{s}}\right)^2 - K^- K^+}{K^- K^+ \left(1 + c_{\mathrm{C}}^{\mathrm{s}} / K_{\mathrm{C}}\right) + K^+ c_{\mathrm{H}}^{\mathrm{s}} + \left(c_{\mathrm{H}}^{\mathrm{s}}\right)^2 \left(1 + c_{\mathrm{A}}^{\mathrm{s}} / K_{\mathrm{A}}\right)}, \qquad [6]$$

where $c_{\mathrm{tot}}^{//}$ is the total amount of surface sites available [mol/m$^2$]. The point of zero charge (PZC) comes into the equation via $K^-$ and $K^+$ since $K^+K^- = c_{\mathrm{PZC}}^2$, with $c_{\mathrm{PZC}}$ the bulk $H^+$ concentration at the point of zero charge. In a different form, $\mathrm{pH_{PZC}} = \frac{1}{2}(\mathrm{p}K + \mathrm{p}K^+)$ (Chan *et al.*, 1975). Other forms of Eq. [6] can be used without changing the essential idea of this report (e.g., by implementing ion-adsorption to neutral sites (Johnson jr., 1984)). In the charge regulation model, the surface charge obtained from Eqs. [4] and [6] are always equal.

## 2.5 Analytical Poisson-Boltzmann expression

The above equations suffice to exactly solve the electrostatic field across the pore. However, apart from the exact solution of the Poisson-Boltzmann relation, we additionally use an analytical solution for monovalent ions in a cylindrical pore based on the Ettelaie-Buscall (1995) approximation of the PB-equation. The latter analytical solution is obtained by approximating the Poisson-Boltzmann relation with a first order Taylor-series in terms of the

potential. For a monovalent electrolyte solution contained in a cylindrical pore with no axial variations, combining Eqs. [2] and [3] results in

$$\frac{1}{\rho}\frac{\mathrm{d}}{\mathrm{d}\rho}\left(\rho\frac{\mathrm{d}\psi}{\mathrm{d}\rho}\right)=\sinh(\psi). \qquad [7]$$

Here, ρ is the dimensionless radius ρ=*r*κ, with κ the inverse of the Debye length, $\kappa=\sqrt{2F^2I/\varepsilon_r\varepsilon_0RT}$, $I$ the ionic strength, $I=1/2\sum_{\ell=1}^{n}z_\ell^2c_\ell^{\mathrm{b}}$, and ψ the dimensionless potential, $\psi=F\phi/RT$. Approximating the right-hand side of Eq. [7] by a first order Taylor polynomial around the dimensionless central-axis potential, $\psi_0$, the PB equation results in

$$\frac{1}{\rho}\frac{\mathrm{d}}{\mathrm{d}\rho}\left(\rho\frac{\mathrm{d}(\psi-\psi_0)}{\mathrm{d}\rho}\right)=\sinh(\psi_0)+(\psi-\psi_0)\cosh(\psi_0). \qquad [8]$$

Now, the dimensionless potential ψ is given by

$$\psi=\psi_0+\tanh(\psi_0)\left[J_0\left(\sqrt{-\cosh(\psi_0)}\rho\right)-1\right], \qquad [9]$$

and the surface charge σ [C/m$^2$] by

$$\sigma=-\sqrt{2IRT\varepsilon_r\varepsilon_0}\tanh(\psi_0)\sqrt{-\cosh(\psi_0)}\,J_1\left(\sqrt{-\cosh(\psi_0)}\rho\right). \qquad [10]$$

The function $J_0$ denotes a Bessel function of zero order, satisfying the relation

$$J_0(x)=\sum_{s=0}^{\infty}\frac{(-1)^s}{2s!}\left(\frac{x}{2}\right)^{2s}. \qquad [11]$$

The Bessel function $J_1$ is of the first order and given by

$$J_1(x)=\sum_{s=0}^{\infty}\frac{(-1)^s}{s!(1+s)!}\left(\frac{x}{2}\right)^{1+2s}. \qquad [12]$$

## 2.6 Equilibrium retention description

The above equations describe equilibrium adsorption behaviour in a cylindrical pore. However, to use this description for the transport through membranes and the resulting separation behaviour, several assumptions have to be made. First, we assume that the ions in the pore are in thermodynamic equilibrium with the feed side of the membrane. Secondly, we use the fact that the pore effluent is electrically neutral (zero electrical current condition, Tsuru *et al.*, 1991; Bowen and Mukhtar, 1996; Bowen, Mohammad and Hildal, 1997). However, the concentration of counterions in a charged membrane is higher than the concentration of co-ions. Therefore, we assume here that the composition of the effluent of the pore is determined by the concentration of those ions that are excluded from the membrane (i.e. the co-ions). This implies that for a monovalent electrolyte the concentration of counterions (and co-ions) in the effluent equals the concentration of the co-ions in the pore. If, additionally, the co-ion concentration is constant with radial coordinate, the retention can be obtained from

$$R = 1 - \frac{c^{\mathrm{p}}_{\text{co-ions}}}{c^{\infty}_{\text{co-ions}}} = 1 - \exp\left(-\left|\psi\right|\right) \qquad [13]$$

with the superscript p denoting the pore.

In reality, $\psi$ changes with pore radius, thus Eq. [13] becomes for plug flow hydrodynamics (zero velocity gradient with pore radial coordinate)

$$R = 1 - \frac{2}{a^2}\int_0^a r \exp\left(-\left|\psi(r)\right|\right) \mathrm{d}r \qquad [14]$$

For a constant viscosity, the flow through a cylinder has a parabolic velocity profile (Wang *et al.*, 1995; chapter 4), given by

$$v(r) = v_0\left(1-\left(\frac{r}{a}\right)^2\right) \qquad [15]$$

with $v_0$ the velocity at $r$=0. Now, $R$ is given by

$$R = 1-\frac{4}{a^2}\int_0^a r\left[1-\left(\frac{r}{a}\right)^2\right]\exp\left(-\left|\psi(r)\right|\right)\mathrm{d}r\,. \qquad [16]$$

Using the analytical EB expression of the Poisson-Boltzmann relation, combination of Eqs. [9] and [16] results in

$$R = 1-\frac{4}{a^2}\int_0^a r\left[1-\left(\frac{r}{a}\right)^2\right]\exp\left\{-\left|\psi_0+\tanh\left(\psi_0\right)\left[J_0\left(\sqrt{-\cosh\left(\psi_0\right)}\,\rho\right)-1\right]\right|\right\}\mathrm{d}r\,. \qquad [17]$$

The above expressions for retention, Eq. [13]-[17], have predictive value for systems containing one type of salt but they will not be able to describe retention of mixtures of ions and certainly not the negative retentions found when ions of the same sign, but of different valencies, are present in the solution (Tsuru *et al.*, 1991; Bowen and Mukhtar, 1996; Schaep *et al.*, 1999). Furthermore, they do not describe the influence of pressure (flux) on retention (Sasidhar and Ruckenstein, 1981; Tsuru *et al.*, 1991; Bowen and Mukhtar, 1996; Bowen, Mohammad and Hildal, 1997; Schaep *et al.*, 1999).

---

$\Delta pK = pK^- - pK^+ = 3$*, $pH_{PZC} = 9.25$ (alumina), $K^- = 1.778\cdot10^{-8}$ mol/m$^3$ and $K^+ = 1.778\cdot10^{-5}$ mol/m$^3$, $K_A = K_C = 0.7$ mol/m$^3$, $c_{tot}^{//} = 8.3\cdot10^{-6}$ mol/m$^2$, which follows from 20 Å$^2$ per site.*

$c_{salt}$=10 mol/m$^3$, pH=3, thus $c^b$=11 mol/m$^3$ and $\kappa^{-1}$=2.89 nm.

For the base case (pore radius $a$=3 nm): $\phi_0$=34.3 mV, $\phi_s$=48.5 mV, $\sigma$=7.64 mC/m$^2$.

---

*Chan *et al.*, 1975.

Table 1: Data used in the simulations.

## 3. Results and Discussion

In this section, the CR model is applied to a cylindrical pore slice omitting axial effects. The ion retention is obtained from the radial potential distribution in the pore. When the potential profile is calculated, the corresponding ion concentration profiles are determined with Eq. [3].

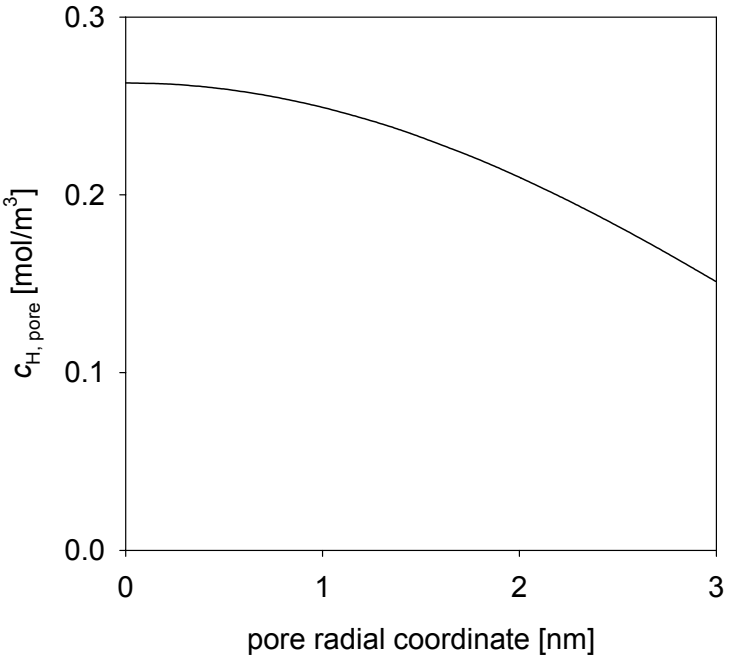


Figure 1: Concentration of protons as function of radial coordinate, *r*, for a cylindrical pore slice at equilibrium with the bulk solution and sufficiently far from the outsides of the membranes for axial gradients to be zero calculated by the charge regulation model. Base case conditions in Table 1.

To show how the retention changes as a function of pore size, bulk electrolyte concentrations and bulk pH, we applied the charge regulation model to a cross-section of a cylindrical pore. The calculations are based on an aqueous monovalent electrolyte solution CA (e.g. NaCl) in contact with a porous γ-alumina matrix of cylindrical pores (see Table 1). For the base case,

the pore radius is 3 nm, which is a typical value for γ-alumina membranes (Schaep *et al.*, 1999).

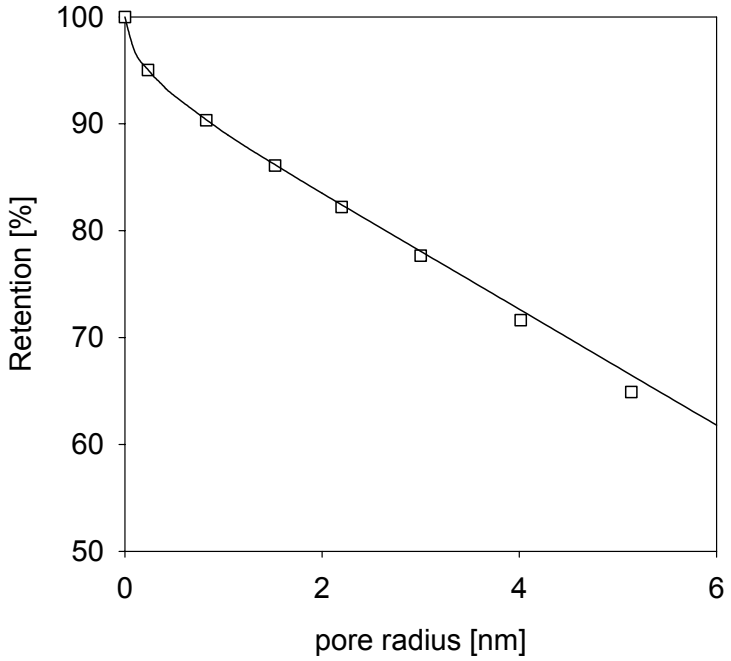


Figure 2: Retention (Eq. [16]) as function of pore radius, *a*, for the equilibrium charge regulation model. Squares are the exact PB-solution, the solid line is based on the EB approximation, Eq. [17]. Except for the pore radius the data in Table 1 are used.

In Figure 1 the concentration change of protons with pore radial coordinate is presented. The concentration of these positive ions decreases toward the pore wall, corresponding to a positively charged membrane surface.

Using Eq. [16], the retention as a function of the pore radius *a* can be determined. The retention decreases with increasing pore size (Figure 2), as expected from practical experience (Schaep *et al.*, 1999) and theory (Tsuru *et al.*, 1991; Wang *et al.*, 1995; Bowen and Mukhtar, 1996; Bowen, Mohammad and Hildal, 1997). Apart from the exact solution using the Poisson-Boltzmann relation (Eqs. [2], [3] and [16]) the retention is calculated with the

EB approximation (Eq. [17]). It can be seen that up to quite a large pore size of 6 nm the EB solutions can accurately describe the retention.

The agreement of the EB solution with the PB equation is also shown in Figure 3 and Figure 4. In Figure 3 the retention is plotted as a function of pH. When the point of zero charge is approached, the retention decreases sharply, in agreement with typical experience with hydrophilic membranes (Schaep *et al.*, 1999). With increasing salt concentration the retention decreases, again in agreement with experimental evidence (Tsuru *et al.*, 1991; Bowen and Mukhtar, 1996; Bowen, Mohammad and Hildal, 1997; Schaep *et al.*, 1999).

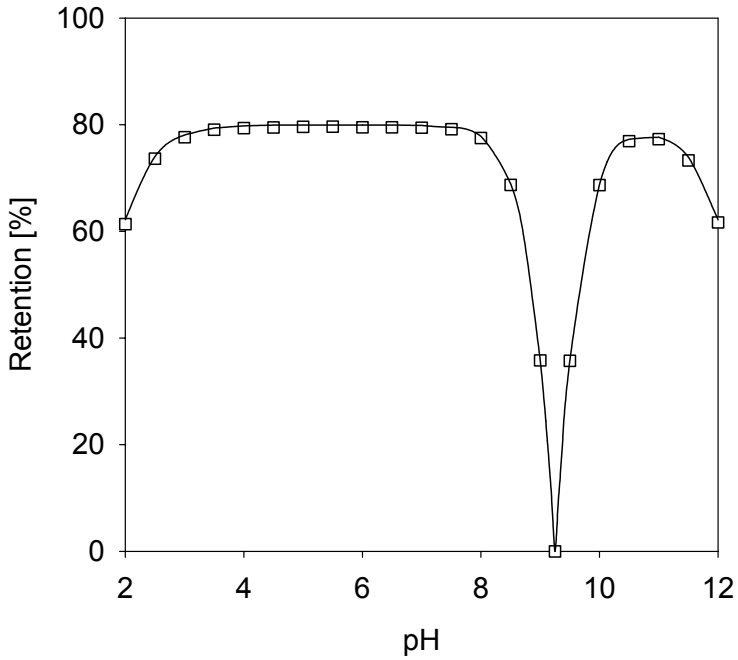


Figure 3: Retention (Eq. [16]) as function of bulk pH based on the equilibrium charge regulation model. Squares denote the exact PB-solution, the solid line is the EB approximation, Eq. [17]. The retention decreases to zero around the point of zero charge. Base case conditions of Table 1 except for the value of pH.

These results resemble typical experimental and theoretical findings on the influence of pore size, pH and salt concentration on the ion-retention behaviour of hydrophilic membranes. The agreement suggests that although the equilibrium calculation based on the charge regulation model is a large simplification of the separation process (no driving forces for transport are considered), the presented modelling approach is a useful and clarifying tool to understand the influence of feed conditions and material properties on membrane separation.

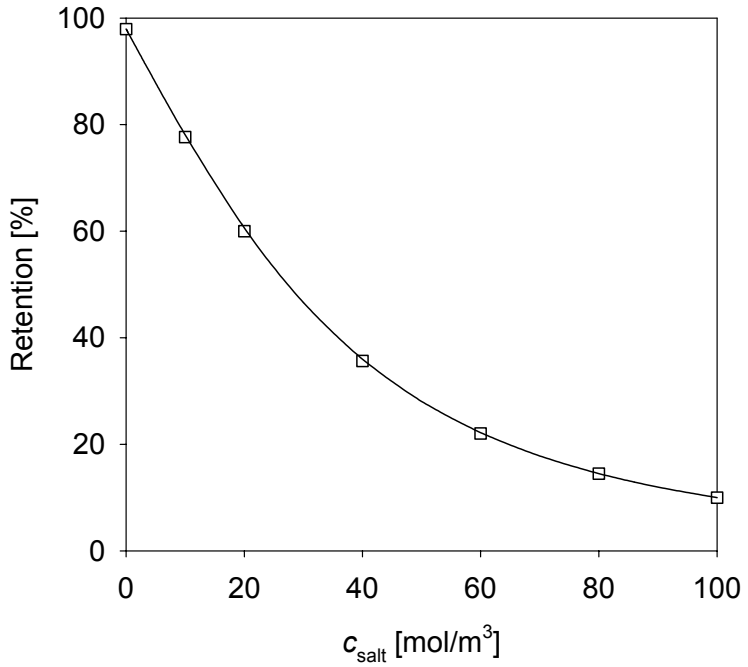


Figure 4: Retention (Eq. [16]) as function of salt concentration in bulk (constant pH) based on the equilibrium charge regulation model. Squares are the exact PB-solution, the solid line is based on the EB approximation, Eq. [17]. Base case conditions of Table 1 except for the value of $c_{salt}$.

Also, in more elaborate non-equilibrium calculations, the charge regulation model (based on combination of Eqs. [4] and [6] as boundary condition) can be implemented to replace the boundary condition of a constant surface

charge or a constant surface potential commonly used in transport descriptions (e.g., Koh and Silverman, 1983; Guzmán-Garcia *et al.*, 1990; Wang *et al.*, 1995; Bowen and Mukhtar, 1996).

## 4. Conclusions

A charge regulation model is a useful tool to describe ion retention by hydrophilic membranes. The model implements material properties, such as the point of zero charge and pore size, in a simple and straightforward manner, as well as solution properties such as pH, concentration and valencies of indifferent ions. For a monovalent salt, an equilibrium calculation based on the absence of pore entrance effects describes observed trends of ion retention versus pH, salt concentration and pore size. A simplification of the full Poisson-Boltzmann equation is derived for monovalent salts, which for the base case could be used for pore sizes up to 6 nm.

## References


1. Alami-Younssi S., Larbot A., Persin M., Sarrazin J., and Cot L., "Rejection of Mineral Salts on a Gamma Alumina Nanofiltration Membrane. Application to Environmental Process," *J. Membrane Sci.*, **102**, 123 (1995).
2. Basu S., and Sharma M.M., "Effect of Dielectric Saturation on Disjoining Pressure in Thin Films of Aqueous Electrolytes," *J. Colloid Interface Sci.*, **165**, 355 (1994).
3. Basu S., and Sharma M.M., "An Improved Space-Charge Model for Flow Through Charged Microporous Membranes," *J. Membrane Sci.,* **124**, 77 (1997).
4. Biesheuvel P.M., "Simplifications of the Poisson-Boltzmann Equation for the Electrostatic Interaction of Close Hydrophilic Surfaces in Water," *J. Colloid Interface Sci.*, **238**, 362 (2001).
5. Biesheuvel P.M., Implications of the Charge Regulation Model for the Interaction of Hydrophilic Surfaces in Water," *Langmuir*, **17**, 3553 (2001).
6. Biesheuvel P.M., and Lange F.F., "Application of the Charge Regulation Model to the Colloidal Processing of Ceramics," *Langmuir*, **17**, 3557 (2001).
7. Bowen W.R., and Mukhtar H., "Characterisation and Prediction of Separation Performance of Nanofiltration Membranes," *J. Membrane Sci.*, **112**, 263 (1996).
8. Bowen W.R., Mohammad A.W., and Hildal N., "Characterisation of Nanofiltration Membranes for Predictive Purposes – Use of Salts, Uncharged Solutes and Atomic Force Microscopy," *J. Membrane Sci.*, **126**, 91 (1997).
9. Chan D.Y.C., Perram J.W., White L.R., and Healy T.W., "Regulation of Surface Potential at Amphoteric Surfaces During Particle-Particle Interaction," *J. Chem. Soc. Faraday Trans. I*, **71**, 1046 (1975).
10. Hawkins Cwirko E., and Carbonell R.G., "Transport of Electrolytes in Charged Pores: Analysis Using the Method of Spatial Averaging," *J. Colloid Interface Sci.*, **129**, 513 (1989).
11. Ettelaie R., and Buscall R., "Electrical Double Layer Interactions for Spherical Charge Regulating Colloidal Particles," *Adv. Colloid Interface Sci.*, **61**, 131 (1995).
12. Fair J.C., and Osterle J.F., "Reverse Electrodialysis in Charged Capillary Membranes," *J. Chem. Phys.*, **54**, 3307 (1971).
13. Gross R.J., and Osterle J.F., "Membrane Transport Characteristics of Ultrafine Capillaries," *J. Chem. Phys.*, **49**, 228 (1968).
14. Guzmán-Garcia A.G., Pintauro P.N., Verbrugge M.W., and Hill R.F., "Development of a Space-Charge Transport Model for Ion-Exchange Membranes," *AIChE J.*, **36**, 1061 (1990).

15. Healy T.W., Chan D., and White L.R., "Colloidal Behaviour of Materials with Ionizable Group Surfaces," *Pure & Appl. Chem.*, **52**, 1207 (1980).
16. Johnson jr. R.E., "A Thermodynamic Description of the Double Layer Surrounding Hydrous Oxides," *J. Colloid Interface Sci.*, **100**, 540 (1984).
17. Koh W.H., and Silverman H.P., "Anion Transport in Thin-Channel Cation Exchange Membranes," *J. Membrane Sci.*, **13**, 279 (1983).
18. Meyer K.H., and Sievers J.-F., "La Permeabilité des Membranes I. Théorie de la Permeabilité Ionique," *Helv. Chim. Acta*, **19**, 649 (1936).
19. Morrison jr. F.A., and Osterle J.F., "Electrokinetic Energy Conversion in Ultrafine Capillaries," *J. Chem. Phys.*, **43**, 2111 (1965).
20. Ninham B.W., and Parsegian V.A., "Electrostatic Potential Between Surfaces Bearing Ionizable Groups in Ionic Equilibrium with Physiologic Saline Solution," *J. Theor. Biol.*, **31**, 405 (1971).
21. Sasidhar V., and Ruckenstein E., "Electrolyte Osmosis Through Capillaries," *J. Colloid Interface Sci.*, **82**, 439 (1981).
22. Schaep J., Vandecasteele C., Peeters B., Luyten J., Dotremont C., and Roels D., "Characteristics and Retention Properties of a Mesoporous $\gamma$-$Al_2O_3$ Membrane for Nanofiltration," *J. Membrane Sci.*, **163**, 229 (1999).
23. Taylor R., and Krishna R., "Multicomponent Mass Transfer," Wiley, New York, 1993, p. 37-49.
24. Teorell T., "An Attempt to Formulate a Quantitative Theory of Membrane Permeability," *Proc. Soc. Exper. Biol. Med.*, **33**, 282 (1935).
25. Teorell T., "Zur quantitativen Behandlung der Membranpermeabilität," *Z. Electrochem.*, **55**, 460 (1951).
26. Tsuru T., Urairi M., Nakao S.-I., and Kimura S., "Negative Rejection of Anions in the Loose Reverse Osmosis Separation of Mono- and Divalent Ion Mixtures," *Desalination*, **81**, 219 (1991).
27. Wang X-L, Tsuru T., Nakao S-I, and Kimura S., "Electrolyte Transport through Nanofiltration Membranes by the Space-Charge Model and the Comparison with Teorell-Meyer-Sievers Model," *J. Membrane Sci.*, **103**, 117 (1995).
28. Westermann-Clark G.B., and Anderson J.L., "Experimental Verification of the Space-Charge Model for Electrokinetics in Charged Microporous Membranes," *J. Electrochem. Soc.*, **130**, 839 (1983).
29. Westermann-Clark G.B., and Christoforou C.C., "The Exclusion-Diffusion Potential in Charged Porous Membranes," *J. Electroanal. Chem.*, **198**, 213 (1986).
30. Zhmud B.V., Meurk A., and Bergström L., "Evaluation of Surface Ionization Parameters from AFM Data," *J. Colloid Interface Sci.*, **207**, 332 (1998).

# Chapter 4

## Application of the Charge Regulation Model to Transport of Ions through Hydrophilic Membranes. One-Dimensional Transport Model for Narrow Pores (Nanofiltration)


### Abstract

Equation Section (Next)The charge regulation concept is combined with the Navier-Stokes and Nernst-Planck equations to describe the ion retention of nanofiltration membranes consisting of narrow cylindrical pores. The charge regulation approach replaces the assumption of a constant charge or a constant potential at the membrane pore surface, and accounts for the influence of pH, salt concentration and type of electrolyte on ion retention. In the current model, radial concentration and potential gradients are considered to be negligibly small (valid for narrow enough pores), resulting in a one-dimensional transport description.

The model describes typical experimental data for nanofiltration membranes, such as the change of ion retention with pore radius, ion concentration, pH and pressure both for monovalent and multivalent ions. For a constant solvent velocity, the model in some cases predicts an optimum pore size for retention. Non-equal retentions for anions and cations are predicted at low and high pH values, as well as a minimum solvent velocity for very low salt concentrations. For higher salt concentrations, and at a fixed pressure difference, an increase in solvent velocity with increasing ion concentrations is predicted, in agreement with other one-dimensional transport descriptions found in literature, but in contrast to some experimental data.


---


Published with minor modifications as: W.B.S de Lint, P.M. Biesheuvel, and H. Verweij, "Application of the Charge Regulation Model to Transport of Ions through Hydrophilic Membranes. One-Dimensional Transport Model for Narrow Pores (Nanofiltration)," *J. Colloid Interface Sci.*, **251**, 131 (2002).

## 1. Introduction

Nanofiltration (NF) membranes consist of a thin separation layer with pore sizes in the 1-10 nm range, in between the pore sizes of reverse osmosis and ultrafiltration membranes. NF membranes can separate ions from aqueous solutions using electrostatic effects and typically have higher solvent fluxes, but lower retentions, than reverse osmosis membranes.

Theoretical studies on mass transport in NF membranes use different approaches, such as models derived from the Generalized Maxwell-Stefan (GMS) theory (Morrison jr. and Osterle, 1965; Gross and Osterle, 1968; Fair and Osterle, 1971; Jacazio *et al.*, 1972; Sonin, 1976; Sasidhar and Ruckenstein, 1981; Westermann-Clark and Anderson, 1983; Hawkins Cwirko and Carbonell, 1989; Tsuru *et al.*, 1991; Basu and Sharma, 1997; Yang and Pintauro, 2000), the concept of hydrodynamics (Deen, 1987), a combination of both (Bowen and Mukthar, 1996; Bowen, Mohammad and Hildal, 1997), or irreversible thermodynamics (De Groot and Mazur, 1962; Spiegler and Kedem, 1966). We use the GMS description, which simplifies to the Nernst-Planck (NP) equation for dilute systems (Taylor and Krishna, 1993). Combining the NP approach with proper descriptions of momentum transfer (Navier-Stokes), electrostatics (Poisson), continuity of mass, electroneutrality, zero electric current and the interactions with the membrane material, suffices to completely specify the mass transport of ions. Because solving the full NP and Poisson equations for the complex structure of a membrane is mathematically formidable, simplifications of the governing relations are very useful. Therefore we assume the membrane to be constructed of a collection of straight capillary pores with a small and uniform radius. For small enough pore radii radial gradients in the electrostatic potential and the concentration of ions can be neglected (Sonin, 1976; Hawkins Cwirko and Carbonell, 1989; Bowen and Mukthar, 1996; Bowen, Mohammad and Hildal, 1997).

To understand the ion retention behaviour of NF membranes as a function of feed solution conditions, pressure and surface charge, mass transport of the ions and solvent through the membrane pore as well as chemical interactions with the membrane pore surface must be considered. Transport descriptions for NF membranes generally assume a constant surface potential or surface charge (Morrison jr. and Osterle, 1965; Gross and Osterle, 1968; Fair and Osterle, 1971; Jacazio *et al.*, 1972; Sonin, 1976; Westermann-Clark and Anderson, 1983; Tsuru *et al.*, 1991; Bowen and Mukthar, 1996; Bowen, Mohammad and Hildal, 1997). However, it is known from practice as well as from theory that the surface charge and surface potential change with pH, salt concentration and the extent of electrostatic double layer overlap (like in narrow pores) because of the specific interaction of ions in solution with the pore surface (Hall, Starov and Lloyd, 1997; Hall, Lloyd and Starov, 1997; Biesheuvel, 2001b; chapter 2 of this thesis; Biesheuvel and Lange, 2001; Starov, Bowen and Welfoot, 2001); the effects of double layer overlap on the potential and charge are considered in the charge regulation (CR) approach (Ninham and Parsesian, 1971; Chan *et al.*, 1975; Healy, Healy and White, 1978; Chan and White, 1980). For charged membranes, Jacazio *et al.* (1972) and Westermann-Clark and Anderson (1983) were the first to realize this dependence of surface charge on material and solution properties, though they did not incorporate the ion-surface interactions in their model description. Bowen and Mukthar (1996) used a Freundlich-like isotherm to determine a homogeneous membrane charge density as a function of the ion concentrations in the feed and found no influence of the type of electrolyte. Sasidhar and Ruckenstein (1982) and Takagi and Nakagaki (1990) followed the same approach and used a Langmuir isotherm to describe specific adsorption of counterions at the membrane surface. Similar to Bowen and Mukthar (1996), Takagi and Nakagaki (1990) related the Langmuir adsorption parameters to the feed concentrations of the species. Basu and Sharma (1997) integrated the charge regulation (CR) concept into a space-charge model for transport

through microporous mica, but they did not focus on the separation properties of the material. Like Basu and Sharma (1997), Hall and co-workers (1997a, b) combined charge regulation with mass transport, but focused more on retention behaviour, see also Starov, Bowen and Welfoot (2001). Also, the transport of hydroxyl ions and protons was explicitly accounted for (Hall, Starov and Lloyd, 1997; Hall, Lloyd and Starov, 1997; Starov, Bowen and Welfoot, 2001). In the work of Hall and co-workers (1997a, b) the charge regulation adsorption parameters were obtained by fitting the model to membrane retention data of binary electrolyte solutions. Starov, Bowen and Welfoot (2001) used charge regulation data (Hall, Starov and Lloyd, 1997; Hall, Lloyd and Starov, 1997) in a homogeneous mass transport model.

In a previous effort (chapter 2 of this thesis), we used the charge regulation concept for a pore at thermodynamic equilibrium to describe the increase of retention with decreasing pore size and the decrease of retention when the pH approaches on the point of zero charge (PZC). In the present effort the equilibrium model (chapter 2 of this thesis) is extended by combining the charge regulation approach with the Nernst-Planck equation, the Navier-Stokes equation and continuity of mass to predict the ion separation behaviour of a hydrophilic NF membrane. The membrane is modelled as a collection of cylindrical pores with the pore-mouths on both sides of the membrane at thermodynamic equilibrium with the adjacent solution phase. Furthermore, we assume the pore radius small enough for the radial concentration and potential gradients to be negligibly small (uniform potential approach (Sonin, 1976; Hawkins Cwirko and Carbonell, 1989; Bowen and Mukthar, 1996; Bowen, Mohammad and Hildal, 1997)). The resulting model is then one-dimensional in the axial direction. Apart from the use of charge regulation, the present model also explicitly takes into account the concentration of protons and hydroxyl ions (i.e. the pH) in the solution (Hall, Starov and Lloyd, 1997; Hall, Lloyd and Starov, 1997; Starov,

Bowen and Welfoot, 2001). Sodium chloride is used as a model electrolyte, which can be acidified or alkalized by addition of HCl or NaOH, respectively. Mixtures with other univalent and divalent cations are also considered. We will confine ourselves to the description of a stationary experiment in a dead-end permeation set-up with a constant feed salt concentration (infinitely large feed reservoir), and without any sweep flow on the effluent side. The ion concentrations on the effluent side are not fixed, but are a unique function of the ion and solvent flow through the membrane.

The transport model predicts well-known NF separation characteristics like an increase in retention with increasing pressure difference as well as negative retentions for multicomponent electrolyte mixtures. Other interesting features of the model are non-equal anion and cation retentions at high and low pH values, as well as an optimum pore size for retention at a fixed pressure difference over the membrane.

## 2. Theory

We will consider a membrane consisting of a set of long and narrow straight cylindrical pores of equal length extending from the feed side to the effluent side and focus on a single pore, see Figure 1. The solution at the left side of the pore is the feed solution, the solution on the right side is the effluent. For long enough pores entrance and exit effects can be neglected. Furthermore, if the pore is narrow enough the ionic concentrations and electrostatic potential are constant with respect to the pore radius, allowing us to neglect radial effects and use a purely one-dimensional description of flow. This approach is referred to as the uniform potential (UP) approach (Sonin, 1976; Hawkins Cwirko and Carbonell, 1989; Bowen and Mukthar, 1996; Bowen, Mohammad and Hildal, 1997).

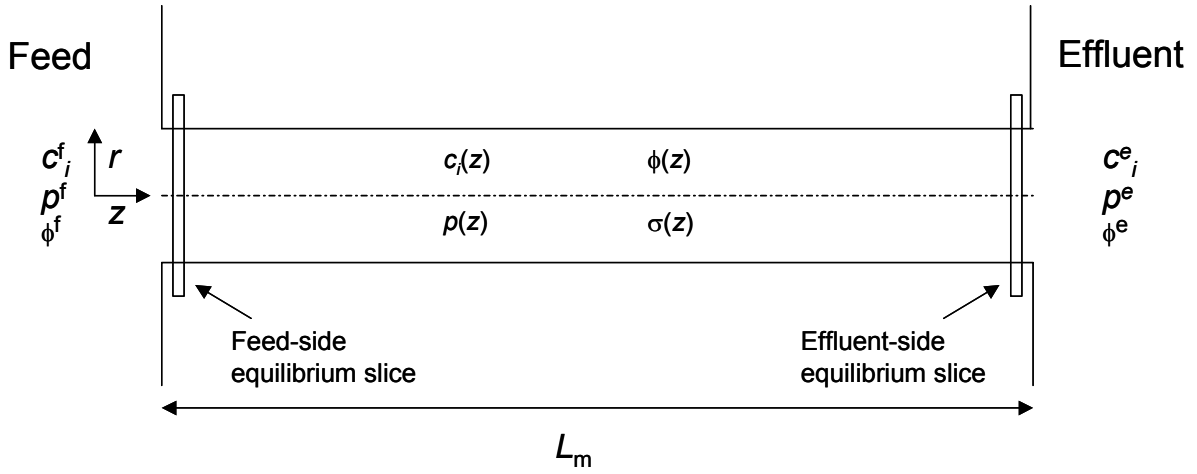


Figure 1: Overview of a cylindrical membrane pore.

On the feed side of the pore, the pressure $p^f$ [Pa], electrostatic potential $\phi^f$ [V] and the concentrations of species $i$, $c^f_i$ [mol/m$^3$], are fixed as well as the pressure on the effluent side $p^e$. The ion concentrations $c^e_i$ and electrostatic potential $\phi^e$ in the effluent are variables in the model and not known a priori. At stationary conditions and without a sweep flow on the effluent side, the concentrations in the effluent are related to the molar flux of ions $N_i$ [mol/m$^2$s] and the mass-average velocity $v$ [m/s] by (Tsuru *et al.*, 1991; Bowen and Mukthar, 1996; Bowen, Mohammad and Hildal, 1997; Hall, Starov and Lloyd, 1997; Starov, Bowen and Welfoot, 2001)

$$c_i^{\mathrm{e}} = \frac{N_i}{v}. \qquad [1]$$

In this work the variables $N_i$ and $v$ are quantities averaged over the pore radius. Since we only consider dilute systems the mass-average velocity is set equal to the solvent velocity.

The pore slices at each end of the membrane are assumed to be in thermodynamic equilibrium with the adjacent solution phases, feed or effluent. This implies that at the solution-pore interfaces the Boltzmann equation (Eq. [4]) can be used (e.g., Jacazio *et al.*, 1972; Westermann-Clark

and Anderson, 1983). All non-equilibrium aspects (i.e. transport) are considered to depend only on the characteristics of the pore in between the two equilibrium slices. Between these equilibrium slices the Boltzmann equation is replaced by the Nernst-Planck equation (Eq. [13]).

For stationary conditions, continuity of mass results in

$$\frac{\mathrm{d}N_i}{\mathrm{d}z} = 0,\ \frac{\mathrm{d}v}{\mathrm{d}z} = 0\,, \qquad [2]$$

with $z$ the axial coordinate. Hence, $N_i$ and $v$ are constant everywhere in the pore.

When the molar fluxes $N_i$ of ions and the solvent velocity $v$ are known, the effluent concentrations can be obtained from Eq. [1]. The retention by the membrane of each ion species $i$ is then given by

$$R_i = \left(1 - \frac{c_i^{\mathrm{e}}}{c_i^{\mathrm{f}}}\right) \cdot 100\%\,. \qquad [3]$$

## 2.1 Thermodynamic equilibrium

For dilute, ideal systems at thermodynamic equilibrium the Boltzmann equation relates ion concentrations $c_i$ [mol/m$^3$] to the electrostatic potential

$$c_i^0 = c_i^{\mathrm{b}} \exp\left[-z_i\left(\psi^0 - \psi^{\mathrm{b}}\right)\right], \qquad [4]$$

with $z_i$ the charge number of species $i$, $\psi$ the dimensionless potential $\psi = F\phi/RT$, with $\phi$ the electrostatic potential [V], $F$ the Faraday constant [C/mol], $R$ the gas constant [J/(mol·K)], and $T$ the temperature [K]. Here we have written the Boltzmann equation for the equilibrium between a bulk ('b') solution (being the feed, f, or the effluent, e), and the solution phase just inside the pore ('0'). In the feed solution we set the dimensionless

electrostatic potential $\psi^f$ to zero, but the potential in the effluent $\psi^e$ is not fixed.

For electric field strengths higher than ≈20 MV/m, the solvent permittivity may decrease with respect to its bulk value (i.e., $\varepsilon_r$<78) and this effect can be incorporated in Eq. [4] (Basu and Sharma, 1997; Yang and Pintauro, 2000).

## 2.2 Charge regulation

Ionic species present in the pore solution adsorb on the membrane pore wall resulting in the formation of a surface charge. When several different ionic species are present, competition for the surface sites, called competitive adsorption, takes place. In this work we assume an oxidic surface with a fixed number of hydroxyl sites $[\text{-OH}]^s$ (Healy and White, 1978; Hall, Starov and Lloyd, 1997; Hall, Lloyd and Starov, 1997; Starov, Bowen and Welfoot, 2001; Biesheuvel, 2001b; chapter 2 of this thesis; Biesheuvel and Lange, 2001). These surface sites are in thermodynamic equilibrium with the ions in the solution next to the surface. Protons may adsorb or desorb at the surface, resulting in the formation of $[\text{-OH}_2^+]^s$ or $[\text{-O}^-]^s$ surface groups. Cations and anions adsorb on these negative and positive surface groups, respectively. This adsorption approach is termed the 2-pK model.

An oxidic material can be characterized in terms of the total fixed number of chargeable hydroxyl groups on the membrane pore wall, $c_{\text{tot}}^{//}$ [mol/m$^2$], the point of zero charge (PZC), which is the pH at which the number of positively and negatively charged surface groups on the material is equal, and $\Delta p\mathit{K}$, the difference between $p\mathit{K}^+$ and $p\mathit{K}^-$ (Ninham and Parsegian, 1971; Chan *et al.*, 1975; Healy, Chan and White, 1980). The parameters $p\mathit{K}^+$ and $p\mathit{K}^-$ describe the equilibrium between the uncharged surface hydroxyl group $[\text{-OH}]^s$ and the charged groups $[\text{-O}^-]^s$ and $[\text{-OH}_2^+]^s$. They are related to the pH at the PZC by

$$\mathrm{pH_{PZC}} = \frac{1}{2}\left(\mathrm{p}K^{+} + \mathrm{p}K^{-}\right). \qquad [5]$$

In this chapter we assume that cations $C^{m+}$ and anions $A^{n-}$ adsorb directly at the surface (i.e., no Stern layer) only on a single charged surface group, irrespective of the ion valency, forming either $[\text{-O}^{-}\text{C}^{m+}]^{s}$ (adsorption constant $K_C$) or $[\text{-OH}_2^{+}\text{A}^{n-}]^{s}$ groups ($K_A$). Note that only for monovalent cations, $C^{1+}$, and monovalent anions $A^{1-}$, these ion pairs are neutral, while for a divalent cation like $Ca^{2+}$, the adsorbed complex has a 1+ charge. More complex surface adsorption reactions (Healy and White, 1978) can be built into the charge regulation model as well as the strong adsorption of specifically adsorbing divalent ions (Huang and Stumm, 1973; He *et al.*, 1997). However, the 2-pK model used here describes the main features of competitive ion adsorption and charge regulation.

The four surface reactions we will consider are

$$\begin{aligned}
\text{-OH}_2^{+} &\overset{K^{+}}{\rightleftharpoons} \text{-OH} + \mathrm{H}^{+}(\mathrm{s}) \\
\text{-OH} &\overset{K^{-}}{\rightleftharpoons} \text{-O}^{-} + \mathrm{H}^{+}(\mathrm{s}) \\
\text{-O}^{-}\mathrm{C}^{m+} &\overset{K_C}{\rightleftharpoons} \text{-O}^{-} + \mathrm{C}^{m+}(\mathrm{s}) \\
\text{-OH}_2^{+}\mathrm{A}^{n-} &\overset{K_A}{\rightleftharpoons} \text{-OH}_2^{+} + \mathrm{A}^{n-}(\mathrm{s})
\end{aligned} \quad ,$$

which are thought to occur in an equipotential plane. The label (s) denotes non-adsorbed virtual proton, cation and anion species. The concentration of these virtual species is related to that in the electrolyte bulk by the Boltzmann relation, Eq. [4]. The equilibrium constants $K$ for these four reactions are defined as

$$K^{+} = \frac{c_{\mathrm{H}}^{\mathrm{s}}\left[\text{-OH}\right]^{\mathrm{s}}}{c^{\mathrm{ref}}\left[\text{-OH}_2^{+}\right]^{\mathrm{s}}},\ K^{-} = \frac{c_{\mathrm{H}}^{\mathrm{s}}\left[\text{-O}^{-}\right]^{\mathrm{s}}}{c^{\mathrm{ref}}\left[\text{-OH}\right]^{\mathrm{s}}},\ K_{\mathrm{C}} = \frac{c_{\mathrm{C}}^{\mathrm{s}}\left[\text{-O}^{-}\right]^{\mathrm{s}}}{c^{\mathrm{ref}}\left[\text{-O}^{-}\mathrm{C}^{m+}\right]^{\mathrm{s}}},\ K_{\mathrm{A}} = \frac{c_{\mathrm{A}}^{\mathrm{s}}\left[\text{-OH}_2^{+}\right]^{\mathrm{s}}}{c^{\mathrm{ref}}\left[\text{-OH}_2^{+}\mathrm{A}^{n-}\right]^{\mathrm{s}}}. \qquad [6]$$

The concentrations of the surface complexes ([-OH]$^s$, [-$OH_2^+$]$^s$, [-$O^-$]$^s$, [-$O^-C^{m+}$]$^s$, [-$OH_2^+A^{n-}$]$^s$) have units [mol/m$^2$], the virtual ion concentrations $c_i^s$ have dimensions [mol/m$^3$], and $c^{ref}$ is the thermodynamic reference concentration ($c^{ref}$=1000 mol/m$^3$, corresponding to 1 mol/dm$^3$). The adsorption equilibrium constants $K^+$, $K^-$, $K_A$, $K_C$ and $c_{tot}^{//}$ describe the interaction of the (membrane) material with the respective ion and the solvent for the given adsorption model and are independent of such factors as pore size, geometry, pH and ion concentration. Because they are material-specific, independent techniques like electrophoretic mobility measurements or electroacoustic methods can help to determine the adsorption constants.

The surface charge σ [C/m$^2$] is given by

$$\sigma = F\left( [\text{-}OH_2^+]^s - [\text{-}O^-]^s + \sum_{\ell=1}^{nC}(m_\ell - 1)[\text{-}O^-C_\ell^{m_\ell +}]^s - \sum_{\ell=1}^{nA}(n_\ell - 1)[\text{-}OH_2^+A_\ell^{n_\ell -}]^s \right), \qquad [7]$$

with $nC$ and $nA$ the total number of cation and anion species, respectively. The total number of surface sites $c_{tot}^{//}$ [mol/m$^2$] is equal to the sum over all surface sites,

$$c_{tot}^{//} = [\text{-}OH]^s + [\text{-}OH_2^+]^s + [\text{-}O^-]^s + \sum_{\ell=1}^{nC}[\text{-}O^-C_\ell^{m_\ell +}]^s + \sum_{\ell=1}^{nA}[\text{-}OH_2^+A_\ell^{n_\ell -}]^s \,. \qquad [8]$$

Combining Eqs. [7] and [8] with the adsorption reactions in Eq. [6] results in a surface charge given by

$$\sigma = Fc_{tot}^{//}\frac{\dfrac{c^{ref}c_H^s}{K^+}\left[1 - \sum_{\ell=1}^{nA}(n_\ell - 1)\dfrac{c_{A,\ell}^s}{c^{ref}K_{A,\ell}}\right] - \dfrac{c^{ref}K^-}{c_H^s}\left[1 - \sum_{\ell=1}^{nC}(m_\ell - 1)\dfrac{c_{C,\ell}^s}{c^{ref}K_{C,\ell}}\right]}{1 + \dfrac{c_H^s}{c^{ref}K^+}\left(1 + \sum_{\ell=1}^{nA}\dfrac{c_{A,\ell}^s}{c^{ref}K_{A,\ell}}\right) + \dfrac{c^{ref}K^-}{c_H^s}\left(1 + \sum_{\ell=1}^{nC}\dfrac{c_{C,\ell}^s}{c^{ref}K_{C,\ell}}\right)}. \qquad [9]$$

In the case of only one type of monovalent anion and one type of monovalent cation, Eq. [9] results in a surface charge given by (Healy, Chan and White, 1980; Basu and Sharma, 1997; Biesheuvel, 2001a; chapter 2 of this thesis)

$$\sigma = Fc_{\mathrm{tot}}^{//}\frac{\left(c_{\mathrm{H}}^{\mathrm{s}}\right)^2 - K^+K^-\left(c^{\mathrm{ref}}\right)^2}{K^+c_{\mathrm{H}}^{\mathrm{s}}c^{\mathrm{ref}} + \left(c_{\mathrm{H}}^{\mathrm{s}}\right)^2 + K^+K^-\left(c^{\mathrm{ref}}\right)^2 + K^+K^-c^{\mathrm{ref}}c_{\mathrm{C}}^{\mathrm{s}}/K_{\mathrm{C}} + \left(c_{\mathrm{H}}^{\mathrm{s}}\right)^2 c_{\mathrm{A}}^{\mathrm{s}}\Big/\left(c^{\mathrm{ref}}K_{\mathrm{A}}\right)}. \qquad [10]$$

In some of the simulations we will use the divalent calcium ion as well. With the assumption that this ion only adsorbs at one single $[\text{-O}^-]^{\mathrm{s}}$ site, the surface charge can be calculated with Eq. [9] ($nA$=1, $nC$=2).

In the model, the surface charge is calculated at every axial position in the membrane and is supplemented by another expression for the surface charge resulting from the constraint of electroneutrality in each pore slice.

## 2.3 Electroneutrality

In every pore slice the sum of the mobile charges (the charges related to the ions in the pore solution) is assumed compensated by the immobile charge on the pore surface. Hence, the surface charge σ [C/m$^2$] is given by

$$\sigma(z) = -\frac{1}{a}\int_0^a F\sum_{i=1}^{ni} z_i c_i(z,r)\, r\, \mathrm{d}r\,, \qquad [11]$$

with $ni$ the number of ionic species ($ni$=$nA$+$nC$), $a$ the pore radius [m], $r$ the radial coordinate [m] and $c_i$ a function of $z$ and $r$. In the uniform potential model (Sonin, 1976; Hawkins Cwirko and Carbonell, 1989; Bowen and Mukthar, 1996; Bowen, Mohammad and Hildal, 1997) the concentrations are constant over the radial coordinate (see Figure 1), and Eq. [11] becomes

$$\sigma(z) = -\frac{Fa}{2}\sum_{\ell=1}^{ni} z_\ell c_\ell(z)\,. \qquad [12]$$

## 2.4 The Nernst-Planck equation

The Nernst-Planck equation can be derived from the full Maxwell-Stephan equation for dilute, ideal systems (Taylor and Krishna, 1993) and is given by

$$N_i = -D_i\left(\frac{\mathrm{d}c_i}{\mathrm{d}z} + z_i c_i \frac{\mathrm{d}\psi}{\mathrm{d}z}\right) + c_i v \,. \qquad [13]$$

The diffusion coefficients $D_i$ [$m^2/s$] are equal to the Maxwell-Stefan ion-solvent diffusion coefficients at infinite dilution (Taylor and Krishna, 1993). The constraints of the porous membrane matrix hinder transport, and the diffusion coefficients as well as the convective velocity can be adjusted to account for these geometrical effects (Wesselingh, Vonk and Kraaijeveld, 1995; Bowen, Mohammad and Hildal, 1997; Krishna and Wesselingh, 1997; Yang and Pintauro, 2000). For example, Bowen, Mohammad and Hildal (1997) use a correction from the theory of hydrodynamics for both diffusion and convection. Another particular elegant manner to include matrix effects - hindered transport of both solvent and ions - is the inclusion of the Einstein correction, simultaneously in the diffusion coefficient $D_i$ (Eq. [13]) as well as in the viscosity $\mu$ (Eq. [15]). This approach was used by Yang and Pintauro (2000) and allowed them to quantitatively describe membrane retention data (their Figure 3). In the present paper we will not apply such corrections and assume that transport by diffusion and convection in the membrane pore is equal to transport in free solution.

In principle, the Nernst-Planck equations should be solved for all charged mobile species (hydroxyl ions, protons, anions and cations). However, for the hydroxyl ions we apply the water dissociation reaction instead, which is fast compared to the transport processes. The water dissociation reaction is given by

$$K_{\mathrm{w}} = c_{\mathrm{H^+}} c_{\mathrm{OH^-}} \,, \qquad [14]$$

where $K_w$ is the water autoprotolysis constant [mol$^2$/m$^6$]. Contrary to (Hall, Starov and Lloyd, 1997; Hall, Lloyd and Starov, 1997; Starov, Bowen and Welfoot, 2001) we assume Eq. [14] to be valid at each location in the membrane. Because the molar fluxes are related to the effluent concentrations by Eq.[1], the flux of hydroxyl ions follows directly from the flux and the effluent concentration of protons (see Eq. [14]).

### 2.5 The Navier-Stokes equation

Solving the full Navier-Stokes (NS) equation is a formidable task. We will therefore limit ourselves to systems with a constant mass density and viscosity. Neglecting radial velocities $v_r$ and radial pressure gradients $\partial p/\partial r$ and using the uniform potential approach, we only have to consider the axial component of the NS equation. At mechanical equilibrium, with cylindrical symmetry (i.e. $\partial/\partial\theta = 0$) and zero tangential velocity, the axial component of the NS equation reads

$$-\frac{\mathrm{d}p}{\mathrm{d}z}+\frac{\mu}{r}\frac{\partial}{\partial r}\left(r\frac{\partial v_z}{\partial r}\right)-RT\sum_{\ell=1}^{ni}z_\ell c_\ell\frac{\mathrm{d}\psi}{\mathrm{d}z}=0\,, \qquad [15]$$

with $p$ the pressure [Pa] and $\mu$ the Newtonian viscosity [Pa·s]. Integrating Eq. [15] twice subject to the boundary conditions

$$\left.\frac{\partial v_z}{\partial r}\right|_{r=0}=0 \quad , \qquad [16]$$
$$v_z\big|_{r=a}=0$$

and using Eq. [2], results in

$$v_z(r)=\frac{a^2}{4\mu}\left[1-\left(\frac{r}{a}\right)^2\right]\left(\frac{\mathrm{d}p}{\mathrm{d}z}+RT\sum_{\ell=1}^{ni}z_\ell c_\ell\frac{\mathrm{d}\psi}{\mathrm{d}z}\right). \qquad [17]$$

Integrating over the pore radius $a$, the average velocity $v$ is obtained (Sonin, 1976)

$$v = -\frac{a^2}{8\mu}\left(\frac{\mathrm{d}p}{\mathrm{d}z} + RT\sum_{\ell=1}^{ni} z_\ell c_\ell \frac{\mathrm{d}\psi}{\mathrm{d}z}\right). \qquad [18]$$

If the electrostatic term in Eq. [18] is neglected the classical parabolic Hagen-Poiseuille flow profile is obtained (Bird, Stewart and Lightfoot, 1960), but the expression shows that also for the uniform potential approach the flow profile is always parabolic.

Instead of the pore-ensemble approach it is also possible to model a membrane as a porous packed bed. In this concept the permeability of the material $B_0$ (see Eq. [2] in chapter 7) replaces the $a^2/8$ term in Eq. [18] (Bird, Stewart and Lightfoot, 1960; Biesheuvel and Verweij, 1999). Please note that the convective velocity in Eq. [18] is defined interstitially (i.e., volume flow per area of pore). When the membrane is considered as a porous packed bed, the velocity is defined superficially (volume flow per total area of membrane). The interstitial and superficial velocities, $v_{\mathrm{int}}$ and $v_{\mathrm{sup}}$, are related by the membrane porosity $\varphi$, $v_{\mathrm{sup}}/v_{\mathrm{int}} = \varphi$. The permeability $B_0$ depends on the porosity, the tortuosity and the size of the particles of which the porous medium consists. In the present paper, however, Eq. [18] is used instead.

## 2.6 Zero electric current

Charged mobile species of opposite sign cannot move through the membrane independently since even minute amounts of charge separation will give rise to very large electrostatic fields. These fields will immediately adjust the ion molar fluxes to obtain a zero electric current,

$$F\sum_{\ell=1}^{ni} z_\ell N_\ell = 0\,. \qquad [19]$$

Note that to obtain a zero current, a constant axial potential difference has to be established over the pore.

## 2.7 Uniform potential assumption

In our model only transport through narrow pores is considered. As a result, gradients in the radial concentrations and radial electrostatic potential can be neglected; this is the uniform potential approach (Sonin, 1976; Hawkins Cwirko and Carbonell, 1989; Bowen and Mukthar, 1996; Bowen, Mohammad and Hildal, 1997). Indeed, this assumption becomes increasingly exact when equally charged opposing surfaces approach each other (Biesheuvel, 2001a). To assess the validity of this assumption for our system of cylindrical pores, and to select a proper base case, we calculated the radial concentration and electrostatic potential profile using the exact Poisson-Boltzmann equation for a system consisting of monovalent ions only,

$$\frac{\lambda^2}{\rho}\frac{\mathrm{d}}{\mathrm{d}\rho}\left(\rho\frac{\mathrm{d}\psi}{\mathrm{d}\rho}\right)=\sinh\left(\psi\right). \qquad [20]$$

The Debye ratio $\lambda$ is the ratio of the Debye length $\lambda_D$ over the pore radius $a$, $\lambda = a\Big/\sqrt{\varepsilon_r\varepsilon_0 RT\Big/\left(2F^2 I\right)}$, with $I$ the ionic strength of the feed solution, and $\rho$ the dimensionless radial coordinate, $\rho = r/a$.

Figure 2 shows the deviation between the coion concentration at the pore surface and at the pore centreline for a monovalent salt as a function of the dimensionless surface potential $\psi^s$ and the Debye ratio $\lambda$ while Figure 3 shows the deviation in electrostatic potential in the centre of the pore $\psi^0$ from its value at the surface $\psi^s$. Bowen, Mohammad and Hildal (1997) made a similar assessment for the applicability of the uniform potential approach. In the calculations for Figure 2 and Figure 3 the radial potential distribution was obtained from Eq. [20] and the coion concentration profile was

calculated using Eq. [4] (setting the electrostatic potential in the feed to zero).

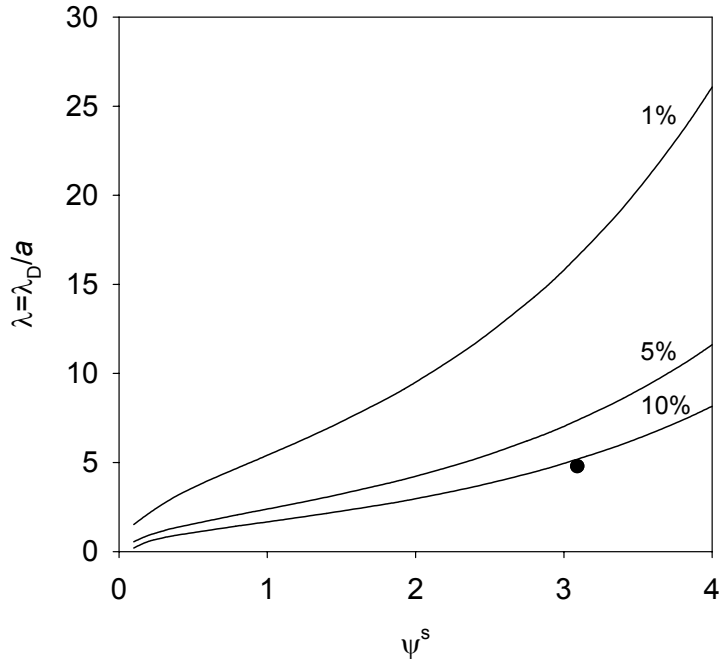


Figure 2: Deviation from the uniform potential in the base case as a function of the dimensionless surface potential $\psi^s$ and the Debye ratio $\lambda$, calculated using the exact Poisson-Boltzmann equation. The single circle is the base case. Solid lines represent the deviation in the coion ($Na^+$) concentration between the pore center ($r$=0) and the pore wall ($r$=$a$).

Analysing Figure 2 and Figure 3 shows that for dimensionless surface potentials $\psi^s$ below 1.0 ($\phi^s$<25.7 mV) the deviation in the radial ion concentration is lower than the deviation in radial potential, while the opposite is true for $\psi^s$>1.0.

To select a proper base case (Table 1), we combined Eq [20] with the charge expression (Eq. [10]) and the electroneutrality condition (Eq. [12]). For our base case a deviation in the concentration of approximately 10% was

considered acceptable and the base case was selected accordingly (the single circle in Figure 2 and Figure 3 shows the position of the base case).

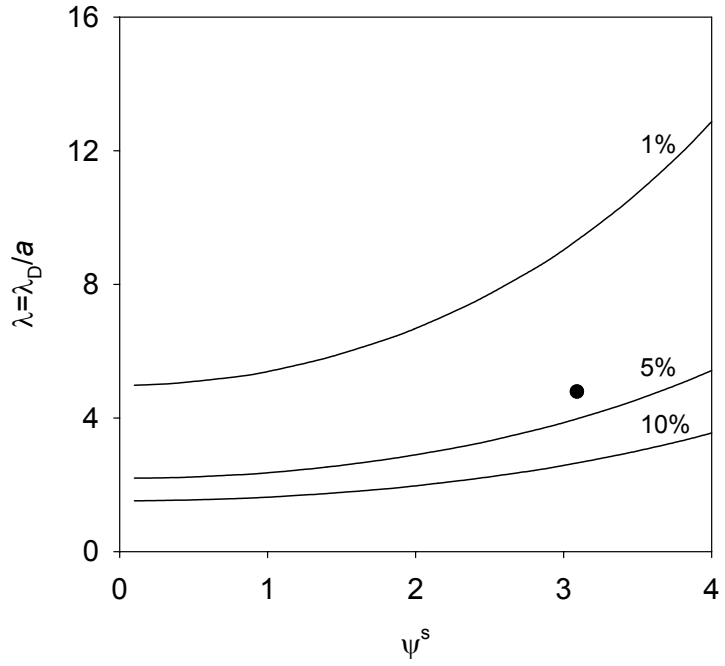


Figure 3: Deviation from the uniform potential in the base case as a function of the dimensionless surface potential $\psi^s$ and the Debye ratio λ, calculated using the exact Poisson-Boltzmann equation. The single circle is the base case. Solid lines represent the deviation in electrostatic potential between the pore centre and the pore wall.

## 2.8 Solution scheme

The 1D transport model consists of a coupled set of 3*ni*+5 differential and algebraic equations (*ni* is the number of ionic species) which is simultaneously solved for the independent variables: the molar fluxes $N_i$, the solvent velocity $v$, the effluent concentrations $c_i^e$ and the dimensionless potential in the effluent $\psi^e$ (all independent of $z$), the concentrations of species $i$, $c_i(z)$, the dimensionless axial potential gradient, $\mathrm{d}\psi(z)/\mathrm{d}z$, the pressure, $p(z)$, and the membrane surface charge $\sigma(z)$ (all a function of the

axial coordinate $z$). The feed concentrations $c^{f}_{i}$ are known a-priori as well as the pressures in both solution phases.

Because of thermodynamic equilibrium, the concentrations and potential in the pore at the left equilibrium slice can be calculated using Eqs. [4] (we define a reference potential by setting the potential in the feed to zero), [10], [12] and [14]. The ion concentrations in the effluent $c^{e}_{i}$ are variables in the model and therefore not known a priori, but are related to the ion fluxes and solvent velocity by Eq. [1]. In between the equilibrium slices in the membrane the Nernst-Planck equation [13] is solved for each of the ionic species as well as the integrated Navier-Stokes equation [18] and charge regulation relations [10] at each pore slice under the conditions of electroneutrality [12] and zero electric current [19].

The system of equations [10], [12], [13] and [18] is discretised and written in a finite difference scheme, resulting in a set of 'pore slices', while Eqs. [1] and [19] are only solved once, independent of the number of pore slices in the model. The unknown parameters are then calculated with a Newton-Raphson iteration procedure. Before implementation, numerical stability was checked by testing different finite discretisation schemes and changing the number of grid points. The complete model is implemented in the mathematical program Maple (Waterloo Maple, Ontario, Canada).

## 3. Results and Discussion

### 3.1 Base case

Model results will be discussed using a base case for which we consider a pore radius $a$ of 2 nm. The feed solution contains 1 mol/m$^3$ NaCl at a pH of 6, obtained by the addition of HCl (for pH>7, NaOH is added). The applied

pressure difference over the membrane is 0.5 MPa. We consider a γ-alumina membrane and use the material parameters given in Table 1.

| |
|---|
| $\Delta pK = pK^- - pK^+ = 3^*$, $pH_{PZC} = 9.25$ (alumina), $K^- = 1.778 \cdot 10^{-11}$ and $K^+ = 1.778 \cdot 10^{-8}$, |
| $K_A = K_C = 7.0 \cdot 10^{-5}$, $c_{tot}^{//} = 8.3 \cdot 10^{-6}$ mol/m$^2$ which follows from 20 Å$^2$ per site.$^*$ |
| Pore size ($2a$)=4 nm and membrane thickness (pore length) $L_M$=1 μm. |
| $K_w = 1 \cdot 10^{-8}$ mol$^2$/m$^6$, $D_{H^+} = 9.31 \cdot 10^{-9}$, $D_{Na^+} = 1.33 \cdot 10^{-9}$, $D_{Cl^-} = 2.03 \cdot 10^{-9}$, $D_{Ca^{2+}} = 0.79 \cdot 10^{-9}$ m$^2$/s.$^+$ |
| For the feed solution $c^f$ =1 mol/m$^3$, $pH^f$=6, $p^f$-$p^e$=0.5 MPa, $\mu = 8.85 \cdot 10^{-4}$ Pa·s. |
| $F$=96485 C/mol, $R$=8.3144 J/(mol·K), $T$=298.15 K, $\varepsilon_r$=78, $\varepsilon_0 = 8.854 \cdot 10^{-12}$ C/(V·m). |

$^*$Chan *et al.*, 1975 ; $^+$Cusler, 1984.

Table 1: Data used in the simulations.

For the base case, the deviation from the uniform potential model assumption is 11.6% for the radial cation concentration, 3.8% for the electrostatic potential and 3.1% for the surface charge (see section 7 of Theory). In all other simulations, the deviation in the radial concentration was smaller than 11.6% unless otherwise specified (see Figure 12).

### 3.2 Limiting retention

It is well known from practice that at increasing pressure differences the retention increases but reaches a limiting retention at very high pressures (Szaniawska and Spencer, 1995; Baticle *et al.*, 1997; Schaep *et al.*, 1999; Yang and Pintauro, 2000); the charge regulation model also predicts this phenomenon (Figure 4).

The initial increase in retention for increasing pressure differences is a result of the fact that water transport is more enhanced than ion transport: the velocity of water is almost proportional to the pressure difference (see Figure 2 in Baticle *et al.*, 1997 as well as Eq. [18], the component with the axial potential gradient is in general very small), while transport of ions is reduced by migration (due to the axial electric field that originates from the condition of zero electrical current). For ever increasing pressure differences,

however, convection becomes the most important transport mechanism for both water and ions, finally resulting in the limiting retention.

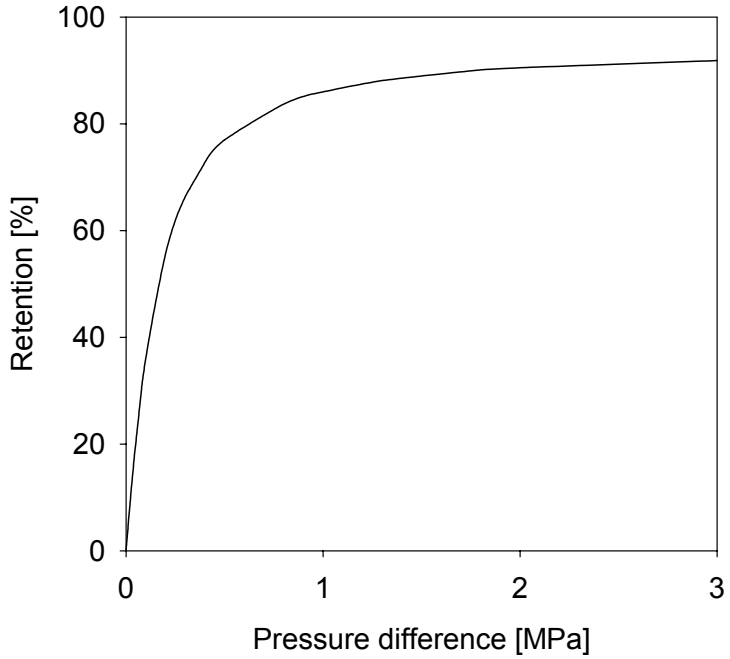


Figure 4: Anion and cation retention (equal) as a function of pressure difference. Base case conditions of Table 1 (NaCl+HCl) except for the pressure.

In chapter 2 of this thesis we modelled the retention of a hydrophilic membrane applying the CR model to a cylindrical pore slice, far enough from either of the pore interfaces for axial concentration gradients to be zero, and in thermodynamic equilibrium with the feed solution. In Figure 5 we compare the cation retention predicted with the equilibrium model (chapter 2 of this thesis) with the results from the present model incorporating transport.

The models coincide only at very low values of the cation diffusion coefficient. This is because for small enough diffusion coefficients, the cation (the co-ion in a positively charged membrane) will be “frozen” in the solvent flow, moving at the same velocity as the solvent; in a binary electrolyte the

counterions are then forced to move with the same molar flux as the co-ions because of the zero-current condition. For negatively charged membranes, the anion is the co-ion and we expect the transport model to approach the equilibrium model for very low anion diffusion coefficients.

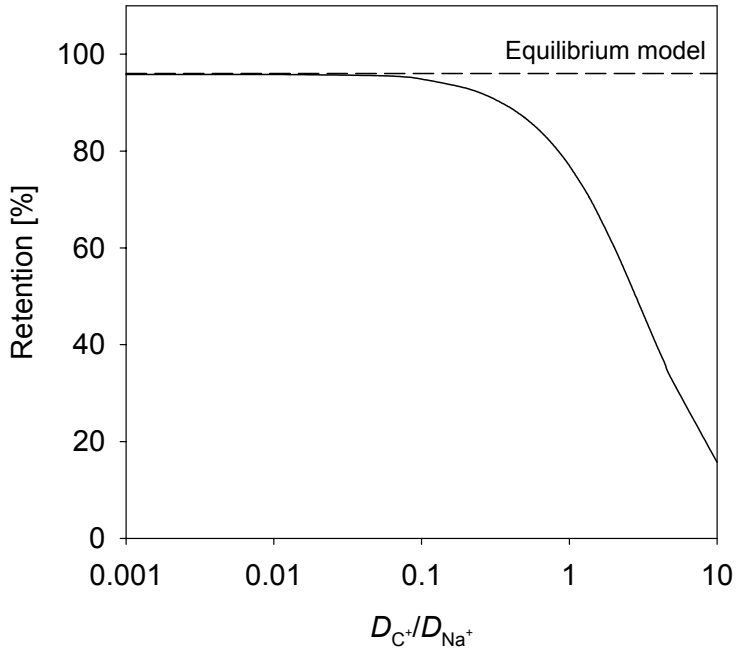


Figure 5: Anion and cation retention (equal) as a function of the diffusion coefficient of the cation, $C^+$, for the equilibrium model, chapter 2 of this thesis, (dotted line) and the transport model (solid line). Base case conditions of Table 1.

### 3.3 Influence of mobility and charge on retention

In Figure 6 we show the effect on retention when instead of one co-ion, two co-ions with different mobilities (diffusion coefficients) are present in the solution. In the simulation a mixture of NaCl and CCl ($C^+$ being an undefined monovalent cation) of equal molarity is considered. Similar to the observations in Figure 5, a lower cation mobility (of $C^+$ compared to $Na^+$) results in a higher retention for $C^+$. The reverse effect occurs at mobilities of $C^+$ higher than that for $Na^+$. For a very high mobility of $C^+$, the model even

predicts negative retentions for $C^+$ but this occurs only at an unrealistically large value of $D_{C+}/D_{Na+}$ (not shown).

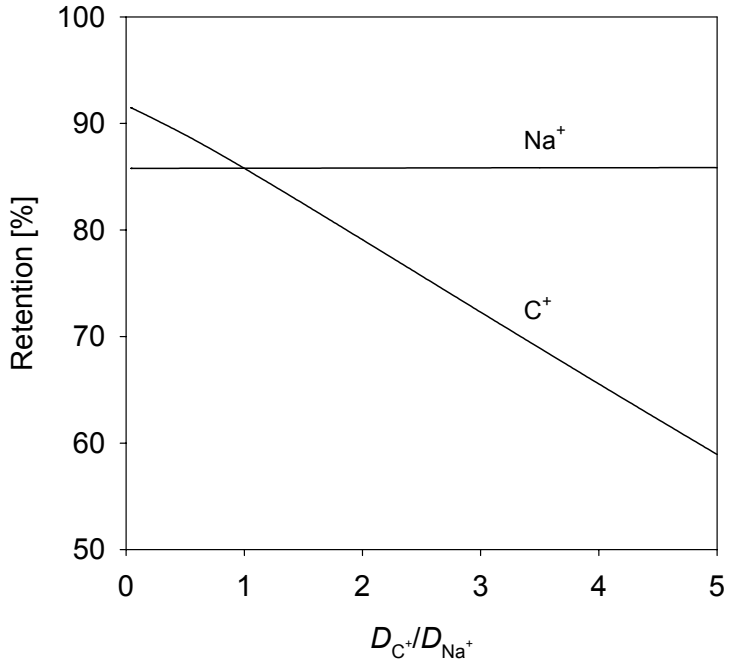


Figure 6: Retention of sodium and another cation $C^+$ as a function of the diffusion coefficient of $C^+$ for a mixture of 1 mol/m$^3$ NaCl and 1 mol/m$^3$ CCl, pH=6. Base case conditions of Table 1.

Yaroshchuk *et al.* (1994) and Bardot, Gaubert and Yaroshchuk (1995) measured retentions in multicomponent mixtures (Cs+Li, Cs+Na+Li, Cs+Na and K+Li) on negatively charged membranes and obtained decreasing retentions for cations with decreasing mobility in the order Cs>Na/K>Li. In mixtures of $Li^+$ with $Cs^+$ or $K^+$, negative retentions for lithium could be found. Interestingly, this experimental behavior seems exactly opposite to what our model predicts, namely that the less mobile cations are better retained. However, both Yaroshchuk *et al.* (1994) and Bardot, Gaubert and Yaroshchuk (1995) measured retentions on a negatively charged membrane, while the membrane considered in Figure 6 is positively charged. Hence, where in our calculations the positive ions are the co-ions, in both latter they

are the counterions, which reverses the retention-mobility behaviour of the cations: in positive membranes a reduced mobility of cations increases the retention while in a negative membrane a reduced mobility of cations decreases the retention, see also Yaroshchuk *et al.* (1994).

Simulations at a pH of 11, where our system becomes negatively charged, indeed showed a decreasing retention with decreasing cation mobility (simulations not reported), confirming that our model results are in qualitative agreement with the experimental results by Yaroshchuk *et al.* (1994) and Bardot, Gaubert and Yaroshchuk (1995).

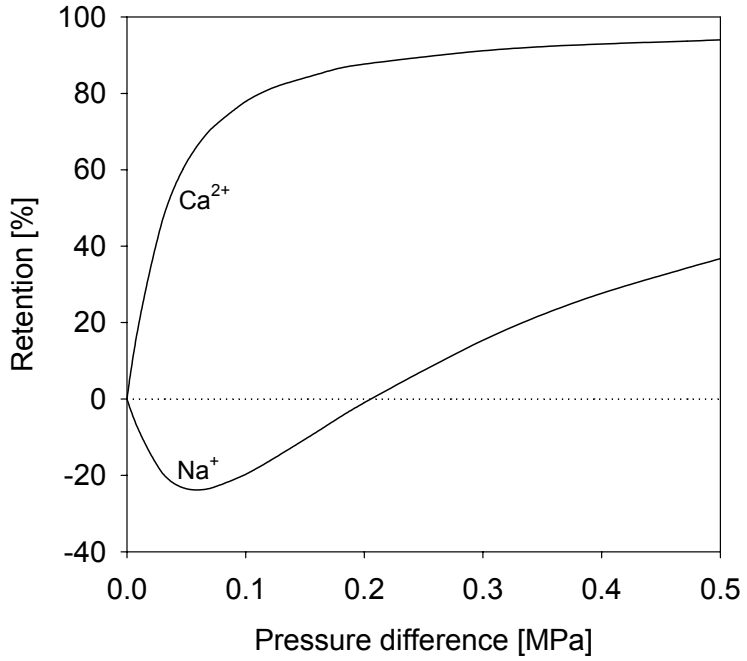


Figure 7: Retention for calcium and sodium ions as a function of pressure in a mixture of 1 mol/m$^3$ $CaCl_2$ and 1 mol/m$^3$ NaCl, pH=6. Base case conditions of Table 1 except for the pressure difference and concentrations.

Retention not only depends on ion mobility but on ion charge as well. Indeed, negative retentions have been found experimentally for mixtures of ions with different valencies (Tsuru *et al.*, 1991; Yaroshchuk *et al.*, 1994;

Bardot, Gaubert and Yaroshchuk, 1995). We show in Figure 7 that the present charge regulation model also predicts this effect. In the simulations for Figure 7 we added 1 mol/m$^3$ calcium chloride to a solution of sodium chloride of the same molarity (pH=6). The adsorption equilibrium constants of sodium and calcium in the charge regulation relation (Eq. [9]) were arbitrarily set equal (i.e. $K_{Na+}=K_{Ca2+}=7\cdot10^{-5}$). Calcium is retained much better than sodium, and negative retentions are found for sodium for low pressure differences (i.e. low solvent velocities). The origin of the higher retention for calcium lies mainly in its higher charge number: it is more effectively excluded from the pores by the positive electrostatic potential, Eq. [4], which is due to the positive surface charge on the membrane. Note that this behaviour only occurs for positively charged membranes. For negatively charged membranes, the retention of divalent cations is lower than the retention for monovalent cations, for binary electrolytes with the same anion.

### 3.4 Retention as a function of pH

The predictive power of the charge regulation model is clearly shown in Figure 8 where the retention is shown as function of the pH in the feed solution. In the pH range commonly used in experimental work (pH 6-7) the retentions of anions and cations are equal. This is because the concentrations of hydroxyl ions and protons ($H_3O^+$) are very low and almost equal. For pH values lower than 4 and higher than 10 the anion and cation retentions clearly start to deviate from each other. The deviation in cation and anion retentions at low and high pH is a result of the fact that we have incorporated transport of protons and hydroxyl ions in the model. At decreasing pH the proton concentration in the system increases and the protons start to influence the retention of the other ions: in the pore and effluent the slow cations (low mobility) are replaced by the much faster protons, causing the higher retention of cations compared to those of the anions (see Figure 6). At pH values above the PZC the situation is reversed:

the hydroxyl ions replace the much slower anions, increasing the retention of the latter (Hall, Starov and Lloyd, 1997; Hall, Lloyd and Starov, 1997).

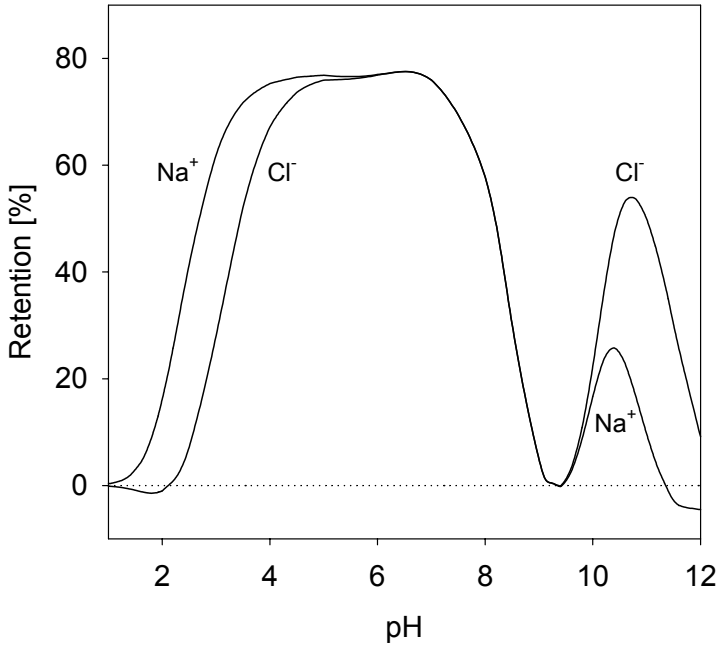


Figure 8: Anion and cation retention for 1 mol/m$^3$ NaCl as a function of pH. Base case conditions of Table 1 (NaCl+HCl) except for the pH.

When the feed salt concentration is increased, the influence of hydroxyl ions and protons is reduced and more extreme pH-values are required to observe the diverging retention of cations and anions (Figure 9).

Apart from the influence of protons and hydroxyl ions (pH), the retention of ions depends also on the surface charge. This is most clearly observed at the PZC of the membrane ($pH_{PZC}$=9.25; Figure 8). Because the effective membrane surface charge is zero at the PZC, zero retention is predicted, see chapter 2 of this thesis as well.

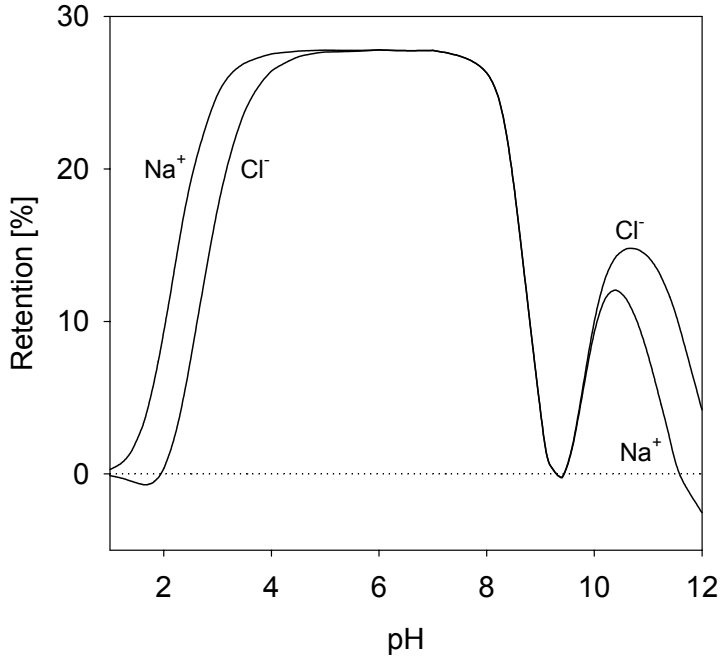


Figure 9: Anion and cation retention for 5 mol/m$^3$ NaCl as a function of pH. Base case conditions of Table 1 (NaCl+HCl) except for the pH.

## 3.5 Retention as a function of feed salt concentration

The CR model predicts that increasing the feed electrolyte concentration will result in a decreasing retention, see Figure 10 (and chapter 2 of this thesis). The reason is the reduced surface charge and electrostatic potential in the pore at increasing feed concentrations. As a result, the concentrations of co-ions and counterions in the pore become more equal to each other and to the feed concentration, leading to higher ion fluxes and therefore lower retentions (see Eq. [1]). Although this behaviour is experimentally found for some (inorganic) materials (Szaniawska and Spencer, 1995; Baticle *et al.*, 1997; Schaep *et al.*, 1999) it does not seem to apply as a rule (Afonso and De Pinho, 2000).

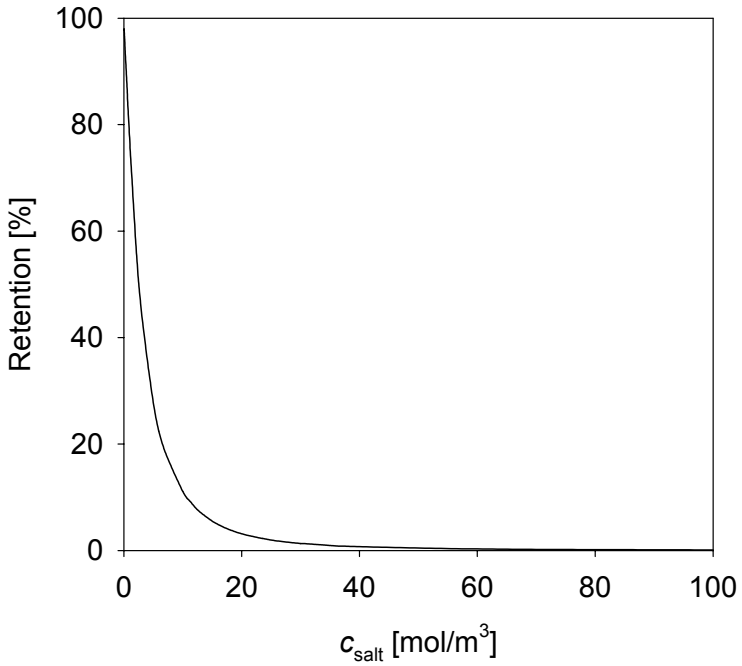


Figure 10: Anion and cation retention (equal) as a function of the electrolyte concentration in the feed. Base case conditions of Table 1 (NaCl+HCl) except for the feed solution concentration.

### 3.6 Retention as a function of pore size

When the pore size of a membrane is reduced the retention will increase (Baticle *et al.*, 1997; Hall, Lloyd and Starov, 1997; Schaep *et al.*, 1999). This behaviour is shown in Figure 11 for a constant solvent velocity $v$. To obtain a constant solvent velocity, the decrease in pore size has to be counterbalanced by an increase in the pressure difference, see Eq. [18]. For such cases the retention always increases continuously with decreasing pore size. However, when the pressure difference $p^e$-$p^f$ is kept constant and the pore size is varied (Figure 12) the retention behaviour is completely different: the retention increases with increasing pore size for most cases considered. For very high pressures of 2 MPa the retention attains a maximum for a pore size of 5.5 nm (optimum pore size). In Figure 12 the optimum pore size is

difficult to distinguish and occurs only at high deviations from the uniform potential model (≈20% deviation). In other simulations (not reported) with lower diffusion coefficients, the optimum in pore size occurs at a lower pore size, within the 10% deviation limit, and is much more pronounced.

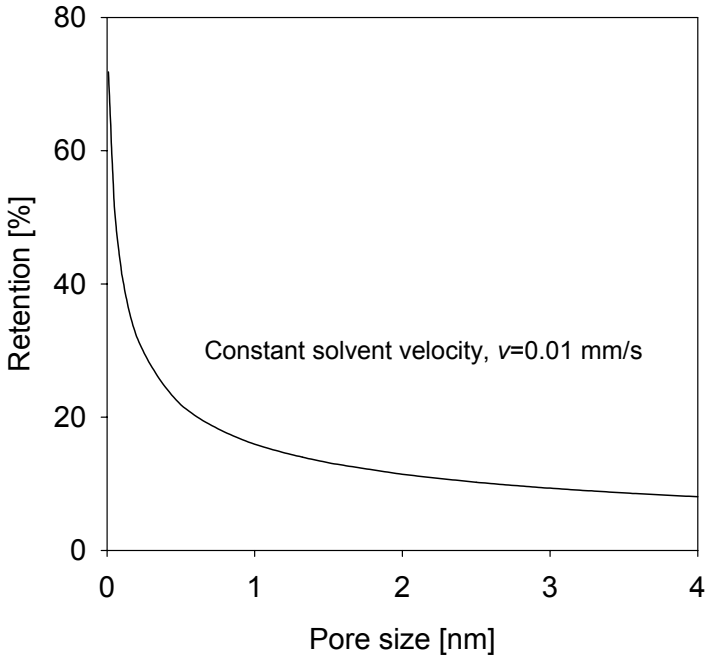


Figure 11: Anion and cation retention (equal) as function of pore size. Base case conditions of Table 1 (NaCl+HCl) except for the pore radius. Constant solvent velocity of 0.01 mm/s.

We examined the influence of pH and feed salt concentration on the location of the optimum pore size. There were only small effects for both parameters. The (constant) pressure difference that we considered, however, had a profound influence on the position of the optimum. For increasing pressure differences, the optimum in pore size shifted to lower values though the effect levels off at higher pressure differences (see Figure 12).

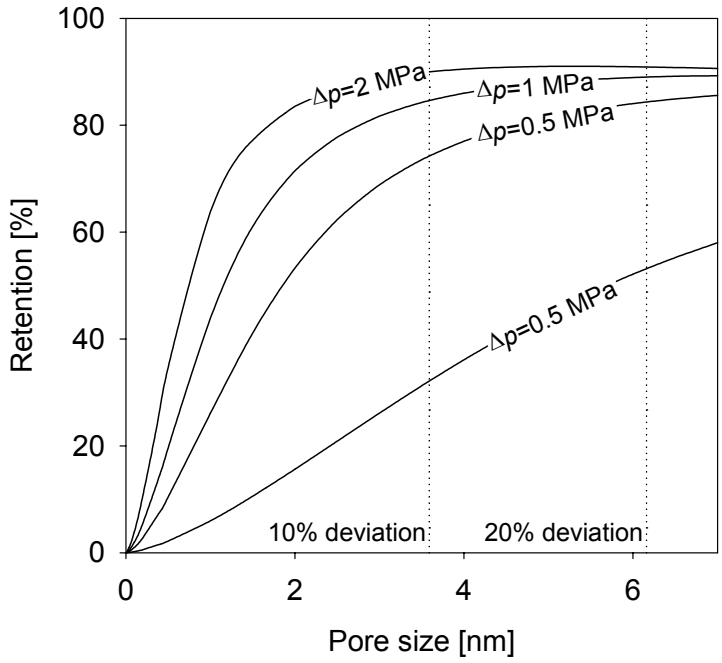


Figure 12: Anion and cation retention (equal) as function of pore size. Base case conditions of Table 1 (NaCl+HCl) except for the pore radius. Constant pressure difference of 0.1, 0.5, 1 and 2 MPa. The dotted lines are the percentage of deviation from the uniform potential assumption.

The finding in Figure 12 is quite remarkable, but understandable as well. A decreasing pore size will cause the double layers to overlap more, thereby excluding more co-ions from the pore but admitting more counterions. Hence, the co-ion concentration in the pore decreases and the concentration of counterions increases, which increases retention. This effect levels off for decreasing pore sizes as the double layers become fully overlapped. A second effect of a decreasing pore size is the decrease in solvent velocity, and as was shown in Figure 4, a decrease in solvent velocity (i.e. a decreasing pressure difference) results in a lower retention. Hence we have two phenomena that counteract each other. Supposedly, with decreasing pore size, the electrostatic exclusion effect becomes important first (before the solvent

velocity effect), but is also the first to level off, resulting in an optimum pore size with respect to retention. Unfortunately, no experimental evidence in literature was found to support the prediction of an optimum pore size for retention.

In other simulations instead of the pore size the pore length $L_M$ was varied, maintaining a constant pressure difference, which showed that the solvent velocity to be inversely proportional to the pore length, as can be expected from Eq. [18]. Interestingly, the ion retention remained constant with varying pore length. This can be explained by the fact the solvent velocity and the ion molar fluxes decrease to the same extent when the pore length is increased, thereby not influencing the retention, see Eq. [1].

### 3.7 Surface Charge

In the present model, the surface charge is calculated at every position in the pore (Figure 13). However, for the base case of Table 1, the change in surface charge across the membrane is quite small and the use of a constant surface charge (independent of axial coordinate) would not have been of much influence for the prediction of retention and solvent velocity. In such a simplified model, the surface charge is calculated for the left equilibrium slice - only dependent on feed conditions, material properties and pore size - and this value used for each position in the membrane pore. This simplified approach using a constant surface charge also gives the possibility to fit the model to experimental retention data to obtain the surface charge of the pores in the membrane (e.g., Tsuru *et al.*, 1991; Bowen and Mukthar, 1996; Bowen, Mohammad and Hildal, 1997).

Note, however, that the surface charge is a function of all experimental variables (feed salt concentration, feed pH, pore size, etc.) and therefore the surface charge would need to be determined for each new experimental condition. The objective of using the charge regulation boundary condition in

this chapter is that when the *K*-values and $c_{tot}^{//}$ have been determined for the membrane material (by some experimental method), surface charge and retention can be predicted a-priori when the experimental conditions are changed.

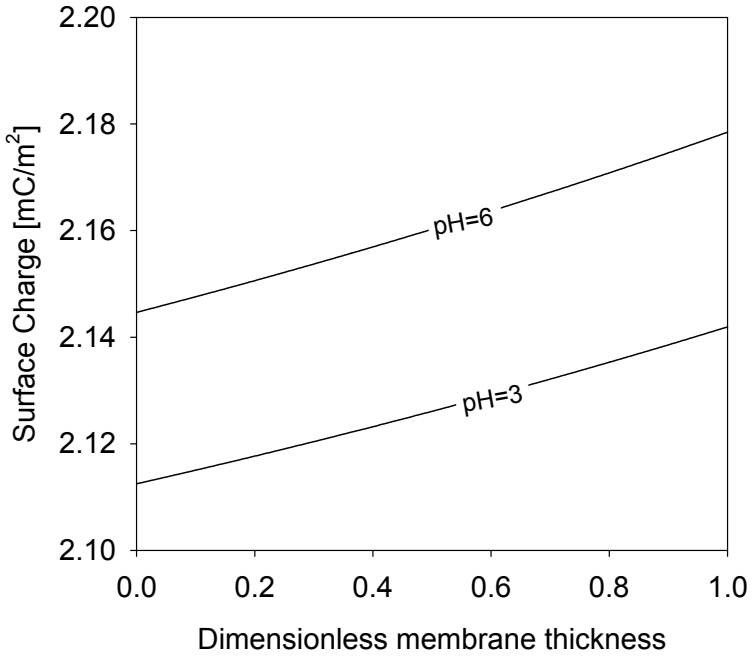


Figure 13: Surface charge across the membrane (dimensionless thickness, 0: feed side; 1: effluent side). Base case conditions of Table 1 (NaCl+HCl) except for the pH.

Besides, the surface charge is not always as constant across the membrane as in Figure 13: for example, in the simulations related to Figure 14 the surface charge decreased up to 95% across the membrane for salt concentrations of ~30 mmol/m$^3$. Furthermore, a large change in surface charge will certainly be the case for membranes with changing material properties over the pore length, as is the case for bipolar membranes. Because the surface charge is calculated in each pore slice, the present model would be naturally suited to describe such non-homogeneous membrane systems.

## 3.8 Solvent velocity

In Figure 14 the solvent velocity $\upsilon$, as predicted by the charge regulation transport model, is plotted on the left $y$-axis as function of salt concentration and pressure difference. The solvent velocity is scaled with respect to the maximum solvent velocity at its corresponding pressure difference, $\upsilon_{max}$, which is given by the Poiseuille equation: Eq. [18] with the (second) electrostatic term omitted. For sufficiently high salt concentrations (>50 mol/m$^3$; not shown in Figure 14), $\upsilon/\upsilon_{max}$ approaches unity because the membrane becomes uncharged and the axial potential gradient vanishes. This charging picture does not agree with the experimentally observed charging behaviour of oxides, which shows an increase of the surface charge and a decrease of the diffuse charge (i.e., the axial potential) with increasing concentration (e.g., Huang and Stumm, 1973; Healy and White, 1978). The inconsistency in our approach is caused by a too simple representation of the double layer. To properly account for the effect of salt concentration increase on the surface charge and axial potential, the double layer model should also contain a Helmholtz layer (see chapters 5 and 6).

For a zero salt concentration and at pH=7, $\upsilon/\upsilon_{max}$=1 as well, because charge separation is impossible (zero electrical current, and anion and cation concentrations are zero). However, in Figure 14 simulations were performed at pH=6 (base case), hence, even for a zero salt concentration $\upsilon/\upsilon_{max}$ was less than unity.

According to the model, see Figure 14, the solvent velocity increases linearly with the pressure difference as long as the salt concentration exceeds the (very low) value of ~0.2 mol/m$^3$. This linear behaviour is well known from experiments (e.g., Szaniawska and Spencer, 1995; chapter 8).

The influence of the salt concentration on the solvent velocity $\upsilon$ is less straightforward. Starting at $c_{salt}$=0, with increasing $c_{salt}$, $\upsilon$ first decreases,

reaches a minimum around ~10-30 mmol/m$^3$ after which $v$ increases and levels off. Let us discuss the minimum, the increase in solvent velocity above the minimum, and the levelling-off of the solvent velocity one after the other.

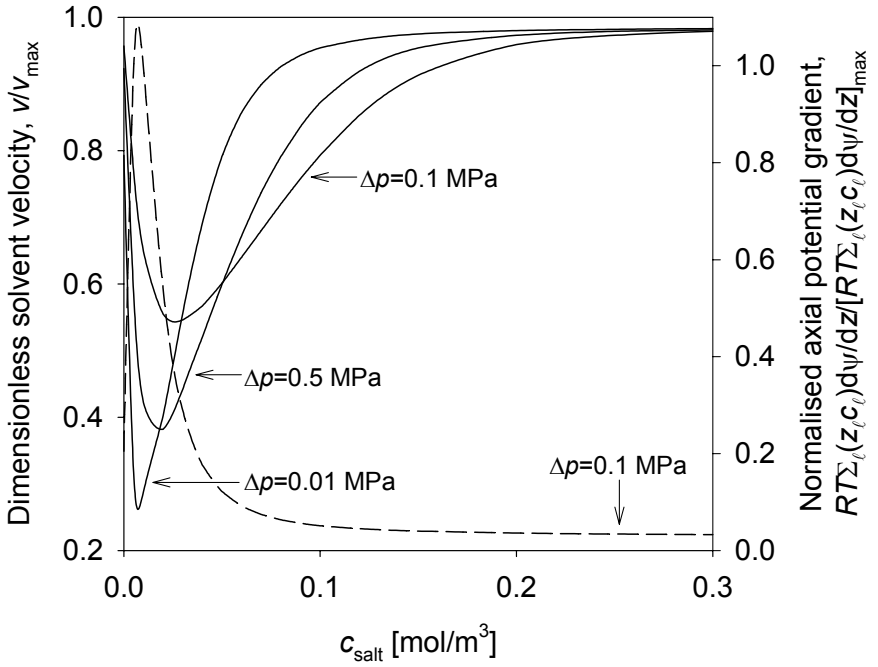


Figure 14: Dimensionless solvent velocity (solid lines) and normalized axial potential gradient term (dashed line, Eq. [18]) as a function of the feed salt concentration for pressure differences of 0.01, 0.05 and 0.1 MPa. Base case conditions of Table 1 (pH=6) except for the pressure difference and the feed concentration.

### 3.8.1 Minimum solvent velocity

The minimum in the solvent velocity predicted by the charge regulation model is caused by the second term between brackets in Eq. [18], $RT\,\mathrm{d}\psi/\mathrm{d}z\sum_{\ell=1}^{ni} z_\ell c_\ell$ . At high salt concentrations the summation over all ions is large but the charge is low. For small charges the electrostatic potential in the pore is low and the co-ion and counterion concentrations approach each other, resulting in a decreasing axial electric field (i.e., $\mathrm{d}\psi/\mathrm{d}z$ is small). For very low salt concentrations, however, $RT\,\mathrm{d}\psi/\mathrm{d}z\sum_{\ell=1}^{ni} z_\ell c_\ell$ is low, but the surface

charge and the axial electric field become very large. These phenomena have an opposite effect on $\sum_{\ell=1}^{ni} z_\ell c_\ell$, and this term attains a maximum value for very small salt concentrations (see Figure 14, right *y*-axis), leading to the observed minimum in the solvent velocity.

### 3.8.2 Increasing solvent velocity

An increasing solvent velocity with increasing salt concentration is not usually reported in membrane literature. However, an increase of solvent velocity with salt concentration was recently reported for the flow through the micro-channels of pit membranes within xylem vessels in plants (Zwieniecki, Melcher and Holbrook, 2001) for salt concentrations of 0-20 mol/m$^3$ and especially in the range 0-1 mol/m$^3$, similar to the increase in solvent velocity predicted by the present model (Figure 14) up to 0.3 mol/m$^3$ (dependent on the pressure difference across the membrane).

This qualitative agreement might suggest that the present model that combines transport by electrostatic and convective mechanisms (electro-viscous effects) with charge-regulation on the pore walls might have relevance for the description of flow through the pit membranes of the xylem vessels in plants. Note that in the experiments of Zwieniecki, Melcher and Holbrook (2001), a minimum in solvent velocity at a critical salt concentration was not found, perhaps because dissolution of ions from the cell surfaces into the water always increased the salt concentration to above the minimum value.

### 3.8.3 Decreasing solvent velocity

Contrary to the prediction of the charge regulation model that the solvent velocity approaches the maximum $v_{max}$ with increasing salt concentration, experiments with nanofiltration membranes (Baticle *et al.*, 1997; Afonso and De Pinho, 2000) show a decreasing solvent velocity with increasing feed salt

concentration in the range of 1-100 mol/m$^3$. To understand the reason for this discrepancy, we performed additional simulations.

First, we used a one-dimensional uniform potential model with a constant surface charge from literature (Tsuru *et al.*, 1991) and found that it predicts an increase in solvent velocity with salt concentration as well.

Second, we focused our attention on osmotic effects. Indeed, some authors have attributed the decreasing solvent velocity to an increase in the osmotic pressure difference (between the feed and permeate) for increasing salt concentrations (Grim and Sollner, 1957; Kobatake and Fujita, 1963; Sasidhar and Ruckenstein, 1982; Afonso and De Pinho, 2000). Others, however, attributed the decrease in solvent velocity only to a minor degree to osmosis but mainly to other effects, such as the degree of dissociated charged groups and a change in the water concentration in the membrane (Szaniawska and Spencer, 1995). Still, to investigate whether osmosis explains the decrease in solvent velocity, we incorporated osmosis into the transport model by adding the term responsible for osmosis, $\bar{V}_i p$, with $\bar{V}_i$ the molar volume [m$^3$/mol] of species $i$ (Atkins, 1990), and used the full Maxwell-Stefan transport description (Taylor and Krishna, 1993; Krishna and Wesselingh, 1997) for the molar fluxes of all mobile species, including water. Unfortunately, in these simulations (not reported), the same result was obtained: the solvent velocity increases with feed salt concentration and levels off, without decreasing at higher salt concentrations. We therefore believe the decreasing solvent velocity with increasing salt concentration (1-100 mmol/m$^3$ range) in dead-end permeation set-ups is not related directly to osmotic effects, but must be due to another phenomenon, e.g., a transport resistance leading to concentration polarization outside the membrane. These effects can be incorporated using film models that are well known and available in literature (e.g., Bird, Stewart and Lightfoot, 1960; Taylor and Krishna, 1993; Bowen and Mukthar, 1996).

## 4. Conclusions

We combined charge regulation with the relevant transport relations to describe ion retention of and solvent flow through a charged nanofiltration membrane consisting of cylindrical capillaries. For the base case with a pore size of 4 nm, the deviation from the uniform potential assumption was 11.6% for the cation concentration and 3.8% for the electrostatic potential. The model results are in agreement with experimental evidence for nanofiltration membranes and describe the changes of ion retention with pore radius, ion concentrations, pH and pressure for a binary electrolyte as well as for multi-component mixtures with cations of different mobility and/or charge. Because protons and hydroxyl ions are taken into account, markedly different retentions for anions and cations are predicted at pH values below 4 and above 10. A minimum solvent velocity is predicted for a low feed salt concentration of 10-30 mmol/$m^3$.

## Nomenclature

| | | |
|---|---|---|
| $a$ | pore radius | [m] |
| $B_0$ | permeability (superficial) | [$m^2$] |
| $c_i^b$ | bulk concentration of species $i$ | [mol $m^{-3}$] |
| $c_i^e$ | concentration of species $i$ in the effluent | [mol $m^{-3}$] |
| $c^f$ | feed salt concentration | [mol $m^{-3}$] |
| $c_i^f$ | concentration of species $i$ in the feed solution | [mol $m^{-3}$] |
| $c_i^0$ | concentration of species $i$ at the membrane interface | [mol $m^{-3}$] |
| $c_A^s$ | concentration of anions at the pore surface | [mol $m^{-3}$] |
| $c_C^s$ | concentration of cations at the pore surface | [mol $m^{-3}$] |
| $c_H^s$ | concentration of protons at the pore surface | [mol $m^{-3}$] |
| $c_{tot}^{//}$ | total number of surface sites | [mol $m^{-2}$] |
| $D_i$ | Maxwell-Stefan diffusion coefficients at infinite dilution | [$m^2$ $s^{-1}$] |
| $F$ | Faraday constant | [C $mol^{-1}$] |
| $I$ | ionic strength | [mol $m^{-3}$] |
| $K_A$ | anion adsorption equilibrium constant | [-] |
| $K_C$ | cation adsorption equilibrium constant | [-] |
| $K^+$ | proton adsorption equilibrium constant | [-] |
| $K^-$ | proton desorption equilibrium constant | [-] |
| $K_w$ | water autoprotolysis equilibrium constant | [$mol^2$ $m^{-6}$] |
| $N_i$ | molar flux of species $i$ in a fixed coordinate system | [mol $m^{-2}$ $s^{-1}$] |
| ni | number of ionic species | [-] |
| $p$ | pressure | [Pa] |
| $pH_{PZC}$ | pH at the point of zero charge | [-] |
| $R$ | ideal gas constant | [J $mol^{-1}$ $K^{-1}$] |
| $R_i$ | retention of species $i$ | [-] |
| $r$ | radial coordinate | [m] |
| $T$ | temperature | [K] |
| $v$ | velocity | [m $s^{-1}$] |
| $z$ | axial coordinate | [m] |
| $z_i$ | charge number of species $i$ | [-] |

Greek

| | | |
|---|---|---|
| $\varepsilon_0$ | dielectric constant of vacuum | [C $V^{-1}$ $m^{-1}$] |
| $\varepsilon_r$ | relative dielectric constant | [-] |
| $\lambda$ | Debye ratio | [-] |
| $\mu$ | Newtonian viscosity | [Pa s] |
| $\rho$ | dimensionless radial coordinate | [-] |
| $\sigma$ | surface charge | [C $m^{-2}$] |
| $\phi$ | electrostatic potential | [V] |
| $\phi^s$ | electrostatic potential at the pore surface | [V] |
| $\psi$ | dimensionless electrostatic potential | [-] |
| $\psi^b$ | dimensionless electrostatic potential in the bulk solution | [-] |
| $\psi^e$ | dimensionless electrostatic potential in the effluent | [-] |
| $\psi^s$ | dimensionless electrostatic potential at the pore surface | [-] |
| $\psi^0$ | dimensionless electrostatic potential at the membrane interface | [-] |

## References


1. Afonso M.D., and De Pinho M.N., "Transport of $MgSO_4$, $MgCl_2$ and $Na_2SO_4$ across an Amphoteric Nanofiltration Membrane," *J. Membrane Sci.*, **179**, 137 (2000).
2. Atkins P.W., "Physical Chemistry," fourth edition, Oxford University Press, Oxford, 1990, pp. 171-173.
3. Bardot C., Gaubert E., and Yaroshchuk A.E., "Unusual Mutual Influence of Electrolytes during Pressure-Driven Transport of their Mixtures across Charged Porous Membranes," *J. Membrane Sci.*, **103**, 11 (1995).
4. Basu S., and Sharma M.M., "An Improved Space-Charge Model for Flow Through Charged Microporous Membranes," *J. Membrane Sci.,* **124**, 77 (1997).
5. Baticle P., Kiefer C., Lakhchaf N., Larbot A., Leclerc O., Persin M., and Sarrazin J., "Salt Filtration on Gamma Alumina Nanofiltration Membranes Fired at Two Different Temperatures," *J. Membrane Sci.*, **135**, 1 (1997).
6. Biesheuvel P.M., and Verweij H., "Design of ceramic membrane supports: permeability, tensile strength and stress," *J. Membrane Sci.*, **156**, 141 (1999).
7. Biesheuvel P.M., "Simplifications of the Poisson-Boltzmann Equation for the Electrostatic Interaction of Close Hydrophilic Surfaces in Water," *J. Colloid Interface Sci.*, **238**, 362 (2001).
8. Biesheuvel P.M., Implications of the Charge Regulation Model for the Interaction of Hydrophilic Surfaces in Water," *Langmuir*, **17**, 3553 (2001).
9. Biesheuvel P.M., and Lange F.F., "Application of the Charge Regulation Model to the Colloidal Processing of Ceramics," *Langmuir*, **17**, 3557 (2001).
10. Bird R.B., Stewart W.E., Lightfoot E.N., "Transport Phenomena," Wiley, Singapore, 1960, pp. 149-150, 196-200.
11. Bowen W.R., and Mukhtar H., "Characterisation and Prediction of Separation Performance of Nanofiltration Membranes," *J. Membrane Sci.*, **112**, 263 (1996).
12. Bowen W.R., Mohammad A.W., and Hildal N., "Characterisation of Nanofiltration Membranes for Predictive Purposes – Use of Salts, Uncharged Solutes and Atomic Force Microscopy," *J. Membrane Sci.*, **126**, 91 (1997).
13. Chan D.Y.C., Perram J.W., White L.R., and Healy T.W., "Regulation of Surface Potential at Amphoteric Surfaces During Particle-Particle Interaction," *J. Chem. Soc. Faraday Trans. I*, **71**, 1046 (1975).
14. Cussler E.L., "Diffusion. Mass Transfer in Fluid Systems," Cambridge University Press, Cambridge, 1984, p. 147.
15. De Groot S.R., and Mazur P., "Non-Equilibrium Thermodynamics," Interscience, New York, 1962, pp. 423-426.

16. Deen W.M., "Hindered Transport of Large Molecules in Liquid-Filled Pores," *AIChE J.*, **33** (9), 1409 (1987).
17. Fair J.C., and Osterle J.F., "Reverse Electrodialysis in Charged Capillary Membranes," *J. Chem. Phys.*, **54**, 3307 (1971).
18. Grim E., and Sollner K., "The Contributions of Normal and Anomalous Osmosis to the Osmotic Effects Arising across Charged Membranes with Solutions of Electrolytes," *J. Gen. Physiol.*, **40**, 887 (1957).
19. Gross R.J., and Osterle J.F., "Membrane Transport Characteristics of Ultrafine Capillaries," *J. Chem. Phys.*, **49**, 228 (1968).
20. Hall M.S., Starov V.M., and Lloyd D.R., "Reverse Osmosis of Multicomponent Electrolyte Solutions. Part I. Theoretical Development," *J. Membrane Sci.*, **128**, 23 (1997).
21. Hall M.S., Lloyd D.R., and Starov V.M., "Reverse Osmosis of Multicomponent Electrolyte Solutions. Part II. Experimental Verification," *J. Membrane Sci.*, **128**, 39 (1997).
22. Hawkins Cwirko E., and Carbonell R.G., "Transport of Electrolytes in Charged Pores: Analysis Using the Method of Spatial Averaging," *J. Colloid Interface Sci.*, **129**, 513 (1989).
23. He L.M., Zelazny L.W., Baligar V.C., Ritchey K.D., and Martens D.C., "Ionic Strength Effects on Sulfate and Phosphate Adsorption on γ-Alumina and Kaolinite: Triple-Layer-Model," *Soil Sci. Soc. Am. J.*, **61**, 784 (1997).
24. Healy T.W., and White L.R., "Ionizable Surface Group Models of Aqueous Interfaces," *J. Colloid Interface Sci.*, **9**, 303 (1978).
25. Healy T.W., Chan D., and White L.R., "Colloidal Behaviour of Materials with Ionizable Group Surfaces," *Pure & Appl. Chem.*, **52**, 1207 (1980).
26. Huang C.P., and Stumm W., "Specific Adsorption of Cations on Hydrous γ-$Al_2O_3$," *J. Colloid Interface Sci.*, **43**, 409 (1973).
27. Jacazio G., Probstein R.F., Sonin A.A., and Yung D., "Electrokinetic Salt Rejection in Hyperfiltration through Porous Materials. Theory and Experiment," *J. Phys. Chem.*, **26**, 4015 (1972).
28. Kobatake Y., and Fujita H., "Osmotic Flow in Charged Membranes. I. Anomalous Osmosis," *Kolloid Z.*, **196**, 58 (1963).
29. Krishna R., and Wesselingh J.A., "The Maxwell-Stefan Approach to Mass Transfer," *Chem. Eng. Sci.*, **52**, 861 (1997).
30. Morrison jr. F.A. and Osterle J.F., "Electrokinetic Energy Conversion in Ultrafine Capillaries," *J. Chem. Phys.*, **43**, 2111 (1965).
31. Ninham B.W., and Parsegian V.A., "Electrostatic Potential Between Surfaces Bearing Ionizable Groups in Ionic Equilibrium with Physiologic Saline Solution," *J. Theor. Biol.*, **31**, 405 (1971).

32. Sasidhar V., and Ruckenstein E., "Electrolyte Osmosis Through Capillaries," *J. Colloid Interface Sci.*, **82**, 439 (1981).
33. Sasidhar V., and Ruckenstein E., "Anomalous Effects during Electrolyte Osmosis across Porous Membranes," *J. Colloid Interface Sci.*, **85**, 332 (1982).
34. Schaep J., Vandecasteele C., Peeters B., Luyten J., Dotremont C., and Roels D., "Characteristics and Retention Properties of a Mesoporous $\gamma$-$Al_2O_3$ Membrane for Nanofiltration," *J. Membrane Sci.*, **163**, 229 (1999).
35. Sonin A.A., "Osmosis and Ion Transport in Charged Porous Membranes: a Macroscopic, Mechanistic Model," in "Charged Gels and Membranes I", Reidel, Dordrecht, 1976, pp. 255-265.
36. Spiegler K.S., and Kedem O., "Thermodynamics of Hyperfiltration (Reverse Osmosis). Criteria for Efficient Membranes," *Desalination*, **1**, 311-326 (1966).
37. Starov V.M., Bowen W.R., and Welfoot J.S., "Flow of Multicomponent Electrolyte Solutions through Narrow Pores of Nanofiltration Membranes," *J. Colloid Interface Sci.*, **240**, 509 (2001).
38. Szaniawska D., and Spencer H.G., "Non-Equilibrium Thermodynamics Analysis of the Transport Properties of Formed-In-Place Zr(IV) Hydrous Oxide-PAA Membranes: II. NaCl-water solutions," *Desalination*, **101**, 31 (1995).
39. Takagi R., and Nakagaki M., "Theoretical Study of the Effect of Ion Adsorption on Membrane Potential and its Application to Collodion Membranes," *J. Membrane Sci.*, **53**, 19 (1990).
40. Taylor R., and Krishna R., "Multicomponent Mass Transfer," Wiley, New York, 1993, pp. 37-49.
41. Tsuru T., Urairi M., Nakao S.-I., and Kimura S., "Negative Rejection of Anions in the Loose Reverse Osmosis Separation of Mono- and Divalent Ion Mixtures," *Desalination*, **81**, 219 (1991).
42. Wesselingh J.A., Vonk P., and Kraaijeveld G., "Exploring the Maxwell-Stefan Description of Ion Exchange," *Chem. Eng. J.*, **57**, 75 (1995).
43. Westermann-Clark G.B., and Anderson J.L., "Experimental Verification of the Space-Charge Model for Electrokinetics in Charged Microporous Membranes," *J. Electrochem. Soc.*, **130**, 839 (1983).
44. Yang Y., and Pintauro P.N., "Multicomponent Space-Charge Transport Model for Ion-Exchange Membranes," *AIChE J.*, **46**, 1177 (2000).
45. Yaroshchuk A.E., Bardot C., Gaubert E., Kulov N.N., and Nechaev A.N., "Modeling of the Pressure-Driven Transport of Single and Mixed Electrolyte Solutions across Fine-Porous Inorganic Membranes. Criteria for Efficient Rejection and Separation," Presented at ICIM3, Worcester, USA, (1994).
46. Zwieniecki M.A., Melcher P.J., and Holbrook N.M., "Hydrogel Control of Xylem Hydraulic Resistance in Plants, Science, **291**, 1059-1062 (2001).

# Chapter 5

## Derivation of Adsorption Parameters for Nanofiltration Membranes using a 1-pK Basic Stern Model


### Abstract

Equation Section (Next)The ion retention and flux of nanofiltration (NF) membranes are to a large extent determined by the membrane surface charge. This surface charge is in turn strongly influenced by adsorption of ions from the solution onto the membrane material. A 1-pK adsorption model with a Basic Stern electrostatic double layer model is used to describe ion adsorption, and the sensitivity of this model for various parameters is discussed. From a non-linear regression analysis of literature data (Sprycha, 1989a, b) regarding the surface charge and the zeta potential, adsorption parameters for the 1-pK model are obtained for sodium chloride on γ-alumina. The 1-pK Basic Stern model can predict the surface charge well, except for the highest concentration of 1000 mol/m$^3$. Reasonable agreement is found between the measured zeta potentials and the model predictions.



Published with minor modifications as: W.B.S. de Lint, N.E. Benes, A.P. Higler, and H. Verweij, "Derivation of Adsorption Parameters for Nanofiltration Membranes using a 1-pK Basic Stern Model," *Desalination*, **145**, 87 (2002).

## 1. Introduction

Nanofiltration (NF) of electrolyte solutions is mainly determined by electrostatic effects, which are governed by the surface charge, $\sigma_0$, of the membrane and the relationship between this quantity and the diffuse double layer charge, $\sigma_d$, governing the double layer part that is relevant for transport. The surface charge depends on the composition of the solution (concentrations, pH) and adsorption parameters. These parameters can be determined from a variety of methods, including potentiometric titration ($\sigma_0$), electrophoretic mobility experiments (Huang and Stumm, 1973; Sprycha, 1989a), $\sigma_{ek} \approx \sigma_d$, acoustic techniques (Johnson, Scales and Healy, 1999), $\sigma_{ek} \approx \sigma_d$, and colloidal probe or surface-force techniques (Zhmud, Meurk and Bergström, 1998), $\sigma_d$, and can be used in transport models for predicting membrane separation behaviour, that is, ion retention and flux (Hall, Starov and Lloyd, 1997; Hall, Lloyd and Starov, 1997; Starov, Bowen and Welfoot, 2001; chapters 2 and 3 of this thesis).

Numerous adsorption models for oxides have been presented in literature, such as the porous gel model (Lyklema, 1971) and several site-binding models (e.g., Yates, Levine and Healy, 1974; Davis, James and Leckie, 1978; Healy and White, 1978). We will restrict the discussion to a site-binding model in which the charged surface is thought to consist of discrete surface sites that can interact with the various ions in the electrolyte solution. Generally it is assumed that the surface is in thermodynamic equilibrium with the solution phase next to the surface, as well as with the bulk solution. Furthermore, we consider a simple 1-pK adsorption scheme, in which the hydroxyl surface groups are charged (Hiemstra, Van Riemsdijk and Bruggenwert, 1987; Hiemstra, Van Riemsdijk and Bolt, 1989; Hiemstra, De Wit and Van Riemsdijk, 1989) and can only adsorb a proton (i.e., desorption of protons from hydroxyl surface sites is not considered), and an electrostatic Basic Stern model (Hiemstra, Van Riemsdijk and Bruggenwert,

1987; Hiemstra, Yong and Van Riemsdijk, 1999). Other site-binding models may be equally appropriate (see Westall and Hohl, 1980). Subsequent to a parametric study, the 1-pK Basic Stern model is combined with a non-linear regression algorithm and applied to literature data (Sprycha, 1989a, b) for the surface charge and the zeta potential of γ-alumina in a NaCl solution at various pH values to extract the corresponding adsorption parameters.

## 2. Theory

Inorganic NF membranes generally consist of oxides (e.g., $Al_2O_3$, $TiO_2$, $ZrO_2$), which form surface hydroxyl groups [-OH] in aqueous solutions. These groups are considered to be the adsorption sites at which competitive adsorption of ions (including $H^+$) can occur. In this work the discussion is restricted to a simple adsorption scheme in which the hydroxyl surface groups are charged (Hiemstra, Van Riemsdijk and Bruggenwert, 1987; Hiemstra, Van Riemsdijk and Bolt, 1989; Hiemstra, De Wit and Van Riemsdijk, 1989) and can only adsorb a proton (i.e., no desorption of protons from hydroxyl surface sites occurs). Cations ($C^+$) and anions ($A^-$) then adsorb on the formed charged sites (extension to multivalent ions is straightforward). This model is often referred to as the 1-pK model (Hiemstra, Van Riemsdijk and Bruggenwert, 1987). The corresponding surface reactions are

$$\begin{aligned} \text{Al-OH}^{-1/2} + \text{H}^+(\text{s}) &\overset{K^+}{\rightleftharpoons} \text{Al-OH}_2^{+1/2} \\ \text{Al-OH}^{-1/2} + \text{C}^+(\text{s}) &\overset{K_\text{C}}{\rightleftharpoons} \text{Al-OH}^{-1/2}\text{C}^+ \\ \text{Al-OH}_2^{+1/2} + \text{A}^-(\text{s}) &\overset{K_\text{A}}{\rightleftharpoons} \text{Al-OH}^{+1/2}\text{A}^- \end{aligned} \quad . \qquad [1]$$

The non-adsorbed species with the addition (s), e.g., $C^+$, in Eq. [1] are assumed to be located in a plane with the same (averaged) potential (equipotential plane) as their corresponding surface complexes (e.g., $\text{Al-OH}^{-1/2}\text{C}^+$) and are virtual in this plane.

γ-Alumina will be used as a reference material in this paper. The equilibrium constants $K$ for these reactions are

$$K^{+} = \frac{c_{\text{Al-OH}_2^{+1/2}} c^{\text{ref}}}{c^{\text{s}}_{\text{H}^+} c_{\text{Al-OH}^{-1/2}}}, K_C = \frac{c_{\text{Al-OH}^{-1/2}\text{C}^+} c^{\text{ref}}}{c^{\text{s}}_{\text{C}^+} c_{\text{Al-OH}^{-1/2}}}, K_A = \frac{c_{\text{Al-OH}_2^{+1/2}\text{A}^-} c^{\text{ref}}}{c^{\text{s}}_{\text{A}^-} c_{\text{Al-OH}_2^{+1/2}}}, \quad [2]$$

where $c_i^{\text{s}}$ are the concentrations of non-adsorbed ions [mol/m$^3$] and $c^{\text{ref}}$ is the thermodynamic reference concentration of $10^3$ mol/m$^3$ (1 mol/dm$^3$).

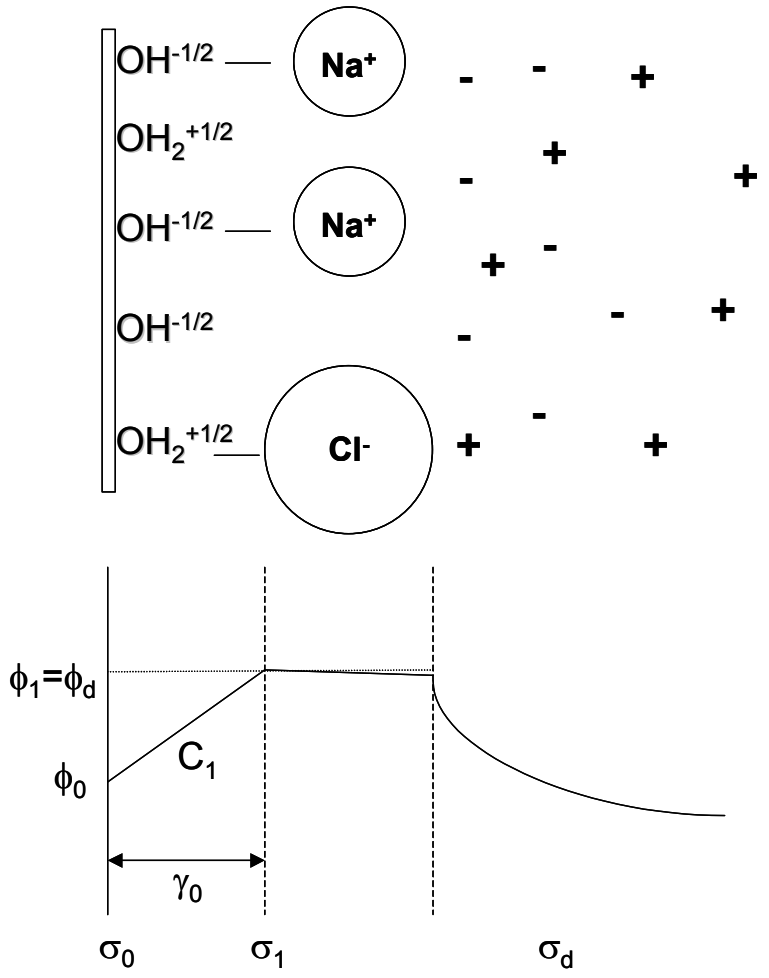


Figure 1: Schematic representation of the electrostatic double layer model (not drawn to scale).

The electrostatic double layer model adopted in this study is a two-layer model, consisting of one Helmholtz plane and a diffuse (Gouy-Chapman) double layer, which is displaced from the Helmholtz plane by a certain

distance (see Figure 1). The capacity of the empty layer between the Helmholtz plane and the Gouy-Chapman layer is assumed infinite (i.e., $\phi_1=\phi_d$). The model is generally referred to as the Basic Stern (BS) model, and has been widely accepted as applicable for AgI systems (Westall and Hohl, 1980; Hiemstra, Van Riemsdijk and Bruggenwert, 1987). In the BS model, protons (or hydroxyl ions) adsorb directly at the surface, screening some of the surface charge $\sigma_0$. Due to their size, electrolyte ions (cations and anions) adsorb at the Helmholtz plane (i.e., the 1-plane).

The surface concentrations are related to the bulk concentrations using the Boltzmann equation

$$c^{s}_{H^+} = c^{b}_{H^+} \exp\left(\frac{-F}{RT}\phi_0\right),\ c^{s}_{C^+} = c^{b}_{C^+} \exp\left(\frac{-F}{RT}\phi_1\right),\ c^{s}_{A^-} = c^{b}_{A^-} \exp\left(\frac{F}{RT}\phi_1\right), \qquad [3]$$

where $c_i^b$ is the bulk concentration of species $i$ and the choice for either $\phi_0$ or $\phi_1$ is determined by the plane a (virtual) species is located in.

For the BS model, the surface charge $\sigma_0$ is

$$\sigma_0 = \frac{F}{2}\left(c_{\text{Al-OH}_2^{+1/2}} - c_{\text{Al-OH}^{-1/2}} + c_{\text{Al-OH}_2^{+1/2}\text{A}^-} - c_{\text{Al-OH}^{-1/2}\text{C}^+}\right). \qquad [4]$$

Note that we have two types of sites in the 0-plane, free sites (Al-$OH^{-1/2}$, Al-$OH_2^{+1/2}$) and occupied sites (Al-$OH^{-1/2}C^+$, Al-$OH_2^{+1/2}A^-$), which both sites contribute to $\sigma_0$. The surface charge is related to the potential difference between the surface and the Helmholtz plane by

$$\sigma_0 = C_1\left(\phi_0 - \phi_1\right), \qquad [5]$$

where $C_1$ is the differential or Helmholtz capacity.

The charge due to electrolyte adsorption on the Helmholtz plane is

$$\sigma_1 = F\left(c_{\text{Al-OH}^{-1/2}\text{C}^+} - c_{\text{Al-OH}_2^{+1/2}\text{A}^-}\right). \qquad [6]$$

Because the electric double layer is electrically neutral, the sum of the charge on the 0-plane and 1-plane has to be compensated in the diffuse double layer (Westall and Hohl, 1980; Hiemstra, Van Riemsdijk and Bruggenwert, 1987),

$$\sigma_1 = -\left(\sigma_0 + \sigma_d\right) = C_1\left(\phi_1 - \phi_0\right) + \text{sign}\left(\phi_1\right)\sqrt{2\varepsilon_0\varepsilon_r RT\sum_{\ell=1}^{n} c_\ell^b\left[\exp\left(\frac{-z_\ell F}{RT}\phi_1\right) - 1\right]}. \qquad [7]$$

with $\sigma_d$ the charge in the diffuse double layer, sign($\phi_1$) the sign of $\phi_1$ (+1 or -1), $\varepsilon_0$ the permittivity of vacuum, $\varepsilon_r$ the relative permittivity ($\varepsilon_r$=78 for water), $R$ the ideal gas constant, $T$ the temperature, $z_i$ the charge number of species $i$, and $F$ the Faraday constant. The summation in Eq. [7] has to be performed over all mobile (i.e. bulk) species, $n$, this means including the bulk protons and hydroxyl ions.

The bulk concentrations of protons (formally $H_3O^+$) and hydroxyl ions are not independent but related by the water autoprotolysis equilibrium reaction

$$\text{H}_2\text{O} \quad \overset{K_w}{\rightleftharpoons} \quad \text{H}^+ + \text{OH}^- \qquad K_w = c_{\text{H}^+}^b c_{\text{OH}^-}^b \qquad [8]$$

In writing Eqs. [7] we have assumed that the bulk solution is in thermodynamic equilibrium with any position in the electrostatic double layer, the double layer thickness is much smaller than the radius of the particle, the relative permittivity is independent of the electric field (see Basu and Sharma, 1997), and there is no double layer overlap. Furthermore, the electrostatic (reference) potential in the bulk is set equal to zero.

The adsorption model is completed by an expression for the total fixed number of surface sites $c_{\text{tot}}^{//}$,

$$c''_{\text{tot}} = \left( c_{\text{Al-OH}^{-1/2}} + c_{\text{Al-OH}_2^{+1/2}} + c_{\text{Al-OH}^{-1/2}\text{C}^+} + c_{\text{Al-OH}_2^{+1/2}\text{A}^-} \right). \quad [9]$$

### 2.1 Solution procedure

Eqs. [2]-[9] is a set of 8 relations containing 8 variables ($c_{\text{Al-OH}^{-1/2}}$, $c_{\text{Al-OH2}^{+1/2}}$, $c_{\text{Al-OH}^{-1/2}\text{C}^+}$, $c_{\text{Al-OH2}^{+1/2}\text{A}^-}$, $\sigma_0$, $\sigma_1$, $\phi_0$ and $\phi_1$) that can be solved for a given set of adsorption parameters ($K^+$, $K_C$, $K_A$, $C_1$, $c''_{\text{tot}}$) and bulk concentrations $c^b{}_i$ (Westall and Hohl, 1980). Variables that are experimentally available are $\sigma_0$ (from titration experiments, e.g., Huang and Stumm, 1973; Sprycha, 1989a), $\sigma_1$ (from radiotracer techniques, e.g., Sprycha, 1989b), $\phi_0$ (potential characteristics on ISFETS, Bousse, De Rooij and Bergveld, 1983) and $\phi_1$ (from electrophoretic mobility measurements on isolated particles, e.g., Huang and Stumm, 1973; Sprycha, 1989a; Johnson, Scales and Healy, 1999). By utilising a minimisation algorithm the adsorption parameters can be changed to achieve optimal agreement between model and experiment. In this work we will use the Simplex minimisation algorithm by Nelder and Mead (Press, Teukolsky, Vetterling and Flannery, 1992) to connect the adsorption parameters to experimental data.

## 3. Results and Discussion

The sensitivity of the charge and potential predicted by the 1-pK Basic Stern model for the adsorption parameters is numerically investigated. Secondly, the minimisation algorithm is used to obtain values for the adsorption parameters from literature data. The sensitivity analysis is based on a 1-1 10.0 mol/m$^3$ electrolyte interacting with an oxidic material, at different pH-values (Table 1).

| |
|---|
| $pK^+$=-8.1, $pH_{PZC}$=8.1 for a γ-alumina.* |
| $pK_C=pK_A$=8.0, $C_1$=1.4 C/(V·m²), $c_{tot}^{//}$ =8.3·10⁻⁶ mol/m² (i.e., 5.0 sites/nm²).+ |
| For the feed solution $c^f$=10.0 mol/m³, $K_w$=1·10⁻⁸ mol²/m⁶. |
| $F$=96485 C/mol, $R$=8.3144 J/(mol·K), $T$=298.15 K, $\varepsilon_0$=8.854·10⁻¹² C/(V·m), $\varepsilon_r$=78. |

*Sprycha, 1989a; +Chan *et al.*, 1975.

Table 1: Data used in the simulations for the base case.

### 3.1 Influence of proton affinity constant, $K^+$

At a certain pH the surface charge is zero ($\sigma_0$=0). This pH is referred to as the point of zero charge, PZC, (Lyklema, 1995). Similarly, the pH at which $\sigma_0+\sigma_1=\sigma_d$=0 is called iso-electric point (IEP).

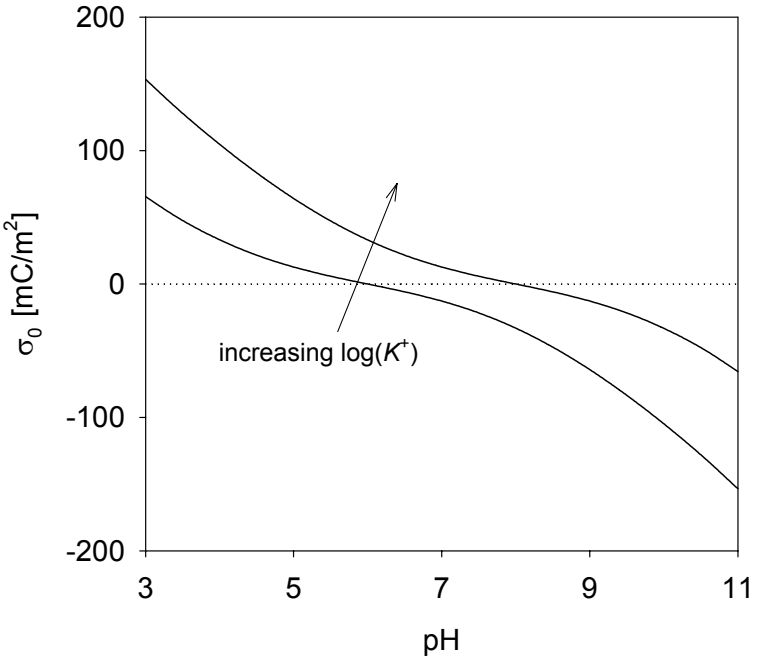


Figure 2: Dependence of the surface charge on log($K^+$) for log($K^+$) values of 6.0 and 8.0 (base case). Other parameters as in Table 1.

Figure 2 and Figure 3 show that increasing $K^+$ shifts $\sigma_0$, $\phi_0$ and $\phi_1$ to higher pH (PZC and IEP are both increased). According to Eq. [3], a rise the surface

charge requires an increase in ($\phi_0$- $\phi_1$), as can be observed in Figure 2. Since we set $K_C$=$K_A$≈0 for the simulations presented in Figure 2 and Figure 3, $\sigma_0$=-$\sigma_d$ ($\sigma_1$≈0). Consequently, an increase in $\sigma_0$ results in a decreased $\sigma_d$. From Eq. [7] it is clear that a decrease of charge in the diffuse double layer ($\sigma_d\downarrow$) corresponds to an increase in the potential at plane 1 ($\phi_1\uparrow$). From ($\phi_0$-$\phi_1$)$\uparrow$ and $\phi_1\uparrow$ it follows that the surface potential should increase ($\phi_0\uparrow$), and rise more strongly than the potential at the 1-plane ($\Delta\phi_0>\Delta\phi_1$, see Figure 3).

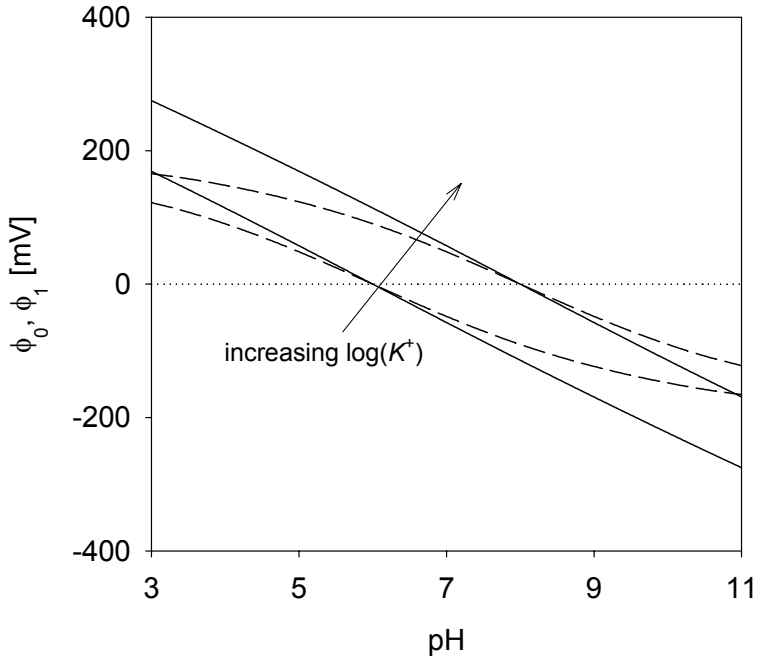


Figure 3: Dependence of the surface potential (solid lines) and the 1-plane potential (dashed lines) on log($K^+$) for log($K^+$) values of 6.0 and 8.0 (base case). Other parameters as in Table 1.

### 3.2 Degree of cation adsorption, $K_C$

Figure 4 and Figure 5 show that an increase of $K_C$ is only visible in $\sigma_0$, $\sigma_1$ and $\phi_1$ and at high pH values (basic region). The surface charge becomes less positive, while $\sigma_1$ and $\phi_1$ increase ($\phi_0$ increases as well, but only marginally).

This is because in this region, $\sigma_0$ and $\sigma_1$ are almost completely determined by the number of Al-$OH^{-1/2}$ and Al-$OH^{-1/2}C^+$ species (the protonated and anion-complex species concentrations are very small). At high pH and for increasing $K_C$ (see Eq. [4]), $\sigma_0$ decreases and $\sigma_1$ increases (Figure 4), but the surface charge decreases less than the 1-plane charge, $\Delta\sigma_1 > \Delta\sigma_0$.

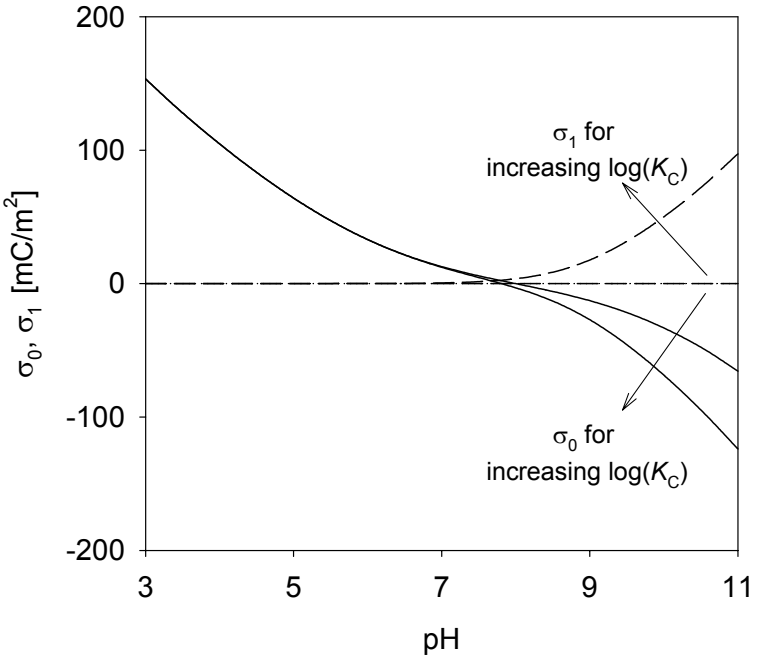


Figure 4: Dependence of the surface charge (solid lines) and the 1-plane charge (dashed lines) on log($K_C$) for log($K_C$) values of 0.0 and 8.0 (base case). Other parameters as in Table 1.

Initially, $K_C$ and $K_A$ were set to be almost equal to zero (i.e., $\sigma_1 \approx 0$) and hence the concentration of Al-$OH^{-1/2}C^+$ and Al-$OH_2^{+1/2}A^-$ species was very low. With increasing $K_C$ (increased cation adsorption), however, cations will replace the protons on the surface groups (Al-$OH_2^{+1/2} \rightarrow$ Al-$OH^{-1/2}C^+$) by creating a higher potential in the 1-plane, resulting in a lower surface charge. Since at high pH there are already few Al-$OH_2^{+1/2}$ groups at the surface, this effect of proton replacement by cations is rather limited in the 0-plane. The surface charge in the 1-plane is, however, directly proportional to the number of

Al-$OH^{-1/2}C^{+}$ groups and $\sigma_1$ will consequently rise more than $\sigma_0$ decreases ($\Delta\sigma_1 > \Delta\sigma_0$).

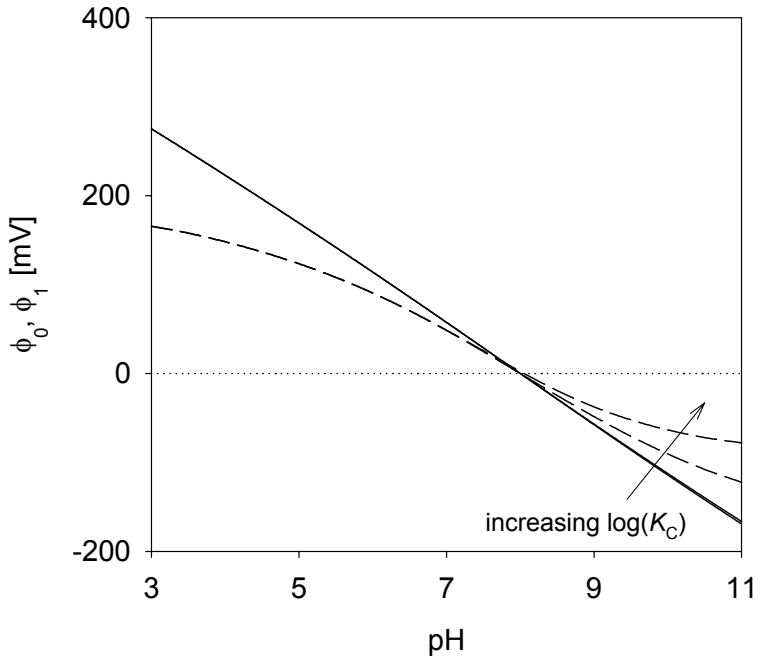


Figure 5: Dependence of the surface potential (solid lines) and the 1-plane potential (dashed lines) on log($K_C$) for log($K_C$) values of 0.0 and 8.0 (base case). Other parameters as in Table 1.

Because the decrease in surface charge is less than the rise in $\sigma_1$, the diffuse double layer charge decreases ($\sigma_d\downarrow$). Less charge in the diffuse double layer implies that the 1-plane potential, $\phi_1$, has to increase. Since $\sigma_0$ decreases, consequently ($\phi_0 - \phi_1$) has to go down. Because of the competition with cations, the concentration of protons in the 0-plane will go down and, according to Eq. [3], this implies that the surface potential has to increase at pH>PZC (were $\phi_0<0$), that is, it becomes less favourable for the protons to be situated near the surface. The behaviour for $\phi_0$ and $\phi_1$ is shown in Figure 5, though the change in the surface potential is hardly visible.

The behaviour of $\sigma_0$, $\sigma_1$, $\phi_0$ and $\phi_1$ for increasing values of the anionic equilibrium constant ($K_A$) is the reverse (not shown) of that for increasing $K_C$. Here the effects of $K_A$ are largest in the low pH range (acidic region).

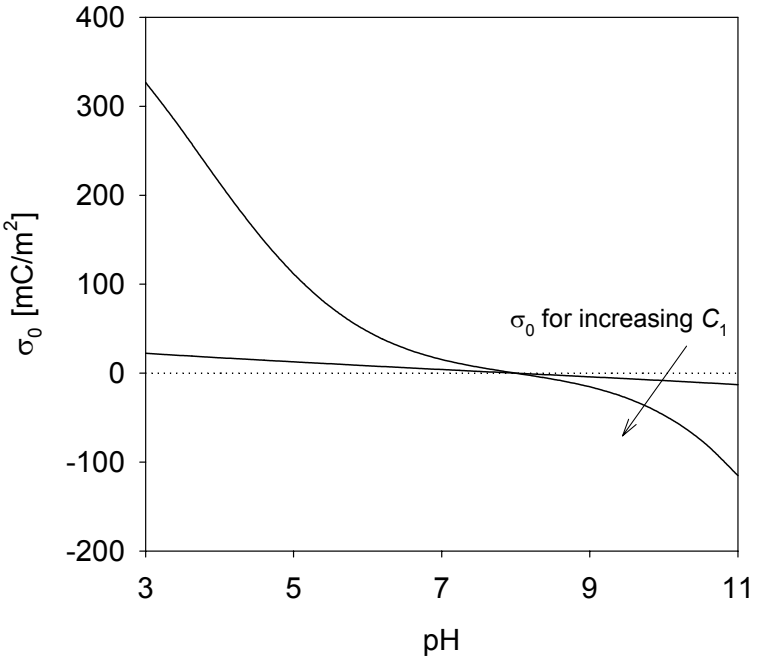


Figure 6: Dependence of the surface charge on the Helmholtz capacity ($C_1$) for $C_1$ values of 0.1 and 10.0 C/(V·m$^2$). Other parameters as in Table 1.

### 3.3 Helmholtz capacity dependence, $C_1$

The Helmholtz capacity is defined by the ratio of vacuum and relative permittivity over the thickness of the Helmholtz layer $\gamma_0$ (Lyklema, 1995; Hiemstra, Yong and Van Riemsdijk, 1999; Bockris, Reddy and Gamboa-Aldeco, 2000),

$$C_1 = \frac{\varepsilon_0 \varepsilon_r}{\gamma_0}. \qquad [10]$$

When $C_1$ approaches large values it means that the thickness of the Helmholtz layer decreases. As a result, the 1-plane potential and surface

potential should move closer together, that is, ($\phi_0$- $\phi_1$) decreases. For pH>PZC, $\phi_0$ is negative and more negative than $\phi_1$, and consequently $\phi_1$ will decrease for increasing $C_1$. For pH values below the PZC the situation is reversed (initially $\phi_0>0$, $\phi_1>0$ and $\phi_0>\phi_1$) and $\phi_1$ should increase when the capacity increases. Both effects are clearly shown in Figure 7.

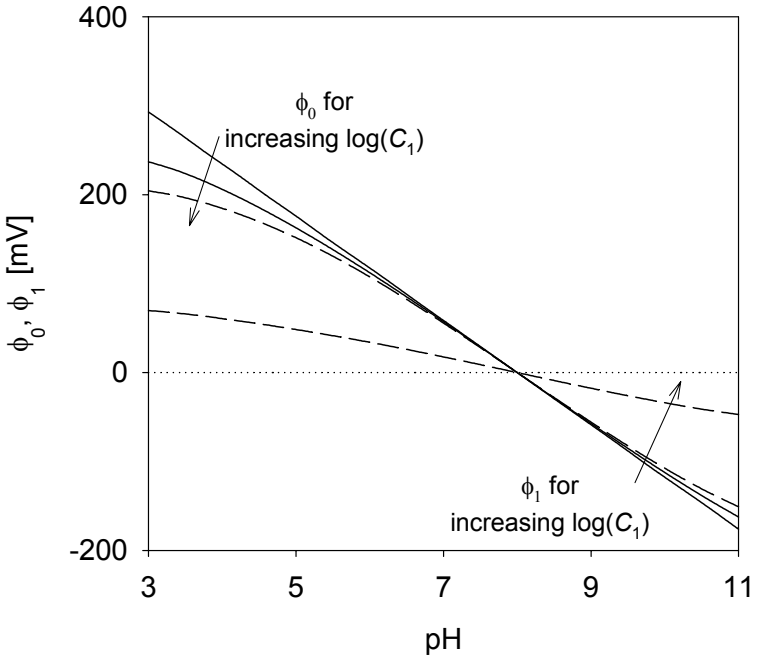


Figure 7: Dependence of the surface potential (solid lines) and the 1-plane potential (dashed lines) on the Helmholtz capacity ($C_1$) for $C_1$ values of 0.1 and 10.0 C/(V·m$^2$). Other parameters as in Table 1.

For the capacitance simulations, $K_C$ and $K_A$ were set to almost zero and it follows that the 1-plane charge is almost zero and the surface charge is completely compensated in the diffuse double layer (i.e., $\sigma_0$=-$\sigma_d$). The diffuse double layer charge is directly related to the 1-plane potential (Eq. [7]) and follows the reverse behaviour described for $\phi_1$: for high pH ($\phi_1\downarrow$), $\sigma_d$ increases and for low pH ($\phi_1\uparrow$), $\sigma_d$ decreases. Because the surface charge behaves opposite to $\sigma_d$, $\sigma_0$ is expected to decrease for high pH and increase for low pH (see Figure 6).

## 3.4 Deriving adsorption parameters from literature data

Sprycha (1989a) performed measurements of the surface charge and the zeta potential, $\zeta$ (defined as the potential located at the shear plane of an interface), for monovalent electrolytes on a $\gamma$-alumina as a function of pH. We applied our adsorption model to the data of Sprycha. For the fitting of $\sigma_0$ this was quite straightforward since this variable follows directly from the electrostatic model (see Eq. [3]; $\phi_0$ and $\phi_1$ are determined by the model). For $\zeta$ we assumed that it is situated at the head-end of the diffuse double layer (i.e. $\zeta = \phi_1$).

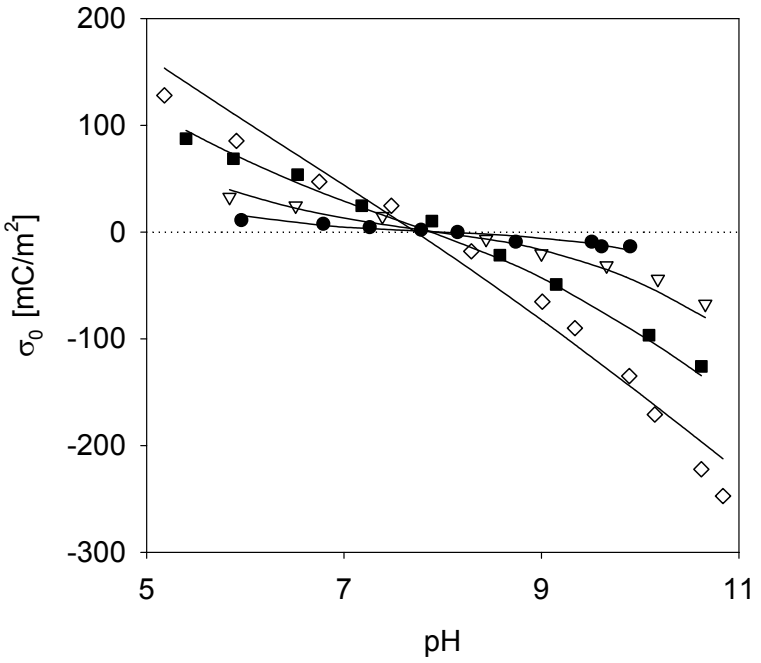


Figure 8: 1-pK BS model fit of the surface charge $\sigma_0$ (solid lines) based on data from Sprycha (1989a, b) for adsorption of NaCl on $\gamma$-alumina: 1 mol/m$^3$ (filled circles), 10 mol/m$^3$ (triangles), 100 mol/m$^3$ (filled squares) and 1000 mol/m3 (diamonds). $\log(K^+)$=8.1, $\log(K_C)$=-1.0, $\log(K_A)$=-2.5, $C_1$=1.6 C/(V·m$^2$), $c_{tot}^{//}$ =1.33·10$^{-5}$ mol/m$^2$ (Sahai and Sverjensky, 1997).

In the fitting procedures for $\sigma_0$ and $\zeta$ we have kept the values of $K^+$ and $c_{tot}^{//}$ fixed since $K^+$ follows directly from the PZC ($\sigma_0$=0). The fixed surface site concentration $c_{tot}^{//}$ is highly correlated to the other adsorption parameters and hence it cannot be determined from these experimental data. We have used $c_{tot}^{//}$=1.33·10$^{-5}$ mol/m$^2$ (i.e., 8 sites/nm$^2$) as obtained from infrared experiments (Sahai and Sverjensky, 1997).

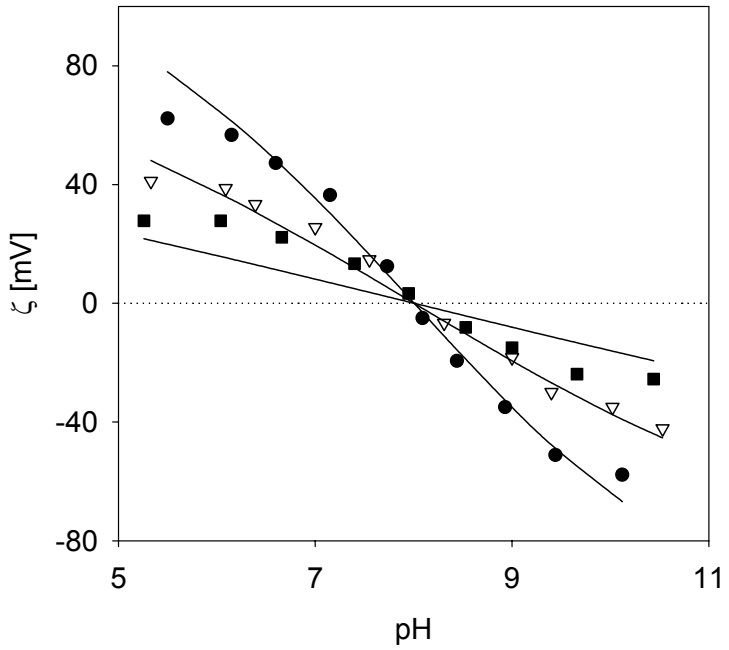


Figure 9: 1-pK BS model fit of the zeta potential, $\zeta=\phi_1$, (solid lines) based on data from Sprycha (1989a, b) for adsorption of NaCl on a γ-alumina: 1 mol/m$^3$ (filled circles), 10 mol/m$^3$ (triangles), 100 mol/m$^3$ (filled squares). log($K^+$)=8.1, log($K_C$)=-8.7, log($K_A$)=-2.2, $C_1$=0.12 C/(V·m$^2$), $c_{tot}^{//}$=1.33·10$^{-5}$ mol/m$^2$ (Sahai and Sverjensky, 1997).

The adsorption model yields good predictions for the surface charge as a function of pH (Figure 8). Only at high concentrations of 1000 mol/m$^3$ the fit deteriorates. When the model parameters from Figure 8 are used to calculate

the zeta potential (i.e., $\phi_1$), $\zeta$ is underestimated (plot not shown), though predictions are much better than for the reversed procedure. The fit for the zeta potential is rather poor (Figure 9). The model is not capable of describing the limiting $\zeta$ values at very high and low pH. Also, if we use the obtained parameters to calculate the surface charge, they grossly underestimate $\sigma_0$ (up to 5x as low) as found from titration experiments (comparison not shown). The model parameters that were calculated for the fit of $\sigma_0$ (Figure 8) are, however, very different from the results found for the zeta potential fit. Apart from the poor fit for $\zeta$, it was possible to obtain multiple solutions that described the experimental data equally well. Instead of $\log(K_C)$=-8.7 and $\log(K_A)$=-2.2 (see Figure 9) the same model data set could be obtained with the parameters $\log(K_C)$=-10.6 and $\log(K_A)$=-2.5 (all other parameters remained constant). The absence of a unique parameter solution is known from model investigations in literature (Westall and Hohl, 1980; Koopal, Van Riemsdijk and Roffey, 1987).

The observed model behaviour is not typical for this case, however. A consistent description of the surface charge and zeta potential within the framework of one site-binding model has proven to be quite difficult (Davis, James and Leckie, 1978; Hiemstra, Yong and Van Riemsdijk). One reason for this is that for many oxides there is only a small difference between $\sigma_0$ and $\sigma_1$. Since the zeta potential is directly related to this difference ($\sigma_d \rightarrow \zeta$), errors in the experimental determination of $\sigma_0$ and $\sigma_1$ can have a major impact on the calculated value for $\zeta$. Furthermore, electrostatic site-binding models, like the one used in this chapter, do not contain any information about the (hydrodynamic) movement of ions directly at the surface (e.g., location of the shear plane). Model predictions can sometimes be improved by using a more elaborate double layer model or multiple adsorption sites, but it is questionable if this approach improves the physical representation of the oxide material, even more so when we would like to describe adsorption in

inorganic NF membranes that consist of highly porous materials. For materials with a high porosity it is uncertain if the Helmholtz capacity (Eq. [3]) can still be considered constant (Hiemstra, Yong and Van Riemsdijk, 1999). Also, we question the assumptions used to arrive at the expression for the diffusive double layer charge (second term in Eq. [7]).

## 4. Conclusions

A 1-pK adsorption model was combined with a Basic Stern electrolyte double layer model and used to describe adsorption of ions on an oxidic surface to derive the adsorption parameters for application in a transport model for NF membranes. The dependence of the surface charge, $\sigma_0$, and the 1-plane potential, $\phi_1$, on the model parameters was investigated. Also the model was applied to extract adsorption parameters from an experimental study of sodium chloride adsorption on a γ-alumina. When the model was fitted to the experimental $\zeta$ potential data the model parameters were $\log(K^+)$=8.1, $\log(K_C)$=-8.7, $\log(K_A)$=-2.2, $C_1$=0.12 C/(V·m$^2$), $c_{tot}^{//}$=1.33·10$^{-5}$ mol/m$^2$ (i.e., 8.0 sites/nm$^2$). Estimated model parameters for the surface charge measurements were $\log(K^+)$=8.1, $\log(K_C)$=-1.0, $\log(K_A)$=-2.5, $C_1$=1.6 C/(V·m$^2$), $c_{tot}^{//}$=1.33·10$^{-5}$ mol/m$^2$ (8.0 sites/nm$^2$). Discrepancies between the parameter predictions and the surface charge or zeta potential obtained with both methods are caused by the lack of knowledge about the physical properties of the oxide material as well as by questionable assumptions made in the site-binding model. Still, the model predicts surface charge and zeta potential qualitatively and may be suitable for the description of surface adsorption behaviour in nanofiltration membranes.

## Nomenclature

| | | |
|---|---|---|
| $C_1$ | Helmholtz capacity | [C $V^{-1}$·$m^{-2}$] |
| $c_i^{sc}$ | concentration of surface complexes $i$ | [mol $m^{-2}$] |
| $c^{ref}$ | thermodynamic reference concentration | [mol $m^{-3}$] |
| $c^{s}_i$ | surface concentration of non-adsorbed ions $i$ | [mol $m^{-3}$] |
| $c^{b}_i$ | bulk concentration of species $i$ | [mol $m^{-3}$] |
| $c^{//}_{tot}$ | total concentration of surface sites | [mol $m^{-2}$] |
| $F$ | Faraday constant | [C $mol^{-1}$] |
| $K^+$ | proton adsorption equilibrium constant | [-] |
| $K_A$ | anion adsorption equilibrium constant | [-] |
| $K_C$ | cation adsorption equilibrium constant | [-] |
| $K_w$ | water autoprotolysis equilibrium constant | [$mol^2$ $m^{-6}$] |
| $R$ | ideal gas constant | [J $mol^{-1}$ $K^{-1}$] |
| $T$ | temperature | [K] |
| $z_i$ | charge number of species $i$ | [-] |

Greek

| | | |
|---|---|---|
| $\varepsilon_0$ | vacuum permittivity | [C $V^{-1}$ $m^{-1}$] |
| $\varepsilon_r$ | relative permittivity | [-] |
| $\sigma_0$ | surface charge | [C $m^{-2}$] |
| $\sigma_1$ | charge at the 1-plane | [C $m^{-2}$] |
| $\sigma_d$ | diffuse double layer charge | [C $m^{-2}$] |
| $\phi_0$ | surface potential | [V] |
| $\phi_1$ | potential at the 1-plane | [V] |
| $\zeta$ | zeta potential | [V] |

## References


1. Basu S., and Sharma M.M., "An Improved Space-Charge Model for Flow Through Charged Microporous Membranes," *J. Membrane Sci.*, **124**, 77 (1997).
2. Bockris J.O'M., Reddy A.K.N., and Gamboa-Aldeco M., "Modern Electrochemistry 2A. Fundamentals of Electrodics," 2nd edition, Kluwer Academic/Plenum Publishers, New York, 2000, pp. 871-887.
3. Bousse L., De Rooij N.F., and Bergveld P., "The Influence of Counter-Ion Adsorption on the $\psi_0$/pH Characteristics of Insulator Surfaces," *Surf. Sci.*, **135**, 479 (1983).
4. Chan D.Y.C., Perram J.W., White L.R., and Healy T.W., "Regulation of Surface Potential at Amphoteric Surfaces During Particle-Particle Interaction," *J. Chem. Soc. Faraday Trans. I*, **71**, 1046 (1975).
5. Davis J.A., James R.O., and Leckie J.O., "Surface Ionization and Complexation at the Oxide/Water Interface. I. Computation of Electrical Double Layer Properties in Simple Electrolytes," *J. Colloid Interface Sci.*, **63**, 480 (1978).
6. Hall M.S., Starov V.M., and Lloyd D.R., "Reverse Osmosis of Multicomponent Electrolyte Solutions. Part I. Theoretical Development," *J. Membrane Sci.*, **128**, 23 (1997).
7. Hall M.S., Lloyd D.R., and Starov V.M., "Reverse Osmosis of Multicomponent Electrolyte Solutions. Part II. Experimental Verification," *J. Membrane Sci.*, **128**, 39 (1997).
8. Healy T.W., and White L.R., Ionizable Surface Group Models of Aqueous Interfaces, *Adv. Colloid Interface Sci.*, **9**, 303 (1978).
9. Hiemstra T., Van Riemsdijk W.H., and Bruggenwert M.G.M., "Proton Adsorption Mechanism at the Gibbsite and Aluminium Oxide Solid/Solution Interface," *Neth. J. Agric. Sci.*, **35**, 281 (1987).
10. Hiemstra T., Van Riemsdijk W.H., and Bolt G.H., "Multisite Proton Adsorption Modeling at the Solid/Solution Interface of (Hydr)oxides: A New Approach. I. Model Description and Evaluation of Intrinsic Reaction Constants," *J. Colloid Interface Sci.*, **133**, 91 (1989).
11. Hiemstra T., De Wit J.C.M., and Van Riemsdijk W.H., "Multisite Proton Adsorption Modeling at the Solid/Solution Interface of (Hydr)oxides: A New Approach. II. Application to Various Important (Hydr)oxides," *J. Colloid Interface Sci.*, **133**, 105 (1989).
12. Hiemstra T., Yong H., Van Riemsdijk W.H., "Interfacial Charging Phenomena of Aluminium (Hydr)oxides," *Langmuir*, **15**, 5942 (1999).
13. Huang C-P., and Stumm W., "Specific Adsorption of Cations on Hydrous $\gamma$-$Al_2O_3$," *J. Colloid Interface Sci.*, **43**, 409 (1973).

14. Johnson S.B., Scales P.J., and Healy T.W., "The Binding of Monovalent Electrolyte Ions on α-Alumina. I. Electroacoustic Studies at High Electrolyte Concentrations," *Langmuir*, **15**, 2836 (1999).
15. Koopal L.K., Van Riemsdijk W.H., and Roffey M.G., "Surface Ionization and Complexation Models: A Comparison of Methods for Determining Model Parameters," *J. Colloid Interface Sci.*, **118**, 117 (1987).
16. Lyklema J., "The Electrical Double Layer on Oxides", *Croat. Chem. Acta.*, **43**, 249 (1971).
17. Lyklema J., "Fundamentals of Interface and Colloid Science. Volume II: Solid-Liquid Interfaces," Academic Press, London, 1995, chapter 3.
18. Press W.H., Teukolsky S.A., Vetterling W.T., and Flannery B.P., "Numerical Recipes in Fortran 77," 2nd edition, Cambridge University Press, Cambridge, 1992, pp. 402-406.
19. Sahai N., and Sverjensky D.A., "Evaluation of Internally Consistent Parameters for the Triple-Layer Model by the Systematic Analysis of Oxide Surface Titration Data," *Goechim. Cosmochim. Acta*, **61**, 2801 (1997).
20. Sprycha R., "Electrical Double Layer at Alumina/Electrolyte Interface. I. Surface Charge and Zeta Potential," *J. Colloid Interface Sci.*, **127**, 1 (1989).
21. Sprycha R., "Electrical Double Layer at Alumina/Electrolyte Interface. II. Adsorption of Supporting Electrolyte Ions," *J. Colloid Interface Sci.*, **127**, 12 (1989).
22. Starov V.M., Bowen W.R., and Welfoot J.S., "Flow of Multicomponent Electrolyte Solutions through Narrow Pores of Nanofiltration Membranes," *J. Colloid Interface Sci.*, **240**, 509 (2001).
23. Westall J., and Hohl H., "A Comparison of Electrostatic Models for the Oxide/Solution Interface," *Adv. Colloid Interface Sci.*, **12**, 265 (1980).
24. Yates D.E., Levine S., and Healy T.W., "Site-binding Model of the Electrical Double Layer at the Oxide/Water Interface," *J. Chem. Soc. Faraday Trans. I*, **70**, 1807 (1974).
25. Zhmud B.V., Meurk A., and Bergström L., "Evaluation of Surface Ionization Parameters from AFM Data," *J. Colloid Interface Sci.*, **207**, 332 (1998).

# Chapter 6

## Ion-Adsorption Parameters determined from Zeta Potential and Titration Data for a γ-Alumina Nanofiltration Membrane


### Abstract

Theoretical models for the prediction of nanofiltration separation performance as a function of, e.g., pH and electrolyte composition require knowledge on the ion-surface adsorption chemistry. Adsorption parameters have been extracted from electrophoretic mobility measurements on a ceramic γ–alumina NF membrane material in aqueous solutions of NaCl, $Na_2SO_4$ and $CaCl_2$, and literature potentiometric titration data on γ–alumina. Various adsorption reaction models and descriptions of the electrostatic double layer have been tested. The adsorption parameters are obtained using a 1-pK triple-layer model.

The zeta potential data indicate that on this γ-alumina NaCl acts as an indifferent electrolyte, resulting in an iso-electric point (IEP) of pH=8.3. The data can be accurately described with the 1-pK triple-layer model. Furthermore, the surface charge model predictions are in good agreement with literature titration data for this 1:1 electrolyte. Strong adsorption of $Ca^{2+}$ ions leads to positive zeta potentials over the entire concentration and pH range studied. The model is capable of fitting the potential data reasonably well. Strong adsorption of sulphate ions causes a shift of the iso-electric point to lower pH values. For a bulk concentration of 100 mol/$m^3$ $Na_2SO_4$ only negative zeta potentials are observed.

## 1. Introduction

Nanofiltration (NF) membranes can be used to selectively remove ions from aqueous electrolyte solutions. Since these membranes contain pores much larger ($1<d_p<4$ nm) than the hydrated size of ions ($d^h_{ion}\approx0.4$ nm), separation is not solely based on size exclusion. Rather, it is due to electrostatic interactions between ions in the electrolyte solution and the charge on the surface of the membrane (internal and external). Due to these interactions ions can efficiently be retained, while transport of the uncharged solvent (often water) remains largely unaffected.

The surface charge depends on the nature of the membrane material, the composition of the electrolyte solution and the interactions of the ionic species with the surface. These interactions are generally described in terms of adsorption parameters. For a prediction of the separation characteristics of NF membranes as a function of pH and electrolyte composition, these adsorption parameters are required. For membranes they can be obtained from retention measurements. Such an approach was adopted by Hall, Starov and Lloyd (1997), Hall, Lloyd and Starov (1997) and Starov, Bowen and Welfoot (2001) for polymeric NF membranes. In contrast to polymeric membranes, the adsorption parameters for inorganic NF membranes can also be obtained from measurements unrelated (i.e. independent) to retention experiments, as was shown for zirconia by Randon *et al.* (1991a, b). Examples of such techniques include potentiometric titration, electroacoustic experiments or electrophoretic mobility measurements. The objective of the present study will be to determine a consistent set of adsorption parameters for a γ-alumina NF membrane using independent measurements. These parameters can then subsequently be used in a transport description to predict the separation performance of the γ-alumina membrane (see chapters 3, 4 and 7 in this thesis).

Many of the experimental techniques for determining the charging of a material probe the inner as well as the outer surface, which hampers their interpretation since the inner surface area of NF materials can be quite large (e.g., 250 $m^2/g$, see Ulhorn *et al.*, 1992). Furthermore, for NF materials the charge and potential within the narrow pores vary with the degree of double layer overlap, for instance by charge regulation (Ninham and Parsegian, 1971; Chan *et al.*, 1975). Electrophoretic mobility (EM) measurements only probe the outer surface, and by considering only dilute suspensions particle double layer overlap can be avoided. The EM measurements yield information on the potential at the shear plane (i.e., the zeta potential, $\zeta$), which can be interpreted in terms of an electrokinetic charge. Because ions flowing through a membrane will, at steady state, only experience the pore properties beyond this shear plane, the $\zeta$ potential is of primary importance in any NF transport description. Drawbacks of EM measurements may include the unknown position of the shear plane, and the corrections required for retardation and relaxation effects (O'Brien and White, 1978). Despite these drawbacks, we consider EM measurements the best way for characterizing our charged membrane surface.

For the interpretation of EM measurements in terms of adsorption characteristics it is required to adopt a model. Such models generally consist of two parts: one part describing the surface charging reactions and one describing the double layer at the charged interface. In this paper a site-binding model is used to describe the materials' charging behaviour. In site-binding models, ions adsorb on a fixed number of surface sites (Yates, Levine and Healy, 1974; Davis, James and Leckie, 1978; Healy and White, 1978). Many models have been proposed for the ensuing double layer (Yates, Levine and Healy, 1974; Bousse, De Rooij and Bergveld, 1983; Hiemstra, Van Riemsdijk and Bruggenwert, 1987; Hiemstra and Van Riemsdijk, 1996), some of which will be tested here.

# 2. Theory

## 2.1 Charging mechanisms

Inorganic NF membranes consist of (mixed) oxides (e.g., $Al_2O_3$, $TiO_2$, $ZrO_2$), which form surface hydroxyl groups in aqueous solutions. The surface of an oxide is usually heterogeneous, *i.e.*, the surface hydroxyl groups it contains are neither identical nor energetically independent (Morterra and Magnacca, 1996; Sohlberg, Pennycook and Pantelides, 2000). Because adequate information about the heterogeneity is generally missing, in this work the surface will be assumed effectively homogeneous, containing only a single type of averaged surface site [-$OH^q$] ($q$ being the initial charge of the hydroxyl groups). On these surface sites competitive adsorption of protons, cations ($C^{m+}$) and anions ($A^{n-}$) takes place. In this work the focus will be on two well-known site-binding models, the 1-pK and the 2-pK model.

### 2.1.1 1-pK model

In the 1-pK model all surface sites on alumina are assumed to be negatively charged ($q$ = -1/2) hydroxyl groups, which can become positively charged ($q$ = 1/2) via adsorption of a proton (Hiemstra, De Wit and Van Riemsdijk, 1989; Hiemstra, Yong and Van Riemsdijk, 1999). Ions can adsorb on surface sites with opposite charge. The corresponding equilibrium reactions are

$$\begin{aligned} &\text{Al-OH}^{-1/2} + \text{H}^+(\text{s}) && \overset{K_1^+}{\rightleftharpoons} && \text{Al-OH}_2^{+1/2} \\ &v\,\text{Al-OH}^{-1/2} + \text{C}^{m+}(\text{s}) && \overset{K_{\text{C1}}}{\rightleftharpoons} && (\text{Al-OH}^{-1/2})_v\text{C}^{m+}\ . \\ &w\,\text{Al-OH}_2^{+1/2} + \text{A}^{n-}(\text{s}) && \overset{K_{\text{A1}}}{\rightleftharpoons} && (\text{Al-OH}_2^{+1/2})_w\text{A}^{n-} \end{aligned} \qquad [11]$$

A label (s) is used to designate virtual non-adsorbed ions (e.g., $H^+$) located in a plane with the same potential as their surface complexes (e.g., Al-$OH_2^{+1/2}$). Note that the Boltzmann relation, Eq. [13], relates their concentration to that in the bulk of the electrolyte. Additionally in Eq. [11], $v$ and $w$ are

stoichiometric constants, and $m$ and $n$ are the absolute charges of the cations and anions, respectively. The term surface complex is used here to define species that, in addition to electrostatic interactions, exhibit a non-coulombic or chemical interaction with the surface. This chemical interaction with the surface is referred to as specific adsorption (Koopal, Van Riemsdijk and Roffey, 1987).

The corresponding equilibrium constants are

$$K_1^+ = \frac{c_{\text{Al-OH}_2^{+1/2}} c^{\text{ref}}}{c^{\text{s}}_{\text{H}^+} c_{\text{Al-OH}^{-1/2}}}, K_{\text{C1}} = \frac{c_{\left(\text{Al-OH}^{-1/2}\right)_v \text{C}^{m+}} c^{\text{ref}}}{c^{\text{s}}_{\text{C}^{m+}} \left(c_{\text{Al-OH}^{-1/2}}\right)_v}, K_{\text{A1}} = \frac{c_{\left(\text{Al-OH}_2^{+1/2}\right)_w \text{A}^{n-}} c^{\text{ref}}}{c^{\text{s}}_{\text{A}^{n-}} \left(c_{\text{Al-OH}_2^{+1/2}}\right)_w}. \quad [12]$$

In the 1-pK model the proton adsorption constant is equal to the point of zero charge, $\text{pH}_{\text{PZC}} = \text{p}K_1^+$. In Eq. [12] $c_i^{\text{s}}$ is the concentration of (virtual) non-adsorbed ions [mol/m$^3$] and $c^{\text{ref}}$ is the thermodynamic reference concentration of $10^3$ mol/m$^3$ (1 mol/dm$^3$). The concentrations $c_i^{\text{s}}$ are related to the bulk concentrations by the Boltzmann equation

$$c_i^{\text{s}} = \gamma_i c_i^{\text{b}} \exp\left(\frac{-z_i F}{RT}\phi_{\text{s}}\right), \quad [13]$$

with $\gamma_i$ the bulk activity coefficient of species $i$, b denotes the bulk ($\phi_{\text{b}} \equiv 0$), $z_i$ is the charge number, $F$ is the constant of Faraday, $R$ the ideal gas constant, $T$ the temperature, and $\phi_{\text{s}}$ the potential of the species $c_i^{\text{s}}$. The bulk activity coefficient is related to the ionic strength $I$ by the Davies relation (Davies, 1962)

$$-\log\left(\gamma_i\right) = 0.51 z_i^2 \left(\frac{\sqrt{I}}{1+\sqrt{I}} - 0.2I\right). \quad [14]$$

The bulk concentrations of protons and hydroxyl ions are related by the water autoprotolysis equilibrium reaction

$$\mathrm{H_2O} \quad \overset{K_w}{\rightleftharpoons} \quad \mathrm{H^+ + OH^-} \qquad K_w = c^{\mathrm{b}}_{\mathrm{H^+}} c^{\mathrm{b}}_{\mathrm{OH^-}} \qquad [15]$$

The charge at a specific (double layer) plane *p* is related to the concentration of adsorbed surface complexes $c_i^{\mathrm{sc}}$,

$$\sigma_p = F \sum_{\ell=1}^{n} z_\ell c^{\mathrm{sc}}_{\ell,p} \; . \qquad [16]$$

Protons adsorb directly at the surface, the 0-plane, and monovalent anions and cations adsorb on one surface site. The surface charge $\sigma_0$ then is

$$\sigma_0 = \frac{F}{2}\left( c_{\mathrm{Al\text{-}OH_2^{+1/2}}} - c_{\mathrm{Al\text{-}OH^{-1/2}}} + c_{\mathrm{Al\text{-}OH_2^{+1/2}A^-}} - c_{\mathrm{Al\text{-}OH^{-1/2}C^+}} \right). \qquad [17]$$

Note that Eq. [17] is a sum of the charges over the total number of surface sites, $c^{//}_{\mathrm{tot}}$ (Healy and White, 1978; Koopal, Van Riemsdijk and Roffey, 1987). This total number of surface sites obeys

$$c^{//}_{\mathrm{tot}} = \left( c_{\mathrm{Al\text{-}OH^{-1/2}}} + c_{\mathrm{Al\text{-}OH_2^{+1/2}}} + c_{\mathrm{Al\text{-}OH^{-1/2}C^+}} + c_{\mathrm{Al\text{-}OH_2^{+1/2}A^-}} \right). \qquad [18]$$

### 2.1.2 2-pK model

The major difference between the 1-pK and 2-pK models is related to the charge of the surface sites. In the 2-pK model these sites are assumed initially uncharged (*q* = 0). Charging occurs via adsorption or desorption of a proton. Again, ions can adsorb on surface sites with opposite charge. The corresponding reactions are

$$\begin{aligned}
&\mathrm{Al\text{-}OH + H^+ (s)} && \overset{K_2^+}{\rightleftharpoons} && \mathrm{Al\text{-}OH_2^{+1}} \\
&\mathrm{Al\text{-}OH} && \overset{K_2^-}{\rightleftharpoons} && \mathrm{Al\text{-}O^{-1} + H^+ (s)} \\
&v\,\mathrm{Al\text{-}O^{-1} + C^{m+} (s)} && \overset{K_{C2}}{\rightleftharpoons} && \mathrm{(Al\text{-}O^{-1})_v C^{m+}} \\
&w\,\mathrm{Al\text{-}OH_2^{+1} + A^{n-} (s)} && \overset{K_{A2}}{\rightleftharpoons} && \mathrm{(Al\text{-}OH^{+1})_w A^{n-}}
\end{aligned} \quad , \qquad [19]$$

The 2-pK model relations can be derived analogously to those of the 1-pK model.

In the 2-pK model, proton interaction is described by two reactions and two parameters are defined to characterize this charging behaviour, the point of zero charge ($pH_{PZC}$ or simply PZC) and $\Delta pK$*

$$\begin{aligned} pH_{pzc} &= \frac{1}{2}\left(pK_2^- - pK_2^+\right) \\ \Delta pK &= pK_2^- + pK_2^+ \end{aligned} \quad . \qquad [20]$$

## 2.2 Electrostatic double layer

The background and structure of several double layer models have been well described by Lyklema (1995) and Westall and Hohl (1980) and we will only briefly mention the features important here. In the double layer models, the surface charge can be compensated by counter charge in one or more Helmholtz layers, a diffuse layer, or several combinations of both. Adsorbed ions are assumed to be only present on the Helmholtz planes located at discrete distances from the material surface. In the diffuse double layer no discrete effects are present and this layer only contains ions that are weakly electrostatically adsorbed. An illustration of a double layer model is presented in Figure 1.

For any Helmholtz plane $p$ the charge $\sigma_p$ is related to the potential $\phi$ drop across the layer, following it in outward direction via

$$\sigma_p = C_{p+1}\left(\phi_p - \phi_{p+1}\right) - \sigma_{p-1} \qquad \text{for } p=0..np \text{ and } \sigma_{-1}=0, \qquad [21]$$

---

* Note that the definition for $pH_{PZC}$ and $\Delta pK$ used here is different from expressions generally given (e.g., Chan *et al.*, 1975; Davis, James and Leckie, 1978; Yates and White, 1978). This is because the proton adsorption reaction is defined differently here. Still, the same nomenclature is retained.

where $C_{p+1}$ is the double layer capacitance, given by $C_{p+1} = \varepsilon_0 \varepsilon_{r,p+1} / \gamma_p$, the ratio between the dielectric permittivity ($\varepsilon_0$, $\varepsilon_r$) and the thickness $\gamma$ of the following Helmholtz plane. The charge in the diffuse layer $\sigma_d$ is (Lyklema, 1995)

$$\sigma_d = -\text{sign}(\phi_d)\sqrt{2\varepsilon_0\varepsilon_r RT\sum_{\ell=1}^{n} c_\ell^b\left[\exp\left(\frac{-z_\ell F}{RT}\phi_d\right)-1\right]}, \qquad [22]$$

with $c^b_\ell$ the bulk concentration of species $\ell$.

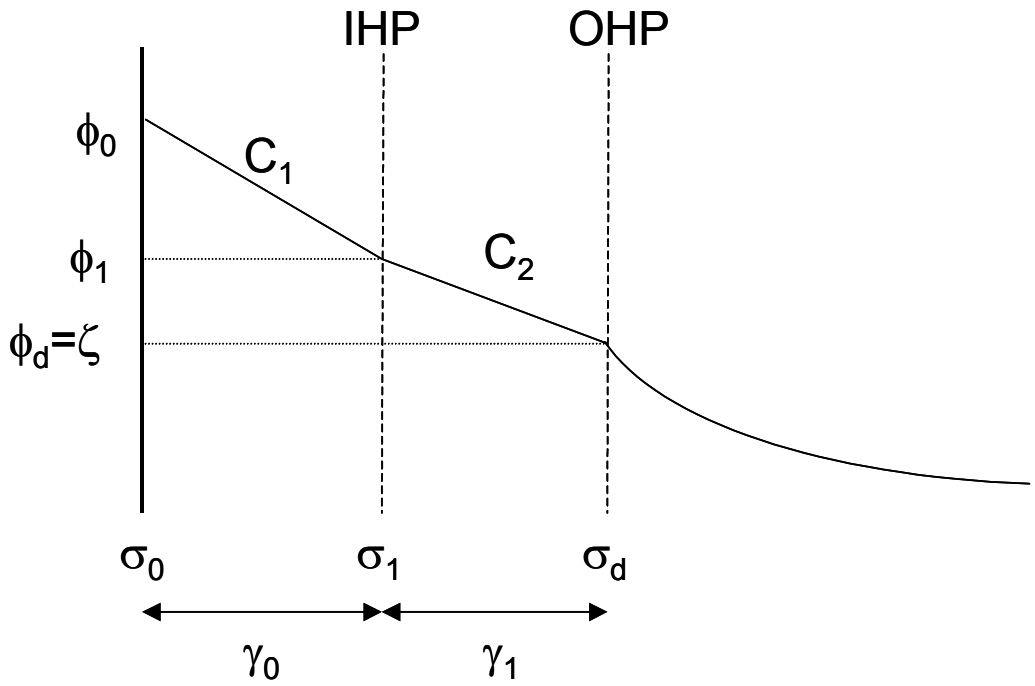


Figure 1: Schematic description of our triple-layer model (not to scale; mostly the diffuse part is much more extended than the Stern layer).

### 2.3 Mobility conversion to zeta potential

The electrophoretic mobility is directly related to the electrokinetic charge (O'Brien and White, 1978). The plane of shear in a system is fixed by hydrodynamics and not related to the system's electrostatic properties. Generally, the shear plane is assumed to be identical to the OHP because

ions residing between the surface of a particle and the shear plane are commonly assumed immobile. Recently, however, it has been shown experimentally that ions in the Helmholtz layer(s) can also contribute to the conductivity of the solution (Minor, Van der Linde and Lyklema, 1998) and therefore influence the mobility of particles (Lyklema and Minor, 1998). Mangelsdorf and White (1990) have proposed to modify the mobility approach of O'Brien and White by introducing a Stern conduction parameter $\delta$ but they state that an unambiguous determination of this parameter is complicated. Hiemstra, Yong and Van Riemsdijk (1999) concluded that for a consistent description of the zeta potential data of Rowlands *et al.* (1997) the $\zeta$-plane should be a function of the square root of the bulk ionic strength.

In this work we account for the additional Stern conductance by the introduction of an apparent $\zeta$-plane. The location of this apparent $\zeta$-plane and the shear plane do not necessarily coincide. The location of the apparent* $\zeta$-plane is assumed a function of the (adsorbed) ion concentrations in the Stern layer. Although there is no direct physical justification for this assumption, it serves as a simple mathematical device, while avoiding the need for a more complex description of the additional Stern conductivity.

For the lowest electrolyte concentration considered in the present study (i.e., 1 mol/m$^3$), the contribution the Stern conductance is assumed negligible and the $\zeta$-plane is assumed to be located at the OHP, but, to obtain consistency, for higher concentrations it must be assumed that the $\zeta$-plane moves closer to the inner Helmholtz plane (see Figure 1). The $\zeta$-plane location is treated as a fitting parameter.

* In the remainder of this work the adjective 'apparent' is omitted.

## 2.4 Numerical solution

The set of equations [12]-[18], [3], and [4] can be solved for a given set of adsorption parameters ($K^+$, $K^-$, $K_C$, $K_A$, $C_1$, $C_2$, $c_{tot}^{//}$, $\zeta$-plane) and bulk concentrations $c_i^b$. The solution is obtained using a modelling scheme similar to that of Westall (1980) and Westall and Hohl (1980), with the exception that changes in the bulk concentrations as a result of adsorption are neglected. The adsorption parameters are obtained by fitting the set of equations to experimental $\zeta$ (mobility) data using a multi-dimensional non-linear Simplex routine (Press *et al.*, 1992).

### 2.4.1 Interdependence of adsorption parameters

For a model combining site-binding with an electrostatic double layer description there is considerable interdependence between the model parameters (Johnson jr., 1984; Koopal, Van Riemsdijk and Roffey, 1987), making it difficult to obtain a unique set of adsorption parameters. Hiemstra and co-workers (1989a, 1989b, 1999) tried to overcome this problem by utilizing a-priori information (e.g., crystallographic and spectroscopic data), thus fixing some of the adsorption parameters. Their approach relies on detailed knowledge of the structure and properties of the material, which is missing for the $\gamma$-alumina NF membrane considered here. However, since the interdependence of model parameter is considered important, in this paper the adsorption parameters are not freely adjustable variables. The total number of adsorption sites $c_{tot}^{//}$ is set at a fixed value of $1.33 \cdot 10^{-5}$ mol/m$^2$ (8 sites/nm$^2$), as obtained by Peri (1966) from infrared experiments and very close to the total site concentration of $1.41 \cdot 10^{-5}$ mol/m$^2$ (8.5 sites/nm$^2$) found by Kummert and Stumm (1980). In the 1-pK calculations for NaCl $\log(K^+)$ is set equal to the iso-electric point of the alumina, since in the absence of specific adsorption p$K^+$=PZC=IEP (PZC=point of zero charge). For the 2-pK approach however, the PZC is determined by proton adsorption and

desorption (see Eq. [20]) and various parameter combinations can lead to the same PZC. Since the magnitude of $\Delta pK$ is a matter of debate (Koopal, Van Riemsdijk and Roffey, 1987), it is not possible to fix either $pK_2^-$ or $pK_2^+$ in the fitting, as is possible for the 1-pK model.

### 2.4.2 Fitting procedure

The fitting is performed in three steps. First the literature titration data are used to obtain an initial guess for the adsorption parameters $K^+$, $K^-$ (only 2-pK model), $K_C$, $K_A$, $C_1$, and $C_2$ (1-pK and 2-pK model). Subsequently, the adsorption parameters' final value is determined by a fit to the experimental $\zeta$ data at 1 mol/m$^3$, where the $\zeta$-plane is held fixed at the OHP. With the parameters obtained in this way, the $\zeta$ measurements at the higher concentrations (10 mol/m$^3$ and 100 mol/m$^3$) are fitted using the location of the $\zeta$-plane as a variable.

## 3. Experimental

Suspensions of $\gamma$-alumina powders in ultrapure water were prepared for the mobility experiments using unsupported alumina films. The preparation of unsupported and supported $\gamma$-alumina has been described in detail elsewhere (Leenaars and Burggraaf, 1985; Uhlhorn *et al.*, 1992). The unsupported material exhibits the same surface properties as the supported NF membrane material (Uhlhorn *et al.*, 1992) and has an average pore size of ≈4 nm (Nijmeijer *et al.*, 2001) and a specific surface area of ≈250 m$^2$/g (Lin, De Vries and Burggraaf, 1991; Uhlhorn *et al.*, 1992). The porosity of the material is ≈50% (Uhlhorn *et al.*, 1992; Benes *et al.*, 2001). After grinding in a mortar, the films were suspended in ultrapure water. The solid concentration was 1 kg/m$^3$. Vigorous ultrasonic treatment and consecutive fractionation after sedimentation was applied to reduce the particle size from

≈2 μm (after grinding in the mortar) to ≈0.5 μm. Subsequently, the alumina suspension was concentrated by evaporating most of the ultrapure water.

Aqueous electrolyte solutions were prepared from high-grade chemicals (Merck Eurolab) in ultrapure water. To obtain the desired pH, 0.25M HCl and 0.25M NaOH was added for the NaCl and $CaCl_2$ solutions, while 0.25M $H_2SO_4$ and 0.25M NaOH was used for the $Na_2SO_4$ solutions. Of the concentrated suspension, 1 ml was added to 80 ml of electrolyte solution at the desired pH in a polyethylene bottle. The system was then left to equilibrate for 12-24 hours after which the pH was readjusted to the desired value and equilibrated for another 12 hours before measurement. Mobility to zeta potential conversion is done using the theory of O'Brien and White (1978).

The electrophoretic mobility and particle size measurements were performed using a Malvern ZetaSizer 3000HSa. The temperature of the samples during the measurements was maintained at 25 ± 0.2 °C using a Haake D8 water bath with water-cooling.

## 4. Results and Discussion

In chapter 5 of this thesis a Basic Stern (BS) double layer description (see Westall and Hohl, 1980) was used for the fitting of NaCl zeta potential and surface charge data of Sprycha (1989). Using the adsorption parameters derived from the zeta potential fit, the surface charge was calculated. It was shown that using the BS approach the predicted surface charge values grossly underestimated the measured $\sigma_0$-pH data. For the electrophoretic mobility measurements in this paper the BS double layer description was not only tested for NaCl but also for $CaCl_2$ and $Na_2SO_4$. The BS predictions showed that it was not possible to obtain a good description of all zeta potential curves, and predict the surface charge data satisfactorily as well.

Various other double layer models were tested; the most satisfactory results were obtained with the triple-layer (TL) model due to Yates, Levine and Healy (1974), see Figure 1, which was extended by considering the ζ–plane to be variable. The TL model is used for all the model predictions presented below.

## 4.1 Zeta potential data

### 4.1.1 NaCl

Figure 2 shows ζ as a function of pH for three NaCl concentrations. The iso-electric point (IEP) is observed at pH = 8.3 (the variation of the IEP with bulk concentration is within experimental error). This value agrees well literature data for γ-alumina (Parks, 1965; Sprycha, 1989). The symmetry in the curves indicates equally strong adsorption of sodium and chloride ions, $\log(K_{Na})= \log(K_{Cl})$, which is typical for an electrolyte that does not specifically adsorb like NaCl. Hence for the 1-pK model $pK_1^+=8.3$ (as there is no specific adsorption, the IEP coincides with the PZC).

The solid lines in Figure 2 indicate model predictions for ζ, in which the 1-pK model is combined with a TL model. For the 1-pK model, the restrictions $\log(K^+)=8.3$ and $\log(K_{Na})=\log(K_{Cl})$ were used in the model calculations. The model parameters are listed in Table 1.

For the logarithm of the adsorption equilibrium constants for $Na^+$ and $Cl^-$ a value of –0.7 was obtained, in between the data of Hiemstra, Yong and Van Riemsdijk (1999) who used two adsorption sites (s1, s2) and found $\log(K_{Na,\,s1})=0.2$, $\log(K_{Cl,\,s1})=-0.2$, and $\log(K_{Na,\,s2})=\log(K_{Cl,\,s2})=-1.5$. In literature typically a value of ≈1 C/(V·m2) is found for $C_1$ (e.g., Yates, Levine and Healy, 1974; Davis, James and Leckie, 1978; He *et al.*, 1997; Sahai and Sverjensky, 1997; Hiemstra, Yong and Van Riemsdijk, 1999), and the value of 1.2 C/(V·m2) we obtained is in good agreement with literature. The capacity of the outer Helmholtz plane, $C_2$, is very low ($C_2$=0.05 C/(V·m2)) and does not

relate well to literature (Yates, Levine and Healy, 1974; Davis, James and Leckie, 1978; He *et al.*, 1997; Sahai and Sverjensky, 1997) were generally a value of 0.2 C/(V·m2) is used. It is unclear what causes this discrepancy. However, recently Hiemstra, Yong and Van Riemsdijk (1999) derived a value of 5.0 C/(V·m2). It therefore remains difficult to say what a realistic value is for $C_2$.

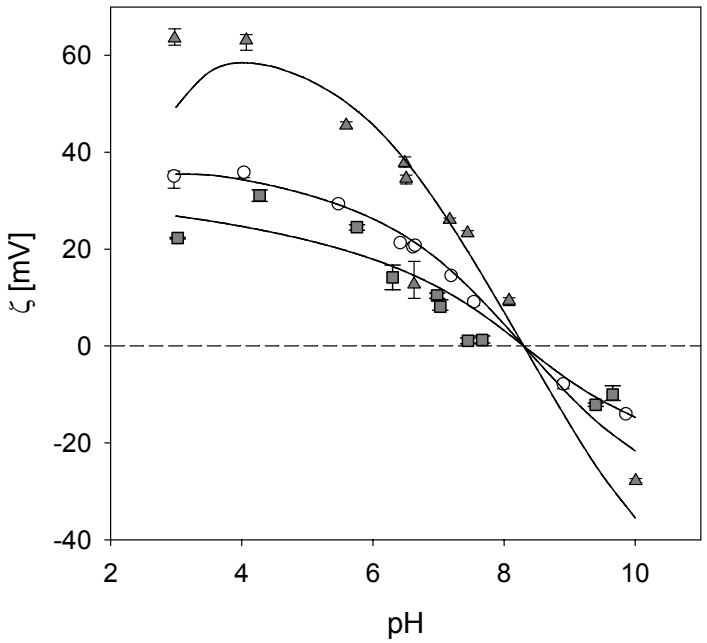


Figure 2: Zeta-potential of γ-alumina as function of pH for NaCl solutions of 1 mol/m$^3$ (triangles), 10 mol/m$^3$ (circles), and 100 mol/m$^3$ (squares). Solid lines are model calculations of the triple-layer model combined with a 1-pK description of the surface adsorption chemistry. The ζ-plane was located at $1\gamma_1$ (1 mol/m$^3$), $0.87\gamma_1$ (10 mol/m$^3$) and $0.7\gamma_1$ (100 mol/m$^3$) of the outer Helmholtz plane.

A 2-pK surface chemistry model in conjunction with the TL model description was also used to model the zeta potential data for NaCl (parameters in Table 1, between brackets). The agreement was not as good (not shown) as for the 1-pK model. Because of the uncertainty in $\Delta pK$ (see

Numerical Solution section) and the fact that the introduction of a proton desorption parameter did not lead to a closer agreement between the predicted and measured ζ data, the 2-pK model was not further explored.

### 4.1.2 $CaCl_2$

Calcium ions are known to exhibit specific adsorption on oxides. Huang and Stumm (1973) showed that the negative zeta potentials of γ-alumina for 0.15 mol/m3 $CaCl_2$, at pH>IEP, became positive if the electrolyte concentration was increased to 1 mol/$m^3$. The calcium concentrations used in NF are often orders of magnitude larger than those used by Huang and Stumm.

Figure 3 shows that for such higher concentrations ζ is positive over the entire pH range for our γ-alumina NF material, indicating super-equivalent adsorption, that is, overcompensation of the surface charge (see Lyklema, 1995) of $Ca^{2+}$. At low pH and 1 mol/$m^3$ the zeta potential for $CaCl_2$ decreases similarly to that for NaCl. This is probably caused by the high positive surface charge of the material that prevents the specific adsorption of calcium ions by means of electrostatic repulsion (note that for the calcium chloride mobility measurements, HCl and NaOH were used to adjust the pH, resulting in the presence of an additional cation ($Na^+$) at alkaline pH). Because of specific adsorption, ζ increases at high pH for the highest calcium concentrations, overcompensating the negative surface charge.

Contrary to the fit for NaCl, the calcium chloride mobility data cannot be accurately described with the 1-pK TL model. Especially the variations in ζ at 10 and 100 mol/$m^3$ cannot be represented well (Figure 3). For the fit it was assumed that NaCl adsorption equilibrium constants are not influenced by the presence of the calcium ions, and hence p$K^+$, p$K_{Cl}$ and p$K_{Na}$ were kept at the fixed value derived from the experiments with NaCl. Only $C_1$, $C_2$ and p$K_{Ca}$ were allowed to vary. For the best fit, $C_1$ and $C_2$ could be maintained

identical to the values for NaCl, as expected. The logarithm of the adsorption constant for calcium was 3.4. Huang and Stumm (1973) only calculated 'operational' (including the Boltzmann term $\exp(-F\phi/RT)$) equilibrium constants for the complexation of calcium. It is therefore not possible to relate our $\log(K_{Ca})$ to their results.

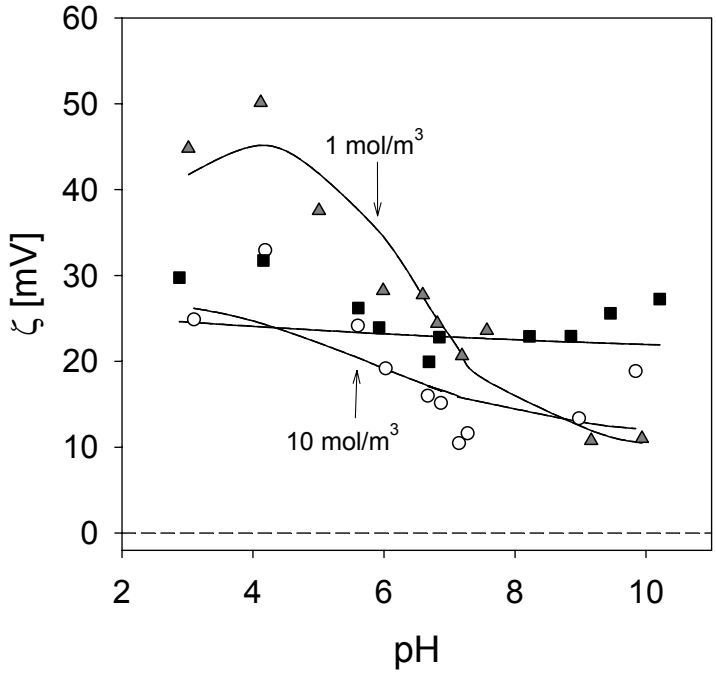


Figure 3: Zeta potential of γ-alumina as function of pH for $CaCl_2$ solutions of 1 mol/m³ (triangles), 10 mol/m³ (circles), and 100 mol/m³ (squares). Error bars are omitted for clarity. Solid lines are model calculations of the triple-layer model combined with a 1-pK description of the surface adsorption chemistry. The ζ-plane was located at $1\gamma_1$ (1 mol/m³), $0.87\gamma_1$ (10 mol/m³) and $0.7\gamma_1$ (100 mol/m³) of the outer Helmholtz plane.

### 4.1.3 $Na_2SO_4$

Sulphate ions interact quite strongly with γ-alumina, sometimes irreversibly changing the surface structure. Fortunately, for the γ-alumina NF membrane material studied here, adsorbed $SO_4^{2-}$ ions can be removed by thoroughly

rinsing the membrane with ultrapure water and no irreversible behaviour is observed. This reversibility effect might be an indication that sulphate is not strongly chemically adsorbed on this γ-alumina, as is commonly assumed. However, due to sulphate adsorption a large decrease of ζ at low pH values and a shift of the IEP to lower pH is observed (Figure 4). For 100 mol/m$^3$ the potential is negative throughout the entire pH range. The latter behaviour was also found for zirconia NF materials by Randon *et al.* (1991a, b) and Vacassy *et al.* (1997).

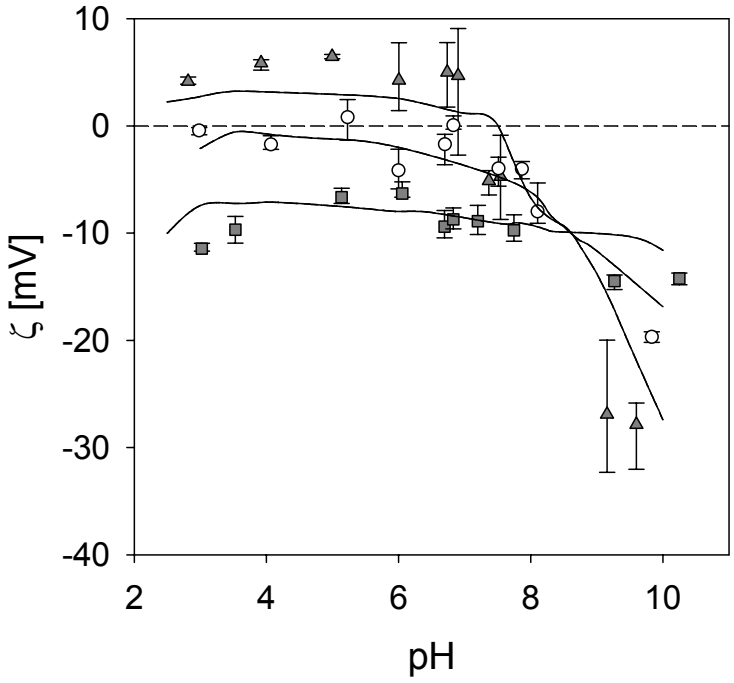


Figure 4: Zeta potential of γ-alumina as function of pH for $Na_2SO_4$ solutions of 1 mol/m$^3$ (triangles), 10 mol/m$^3$ (circles), and 100 mol/m$^3$ (squares). Solid lines are model calculations of the triple-layer model combined with a 1-pK description of the surface adsorption chemistry. The ζ-plane was located at $1\gamma_1$ (1 mol/m$^3$), $0.75\gamma_1$ (10 mol/m$^3$) and $0.65\gamma_1$ (100 mol/m$^3$) of the outer Helmholtz plane.

The complicated variation in ζ is difficult to describe with the 1-pK TL model (Figure 4), though the agreement between the solid model lines and the

measurement data is acceptable. The $SO_4^{2-}$ and $HSO_4^-$ ions are assumed to be the adsorbing species. Due to a lack of detailed surface information the adsorption constants for both ions are set equal, which results in $\log(K_{SO4})=\log(K_{HSO4})=2.5$. This value is significantly lower than the results from He *et al.* (1997), $\log(K_{SO4})\approx11.5$, $\log(K_{HSO4})\approx16.5$, and the data from Jablonski *et al.* (2000), $\log(K_{SO4})\approx7.1$. For a good fit, the ζ–plane for 10 mol/m$^3$ and 100 mol/m$^3$ is placed at 0.75 and 0.65 times the thickness $\gamma_1$ of the OHP (compared to $0.87\gamma_1$ and $0.7\gamma_1$ for NaCl and $CaCl_2$).

| | NaCl | $CaCl_2$ | $Na_2SO_4$ |
|---|---|---|---|
| $\log(K^+)$ | 8.3 (5.2) | 8.3 | 8.3 |
| $\log(K^-)$ | (11.6) | | |
| $\log(K_{Na})$ | -0.7 (1.1) | -0.7 | -0.7 |
| $\log(K_{Cl})$ | -0.7 (1.3) | -0.7 | |
| $\log(K_{Ca})$ | | 3.4 | |
| $\log(K_{SO4})$ | | | 2.5 |
| $\log(K_{HSO4})$ | | | 2.5 |
| $C_1$ [C/(V·m$^2$)] | 1.2 (1.3) | 1.2 | 1.2 |
| $C_2$ [C/(V·m$^2$)] | 0.05 (0.022) | 0.05 | 0.05 |
| ζ-plane* | $1\gamma_1$, $0.87\gamma_1$, $0.7\gamma_1$ | $1\gamma_1$, $0.87\gamma_1$, $0.7\gamma_1$ | $1\gamma_1$, $0.75\gamma_1$, $0.65\gamma_1$ |
| $c_{tot}^{//}$ [mol/m$^2$] | $1.33\cdot10^{-5}$ | $1.33\cdot10^{-5}$ | $1.33\cdot10^{-5}$ |

* For 1, 10 and 100 mol/m$^3$, respectively.

Table 1: Overview of the adsorption parameters obtained from zeta potential fits. 2-pK model parameters between brackets.

## 4.2 Comparison of model surface charge predictions with literature titration data

Having established the required adsorption parameters with an adsorption model, the surface charge, $\sigma_0$, can be calculated. To test the applicability of our approach, the surface charge predicted with the 1-pK TL model was compared with $\sigma_0$ from potentiometric titration experiments from literature (Huang and Stumm, 1973; Sprycha, 1989; Jablonski *et al.*, 2000).

Previously, this approach was only taken the other way around, i.e., zeta potentials were predicted using adsorption parameters fitted on experimental surface charge data (Yates, Levine and Healy, 1974; Hiemstra, Yong and Van Riemsdijk, 1999). Titration data were used for the comparison since with this technique $\sigma_0$ can be directly obtained from experiments.

For the modelling of the surface charge, the adsorption parameters in Table 1 were used with the exception of the proton adsorption constant. The value of $\log(K^+)$ was adjusted to the point of zero charge (PZC) of the literature γ-alumina involved.

For a γ-alumina with a PZC of 8.1, Sprycha (1989) performed titration experiments at different NaCl concentrations. The surface charge he obtained is compared to our model predictions in Figure 5. Considering the possible variations in experimental procedures between our electrophoretic mobility experiments and the titration experiments of Sprycha, as well as the potential difference in the surface (crystal) structure of both γ-alumina materials, the model predictions and the titration data are in fair agreement. In retrospect, the model predictions in chapter 5 underestimated $\sigma_0$ by a factor of 5.

Apart from mobility experiments, Huang and Stumm (1973) also performed titration experiments on a γ-alumina (PZC=8.5) in the presence of calcium chloride. We calculated $\sigma_0$ from their titration results but obtained unreasonably small values at high pH values for the lowest concentration they used (0.15 mol/m$^3$) and a behaviour for the highest concentration (1 mol/m$^3$) and pH values that was difficult to interpret (data not shown). Therefore it was decided not to use the titration data of Huang and Stumm for a qualitative comparison.

Recently, Jablonski *et al.* (2000) presented $\sigma_0$-pH data for sodium sulphate adsorption on a γ-alumina with a PZC of 7.6 for $SO_4^{2-}$ concentrations of 1, 10

and 100 mol/m$^3$. They found a considerable effect of the $Na_2SO_4$ concentration on the PZC, which shifted to higher pH for increasing concentrations (PZC=8.1 at 1 mol/m3, PZC=8.5 at 100 mol/m$^3$) as expected. However, according to the data of Jablonski *et al.* the surface charge of 1 and 10 mol/m$^3$ are equal for pH>PZC. Secondly, at 100 mol/m$^3$ they find a lower $\sigma_0$ for pH>PZC than for lower concentrations. Both results are quite unexpected. It was therefore decided not to use their titration data to determine the sulphate adsorption parameters.

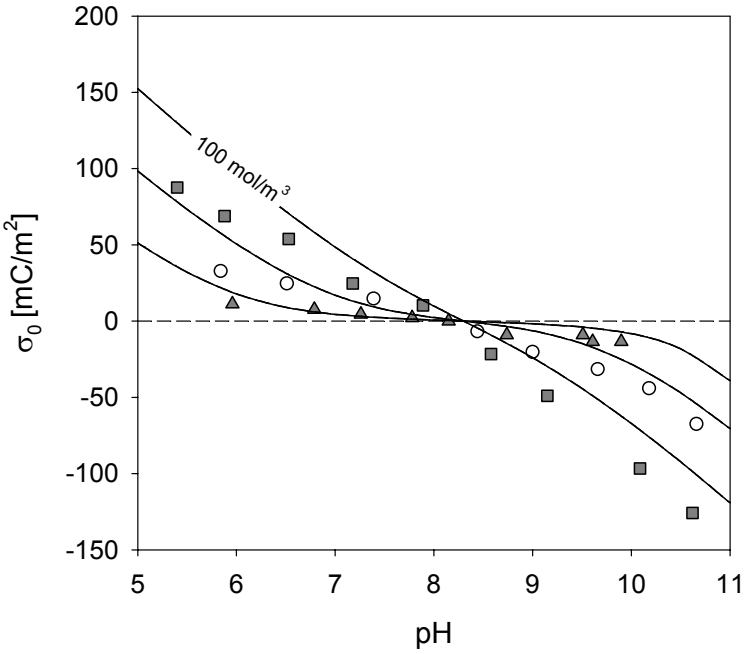


Figure 5: Surface charge of γ-alumina as function of pH for NaCl solutions of 1 mol/m$^3$ (triangles), 10 mol/m$^3$ (circles), and 100 mol/m$^3$ (squares). Data obtained by Sprycha (1989) from potentiometric titration experiments. Solid lines are model calculations.

## 4.3 Predicting NF separation performance using ion-adsorption

Taking the zeta potential and surface charge results into account, the proposed 1-pK TL model approach appears to be a usable description for the ion adsorption behaviour on γ-alumina. Due to a lack of available

experimental (titration) data on the adsorption of divalent ions, estimations of some model parameters for such systems may be uncertain and more detailed experimental studies on the NF material should be conducted to improve the model predictions.

The electrophoretic mobility measurements have shown that the type of electrolyte, its concentration and the solution pH strongly determine the surface properties of the NF material. As the charging behaviour is directly related to the separation performance of a NF membrane, the importance of ion-adsorption in the understanding and characterization of NF separation should be clear.

### 4.4 pH stability of γ-alumina

For the applicability of the discussed surface chemistry characterization it is important to briefly address the matter of γ-alumina stability at extreme pH. Experimental evidence suggests that the material is stable at pH>3 (Hofman-Züter, 1995), and for this reason we have chosen this pH as the lower limit for our mobility experiments. Of the stability in the alkaline region little is known as yet. Preliminary experiments in our own lab suggest that pH=10 is the upper stability limit and consequently this value was not exceeded in our electrophoretic mobility measurements. It should be remarked that it is difficult to define a proper pH-stability criterion since at all pH values alumina will dissolve to some extent in aqueous solutions. Horst and Höll (1997) for example investigated the pH stability of the commercial γ-aluminas Compalox AN/V800 and Alcoa/F1 and they found a stable pH range of 5<pH<10.

## 5. Conclusions

Electrophoretic mobility measurements on γ-alumina NF membrane particle suspensions were performed in 1, 10 and 100 mol/m$^3$ electrolyte solutions of NaCl, $CaCl_2$ and $Na_2SO_4$. On the basis of these measurements and supporting titration evidence from literature, an internally consistent adsorption model was constructed. This model was applied to extract the ion-material adsorption parameters from the mobility measurements.

A 1-pK modified triple-layer model was able to predict the experimentally observed zeta potential behaviour. It was found that for a proper adsorption description the overall ionic conductivity was not only determined by the concentration of ions in the diffuse double layer, but also partly by ions in the outer Helmholtz plane. The zeta potential was therefore assumed to be located at a certain fraction within the OHP.

Generally, the obtained adsorption parameters were in reasonable agreement with literature values. An implication of this work for the understanding of NF separation behaviour is illustrated below for a γ-alumina membrane used to retain a 5 mol/m$^3$ sodium sulphate solution. Operating the NF process in the commonly used neutral pH range (5<pH<7), the retention will be undesirably low, as ζ is very low in that pH range (see Figure 4). Instead, operating this membrane at much higher pH values of around 10, the retention can be expected to increase considerably. This effect was indeed observed experimentally by Hofman-Züter (1995) who measured the retention of a γ-alumina membrane for a 5 mol/m$^3$ $Na_2SO_4$ solution at a pressure difference of 0.5 MPa. At pH=5.6 she observed zero retention, while for the solution at pH=10.2 the retention increased to 50%.

## References


1. Benes N.E., Spijksma G., Verweij H., Wormeester H., and Poelsema B., "CO2 Sorption of a Thin Silica Layer determined by Spectroscopic Ellipsometry,", *AIChE J.*, **47**, 1212 (2001).
2. Bousse L., de Rooij N.F., and Bergveld P., "The Influence of Counter-Ion Adsorption on the ψ0/pH Characteristics of Insulator Surfaces," *Surf. Sci.*, **135**, 479 (1983).
3. Chan D.Y.C., Perram J.W., White L.R., and Healy T.W., "Regulation of Surface Potential at Amphoteric Surfaces During Particle-Particle Interaction," *J. Chem. Soc. Faraday Trans. I*, **71**, 1046 (1975).
4. Curtin D., and Syers J.K., "Mechanism of Sulfate Adsorption by Two Tropical Soils," *J. Soil Sci.*, **41**, 295 (1990).
5. Davies C.W., "Ion Association," Butterworths, London, 1962, p. 41.
6. Davis J.A., James R.O., and Leckie J.O., "Surface Ionization and Complexation at the Oxide/Water Interface. I. Computation of Electrical Double Layer Properties in Simple Electrolytes," *J. Colloid Interface Sci.*, **63**, 480 (1978).
7. Hall M.S., Starov V.M., and Lloyd D.R., "Reverse Osmosis of Multicomponent Electrolyte Solutions. Part I. Theoretical Development," *J. Membrane Sci.*, **128**, 23 (1997).
8. Hall M.S., Lloyd D.R., and Starov V.M., "Reverse Osmosis of Multicomponent Electrolyte Solutions. Part II. Experimental Verification," *J. Membrane Sci.*, **128**, 39 (1997).
9. He L.M., Zelazny L.W., Baligar V.C., Ritchey K.D., and Martens D.C., "Ionic Strength Effects on Sulfate and Phosphate Adsorption on γ-Alumina and Kaolinite: Triple-Layer Model," *Soil Sci. Soc. Am. J.*, **61**, 784 (1997).
10. Healy T.W., and White L.R., "Ionizable Surface Group Models of Aqueous Interfaces," *Adv. Colloid Interface Sci.*, **9**, 303 (1978).
11. Hiemstra T., Van Riemsdijk W.H., and Bruggenwert M.G.M., "Proton Adsorption Mechanism at the Gibbsite and Aluminium Oxide Solid/Solution Interface," *Neth. J. Agric. Sci.*, **35**, 281 (1987).
12. Hiemstra T., Van Riemsdijk W.H., and Bolt G.H., "Multisite Proton Adsorption Modeling at the Solid/Solution Interface of (Hydr)oxides: A New Approach. I. Model Description and Evaluation of Intrinsic Reaction Constants," *J. Colloid Interface Sci.*, **133**, 91 (1989).
13. Hiemstra T., De Wit J.C.M., and Van Riemsdijk W.H., "Multisite Proton Adsorption Modeling at the Solid/Solution Interface of (Hydr)oxides: A New Approach. II. Application to Various Important (Hydr)oxides," *J. Colloid Interface Sci.*, **133**, 105 (1989).

14. Hiemstra T., and Van Riemsdijk W.H., "A Surface Structural Approach to Ion Adsorption: The Charge Distribution (CD) Model," *J. Colloid Interface Sci.*, **179**, 488 (1996).
15. Hiemstra T., Yong H., and Van Riemsdijk W.H., "Interfacial Charging Phenomena of Aluminium (Hydr)oxides," *Langmuir*, **15**, 5942 (1999).
16. Hofman-Züter J.M., "Chemical and Thermal Stability of (Modified) Mesoporous Ceramic Membranes," Ph.D. Thesis, University of Twente, The Netherlands, 1995.
17. Horst J., and Höll W.H., "Application of the Surface Complex Formation Model to Ion Exchange Equilibria. Part IV: Amphoteric Sorption onto γ-Aluminum Oxide," *J. Colloid Interface Sci.*, **195**, 250 (1997).
18. Huang C-P., and Stumm W., "Specific Adsorption of Cations on Hydrous γ-$Al_2O_3$," *J. Colloid Interface Sci.*, **43**, 409 (1973).
19. Jablonski J., Janusz W., Reszka M., Sprycha R., and Szczypa J., "Mechanism of Adsorption of Selected Monovalent and Divalent Inorganic Ions at the Alumina/Electrolyte Interface," *Polish J. Chem.*, **74**, 1399 (2000).
20. Johnson jr. R.E., "A Thermodynamic Description of the Double Layer Surrounding Hydrous Oxides," *J. Colloid Interface Sci.*, **100**, 540 (1984).
21. Koopal L.K., Van Riemsdijk W.H., and Roffey M.G., "Surface Ionization and Complexation Models: A Comparison of Methods for Determining Model Parameters," *J. Colloid Interface Sci.*, **118**, 117 (1987).
22. Kummert R., and Stumm W., "The Surface Complexation of Organic Acids on Hydrous γ-$Al_2O_3$," *J. Colloid Interface Sci.*, **75**, 373 (1980).
23. Leenaars A.F.M., and Burggraaf A.J., "The Preparation and Characterization of Alumina Membranes with Ultrafine Pores. 2. The Formation of Supported Membranes," *J. Colloid Interface Sci.*, **105**, 27 (1985).
24. Lin Y.S., De Vries K.J., and Burggraaf A.J., "Thermal Stability and its Improvement of the Alumina Membrane Top-Layers prepared by Sol-Gel Methods," *J. Mater. Sci.*, **26**, 715 (1991).
25. Lyklema J., "Fundamentals of Interface and Colloid Science. Volume II: Solid-Liquid Interfaces," Academic Press, London, 1995, chapter 3.
26. Lyklema J., Minor M., "On Surface Conduction and its Role in Electrokinetics," *Coll. Surf. A*, **140**, 33 (1998).
27. Mangelsdorf C.S., and White L.R., "Effects of Stern-layer Conductance on Electrokinetic Transport Properties of Colloidal Particles," *J. Chem. Soc. Faraday Trans.*, **86**, 2859 (1990).
28. Minor M., Van der Linde A.J., and Lyklema J., "Streaming Potentials and Conductivities of Latex Plugs in Indifferent Electrolytes," *J. Colloid Interface Sci.*, **203**, 177 (1998).

29. Morterra C., and Magnacca G., "A Case Study : Surface Chemistry and Surface Structure of Catalytic Aluminas, as studied by Vibrational Spectroscopy of Adsorbed Species," *Catal. Today*, **27**, 497 (1996).
30. Nijmeijer A., Kruidhof H., Bredesen R., and Verweij H., "Preparation and Properties of Hydrothermally Stable γ-Alumina Membranes," *J. Am. Ceram. Soc.*, **84**, 136 (2001).
31. Ninham B.W., and Parsegian V.A., "Electrostatic Potential Between Surfaces Bearing Ionizable Groups in Ionic Equilibrium with Physiologic Saline Solution," *J. Theor. Biol.*, **31**, 405 (1971).
32. O'Brien R.W., and White L.R., "Electrophoretic Mobility of a Spherical Colloidal Particle," *J. Chem. Soc. Faraday Trans. II*, **74**, 1607 (1978).
33. Parks G.A., "The Isoelectric Points of Solid Oxides, Solid Hydroxides, and Aqueous Hydroxo Complex Systems," *Chem. Rev.*, **65**, 177 (1965).
34. Peri J.B., "Infrared Study of Adsorption of Carbon Dioxide, Hydrogen Chloride and Other Molecules on Acid Sites on "Dry" Silica-Alumina and γ-alumina," *J. Phys. Chem.*, **70**, 3168 (1966).
35. Press W.H., Teukolsky S.A., Vetterling W.T., and Flannery B.P., "Numerical Recipes in Fortran 77, 2nd edition, Cambridge University Press, Cambridge," 1992, pp. 402-406.
36. Randon J., Larbot A., Cot L., Lindheimer M., and Partyka S., "Sulfate Adsorption on Zirconium Dioxide," *Langmuir*, **7**, 2654 (1991).
37. Randon J., Larbot A., Guizard C., Cot L., Lindheimer M., and Partyka S., "Interfacial Properties of Zirconium Dioxide Prepared by the Sol-Gel Process," *Colloids and Surfaces*, **52**, 241 (1991).
38. Rowlands W.N., O'Brien R.W., Hunter R.J., and Patrick V., "Surface Properties of Aluminum Hydroxide at High Salt Concentrations," *J. Colloid Interface Sci.*, **188**, 325 (1997).
39. Sahai N., and Sverjensky A., "Evaluation of Internally Consistent Parameters for the Triple-Layer Model by the Systematic Analysis of Oxide Surface Titration Data," *Geochim. Cosmochim. Acta*, **61**, 2801 (1997).
40. Sohlberg K., Pennycook S.J., and Pantelides S.T., "The Bulk and Surface Structure of γ-Alumina," *Chem. Eng. Comm.*, **181**, 107 (2000).
41. Sprycha R., "Electrical Double Layer at Alumina/Electrolyte Interface. I. Surface Charge and Zeta Potential," *J. Colloid Interface Sci.*, **127**, 1 (1989).
42. Starov V.M., Bowen W.R., and Welfoot J.S., "Flow of Multicomponent Electrolyte Solutions through Narrow Pores of Nanofiltration Membranes," *J. Colloid Interface Sci.*, **240**, 509 (2001).

43. Uhlhorn R.J.R., Huis in't Veld M.H.B.J., Keizer K., and Burggraaf A.J., "Synthesis of Ceramic Membranes. Part I. Synthesis of Non-Supported and Supported γ-Alumina Membranes without Defects," *J. Mater. Sci.*, **27**, 527 (1992).
44. Vacassy R., Guizard C., Thoraval V., and Cot L., "Synthesis and Characterization of Microporous Zirconia Powders: Application in Nanofilters and Nanofiltration Characteristics," *J. Membrane Sci.*, **132**, 109 (1997).
45. Westall J., "Chemical Equilibrium Including Adsorption of Charged Surfaces," in Advances in Chemistry Series, Leckie J., and Kavanaugh M. (eds.), *Am. Chemical Soc.*, Washington, 1980, pp. 33-44.
46. Westall J., and Hohl H., "A Comparison of Electrostatic Models for the Oxide/Solution Interface," *Adv. Colloid Interface Sci.*, **12**, 265 (1980).
47. Yates D.E., Levine S., and Healy T.W., "Site-binding Model of the Electrical Double Layer at the Oxide/Water Interface," *J. Chem. Soc. Faraday Trans. I*, **70**, 1807 (1974).

# Appendix

| Model variables | $\exp\left(\frac{-F\phi_0}{RT}\right)$ | $\exp\left(\frac{-F\phi_1}{RT}\right)$ | $\exp\left(\frac{-F\phi_2}{RT}\right)$ | $AlOH^{-1/2}$ | $H^+$ | $Na^+$ | $Cl^-$ | log(*K*) |
|---|---|---|---|---|---|---|---|---|
| Species | | | | | | | | |
| $OH^-$ | | | | | -1 | | | $\log(K_w)$ |
| $H^+$ | | | | | 1 | | | 0 |
| $Na^+$ | | | | | | 1 | | 0 |
| $Cl^-$ | | | | | | | 1 | 0 |
| $AlOH^{-1/2}$ | | | | 1 | | | | 0 |
| $AlOH_2^{+1/2}$ | 1 | | | 1 | 1 | | | $\log(K^+)$ |
| $AlOH^{-1/2}$-$Na^+$ | | 1 | | 1 | | 1 | | $\log(K_{Na})$ |
| $AlOH_2^{+1/2}$-$Cl^-$ | 1 | -1 | | 1 | 1 | | 1 | $\log(K^+)+\log(K_{Cl})$ |
| Sum | $\frac{\left(\sigma_0 - Fz_{AlOH^{-1/2}} c_{tot}^{//}\right)}{F}$ | $\frac{\sigma_1}{F}$ | $\frac{\sigma_2}{F}$ | $c_{tot}^{//}$ | | | | |

Table A1. Speciation table for calculation of the adsorption parameters from the zeta potential data measured for NaCl.

| Model variables | $\exp\left(\frac{-F\phi_0}{RT}\right)$ | $\exp\left(\frac{-F\phi_1}{RT}\right)$ | $\exp\left(\frac{-F\phi_2}{RT}\right)$ | $AlOH^{-1/2}$ | $H^+$ | $Ca^{2+}$ | $Cl^-$ | $Na^+$ | log(*K*) |
|---|---|---|---|---|---|---|---|---|---|
| Species | | | | | | | | | |
| $OH^-$ | | | | | -1 | | | | $\log(K_w)$ |
| $H^+$ | | | | | 1 | | | | 0 |
| $Ca^{2+}$ | | | | | | 1 | | | |
| $Cl^-$ | | | | | | | 1 | | 0 |
| $Na^+$ | | | | | | | | 1 | 0 |
| $AlOH^{-1/2}$ | | | | 1 | | | | | 0 |
| $AlOH_2^{+1/2}$ | 1 | | | 1 | 1 | | | | $\log(K^+)$ |
| $AlOH^{-1/2}$-$Ca^{2+}$ | | 2 | | 1 | | 1 | | | $\log(K_{Ca})$ |
| $AlOH_2^{+1/2}$-$Cl^-$ | | -1 | | 1 | | | 1 | | $\log(K^+)+\log(K_{Cl})$ |
| $AlOH^{-1/2}$-$Na^+$ | 1 | 1 | | 1 | 1 | | | 1 | $\log(K_{Na})$ |
| Sum | $\frac{\left(\sigma_0 - Fz_{AlOH^{-1/2}} c_{tot}^{//}\right)}{F}$ | $\frac{\sigma_1}{F}$ | $\frac{\sigma_2}{F}$ | $c_{tot}^{//}$ | | | | | |

Table A2. Speciation table for calculation of the adsorption parameters from the zeta potential data measured for $CaCl_2$.

| Model variables | $\exp\left(\frac{-F\phi_0}{RT}\right)$ | $\exp\left(\frac{-F\phi_1}{RT}\right)$ | $\exp\left(\frac{-F\phi_2}{RT}\right)$ | $AlOH^{-1/2}$ | $H^+$ | $Na^+$ | $SO_4^{2-}$ | $HSO_4^-$ | log($K$) |
|---|---|---|---|---|---|---|---|---|---|
| Species | | | | | | | | | |
| $OH^-$ | | | | | -1 | | | | log($K_w$) |
| $H^+$ | | | | | 1 | | | | 0 |
| $Na^+$ | | | | | | 1 | | | 0 |
| $SO_4^{2-}$ | | | | | | | 1 | | 0 |
| $HSO_4^-$ | | | | | | | | 1 | 0 |
| $AlOH^{-1/2}$ | | | | 1 | | | | | 0 |
| $AlOH_2^{+1/2}$ | 1 | | | 1 | 1 | | | | log($K^+$) |
| $AlOH^{-1/2}$-$Na^+$ | | 1 | | 1 | | 1 | | | log($K_{Na}$) |
| $AlOH_2^{+1/2}$-$SO_4^{2-}$ | 1 | -2 | | 1 | 1 | | 1 | | log($K^+$)+log($K_{SO4}$) |
| $AlOH_2^{+1/2}$-$HSO_4^-$ | 1 | -1 | | 1 | 1 | | | 1 | log($K^+$)+log($K_{HSO4}$) |
| Sum | $\frac{\left(\sigma_0 - Fz_{AlOH^{-1/2}}c_{tot}^{//}\right)}{F}$ | $\frac{\sigma_1}{F}$ | $\frac{\sigma_2}{F}$ | $c_{tot}^{//}$ | | | | | |

Table A3. Speciation table for the calculation of the adsorption parameters from the zeta potential data measured for $Na_2SO_4$.

# Chapter 7

## Predictive Charge-Regulation Transport Model for Nanofiltration from the Theory of Irreversible Processes


### Abstract

Equation Section (Next)The charge-regulation concept and theory of irreversible processes are combined to predict multi-component electrolyte transport in NF. Membrane surface charging is described using a 1-pK site-binding model with a triple-layer electrostatic description. Mass transport is described using Maxwell-Stefan relations, based on the uniform potential approach. A predictive model with no adjustable parameters is presented. Input data is obtained from independent measurements, e.g., electrophoretic mobility data. Model predictions for retention and flux are discussed for an asymmetric γ-alumina NF membrane for NaCl and a mixture of NaCl with $CaCl_2$. Double layer overlap in the pores, leading to charge regulation, appears to have a marked influence on the potential across the pore ($\Delta\phi$=59-88 % for 4 nm pores), and thus on separation. Furthermore, the membrane surface charge and potential vary significantly over the pore length, rendering the assumption of a constant charge and potential generally applied in literature questionable. Additionally, the model predicts typical NF behaviour, including non-equal cation and anion retention at extreme pH values, dependencies of retention and flux on the permeability and thickness of the top-layer and the support, and the influence of an additional external mass transport resistance. A sensitivity analysis suggests that for an accurate quantitative prediction of the separation behaviour of inorganic NF membranes it is not possible to use more simple descriptions for ion adsorption and mass transport than the 1-pK triple-layer model and the Maxwell-Stefan relations.

## 1. Introduction

Nanofiltration (NF) of aqueous electrolyte solutions combines high fluxes with acceptable retentions at low pressure differences (Strathmann, 1984; Ho and Sirkar, 1992). This attractive separation behaviour is due to the fact that NF does not rely only on size exclusion, but is mainly governed by electrostatic effects, i.e., repulsion of coions by the surface charge of the membrane. A proper understanding of NF requires adequate understanding of these electrostatic effects, combined with appropriate flux expressions.

Currently, model descriptions of NF systems are generally based on the (extended) Nernst-Planck (NP) transport relations, combined with a Boltzmann-like equilibrium relation at the interfaces and some relation for the membrane charge (Guzmán-Garcia *et al.*, 1990; Bowen and Mukthar, 1996; Hall, Starov and Lloyd, 1997; Hall, Lloyd and Starov, 1997; Yang and Pintauro, 2000; Bowen and Welfoot, 2002). Model variables typically include the surface charge, the pore radius, and an effective membrane thickness. Often these parameters are fitted to retention experiments (Bowen and Mukthar, 1996; Hall, Starov and Lloyd, 1997; Hall, Lloyd and Starov, 1997; Bowen and Welfoot, 2002). For most polymeric membranes this is an acceptable procedure since structural material information is often lacking and the influence of swelling on the membrane properties is not well understood. Guzman-Carcia *et al.* (1990) and Yang and Pintauro (2000) eliminated the need for fitting by obtaining the model parameters, such as the pore radius and membrane charge, from independent experimental measurements. The incorporation of *a-priori* information in their transport model improves its predictive nature. However, both authors (Guzmán-Garcia *et al.*, 1990; Yang and Pintauro, 2000) assume a constant membrane charge, independent of the electrolyte concentration, type of electrolyte and pH, though it is well known that the charge on an amphoteric

material is directly determined by the solution properties (Ninham and Parsegian, 1971; Chan *et al.*, 1975; Davis, James and Leckie, 1978; Healy and White, 1978; chapters 3 and 4 of this thesis).

Compared to organic membranes, the swelling of inorganic membranes is negligible and structural features can be better characterised (Leenaars and Burggraaf, 1984; Leenaars and Burggraaf, 1985a; Leenaars & Burggraaf, 1985b; Uhlhorn *et al.*, 1992; Benes, 2000; Benes *et al.*, 2001; Nijmeijer *et al.*, 2001). Furthermore, the charging behaviour of inorganic membranes can be predicted from independent measurements (Combe *et al.*, 1997; Palmeri *et al.*, 2000; chapter 6 of this thesis). A transport model for inorganic NF membranes can therefore be made without any adjustable parameters, making it truly predictive.

In chapter 4 of this thesis a predictive NF model was developed based on a combination of the Nernst-Planck (NP) flux equations with the theory of charge regulation (CR). The CR model consisted of a 2-pK site-binding description and a diffuse double layer model to describe ion adsorption and account for double layer overlap in the membrane pores (Ninham and Parsegian, 1971; Chan *et al.*, 1975). This transport model was able to qualitatively predict separation on a ceramic γ-alumina membrane for a binary electrolyte solution and multi-component mixtures.

Electrophoretic mobility studies on γ-alumina (chapter 6 of this thesis) suggest that a more complicated double layer model, a triple-layer model, is required to describe membrane charging. Furthermore, for a correct quantitative description of the membrane separation behaviour the NP expressions used in chapter 4 of this thesis have to be extended. Electrolyte transport in the membrane, for example, has to be corrected for the constraints imposed by the porous matrix. To avoid the implicit assumptions underlying the NP expressions, our starting point in this work is therefore the general Maxwell-Stefan approach.

In the current effort, the approach in chapter 4 is elaborated and a quantitative transport description for ceramic NF membranes is developed without any adjustable parameters. The charging properties (i.e., charge and potential) are obtained from independent zeta potential measurements on isolated particles (chapter 6) and additional material properties are obtained using various experimental techniques. The charge regulation (CR) concept is invoked to account for double layer overlap in the membrane. Both approaches are combined with the Maxwell-Stefan transport relations. The model is applied to study the separation properties of an asymmetric α-alumina supported γ-alumina membrane.

## 2. Theory

### 2.1 One-dimensional NF membrane model

In this section the Maxwell-Stefan transport relations, Eq. [1], are combined with the concept of charge regulation to predict mass transport of simple electrolytes in an α–alumina supported γ-alumina NF membrane (Leenaars and Burggraaf, 1984; Leenaars and Burggraaf, 1985a; Leenaars and Burggraaf, 1985b; Uhlhorn *et al.*, 1992) in a pressure-driven dead-end permeation set-up (see Figure 1).

$$-x_i\nabla\ln\left(\gamma_i x_i\right)-\frac{\bar{V}_i}{RT}x_i\nabla p-\frac{F}{RT}x_i z_i\nabla\phi-H_i^{\mathrm{c}}\frac{x_i}{\mathcal{D}_{i\mathrm{M}}^{\mathrm{eff}}}\mathbf{v}=\sum_{\ell=1}^{n}\frac{x_\ell\mathbf{N}_i-x_i\mathbf{N}_\ell}{c\mathcal{D}_{i\ell}^{\mathrm{eff}}}+\frac{\mathbf{N}_i}{c\mathcal{D}_{i\mathrm{M}}^{\mathrm{eff}}}. \qquad [1]$$

#### 2.1.1 Model restrictions

The major assumptions in the model include:

- isothermal,

- 1D transport,
- steady state: $\mathrm{d}N_i/\mathrm{d}z = 0$,
- uniform potential approach (Hawkins Cwirko and Carbonell, 1989; Bowen and Mukthar, 1996; chapter 4 of this thesis).
- external mass transport located in stagnant film

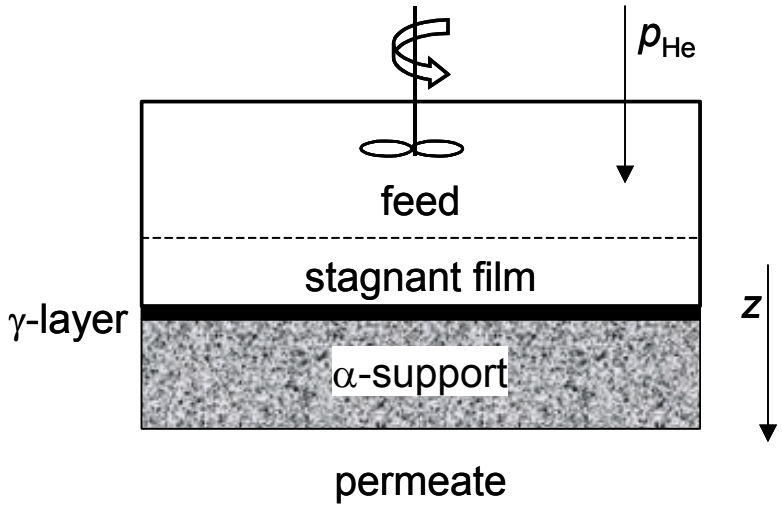


Figure 1: Model of dead-end membrane permeation set-up.

### 2.1.2 Convective flow

Metha *et al.* (1976) showed that for an electrolyte solution the convective velocity $v$ is given by

$$v = -\frac{B_0}{\mu}\left(\frac{\mathrm{d}p}{\mathrm{d}z} + cF\sum_{\ell=1}^{n} x_\ell z_\ell \frac{\mathrm{d}\phi}{\mathrm{d}z}\right) \qquad [2]$$

where the permeability $B_0$ contains the structural properties of the porous matrix ($B_0$ can be obtained from flux measurements of a neutral solvent) and $\mu$ is the Newtonian viscosity. The convective velocity in Eq. [2] is defined as a superficial velocity (i.e., volume flow per area of membrane). Eq. [2] was also

derived in chapter 4 of this thesis although there $v$ is defined interstitially (i.e., volume flow per pore area).

### 2.1.3 Fluxes

The model system can be divided up into three sections: stagnant film, γ-layer, and support. For each section a different flux expression is required. The stagnant film consists of a free solution with no pressure and potential differences. The corresponding terms drop out of the left-hand side of Eq. [1]. At the right-hand side of this expression the contributions from the matrix should be omitted and the stagnant film equation is

$$-x_i \frac{\mathrm{d}\ln\left(\gamma_i x_i\right)}{\mathrm{d}z} = \sum_{\ell=1}^{n} \frac{x_\ell N_i - x_i N_\ell}{c\mathcal{D}_{i\ell}}. \qquad [3]$$

The electrolyte activity coefficients $\gamma_i$ in Eq. [3] are a function of the ionic strength $I$ and can be obtained from the empirical Davies relation (Davies, 1962),

$$-\log\left(\gamma_i\right) = 0.51 z_i^2 \left( \frac{\sqrt{I}}{1+\sqrt{I}} - 0.2I \right). \qquad [4]$$

The water activity is assumed unity.

For the separating γ-layer the full MS expressions, Eq. [1], can be used directly. The support is designed to provide mechanical strength and does not exhibit separating properties. As the pores of the support are large, convection will be the dominating transport mechanism. For the support the MS equations reduce to Darcy's law (Bird, Stewart and Lightfoot, 1960),

$$v = -\frac{B_0^{\mathrm{s}}}{\mu}\frac{\mathrm{d}p}{\mathrm{d}z}. \qquad [5]$$

### 2.1.4 Interfaces

Assuming local thermodynamic equilibrium at the interfaces of the membrane top layer results in the extended Boltzmann expression

$$\gamma_i^{(+)} x_i^{(+)} = h_i \gamma_i^{(-)} x_i^{(-)} \exp\left[\frac{-z_i F}{RT}\left(\phi^{(+)} - \phi^{(-)}\right)\right] \exp\left[\frac{-\bar{V}_i}{RT}\left(p^{(+)} - p^{(-)}\right)\right], \qquad [6]$$

where the superscripts (+) and (-) denote locations just inside and outside the interface, respectively, and the term $h_i$ accounts for steric hindrance effects (see Appendix). The second exponential term in Eq. [6] represents pressure differences due to osmotic effects (e.g., see also Eq. [8] in Noordman *et al.*, 1997).

Eq. [6] can be elaborated by incorporating hydration (or dielectric) effects (Guzmán-Garcia *et al.*, 1990; Yang and Pintauro, 2000; Bowen and Welfoot, 2002). However, generally authors (Combe *et al.*, 1997; Palmeri *et al.*, 2000; Labbez *et al.*, 2002; Van Gestel *et al.*, 2002) have found experimental retentions close to zero at the iso-electric point of inorganic membrane materials, indicating that separation is primarily determined by electrostatic phenomena and dielectric exclusion is probably small.

### 2.1.5 Additional relations

At any location in the system the mole fractions should be equal to one (Noordman *et al.*, 1997)

$$\sum_{\ell=1}^{n} x_\ell = 1, \qquad [7]$$

Electroneutrality must hold everywhere in the system. For the free solution this results in

$$\sum_{\ell=1}^{n} z_\ell x_\ell = 0 \,. \qquad [8]$$

Because in this model separation is assumed to occur only in the membrane top-layer, the surface charge has to be taken into account only in the pores of the γ-alumina layer (see the Appendix). In accordance with the electrostatic model proposed in chapter 6 of this thesis, the double layer consists of two Helmholtz planes *p* and a diffuse layer d containing ions that shield the surface charge $\sigma_0$,

$$\sigma_\mathrm{d} + \sum_{p=0}^{np-1} \sigma_p = 0 \,, \qquad [9]$$

with *np* the number of Helmholtz planes. Due to double layer overlap, the radial potential *outside* the Helmholtz planes, i.e., in the diffuse layer, can be assumed constant. The assumption of zero radial potential (and concentration) gradients is termed the uniform potential (UP) approach (Hawkins Cwirko and Carbonell, 1989; Bowen and Mukthar, 1996; chapter 4 of this thesis). Adopting the UP approach, the charge in the diffuse double layer is given by

$$\sigma_\mathrm{d} = GcF \sum_{\ell=1}^{n} z_\ell x_\ell \,, \qquad [10]$$

The geometrical factor *G* in Eq. [10] is equal to $a/2$ for a membrane consisting of cylindrical pores with radius *a*, and $G = \varphi / \rho_\mathrm{s} S (1-\varphi)$ for a packed-bed pore structure with a specific surface *S*, a porosity φ and a solid density $\rho_\mathrm{s}$. In Eq. [10] the membrane is assumed to consist of cylindrical pores of uniform radius (see also Eq. [12] in chapter 4).

### 2.1.6 Boundary conditions

The set of expressions to be solved contain second order differential expressions in $x_i$, $p$ and $\phi$ and consequently two boundary conditions are required for each of these variables. The boundary conditions are considered at the feed and the permeate. At the feed, an infinitely large volume is assumed, leading to fixed concentrations

$$x_i^{\mathrm{f}} = \text{constant} . \qquad [11]$$

The feed pressure is imposed by helium gas and the potential is set to zero,

$$\begin{aligned} p^{\mathrm{f}} &= p_{\mathrm{He}} \\ \phi^{\mathrm{f}} &\equiv 0 \end{aligned} . \qquad [12]$$

In the permeate 'e' the concentrations are related to the fluxes (Noordman *et al.*, 1997)

$$\frac{N_i}{N_j} = \frac{x_i^{\mathrm{e}}}{x_j^{\mathrm{e}}} . \qquad [13]$$

There are $n$-1 of these expressions. The $n^{\mathrm{th}}$ mole fraction is calculated from the summation of mole fractions, which equals unity. The pressure at the permeate 'e' side pressure is atmospheric,

$$p^{\mathrm{e}} = p_{\mathrm{atm}} . \qquad [14]$$

The boundary condition for the permeate potential is provided by the electroneutrality equation, Eq. [8].

### 2.1.7 Zero-current relation

For each ionic species its mole fraction and flux can be related to those of water, via Eq. [13], $x_i^{\mathrm{e}} = x_{\mathrm{w}}^{\mathrm{e}} N_i / N_{\mathrm{w}}$. Substitution in the electroneutrality equation (Eq. [8]) yields

$$\sum_{\ell}^{ni} z_\ell x_\ell^{\mathrm{e}} = \frac{N_{\mathrm{w}}}{x_{\mathrm{w}}^{\mathrm{e}}} \sum_{\ell}^{ni} z_\ell N_\ell = 0 , \qquad [15]$$

with *ni* the total number of charged species. Eq. [15] shows that in the model presented here, the condition of zero-current (see also Eq. [19] in chapter 4), required for NF systems, is implicitly accounted for.

### 2.1.8 Numerical solution

Equations [3]-[8], [10]-[14], [18]-[20], [22], and [24]-[30] (see Appendix) are solved for the activity coefficients $\gamma_i$, the molar fractions $x_i$, the uniform potential $\phi$, and the pressure $p$ in the stagnant film, the $\gamma$–layer, the $\alpha$-support and the permeate with the boundary conditions Eq. [11]-[14]. Only in the $\gamma$–layer the charge regulation expressions are calculated. Since the difference between the electrolyte activity coefficients at the $\gamma$–interfaces is only small, a linear variation is assumed in the $\gamma$–layer. The additional variables in the model are the molar fluxes $N_i$, the pressure in the support $p^{\mathrm{s}}$, and the permeate potential $\phi^{\mathrm{e}}$.

All layers in the 1D system are discretised using a forward discretisation scheme $((\upsilon_{j+1}-\upsilon_j)/\Delta)$. For the stagnant film, the support, and the permeate, one grid point is used, while in the $\gamma$-layer 6 grid points were taken. Numerical accuracy of the programme was better than 2%. The entire model was implemented in the mathematical software programme Maple (Waterloo Maple, Ontario, Canada), and is available from our website http://ims.ct.utwente.nl/ (downloads).

## 3. Results and Discussion

The model is used to predict the nanofiltration of NaCl by an asymmetric α/γ-alumina membrane. The flux and retention are calculated for various combinations of the model parameters using the structural data given in Table 1. A symmetric electrolyte NaCl at a concentration of 1 mol/m$^3$ and pH=6 is transported through the membrane at a pressure difference of 1 MPa. The physical data for the system is given in Table 2.

| | φ [%] | τ | Pore size [nm] | Thickness [μm] | Permeability [m$^2$] |
|---|---|---|---|---|---|
| stagnant film | | | | 10 | |
| γ-alumina top-layer | 51[+,*] | 3.0 | 4.0[°] | 3.4[*] | 4.8·10$^{-20}$ |
| α-alumina support | 32[#] | 3.2[#] | 88[#] | 2·10$^3$ | 2.4·10$^{-17}$[#] |

[+]Uhlhorn *et al.*, 1992; [*]Benes *et al.*, 2001; [°]Leenaars, Keizer and Burggraaf, 1984; [#]Benes, 2002.

Table 1: Data for the stagnant film, the membrane top-layer and the support: base case.

| Solution properties | $c^f$=1 mol/m$^3$, pH=6, μ=9.0·10$^{-4}$ Pa·s, $K_w$=10$^{-8}$ [mol$^2$/m$^6$], Δ$p$=1 MPa | | | | |
|---|---|---|---|---|---|
| Adsorption parameters[+] | log($K^+$)=8.3, log($K_{Na}$)=log($K_{Cl}$)=-0.7, $C_1$=1.2 [C/(V·m)], $C_2$=50 [mC/(V·m)], $c_{tot}^{//}$=1.33·10$^{-5}$ [mol/m$^2$] | | | | |
| | $OH^-$ | $H^+$ | $Na^+$ | $Cl^-$ | $H_2O$ |
| $\bar{V}_i$ [m$^3$/mol] | -5.3·10$^{-6}$[*] | 0[*] | -1.5·10$^{-6}$[*] | 18.1·10$^{-6}$[*] | 18.0·10$^{-6}$[°] |
| $D_{iw}$ [m$^2$/s][1] | 5.28·10$^{-9}$[#] | 9.31·10$^{-9}$[#] | 1.33·10$^{-9}$[#] | 2.03·10$^{-9}$[#] | |
| $D_{wM}$ [m$^2$/s][1] | | | | | 5.41·10$^{-10}$[§] |

[+]Chapter 6 of this thesis; [*]Horvath, 1985; [°]Atkins, 1990; [#]Cusler, 1984, [§]Lide, 1999.

[1]Effective diffusion coefficients are calculated by $\mathcal{D}_{ij}^{\text{eff}} = \tau \Big/ \left( \varphi H_i^{\text{d}} \right) \mathcal{D}_{ij}$.

Table 2: Physical properties for NaCl: base case.

The data in Table 1 and Table 2 will be referred to as the 'base case' (BC) and model predictions will be discussed in relation to this base case.

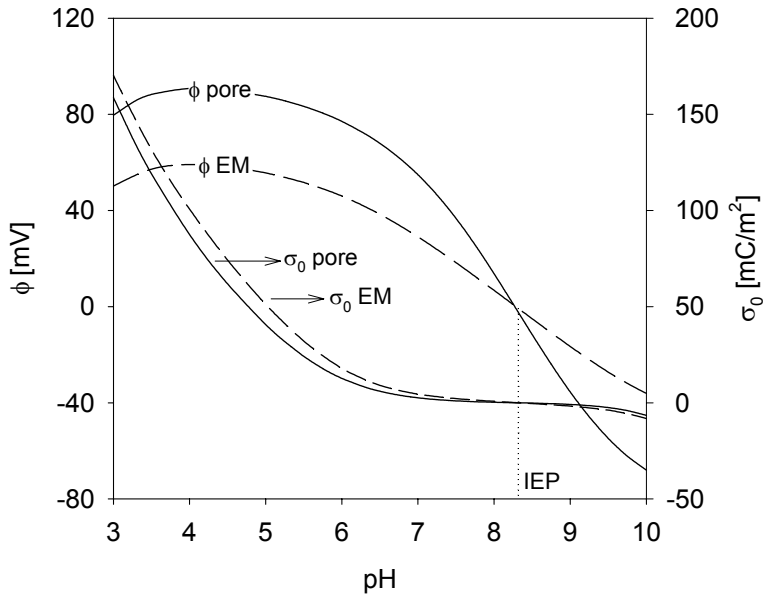


Figure 2: Potential ($\phi$ EM) and surface charge ($\sigma_0$ EM) without double layer overlap (dashed lines) and the axial pore potential ($\phi$ pore) and surface charge ($\sigma_0$ pore) in the middle of 4 nm (base case) membrane pores (solid lines) as a function of pH.

## 3.1 Charge regulation

### 3.1.1 Double layer overlap

Due to double layer overlap the surface charge $\sigma_0$ and potential $\phi$ in NF membrane pores differ significantly from those on isolated membrane particles, as is shown in Figure 2. For our base case $\phi$ increases by 59-88 % and $\sigma_0$ decreases by 7-21 %. Generally the double layer overlap is not accounted for in NF studies, e.g., (Palmeri *et al.*, 2000). Our model suggests that neglecting this effect is generally not justified. Double layer overlap also hampers the comparison between zeta-potential data obtained with

techniques such as mobility and streaming potential measurements (Ricq *et al.*, 1998).

### 3.1.2 Surface charge variation

Figure 3 shows the variation of the surface charge and potential with axial position in the pore. The variation is considerable (30% and 8% for $\sigma_0$ and $\phi$, respectively) and renders the assumption of a constant (effective) membrane charge in the pores (Guzmán-Garcia *et al.*, 1990; Bowen and Mukthar, 1996; Palmeri *et al.*, 2000; Yang and Pintauro, 2000; Bowen and Welfoot, 2002; Labbez *et al.*, 2002) questionable. In a previous effort (chapter 4 of this thesis) even stronger variations in the surface charge were reported.

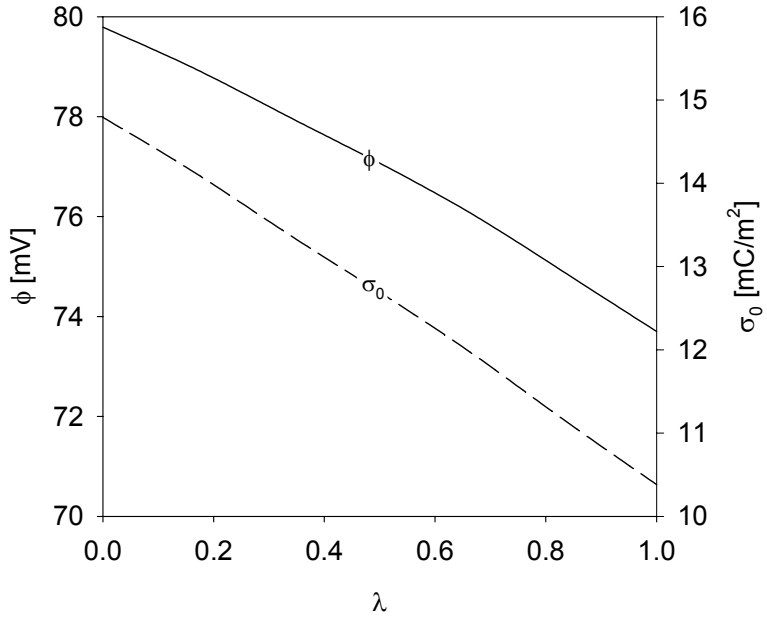


Figure 3: Potential $\phi$ (solid line) and surface charge $\sigma_0$ (dashed) over the (dimensionless) membrane thickness $\lambda$.

For studies in which a fixed membrane charge is fitted to experimental retention data (Bowen and Mukthar, 1996; Bowen and Welfoot, 2002) or in which the variation in the charge is only small the fixed charge assumption may still be usable.

## 3.2 Effect of pH on retention

The pH directly influences the axial pore potential $\phi$, and hence the retention, as can be seen in Figure 4. A similar behaviour of the pH-dependence on retention was also predicted in chapter 4 of this thesis.

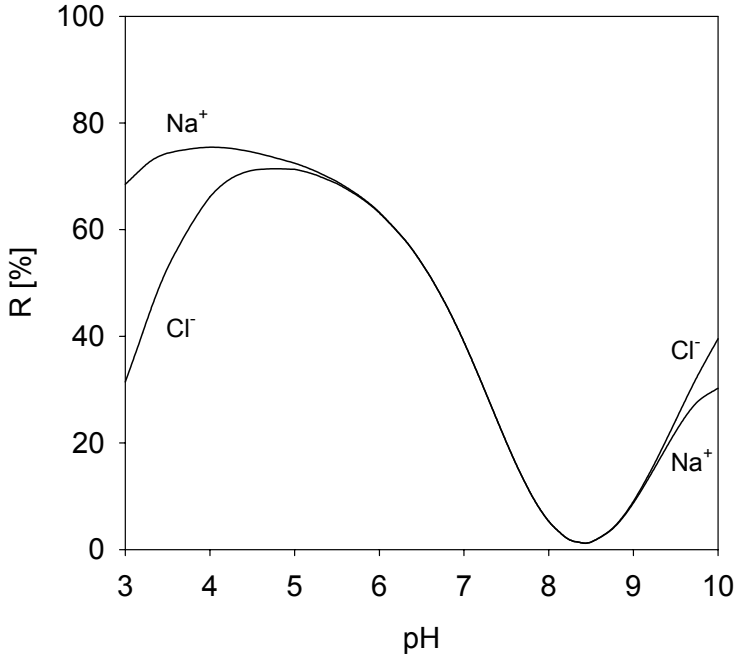


Figure 4: NaCl retention as function of feed solution pH.

At a pH corresponding to the iso-electric point (IEP) the uniform potential (not the surface charge) in the pore is zero by definition. Consequently, no retention due to electrostatic interactions is expected. Indeed Figure 4 shows that the retention reaches a minimum value of about 1.5 % at the IEP. The low predicted retention at the IEP clearly shows that electrostatic interactions are the dominant exclusion mechanism for this ceramic NF membrane. Note that the retention at the IEP cannot be due to dielectric exclusion effects (Guzmán-Garcia *et al.*, 1990; Bowen and Welfoot, 2002) since this phenomenon is neglected in this study.

For pH values exceeding the IEP, the pore potential becomes negative in sign and anions are repelled from the pores (Eq. [6]), reducing the flux of anions. To satisfy the zero-current relation the flux of cations decreases to the same extent. For pH values below the IEP the potential is positive and the cations are repelled from the pores. For a non-specifically adsorbing electrolyte such as NaCl, the potential is symmetric around the IEP (chapter 6 of this thesis). This effect results in the analogous symmetric retention behaviour predicted for IEP-1.5<pH<IEP+1.5.

At extreme pH values the retention of cations and anions becomes dissimilar (e.g., Hall, Starov and Lloyd, 1997; Hall, Lloyd and Starov, 1997; chapter 4 of this thesis). This can be explained by the high concentration of extremely mobile protons or hydroxyl ions, at these pH values (chapter 4). At low pH the large number of protons has a positive effect on the cation retention, while at high pH the high hydroxyl ion concentration increases the anion retention.

### 3.3 Influence of electrolyte concentration

The trend of decreasing retention with increasing electrolyte concentration is well documented in literature (e.g., Szaniawska and Spencer, 1995; Baticle *et al.*, 1997; Schaep *et al.*, 1999;), and shown in Figure 5 as a function of the pressure difference for a concentration increase of 1 mol/m$^3$ to 100 mol/m$^3$. Note that the limiting retention is not reached even at 4 MPa. The decrease in retention with increased concentration is caused by a reduced potential, which is directly concentration dependent (e.g., Lyklema, 1995; Bockris, Reddy and Gamboa-Aldeco, 2000; chapter 6).

Generally, a decrease in the flux is found for increasing concentrations (e.g., Baticle *et al.*, 1997; Afonso and De Pinho, 2000). This effect is due to an osmotic pressure difference over the membrane. The current transport model predicts the same trans-membrane flux for concentrations increasing from 1

to 100 mol/m$^3$ (dashed line in Figure 5). The concentration of 100 mol/m$^3$ represents a considerable osmotic pressure (≈0.5 MPa, calculated with van't Hoff's equation). However, the low retention at this concentration causes the osmotic pressure to be almost similar on both sides of the membrane, thereby making the flux decline due to osmotic effects vanish. Preliminary experiments in our lab confirm this model result.

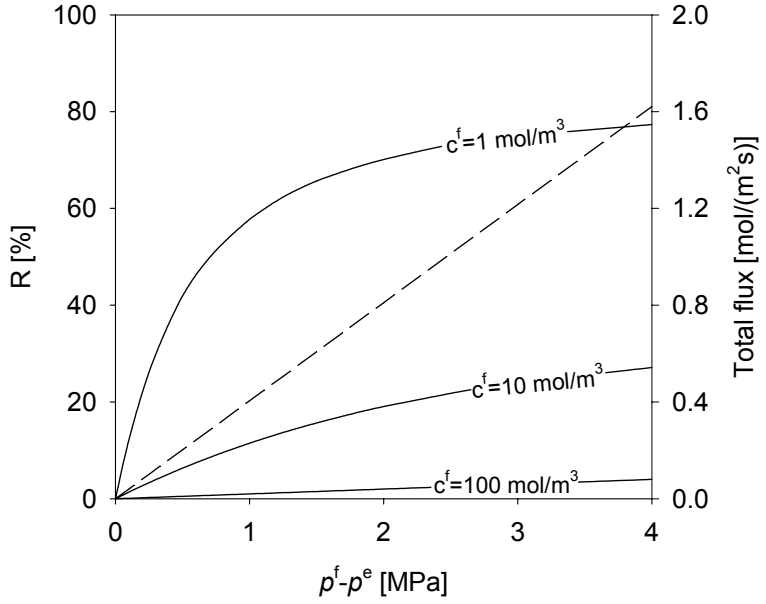


Figure 5: Retention of NaCl (solid line) and membrane flux (dashed) for feed concentrations $c^f$ of 1, 10 and 100 mol/m$^3$ and as a function of pressure.

### 3.4 Ternary mixture

Introducing a divalent ion like $Ca^{2+}$ with NaCl at pH<IEP (i.e., a positive axial pore potential) will lead to negative retentions for $Na^+$ at low trans-membrane pressure drops (Figure 6). This behaviour originates from two effects: the lower mobility, and the higher valency of calcium compared to sodium (chapter 4). Due to a higher valency, the $Ca^{2+}$ concentration in the membrane is considerably lower than the concentration of $Na^+$ (Eq. [6]), while additionally the electric field in the membrane will enhance the

transport of the more mobile $Na^+$. For a more detailed description of negative retention the reader is referred to the work of Yaroshchuk *et al.* (1994).

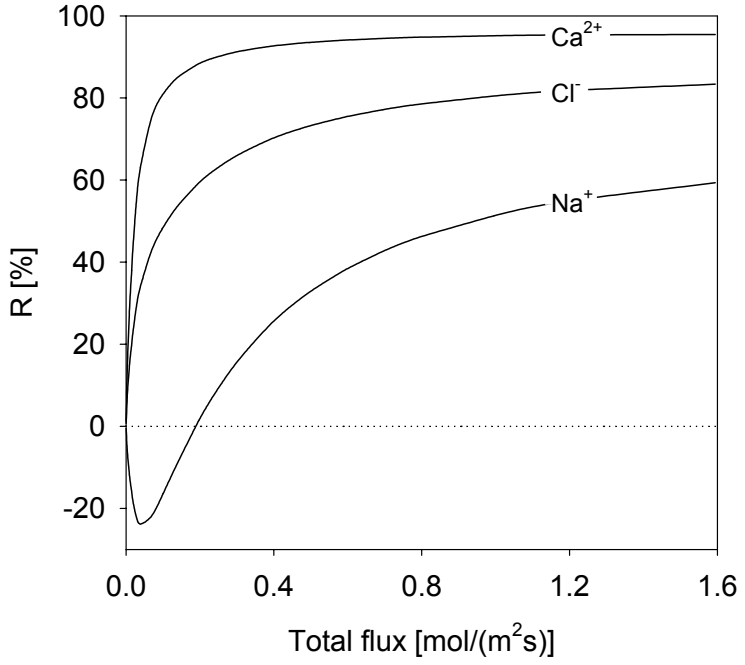


Figure 6: Retention for a mixture of 1 mol/m$^3$ NaCl with 1 mol/m$^3$ $CaCl_2$ as function of the total flux.

### 3.5 Influence of external and membrane transport resistances

NF membranes retain charged species more than the solvent. As a result, if the feed solution is not ideally mixed, a more concentrated region of charged species develops close to the feed-membrane interface. Various methods have been proposed to account for this effect (Taylor and Krishna, 1993), we have adopted the stagnant film model, Eq. [3]. The thickness of the stagnant film is determined by hydrodynamics and for instance reduces with increasing stirrer speed.

When the thickness of the stagnant layer increases, the concentration of electrolyte at the membrane interface will increase accordingly, resulting in a decrease of the observed retention (see Figure 5). At the base case film thickness $L_{sf}$ of 10 μm, the observed retention decreases only by 2% (see

Figure 7), which generally is within experimental error. Only for $L_{sf}$>40 μm, a >10% change in retention is observed. Typical values for the film thickness are in the range 50 and 250 μm (Malone and Anderson, 1977). It is therefore evident that the influence of the stagnant film in these cases cannot be neglected.

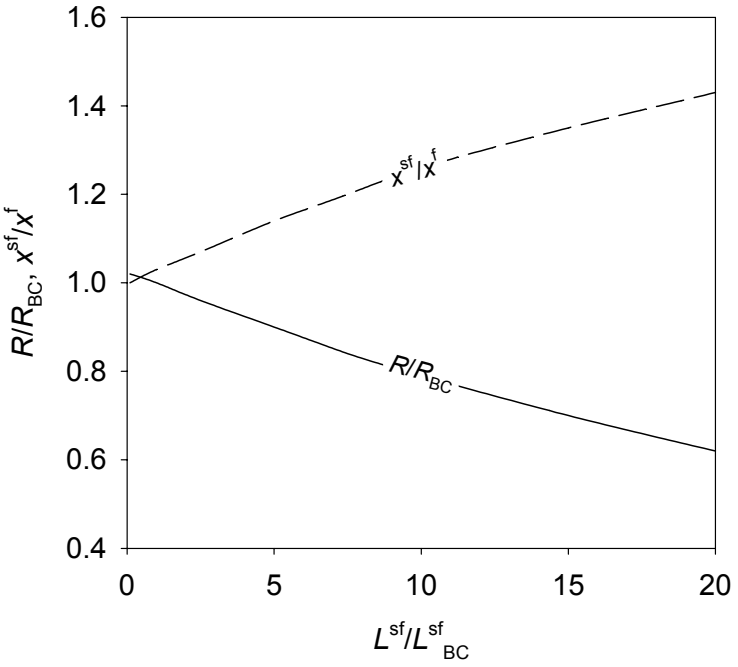


Figure 7: Normalised observed retention (solid line) and electrolyte concentration increase (dashed) of NaCl over the stagnant film as a function of the normalised stagnant film thickness.

Apart from external mass transport resistances, the membrane acts as a resistance as well. In the membrane two parameters determine its resistance: the thickness $L_M$ and the permeability $B_0^M$. As can be expected, an increased thickness or a decrease in permeability $B_0^\gamma$ of the γ–layer increases the retention and decreases the flux. For the support it works differently, overall membrane retention and flux increase with increasing permeability $B_0^s$ and decreasing support thickness. This is because the contribution of convection to the total flux of a species increases when $B_0^s$

increases or $L_s$ decreases (see Eq. [5]). In this way the limiting retention (the highest achievable retention) is reached at much lower pressure differences.

Because of the large thickness of the support on inorganic membranes (2 mm in our case), the pressure drop over the support can be about 50% of the total pressure difference over the system, which is clearly undesired. A reduction of the support thickness from 2 mm to 1 mm can therefore have a tremendously beneficial effect on the separation properties of such membranes. Our calculations (not reported) show that a 1 mm decrease in support thickness increases the overall retention by 9% and the flux by 37% (compared to the base case). It would be even better to increase the support pore size, since this parameter scales quadratically (assuming cylindrical pores) with the flux.

### 3.6 Influence of adsorption model and mass transport description on predicted overall retention and flux

In chapter 4 a predictive model was developed based on the Nernst-Planck flux expressions where ion adsorption was described using a 2-pK site-binding concept and a Gouy-Chapman electrostatic double layer model. This transport model could *qualitatively* predict NF separation. For an accurate *quantitative* prediction of retention data, however, it is necessary to use the more elaborate transport description developed in the present work. To underline this, the most important additions in the current model and their impact on the overall membrane retention and flux predictions will be briefly discussed below.

To derive ion adsorption parameters from electrophoretic mobility data a relatively detailed double layer description is required (see chapter 6). To accurately obtain the adsorption parameters, a triple-layer model (TLM) instead of simpler double layer descriptions like a Basic Stern or a Gouy-Chapman (GC) model has to be used (the TLM reduces to the GC

model for infinitely large Helmholtz capacities, that is, $C_1=C_2=\infty$). Calculations performed for the base case with the Helmholtz capacities increased by 100% (i.e., $C_1$=2.4 C/(V·m$^2$) and $C_2$=0.1 C/(V·m$^2$)) showed an increase in retention by 15% (the flux only decreased by less than 1 %). The increase in retention became even larger at low pressure differences. At $p^f$-$p^e$=0.5 MPa, for example, the retention increased already by 24 %, while the flux still only decreased by less than 1 %.

Correct diffusion coefficients are very important for a realistic predictive transport description of retention (see Figure 5 in chapter 4). The effective diffusion coefficients used in this paper are considerably smaller than the values at infinite dilution ($Đ_i^{eff}/D_{ij}\approx$0.15 for our base case). These lower (effective) diffusion coefficients increase the retention for our base case increases by a factor of 3.4, while the flux only decreases slightly by about 3 %, compared to a case with where diffusion coefficients at infinite dilution are used.

Apart from corrections for diffusion, convective transport is corrected for radial solute distribution effects in the membrane top layer as well (see Eq. [17]). In our model, however, the introduction of a hydrodynamic correction for convection, $H^c_i$, has negligible influence on the retention and overall flux.

Although electrostatic effects are the main separation mechanism for the alumina membrane discussed in this study, steric hindrance (see Eqs. [6] and [18]) can also be important in some cases. In our base case, for example, the contribution of steric exclusion to retention is 12% and becomes somewhat more important at lower trans-membrane pressures (e.g., increase in $R$ by steric exclusion is 16% for $p^f$-$p^e$=0.5 MPa).

The molar volume effect of a species is often neglected in NF studies because the incorporation of $\bar{V}_i$-related terms in model descriptions generally has

only a small influence on retention and flux. This also holds in the current model. For the base case, a reduction in the molar volume of each species by 300 % leads only to an increase in retention and overall flux of ≤1 % (of course this effect increases slightly at more extreme pressure differences).

## 4. Conclusion

Charge regulation is incorporated in a Maxwell-Stefan transport model leading to a model without any adjustable parameters. The applicability of this transport concept to predict retention, flux and charging properties is demonstrated for a real alumina NF membrane, using experimental input parameters. The trend in the modelling results are in accordance with theoretical and experimental evidence for NF systems presented in literature for a binary electrolyte as well as for mixtures with a common anion. It therefore appears that the combination of a 1-pK triple-layer model with a Maxwell-Stefan transport description is a valid approach to predict the separation behaviour of inorganic NF membranes. A sensitivity analysis suggests that for an accurate quantitative prediction of retention and flux it is not possible to use more simple descriptions for adsorption and mass transport.

## Nomenclature

| | | |
|---|---|---|
| $A_i$ | coefficients in Bungay and Brenner Eq. [21] | [-] |
| $a$ | pore radius | [m] |
| $a^{sol}$ | solute radius | [m] |
| $B_i$ | coefficients in Bungay and Brenner Eq. [21] | [-] |
| $B_0$ | permeability | [$m^2$] |
| $C_p$ | Helmholtz capacity of plane $p$ | [C $V^{-1}$ $m^{-2}$] |
| $c$ | total concentration | [mol $m^{-3}$] |
| $c_i$ | concentration of species $i$ | [mol $m^{-3}$] |
| $c^{ref}$ | thermodynamic reference concentration | [mol $m^{-3}$] |
| $c_i^{sc}$ | concentration of surface complexes $i$ | [mol $m^{-2}$] |
| $c_{tot}^{//}$ | total number of surface sites | [mol $m^{-2}$] |
| $Đ_{i\ell}$ | Maxwell-Stefan diffusion coefficient | [$m^2$ $s^{-1}$] |
| $D_{ij}$ | binary diffusion coefficient at infinite dilution | [$m^2$ $s^{-1}$] |
| $\mathbf{d}_i$ | driving force for mass diffusion of species $i$ | [$m^{-1}$] |
| $F$ | constant of Faraday | [C $mol^{-1}$] |
| $\mathbf{F}_i$ | external force on species $i$ | [N $mol^{-1}$] |
| $f_{i\ell}$ | friction coefficient between species $i$ and $\ell$ | [s $m^{-2}$] |
| $G$ | structure parameter | [m] |
| $H^{c}_i$ | hydrodynamic parameter for convection | [-] |
| $H^{d}_i$ | hydrodynamic parameter for diffusion | [-] |
| $H^{s}_i$ | hydrodynamic coefficient | [-] |
| $H^{t}_i$ | hydrodynamic coefficient | [-] |
| $I$ | ionic strength | [mol $m^{-3}$] |
| $\mathbf{J}_i$ | diffusive molar flux | [mol $m^{-2}$ $s^{-1}$] |
| $K^+$ | proton adsorption equilibrium constant | [-] |
| $K_C$ | cation adsorption equilibrium constant | [-] |
| $K_A$ | anion adsorption equilibrium constant | [-] |
| $K_w$ | water autoprotolysis constant | [$mol^2$ $m^{-6}$] |
| $k_L$ | liquid transfer coefficient | [m $s^{-1}$] |
| $L$ | thickness of a layer | [m] |
| $\mathbf{N}_i$ | molar flux at stationary coordinates | [mol $m^{-2}$ $s^{-1}$] |
| $n$ | number of species | [-] |
| $np$ | number of charging planes | [-] |
| $p$ | pressure | [N $m^{-2}$] |
| $R$ | ideal gas constant | [J $mol^{-1}$ $K^{-1}$] |
| $\mathbf{R}_{ij}$ | phenomenological coefficients | [m s $J^{-1}$] |
| $S$ | specific surface | [$m^2$ $kg^{-1}$] |
| $T$ | temperature | [K] |
| $\mathbf{u}_i$ | velocity of species $i$ | [m $s^{-1}$] |
| $\mathbf{v}$ | barycentric velocity | [m $s^{-1}$] |
| $\mathbf{V}$ | arbitrary reference velocity | [m $s^{-1}$] |
| $\bar{V}$ | total molar volume | [$m^3$ $mol^{-1}$] |
| $\bar{V}_i$ | molar volume of species $i$ | [$m^3$ $mol^{-1}$] |
| $x_i$ | molar fraction of species $i$ | [-] |

| | | |
|---|---|---|
| $y_i$ | molar fraction of species $i$ including the porous matrix | [-] |
| $z_i$ | charge number of species $i$ | [-] |

Greek

| | | |
|---|---|---|
| $\gamma_i$ | activity coefficients of species $i$ | [-] |
| $\delta i$ | driving force for diffusion of species $i$ including the porous matrix | [$m^{-1}$] |
| $\zeta_{ij}$ | friction coefficient between species $i$ and $j$ including the porous matrix | [s $m^{-2}$] |
| $\lambda_i$ | ratio of solute radius over the pore radius | [-] |
| $\lambda$ | dimensionless membrane thickness | [-] |
| $\mu$ | Newtonian viscosity | [N s $m^{-2}$] |
| $\mu_i$ | chemical potential of species $i$ | [J $mol^{-1}$] |
| $\mu^0$ | chemical potential at a reference state | [J $mol^{-1}$] |
| $\mathbf{\Pi}$ | viscous pressure tensor | [J $m^{-3}$] |
| $\pi_s$ | entropy production | [J $m^{-3}$ $s^{-1}$ $K^{-1}$] |
| $\rho_s$ | solid density | [kg $m^{-3}$] |
| $\sigma_d$ | diffuse double layer charge | [C $m^{-2}$] |
| $\sigma_p$ | charge at plane $p$ | [C $m^{-2}$] |
| $\tau$ | tortuosity | [-] |
| $\Phi$ | entropy dissipation | [J $m^{-3}$ $s^{-1}$] |
| $\phi$ | potential | [V] |
| $\varphi$ | porosity | [-] |

Super- and subscripts

| | |
|---|---|
| b | bulk |
| e | permeate |
| eff | effective: corrected for the matrix |
| f | feed |
| M | membrane |
| s | support |
| sf | stagnant film |
| w | solvent |
| $\gamma$ | membrane top-layer |
| 0, 1, 2 | charging planes |
| (+) | inside the interface |
| (-) | outside interface |

# Appendix

## Hydrodynamic relations

The movement and entry of a solute in a pore will be constrained when its size is in the order of the pore size. The constrained motion of a particle can be described by hydrodynamic principles (Deen, 1987). The key parameter is such an analysis always is $\lambda_i$, the ratio of the (hydrated) solute radius $a_i^{sol}$ over the pore radius $a$,

$$\lambda_i = \frac{a_i^{sol}}{a}. \qquad [16]$$

The solute radius (Table 3) is calculated using the Stokes-Einstein equation (Einstein, 1956),

$$a_i^{sol} = \frac{RT}{6N_A \pi \mu D_{ij}}, \qquad [17]$$

where $N_A$ is Avogadro's contant.

| | $OH^-$ | $H^+$ | $Na^+$ | $Cl^-$ | $Ca^{2+}$ |
|---|---|---|---|---|---|
| $a_i^{sol}$ [nm] | 0.046 | 0.026 | 0.18 | 0.12 | 0.31 |

Table 3: Hydrodynamic solute radius, calculated with Eq. [17].

Steric hindrance effects may play a role upon entry of a particle in a pore. The term $h_i$ accounts for these effects and is related to $\lambda_i$ by

$$h_i = (1-\lambda_i)^2. \qquad [18]$$

For species within pores of similar size, interaction with the pore wall can cause a variation in their radial location. This effect will influence diffusive and convective transport in the pore and can be described by the

hydrodynamic parameters $H^{d}_{i}$ and $H^{c}_{i}$, respectively. Almost thirty years ago, Bungay and Brenner (1973) formulated expressions to take this variation in radial location of solute species into account (note that for the solvent $H^{d}_{i}=H^{c}_{i}=1$).

$$H_i^{c} = \frac{(2-h_i)H_i^{s}}{2H_i^{t}}, \qquad [19]$$

$$H_i^{d} = \frac{6\pi}{H_i^{t}}, \qquad [20]$$

$$\begin{pmatrix} H_i^{t} \\ H_i^{s} \end{pmatrix} = \frac{9}{4}\pi^2\sqrt{2}\left(1-\lambda_i\right)^{-5/2}\left[1+\sum_{\ell=1}^{2}\begin{pmatrix} A_\ell \\ B_\ell \end{pmatrix}\left(1-\lambda_i\right)^{\ell}\right]+\sum_{\ell=0}^{4}\begin{pmatrix} A_{\ell+3} \\ B_{\ell+3} \end{pmatrix}\lambda_i^{\ell}. \qquad [21]$$

| $i$ | 1 | 2 | 3 | 4 | 5 | 6 | 7 |
|---|---|---|---|---|---|---|---|
| $A_i$ | -1.2167 | 1.5336 | -22.5083 | -5.6117 | -0.3363 | -1.2160 | 1.6470 |
| $B_i$ | 0.1167 | -0.00442 | 4.0180 | -3.9788 | -1.9215 | 4.3920 | 5.0060 |

Table 4: Coefficients for the hydrodynamic relations (Eq. [21]) of Bungay and Brenner (1973).

Noordman (2000) showed that the results obtained with the Bungay and Brenner relations yield results identical (within 3%) to the predictions for $H^{c}_{i}$ and $H^{d}_{i}$ derived by Bowen and Sharif (1994) and Bowen, Mohammad and Hildal (1997). Since the former expressions are valid over the entire range of $\lambda_i$ (from 0 to 1), while the expressions of Bowen are only valid for $0<\lambda_i<0.8$ (Bowen, Mohammad and Hildal, 1997), the results of Bungay and Brenner are used in this work.

## Charge regulation

Surface chemistry

For the inorganic alumina NF membrane, ion adsorption is assumed to occur on a homogeneous surface containing Al-OH$^{-1/2}$ hydroxyl sites (chapter 6) with a total concentration $c_{\mathrm{tot}}^{//}$,

$$c_{\mathrm{tot}}^{//} = \left( c_{\text{Al-OH}^{-1/2}} + c_{\text{Al-OH}_2^{+1/2}} + c_{\text{Al-OH}^{-1/2}\text{C}^+} + c_{\text{Al-OH}_2^{+1/2}\text{A}^-} \right). \qquad [22]$$

Eq. [22] shows that in the 1-pK surface model the hydroxyl groups are charged (Al-OH$^{-1/2}$), and proton charging occurs only by proton adsorption. For the 1-pK model the surface reactions are

$$\begin{aligned} \text{Al-OH}^{-1/2} + \text{H}^+(\text{s}) &\rightleftharpoons^{K^+} \text{Al-OH}_2^{+1/2} \\ \text{Al-OH}^{-1/2} + \text{C}^{m+}(\text{s}) &\rightleftharpoons^{K_\text{C}} \text{Al-OH}^{-1/2}\text{C}^{m+}, \\ \text{Al-OH}_2^{+1/2} + \text{A}^{n-}(\text{s}) &\rightleftharpoons^{K_\text{A}} \text{Al-OH}_2^{+1/2}\text{A}^{n-} \end{aligned} \qquad [23]$$

resulting in the following expressions for the equilibrium constants $K_i$

$$K^+ = \frac{c_{\text{Al-OH}_2^{+1/2}} c^{\text{ref}}}{c^{\text{s}}_{\text{H}^+} c_{\text{Al-OH}^{-1/2}}}, \; K_\text{C} = \frac{c_{\text{Al-OH}^{-1/2}\text{C}^{m+}} c^{\text{ref}}}{c^{\text{s}}_{\text{C}^{m+}} c_{\text{Al-OH}^{-1/2}}}, \; K_\text{A} = \frac{c_{\text{Al-OH}_2^{+1/2}\text{A}^{n-}} c^{\text{ref}}}{c^{\text{s}}_{\text{A}^{n-}} c_{\text{Al-OH}_2^{+1/2}}}. \qquad [24]$$

The concentrations of protons and hydroxyl ions are not independent but related by the water autoprotolysis equilibrium reaction

$$\text{H}_2\text{O} \rightleftharpoons^{K_w} \text{H}^+ + \text{OH}^- \qquad K_w = c^{\text{b}}_{\text{H}^+} c^{\text{b}}_{\text{OH}^-}, \qquad [25]$$

and it is assumed that this equilibrium holds everywhere in the system. The 'surface' concentrations $c_i^{\text{s}}$, are related to the bulk concentrations by the Boltzmann relation.

$$c_i^s = c\gamma_i^{\mathrm{b}} x_i^{\mathrm{b}} \exp\left(\frac{-z_i F}{RT}\phi_s\right). \qquad [26]$$

The charge invoked by the adsorbed surface complexes $c_i^{\mathrm{sc}}$ in Eq. [23] (not $c_i^{\mathrm{s}}$) is related to their concentration on a specific electrostatic plane $p$,

$$\sigma_p = F\sum_{\ell=1}^{n} z_\ell c_{\ell,p}^{\mathrm{sc}} \ . \qquad [27]$$

Double layer description

Apart from the surface chemistry, a double layer model has to be adopted to describe the variation of the potential and charge at the surface. In this work a triple-layer (TL) model is used. The TL model considers three planes (see Figure 1 in chapter 6), the surface or 0-plane, the 1-plane or inner Helmholtz plane (IHP), and the 2-plane or outer Helmholtz plane (OHP). Adsorbed protons are located at the 0-plane while electrolyte adsorption occurs on the 1-plane.

The electrostatic expressions for the charge $\sigma_p$ at the planes $p$ for the TL model are

$$\sigma_0 = C_1\left(\phi_0 - \phi_1\right), \qquad [28]$$

$$\sigma_1 = C_2\left(\phi_1 - \phi_2\right) - C_1\left(\phi_0 - \phi_1\right), \qquad [29]$$

with $C_{p+1}$ the layer capacity. No species adsorb on the 2-plane and therefore the charge (but not the potential) on that plane is zero.

$$\sigma_2 = 0\,. \qquad [30]$$

In the here presented model, only in the γ–layer the surface charge $\sigma_0$, the charge on the inner Helmholtz plane $\sigma_1$, the potentials in the adsorption layers and the diffuse layer $\phi_0$, $\phi_1$, $\phi$ are calculated.

Diffusion coefficients

For application of Eq. [17] to transport in the γ-layer, a whole range of diffusion coefficients has to be determined. The data of Wesselingh, Vonk and Kraaijeveld (1995) show that ion-ion friction is probably only important at very high concentrations (e.g., the cation-anion friction contribution is less than 10% for electrolyte concentrations below 2000 mol/m$^3$ (Krishna and Wesslingh, 1997)). Since this work deals only with dilute solutions, only ion-solvent and solvent-membrane friction are considered.

## References


1. Afonso M.D., and De Pinho M.N., "Transport of $MgSO_4$, $MgCl_2$ and $Na_2SO_4$ across an Amphoteric Nanofiltration Membrane," *J. Membrane Sci.*, **179**, 137 (2000).
2. Atkins P.W., "Physical Chemistry," 4th edition, Oxford University Press, Oxford, Great Britain, 1990, p. 155.
3. Baticle P., Kiefer C., Lakhchaf N., Larbot A., Leclerc O., Persin M., and Sarrazin J., "Salt Filtration on Gamma Alumina Nanofiltration Membranes Fired at Two Different Temperatures," *J. Membrane Sci.*, **135**, 1 (1997).
4. Benes N.E., "Mass Transport in Thin Supported Silica Membranes," Ph.D. Thesis, University of Twente, The Netherlands, 2000, chapter 3.
5. Benes N.E., Spijksma G., Verweij H., Wormeester H., and Poelsema B., "CO2 Sorption of a Thin Silica Layer determined by Spectroscopic Ellipsometry," *AIChE J.*, **47**, 1212 (2001).
6. Bird R.B., Stewart W.E., and Lightfoot E.N., "Transport Phenomena," Wiley, Singapore, 1960, chapter 3.
7. Bockris J.O'M., Reddy A.K.N., and Gamboa-Aldeco M., "Modern Electrochemistry 2A. Fundamentals of Electrodics," 2nd edition, Kluwer Academic/Plenum Publishers, New York, 2000, pp. 871-887.
8. Bowen W.R., and Sharif A.O., "Transport through Microfiltration Membranes – Particle Hydrodynamics and Flux Reduction," *J. Colloid Interface Sci.*, **168**, 414 (1994).
9. Bowen W.R., and Mukthar H., "Characterisation and Prediction of Separation Performance of Nanofiltration Membranes," *J. Membrane Sci.*, **112**, 263 (1996).
10. Bowen W.R., Mohammad A.W., and Hildal N., "Characterisation of Nanofiltration Membranes for Predictive Purposes – Use of Salts, Uncharged Solutes and Atomic Force Microscopy," *J. Membrane Sci.*, **126**, 91 (1997).
11. Bowen W.R., and Welfoot J.S., "Modelling Performance of Membrane Nanofiltration – Critical Assessment and Model Development," *Chem. Eng. Sci.*, **57**, 1121 (2002).
12. Bungay P.M., and Brenner H., "The Motion of a Closely-Fitting Sphere in a Fluid-Filled Tube," *Int. J. Multiphase Flow*, **1**, 25 (1973).
13. Chan D.Y.C., Perram J.W., White L.R., and Healy T.W., "Regulation of Surface Potential at Amphoteric Surfaces During Particle-Particle Interaction," *J. Chem. Soc. Faraday Trans. I*, **71**, 1046 (1975).
14. Combe C., Guizard C., Aimar P., and Sanchez V., "Experimental Determination of Four Characteristics used to predict the Retention of a Ceramic Nanofiltration Membrane," *J. Membrane Sci.*, **129**, 147 (1997).

15. Cussler E.L., "Diffusion. Mass Transfer in Fluid Systems," Cambridge University Press, New York, 1984, p. 147.
16. Davies C.W., Ion Association, Butterworths, London, **1962**, 41.
17. Davis J.A., James R.O., and Leckie J.O., "Surface Ionization and Complexation at the Oxide/Water Interface. I. Computation of Electrical Double Layer Properties in Simple Electrolytes," *J. Colloid Interface Sci.*, **63**, 480 (1978).
18. Deen W.M., "Hindered Transport of Large Molecules in Liquid-Filled Pores," *AIChE J.*, **33**, 1409 (1987).
19. Einstein A., "Investigations on the Theory of the Brownian Movement," Furth R. (ed.), Dover, New York, 1956.
20. Guzmán-Garcia A.G., Pintauro P.N., Verbrugge M.W., and Hill R.F., "Development of a Space-Charge Transport Model for Ion-Exchange Membranes," *AIChE J.*, **36**, 1061 (1990).
21. Hall M.S., Starov V.M., and Lloyd D.R., "Reverse Osmosis of Multicomponent Electrolyte Solutions. Part I. Theoretical Development," *J. Membrane Sci.*, **128**, 23 (1997).
22. Hall M.S., Lloyd D.R., and Starov V.M., "Reverse Osmosis of Multicomponent Electrolyte Solutions. Part II. Experimental Verification," *J. Membrane Sci.*, **128**, 39 (1997).
23. Hawkins Cwirko E., and Carbonell R.G., "Transport of Electrolytes in Charged Pores: Analysis Using the Method of Spatial Averaging," *J. Colloid Interface Sci.*, **129**, 513 (1989).
24. Healy T.W., and White L.R., "Ionizable Surface Group Models of Aqueous Interfaces," *Adv. Colloid Interface Sci.*, **9**, 303 (1978).
25. Ho W.S.W., and Sirkar K.K., "Membrane Handbook," Van Nostrand Reinhold, New York, 1992.
26. Horvath A.L., "Handbook of Aqueous Electrolyte Solutions. Physical Properties, Estimation and Correlation Methods, " Ellis Horwood, Chichester, 1985, p. 132.
27. Krishna R., and Wesselingh J.A., "The Maxwell-Stefan Approach to Mass Transfer," *Chem. Eng. Sci.*, **52**, 861 (1997).
28. Labbez C., Fievet P., Szymczyk A., Vidone A., Foissy A., and Pagetti J., "Analysis of the Salt Retention of a Titania Membrane using the "DSPM" model: Effect of pH, Salt Concentration and Nature," *J. Membrane Sci.*, **208**, 315 (2002).
29. Leenaars A.F.M., Keizer K., and Burggraaf A.J., "The Preparation and Characterization of Alumina Membranes with Ultra-Fine Pores. Part 1. Microstructural Investigations on Non-Supported Membranes," *J. Mater. Sci.*, **19**, 1077 (1984).
30. Leenaars A.F.M., and Burggraaf A.J., "The Preparation and Characterization of Alumina Membranes with Ultrafine Pores. 2. The Formation of Supported Membranes," *J. Colloid Interface Sci.*, **105**, 27 (1985).

31. Leenaars A.F.M., and Burggraaf A.J., "The Preparation and Characterization of Alumina Membranes with Ultra-Fine Pores. Part 3. The Permeability for Pure Liquids," *J. Membrane Sci.*, **24**, 245 (1985).
32. Lide D.L. (ed.), "CRC Handbook of Chemistry and Physics," 79th edition, CRC Press, New York, 1999, p. 5.90.
33. Lyklema J., "Fundamentals of Interface and Colloid Science. Volume II: Solid-Liquid Interfaces," Academic Press, London, 1995, chapter 3.
34. Malone D.M., and Anderson J.L., "Diffusional Boundary-Layer Resistance for Membranes with Low Porosity," *AIChE J.*, **23**, 177 (1977).
35. Metha G.D., Morse T.F., Mason E.A., and Daneshpajooh M.H., "Generalized Nernst-Planck and Stefan-Maxwell Equations for Membrane Transport," *J. Chem. Phys.*, **64**, 3917 (1976).
36. Nijmeijer A., Kruidhof H., Bredesen R., and Verweij H., "Preparation and Properties of Hydrothermally Stable γ-Alumina Membranes," *J. Am. Ceram. Soc.*, **84**, 136 (2001).
37. Ninham B.W., and Parsegian V.A., "Electrostatic Potential Between Surfaces Bearing Ionizable Groups in Ionic Equilibrium with Physiologic Saline Solution," *J. Theor. Biol.*, **31**, 405 (1971).
38. Noordman T.R., Vonk P., Damen V.H.J.T., Brul R., Schaafsma S.H., de Haas M., and Wesselingh J.A., "Rejection of Phosphates by a $ZrO_2$ Ultrafiltration Membrane," *J. Membrane Sci.*, **135**, 203 (1997).
39. Noordman T.R., "High Flux Ultrafiltration," Ph.D. Thesis, University of Groningen, The Netherlands, 2000, chapter 2.
40. Palmeri J., Blanc P., Larbot A., and David P., "Hafnia Ceramic Nanofiltration Membranes. Part II. Modeling of Pressure-Driven Transport of Neutral Solutes and Ions," *J. Membrane Sci.*, **179**, 243 (2000).
41. Randon J., Larbot A., Cot L., Lindheimer M., and Partyka S., "Sulfate Adsorption on Zirconium Dioxide," *Langmuir*, **7**, 2654 (1991).
42. Randon J., Larbot A., Guizard C., Cot L., Lindheimer M., and Partyka S., "Interfacial Properties of Zirconium Dioxide Prepared by the Sol-Gel Process," *Colloids and Surfaces*, **52**, 241 (1991).
43. Ricq L., Pierre A., Reggiani J-C., Pagetti J., and Foissy, "Use of Electrophoretic Mobility and Streaming Potential Measurements to Characterize Electrokinetic Properties of Ultrafiltration and Microfiltration Membranes," *Coll. Surf. A.*, **138**, 301 (1998).
44. Schaep J., Vandecasteele C., Peeters B., Luyten J., Dotremont C., and Roels D., "Characteristics and Retention Properties of a Mesoporous γ-$Al_2O_3$ Membrane for Nanofiltration," *J. Membrane Sci.*, **163**, 229 (1999).

45. Strathmann H., "Ion-Exchange Membranes in Industrial Mass Separation Processes," *J. Separ. Proc. Technol.*, **5**, 1 (1984).
46. Szaniawska D., and Spencer H.G., "Non-Equilibrium Thermodynamics Analysis of the Transport Properties of Formed-In-Place Zr(IV) Hydrous Oxide-PAA Membranes: II. NaCl-water solutions," *Desalination*, **101**, 31 (1995).
47. Taylor R., and Krishna R., "Multicomponent Mass Transfer," Wiley, New York, 1993, chapters 8 and 9.
48. Uhlhorn R.J.R., Huis in't Veld M.H.B.J., Keizer K., and Burggraaf A.J., "Synthesis of Ceramic Membranes. Part I. Synthesis of Non-Supported and Supported γ-Alumina Membranes without Defects," *J. Mater. Sci.*, **27**, 527 (1992).
49. Vacassy R., Guizard C., Thoraval V., and Cot L., "Synthesis and Characterization of Microporous Zirconia Powders: Application in Nanofilters and Nanofiltration Characteristics," *J. Membrane Sci.*, **132**, 109 (1997).
50. Van Gestel T., Vandecasteele C., Buekenhoudt A., Dotremont C., Luyten J., Leysen R., Van der Bruggen B., and Maes G., "Salt Retention in Nanofiltration with Multilayer Ceramic $TiO_2$ Membranes," *J. Membrane Sci.*, **209**, 379 (2002).
51. Wesselingh J.A., Vonk P., and Kraaijeveld G., "Exploring the Maxwell-Stefan Description of Ion Exchange," *Chem. Eng. J.*, **57**, 75 (1995).
52. Yang Y., and Pintauro P.N., "Multicomponent Space-Charge Transport Model for Ion-Exchange Membranes," *AIChE J.*, **46**, 1177 (2000).
53. Yaroshchuk A.E., Bardot C., Gaubert E., Kulov N.N., and Nechaev A.N., "Modeling of the Pressure-Driven Transport of Single and Mixed Electrolyte Solutions across Fine-Porous Inorganic Membranes. Criteria for Efficient Rejection and Separation," Presented at ICIM3, Worcester, USA, (1994).

# Chapter 8

## Separation Properties of γ-Alumina Nanofiltration Membranes Compared to Charge Regulation Model Predictions


### Abstract

Equation Section (Next)The separation behaviour of asymmetric nanofiltration alumina membranes is determined experimentally for binary NaCl and $CaCl_2$ electrolyte solutions and a ternary NaCl-$CaCl_2$ mixture as a function of pH and pressure. Experimental data suggests that the supported alumina membranes are chemically stable over the pH range 4-10. The measured separation behaviour is compared to the results of a predictive charge-regulation transport model with no adjustable parameters.

The model predictions are in good agreement with the experimental data both for the binary as well as for the ternary solutions. At pH values below 6 the retention of $CaCl_2$ is relatively insensitive to the value of the adsorption constant of $Ca^{2+}$. Obtaining the membrane adsorption parameters by fitting a model to retention data, as is often done in nanofiltration literature, can therefore be delicate. Instead, the acquisition of parameters by independent measurement techniques is obviously preferential. Supports with small pore sizes enhance the membrane's mechanical strength but they can exhibit retention and reduce the flux, leading to a decrease of the overall membrane retention. Two supports with pore sizes of 0.20 μm and 0.12 μm are compared. The support with the larger pores increased the trans-membrane flux by ≈40% and the overall membrane retention by ≈30%, compared to the support with the smaller pores.

## 1. Introduction

The separation behaviour of NF membranes is not known in detail and many transport descriptions have been proposed in literature to capture their characteristic features. Generally these models contain some adjustable parameters (Bowen and Mukthar, 1996; Hall, Starov and Lloyd, 1997; Hall, Lloyd and Starov, 1997; Hagmeyer and Gimbel, 1998; Bowen and Welfoot, 2002; Labbez *et al.*, 2002) that are extracted by fitting the model to retention data. Pintauro and co-workers (Guzmán-Garcia *et al.*, 1990; Bontha and Pintauro, 1994; Yang and Pintauro, 2000) were the first to develop a transport model without any adjustable parameters, deriving all model parameters from independent measurements. They showed that it is indeed possible to describe multi-component transport in a Nafion® NF membrane. Palmeri *et al.* (1999) followed a different approach and directly used electrophoretic mobility data to describe the charging of the membrane. By relating the mobility to the electrokinetic charge $\sigma_{ek}$ on the membrane, they could reasonably well calculate the limiting retention of binary electrolytes for a hafnia membrane (Palmeri *et al.*, 2000) without adjustable parameters.

The manner in which the membrane's charging properties are determined is the most important drawback of both these approaches. Pintauro and co-workers measure the membrane surface charge for each specific bulk electrolyte composition. This is not only very time consuming, but it also gives no information about the dependence of the surface charge on the electrolyte solution properties (concentration, type of electrolyte and pH), making an *a-priory* prediction of membrane transport at other bulk compositions impossible. By directly using electrokinetic data instead of parameters describing the underlying adsorption chemistry of individual ions, the approach of Palmeri *et al.* (2000) makes it impossible to predict the retention behaviour for multi-component electrolyte systems. Furthermore, if the membrane can regulate an excess of charge carriers at its surface,

double layer overlap in the membrane pores will considerably increase the zeta potential obtained from electrophoretic mobility studies (chapter 6 of this thesis). This important effect is not accounted for in the work of Palmeri *et al.* (2000).

In chapter 4 a transport approach was developed in which a charge regulation (CR) model describes ion adsorption and accounts for double layer overlap in the membrane pores. The model describes the membrane charging behaviour with a set of ion-material-specific adsorption parameters. They showed that electrolyte retention on a ceramic γ-alumina membrane for a binary electrolyte solution and multi-component mixtures could be qualitatively predicted, using no adjustable parameters.

In chapter 7 this model was extended by introducing a more realistic description of the ion-adsorption chemistry and combined it with the Maxwell-Stefan transport relations. The adsorption parameters in chapter 7 were obtained from independent electrophoretic mobility measurements (chapter 6) and showed that, although the adsorption parameters in the model are derived from mobility data in a binary electrolyte solution, they can also be used to *a-priori* predict the retention for multi-component electrolyte solutions. In the present work the model in chapter 7 is adopted and its predictions are compared with experimental data for the retention on an α-alumina supported γ-alumina NF membrane.

## 2. Experimental

### 2.1 Membrane samples

The alumina membrane materials described in this study are home-made. The α-alumina supports were prepared by filtering stabilised suspensions of AKP powder (Sumitomo Chemicals Ltd.) and consecutive sintering at 1100

°C (AKP30) or 1150 °C (AKP15). Two boehmite sol layers were applied on the support by dip-coating, resulting, after sintering at 600 °C, in the γ-alumina top layer. A more detailed description of the alumina membrane synthesis route has been reported elsewhere (Leenaars and Burggraaf, 1984; Leenaars and Burggraaf, 1985a; Leenaars and Burggraaf, 1985b; Uhlhorn *et al.*, 1992).

| Sample no. | Support | Top layer |
|---|---|---|
| 1 | AKP30 | - |
| 2 | AKP15 | - |
| 3 | AKP30 | 2 γ-layers |
| 4 | AKP30 | 2 γ-layers |
| 5 | AKP15 | 2 γ-layers |
| 6 | AKP15 | 2 γ-layers |
| 7 | AKP15 | 2 γ-layers |

Table 1: Overview of membranes used in this study.

An overview of the seven different membrane samples used in this work is given in Table 1. Supports were prepared from two different starting materials: AKP30 (0.4 μm particle size) and AKP15 (0.7 μm particle size), both from Sumitomo Chemicals Ltd.. After sintering the porosity φ and tortuosity τ of both supports were equal to 0.32 and 3.2 (Benes, 2000), respectively. The separating top layer of the membranes consisted of two γ-alumina layers. Benes *et al.* (2001) determined a top-layer porosity of 0.51 using ellipsometry. The similarity in support and top-layer structure suggests that the tortuosities should also be similar. Abbasi, Evans and Abramson (1983) derived a relation for the tortuosity based on gas diffusion through a porous solid,

$$\tau = \frac{\varphi}{0.4\varphi - 0.0328}. \qquad [1]$$

Using the top-layer porosity (0.51), a value of $\tau$=3.0 is found for the $\gamma$-layer, which is indeed very similar to the support tortuosity, as expected. This value will also be used in the present study. If Eq. [1] is used to calculate the tortuosity of the support (using $\varphi$=0.32), $\tau$=3.4 is obtained, very similar to the value of 3.2 reported in literature (Benes, 2000).

## 2.2 Permporometry

Permporometry is a useful tool to qualitative compare the top layer pore size before and after a series of retention measurements. It is difficult, however, to use this technique for an accurate quantitative determination of the pore radius of an NF membrane top layer. The reason for this is that permporometry is a method that relies on the curvature of an organic liquid (cyclohexane) in a pore at equilibrium conditions.

Ceramic membranes, however, consist of packed spherical particles leading to undulating pore structures. The local Kelvin radius can therefore be quite different from the average pore radius. The results of non-equilibrium (i.e., transport) studies like permeation experiments can be directly interpreted in terms of a hydrodynamic pore size. Since this method operates in the same way as separation experiments, it is our opinion that with this technique the pore size can be most accurately obtained.

Although permporometry should not be used to determine the pore size of an NF membrane top layer, the technique can be very useful to investigate the variation of the pore size.

## 2.3 Gas and liquid permeation

To determine the contribution of the support to the overall mechanical resistance of the membrane, gas permeation experiments can be performed. For gas transport through a membrane, the resistance in the top layer is negligible (Benes, 2000), making this technique a very convenient one, since

it can be used to measure the support properties once the γ-layer(s) are applied on it. In our gas permeation studies we used nitrogen. Benes (2000) has presented a detailed description of the gas permeation set-up.

Gas transport through the support is governed by both convection and diffusion. For porous media these two mechanisms can be assumed additive (Benes, 2000), resulting in a linear dependency of the flux $N$ on the average pressure $p^{avg}$,

$$NRT\frac{L^s}{\Delta p} = -\left( D_{Kn} + \frac{B_0^s}{\mu} p^{avg} \right). \qquad [2]$$

In Eq. [2] $R$ is the ideal gas constant, $T$ the temperature, $L_s$ the support thickness, $\Delta p$ the pressure difference over the material, $D_{Kn}$ the Knudsen diffusion coefficient, $B_0^s$ the support permeability, and μ the gas viscosity. Assuming cylindrical pores, the (hydrodynamic) pore radius of the support $a$ and the ratio $\varphi/\tau$ can be directly calculated from this expression (Benes, 2000).

Similarly to gas permeation experiments, the permeability of a support can be determined from measurement of the ultra-pure water flux (see Figure 1). Once $B_0^s$ is measured, the top-layer permeability can be obtained by measuring the water flux through a complete membrane.

For water permeation, the transport is only driven by convection, and the volume flow rate $v$ is directly proportional to the pressure difference $\Delta p$,

$$v = B_0^M \Delta p\,. \qquad [3]$$

The permeability $B_0^\gamma$ and pore radius of the γ-layer $a$ can be calculated from the pseudo-permeability $B_0^M$. Note that the contribution of the support to the total pressure difference over the membrane is given by

$$\frac{L_s B_0^{\gamma}}{B_0^{s} L_{\gamma}} \qquad [4]$$

The thickness of the γ-layer $L_\gamma$ was experimentally determined by reflectometry (Tompkins and McGahan, 1999).

## 2.4 Retention experiments

The retention and liquid permeation experiments were performed on a home-mode dead-end set-up with a volume of 2 $dm^3$. Special attention was given to the mixing behaviour in the feed cell (Figure 1). Baffles were placed along the wall of the cell where a large stirrer operated at high stirring rates (255 rpm). The mixing behaviour was tested at these operating conditions and at increased stirring rates. No influence on the retention was observed at increased Reynolds numbers. It can therefore be concluded that the influence of external mass transport on retention can be neglected in this study.

Additional cooling was required to prevent an increase in temperature (>15 °C without cooling) as a result of the rapid stirring, and all experiments were performed at a temperature of 25 ± 1 °C.

The retention experiments were conducted with aqueous solutions of 1 $mol/m^3$ NaCl and $CaCl_2 \cdot 2H_2O$ at various pH. The pH was adjusted using 20 $mol/m^3$ NaOH and HCl. The ionic strength of the electrolyte solutions increased by less than 6% as a result of the acid and base additions.

During each pH experiment, samples were collected at pressure differences around 1.5, 1.2, 1.0, 0.7, and 0.4 MPa, in this order (i.e., from high to low $\Delta p$). The ion concentrations in the feed and permeate were determined with a Dionex DX120 ion-chromatograph. Depending on the pressure, a period of 30 to 60 minutes was used to allow both the flux and the permeate concentration to reach steady state. During this equilibration period, the

permeate conductivity and flux were continuously monitored to assure that a steady-state situation had been reached.

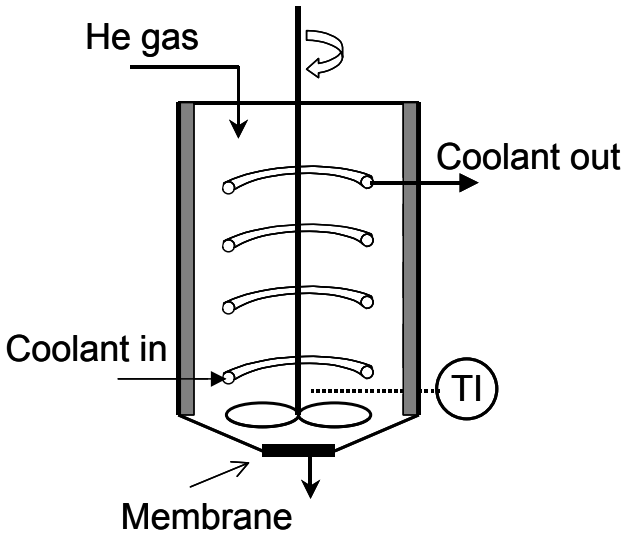


Figure 1: Schematic cross-section of the liquid permeation set-up.

The variation in the pH of the feed solution was determined by measuring the pH at the beginning and the end of every retention experiment (see Table 3). The average of these two pH values was used for the model calculations. Typically variations between the feed and retentate pH were within 0.5 pH unit, except for the pH around the iso-electric point where a pH difference of ≈1.5 was measured.

## 3. Results and Discussion

### 3.1 Osmotic pressure effects

In literature it is generally found that increasing electrolyte feed concentrations reduce the flux through the membrane as a result of osmotic pressure effects (Baticle *et al.*, 1997; Afonso and De Pinho, 2000). In this study, however, the membrane flux (sample no. 4) is found to be constant for ultra-pure water and electrolyte concentrations up to 100 mol/m$^3$ (Figure 2).

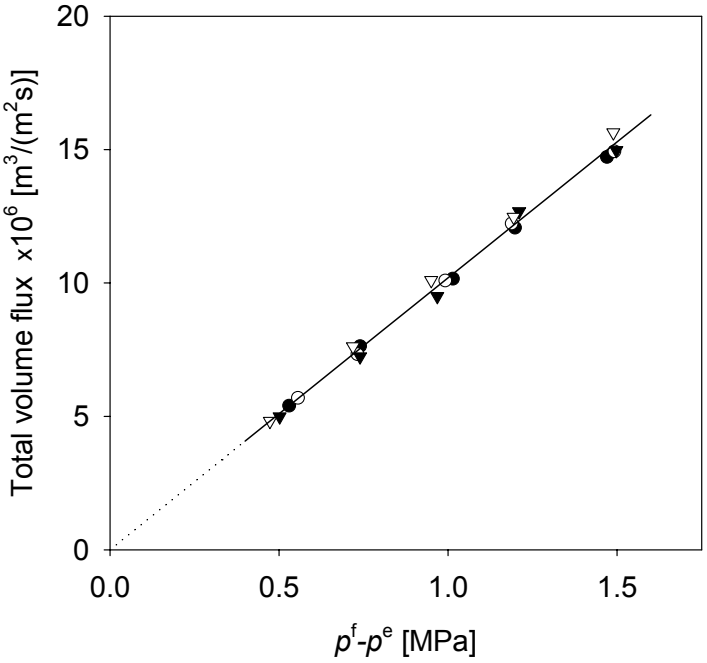


Figure 2: Membrane sample #4 volume flux as function of pressure difference for 1 mol/m$^3$ NaCl at pH$^f$=5.8 (open circles), 100 mol/m$^3$ NaCl at pH$^f$=5.9 (open triangles), ultra-pure water (closed circles) at pH$^f$=5.8, and 1 mol/m$^3$ $Na_2SO_4$ at pH$^f$=5.8 (closed triangles). Line is best fit according to Eq. [3].

In our opinion, this result is caused by the reduction of the retention at increasing concentrations (chapter 7). For example, the limiting retention (not shown) of sample 4 for 1 and 100 mol/m$^3$ NaCl (pH$^f$=5.8) is 75% and 20%, respectively. The lower retention at the higher concentration will nullify the osmotic pressure effect. Our results of a constant volume flux as a function of pressure are in agreement with the findings of Bowen and Welfoot (2002).

### 3.2 Comparison of measured and calculated retention

In this section, the experimentally determined retention is compared to the predictions obtained using the charge regulation transport model

(chapter 7). Because experimental results indicated that the influence of an external mass transport resistance was negligible, all model calculations were performed omitting this contribution.

| Solution properties | $c^f$=1 mol/m$^3$, $\mu$=9.0·10$^{-4}$ Pa·s, $K_w$=10$^{-8}$ [mol$^2$/m$^6$] | | | | | |
|---|---|---|---|---|---|---|
| Adsorption parameters$^+$ | log($K^+$)=8.3, log($K_{Na}$)=log($K_{Cl}$)=-0.7, log($K_{Ca}$)=3.4, $C_1$=1.2 [C/(V·m)], $C_2$=50 [mC/(V·m)], $c_{tot}^{//}$=1.33·10$^{-5}$ [mol/m$^2$] | | | | | |
| | $OH^-$ | $H^+$ | $Na^+$ | $Cl^-$ | $Ca^{2+}$ | $H_2O$ |
| $\bar{V}_i$ [m$^3$/mol] | -5.3·10$^{-6*}$ | 0$^*$ | -1.5·10$^{-6*}$ | 18.1·10$^{-6*}$ | -17.7·10$^{-6*}$ | 18.0·10$^{-6\circ}$ |
| $D_{iw}$ [m$^2$/s][1] | 5.28·10$^{-9\#}$ | 9.31·10$^{-9\#}$ | 1.33·10$^{-9\#}$ | 2.03·10$^{-9\#}$ | 7.9·10$^{-10\#}$ | |
| $D_{wM}$ [m$^2$/s][1] | | | | | | 5.41·10$^{-10\S}$ |

$^+$De Lint *et al.*, 2002c; $^*$Horvath, 1985; $^\circ$Atkins, 1990; $^\#$Cusler, 1984, $^\S$Lide, 1999. [1]Effective diffusion coefficients are calculated by $\mathcal{D}_{ij}^{\text{eff}} = \tau / \left( \varphi H_i^{\text{d}} \right) \mathcal{D}_{ij}$ (chapter 7).

Table 2: Physical properties and adsorption parameters on γ-alumina for NaCl and $CaCl_2$.

Samples 5 to 7 (see Table 1) were used for the retention experiments. The binary electrolytes NaCl and $CaCl_2$ at 1 mol/m$^3$, and a ternary mixture of 1 mol/m$^3$ NaCl with 1 mol/m$^3$ $CaCl_2$ were used at feed pH values around 4.5, 6 (only pH for the ternary mixture), 8.3 (the iso-electric point of the membrane, see chapter 6), and 9.5. The physical data for the electrolytes and the adsorption parameters on γ-alumina are given in Table 2.

### 3.2.1 Independent parameters

For a retention experiment (i.e., a complete pH series) the following parameters were determined experimentally:

- the support thickness (before a top layer was applied),
- the permeability, pore radius and φ/τ of the support (from $N_2$ gas permeation measurements),
- the thickness of the γ-layer (using reflectometry),

- the permeability and pore radius of the γ-layer (using liquid permeation),
- and the Kelvin pore radius before and after the experiment (with permporometry).

The results of these membrane characterisation techniques are summarised in Table 3.

| | Sample | Salt | Feed pH | Thickness [μm] | Permeability $10^{20}$ [$m^2$] | 2a [nm] |
|---|---|---|---|---|---|---|
| γ-layer | 4 | - | - | 1.7 | ≈2.6° | ≈2.2 |
| support | 4 | | | ≈$2 \cdot 10^3$ | ≈$4.6 \cdot 10^{3}$° | ≈124 |
| γ-layer | 5 | NaCl | 4.5-4.7, 5.8-6.4, 8.8-7.0, 9.5-9.2 | 1.5 | 1.7, 2.3, 2.9, 2.6* | 1.8, 2.0, 2.4, 2.2* |
| support | 5 | | | $1.95 \cdot 10^3$ | $15.7 \cdot 10^3$ | 197 |
| γ-layer | 6 | $CaCl_2$ | 4.5-5.0, 5.9-6.2, 8.6-7.1, 9.7-9.4 | 1.6 | 1.9, 2.0, 2.1, 2.6* | 1.9, 1.9, 2.0, 2.2* |
| support | 6 | | | $2.02 \cdot 10^3$ | $11.2 \cdot 10^3$ | 173 |
| γ-layer | 7 | NaCl + $CaCl_2$ | 5.7-6.2 | 1.5 | 1.6 | 1.7 |
| support | 7 | | | $1.99 \cdot 10^3$ | $12.9 \cdot 10^3$ | 160 |

°Not measured, but typical values were used, leading to approximations for the γ-layer and support pore size and permeability. *For the average pH values of NaCl and $CaCl_2$.

Table 3: Measured properties of membrane samples from Table 1.

### 3.2.2 NaCl

Without addition of acid or base, the pH of the NaCl solution is 5.8. This pH is the first value where the retention is measured. Consecutively, an

experiment at pH=8.8 was conducted. The experimental data points and the model results for both measurements are given in Figure 3. Literature data on the porosity and tortuosity and the data in Table 2 and Table 3 are used as input for the model calculations.

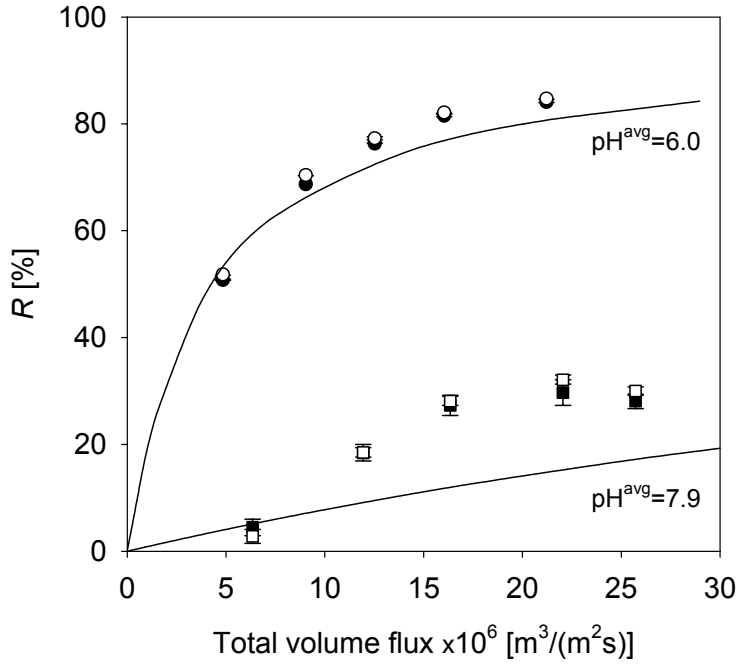


Figure 3: Cation (black) and anion (white) retention of as function of volume flux for 1 mol/m$^3$ NaCl (sample no. 5) at pH$^{avg}$=6.0 (circles) and pH$^{avg}$=7.9 (squares). Lines are model predictions.

Using an average feed pH value of 6.0 (positive membrane charge), the retention for the first experiment was predicted (Figure 3). Taking the accuracy of the model parameters into account, the agreement between model and experiment is very good and the trend of the retention data is predicted well. The retention predictions around the iso-electric point (IEP) are much more inaccurate, but fortunately for practical applications they are less interesting. The primary cause for this discrepancy is the variation in feed pH, which changed from 8.8 to 7.0 during the experiment (see Table 3). Previously performed simulations for NaCl showed that the retention

increases strongly at small deviations in pH from the IEP (chapter 7). A similar result has recently been obtained for indifferent 1:1 electrolytes on a titania NF membrane (Van Gestel *et al.*, 2002). Assuming an average pH for this experiment can therefore lead to a large error in the model predictions. To illustrate this, the retention was calculated at pH=8.8 and pH=7.0 (the feed and permeate pH). At pH=8.8, the limiting *R* was 10%, while at pH=7.0 a limiting retention of ≈66% was calculated. Clearly, for this extremely large variation in the retention, the assumption of an average pH in the model is not justified.

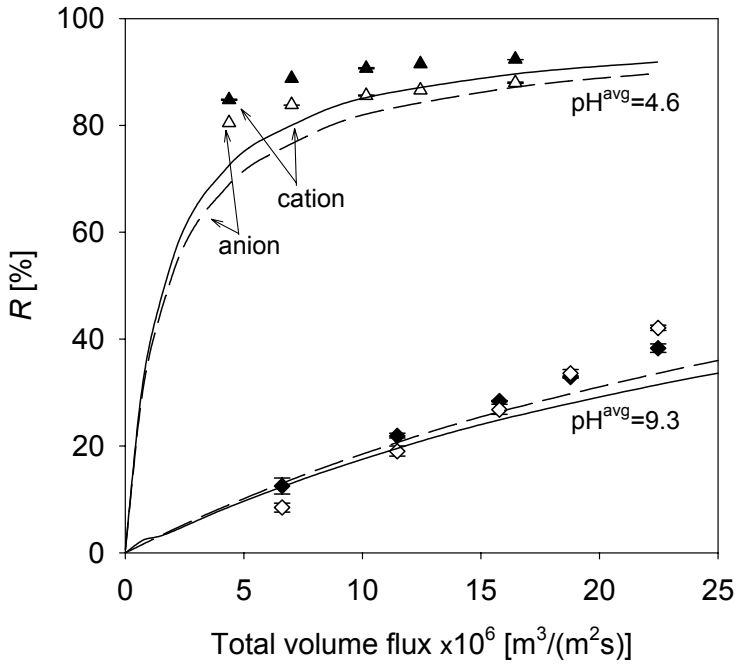


Figure 4: Cation (black) and anion (white) retention as function of volume flux for 1 mol/m$^3$ NaCl (sample no. 5) at pH$^{avg}$=4.6 (triangles) and pH$^{avg}$=9.3 (diamond). Lines are cation (solid) and anion (dashed) model predictions.

Experimental limitations are the reason for the large variation of the feed and retentate pH. Our dead-end set-up has a feed volume of 2 dm$^3$. Unless some kind of buffering effect occurs (like at pH≈6), the pH of any electrolyte solution will always move towards a neutral pH because highly mobile

protons and hydroxyl ions are transported through the membrane more rapidly. For small deviations from the neutral pH a very large feed volume or a continuous adjustment of the feed pH is necessary to compensate for this shift towards a neutral pH.

An increased concentration of protons at $pH^{avg}$=4.6 (positive membrane charge) results in an increased sodium retention compared to the chloride retention. At $pH^{avg}$=9.3 (negative membrane charge), highly mobile hydroxyl ions are added and the situation should be reversed (that is, the retention of $Cl^-$ is higher than that of $Na^+$). Both the model and the experiment show this characteristic behaviour at acidic and alkaline pH (see Figure 4), with fairly good agreement. The expected difference between cation and anion retentions is not found for the experimental data at alkaline pH although the model predicts such an effect. The reason for this discrepancy is not known. The model shows some deviation from the experimental results for the lowest fluxes at pH=4.6 and for the limiting retention at pH=9.3, but besides that its predictions are very good.

The good agreement between model and experiment for NaCl in Figure 3 and Figure 4 are a strong indication that it is well possible to predict NF behaviour for an indifferent (i.e., not specifically adsorbing) binary electrolyte using independent experimental data.

### 3.2.3 $CaCl_2$

Previously it was shown that calcium shows specific adsorption on γ-alumina NF membranes, leading to continuously positive zeta potentials (ζ) for pH values between 3 and 10 (De Lint *et al.*, 2002c). Furthermore, for 1 mol/m$^3$ $CaCl_2$ the drop in ζ over the complete pH range was 45 mV, only half of the variation in ζ for 1 mol/m$^3$ NaCl (chapter 6). The strong dependence of the type of electrolyte on the charging behaviour has not only been observed for inorganic NF membranes (Vacassy *et al.*, 1997; Labbez *et al.,* 2002; Palmeri

*et al.*, 2000; Van Gestel *et al.*, 2002). Schaep *et al.* (1999) studied the retention for four type of polymeric membranes and they concluded that the membrane charge was strongly dependent on the type of salt.

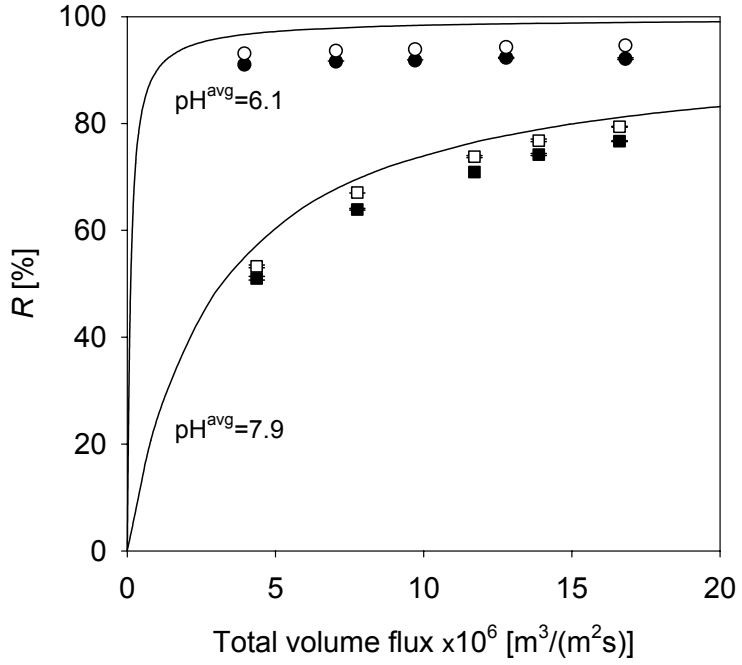


Figure 5: Cation (black) and anion (white) retention of as function of volume flux for 1 mol/m$^3$ $CaCl_2$ (sample no. 6) at $pH^{avg}$=6.1 (circles) and $pH^{avg}$=7.9 (squares). Lines are model predictions.

The increase in the retention of $CaCl_2$ compared to NaCl is clear from Figure 5. The experiments at $pH^{avg}$=6.1 (positive membrane charge) show that apart from a higher absolute retention value (more positive membrane charge due to the strong adsorption of $Ca^{2+}$) the limiting retention is also reached at much lower volume fluxes.

At the limiting retention, migration and viscous flow are the dominating transport mechanisms in the membrane. The effect of diffusion on transport is negligible. In this case, due to the high and positive value of the zeta potential, calcium exclusion from the membrane pore is almost complete

(Boltzmann relation). Since this effect results in a very low concentration of $Ca^{2+}$ in the pores, the influence of electrolyte diffusion on overall membrane transport is already small at very low pressure differences. Consequently, the limiting retention is reached almost immediately.

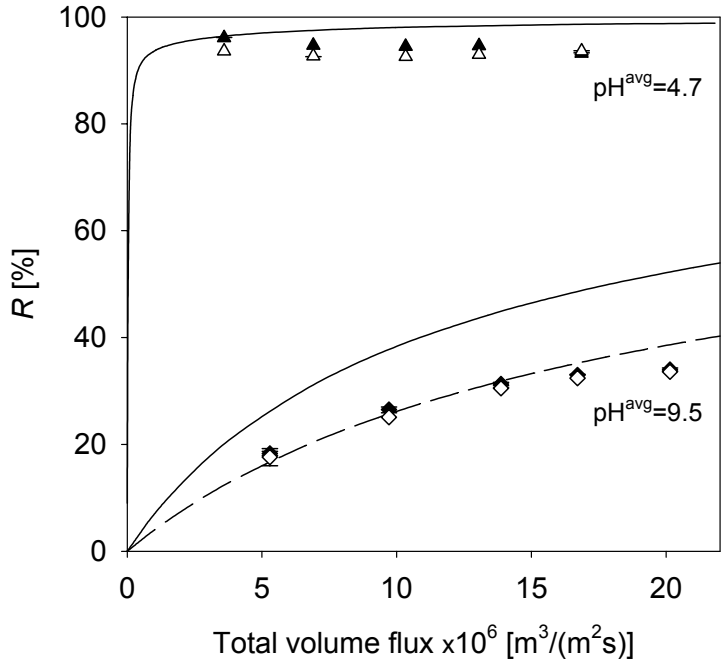


Figure 6: Cation (black) and anion (white) retention as function of volume flux for 1 mol/m$^3$ $CaCl_2$ (sample no. 6) at $pH^{avg}$=4.7 (triangles) and $pH^{avg}$=9.5 (diamond). Solid lines are model predictions. Dashed line is fit for $\log(K_{Ca})$=3.1.

The calcium chloride retention experiment at a pH around the IEP suffered from the same experimental limitations as previously discussed for NaCl. However, for $CaCl_2$ the difference between the (limiting) model retentions for the feed and permeate pH values was much smaller ($\Delta R_{lim}\approx 25\%$, compared to $\Delta R_{lim}\approx 56\%$ for NaCl). Hence, the impact of the pH on retention was much smaller and consequently a more accurate model fit could be obtained for the $pH^{avg}$=7.9 experiment.

The conclusion from the retention data at pH=6.1, that transport processes seem to be of minor importance, is supported by the retention results at $pH^{avg}$=4.7 (positively charged membrane) displayed in Figure 6. Although more mobile protons are present at a lower pH, the retention of $CaCl_2$ does not change in comparison with the situation at pH=6.1. Both the experimental and model retentions show the same behaviour, only the model retention is approximately 4% above the experimental retention.

The model predictions for $pH^{avg}$=9.5 (positively charged membrane) are quite some way of the experimental predictions. This cannot be caused by variations in the pH during the experiment as the feed and permeate pH vary by only 0.3 pH units (see Table 3). Instead, it is likely that this effect is caused by an inaccurate value of the calcium adsorption constant, $\log(K_{Ca})$.

At pH≤6.1, the zeta-potential is so high that the effect of a variation in $\log(K_{Ca})$ is of minor importance as calcium exclusion from the pores is already complete. At 1 mol/m$^3$ $CaCl_2$ and pH≈10, the $\zeta$ obtained from electrophoretic mobility experiments is approximately 10 mV (chapter 6). This low value reduces the degree of double layer overlap in a pore and consequently makes the retention much more sensitive to the absolute value of $\log(K_{Ca})$.

It was found that reducing the $\log(K_{Ca})$ to 3.1 (i.e., a decrease by 9%) resulted in a much better agreement between model and experiment (see Figure 6). The small required variation in $\log(K_{Ca})$ indicates that the ion adsorption parameters extracted from the mobility experiments were reasonably accurate. In our opinion, variation of the other adsorption parameters was not justified, as they are highly correlated (Johnson jr., 1984) and had already produced good predictions for the NaCl case. The influence of the variation in $\log(K_{Ca})$ on the predicted model retention at pH<9.5 was investigated. As expected the retention predictions did not change as a result of the variation in the calcium adsorption constant.

The adjustment of log($K_{Ca}$) clearly indicates that retention experiments at certain pH values can be used to improve the predictions for the adsorption parameters that were obtained from electrophoretic mobility data (chapter 6). Insight into the ion-material charging behaviour is required, however, since some adsorption parameters are insensitive at particular operating conditions.

Please note that to obtain the feed solution of pH=9.7, NaOH was added, resulting in a ternary system. The contribution of $Na^+$ to the $CaCl_2$ retention was so low (≈3%: calculated using the model for a ternary mixture) that it was neglected.

To summarise, despite the complicated interaction of calcium with the alumina NF membrane it is well possible to predict the retention of $CaCl_2$. Furthermore, a combination of retention measurements with zeta-potential data (chapter 6) can help to quantitatively estimate the calcium adsorption constant on γ-alumina. Not all retention experiments are well suited for this last purpose, as the contribution of log($K_{Ca}$) becomes less important at high degrees of double layer overlap.

### 3.2.4 NaCl + $CaCl_2$

The individual ion adsorption parameters were derived from electrophoretic mobility measurements in binary electrolyte solutions. It is therefore very interesting to see how accurate these parameters can predict retention for a ternary mixture of NaCl and $CaCl_2$.

The retention for an equimolar solution of 1 mol/$m^3$ NaCl with $CaCl_2$ at a $pH^{avg}$ of 5.9 is analysed in Figure 7. According to the generally observed behaviour for ternary mixtures (Tsuru *et al.*, 1991; Shenase, Staude and Yaroshchuk, 1995; Bowen, Welfoot and Williams, 2002), it is expected that the addition of $Na^+$ to the $CaCl_2$ solution would increase the $Ca^{2+}$ and reduce

the $Cl^-$ retention, compared to a situation with only calcium chloride. Furthermore, the sodium retention should be negative for low volume fluxes.

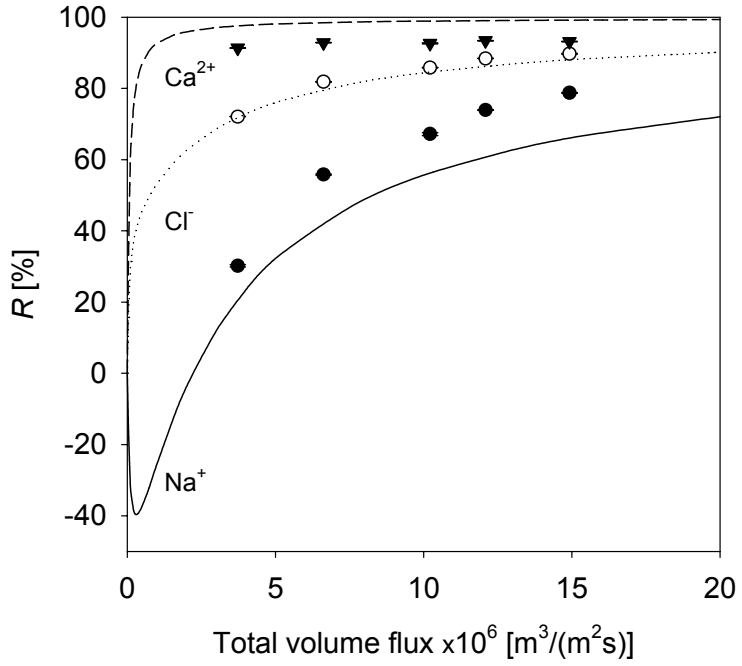


Figure 7: Cation and anion retention of as function of volume flux for a mixture of 1 mol/m³ $CaCl_2$ with 1 mol/m³ NaCl at $pH^{avg}$=5.9. Lines are model predictions.

Figure 7 shows that although a decrease in $R_{Cl}$ is observed, the calcium retention remains practically unchanged. The trend of the sodium ion data suggests that at low volume fluxes negative retentions will be observed. The fact that the $R_{Ca}$ does not increase gives again conformation of the assumption that calcium is almost completely eliminated from the membrane pores (Boltzmann relation) as a result of the high positive pore potential due to calcium adsorption. The lower charge and higher mobility of the sodium ion enables it to enter the pores more easily, and concurrently this effect reduces the chloride retention.

In general, the ternary model predictions agree well with the experimental data. For $Ca^{2+}$ the model deviation is already elaborately discussed. Model

and experiment correspond excellently for $Cl^-$. The difference in retention is largest for $Na^+$ (reaching a maximum of 10% at the highest volume flux), although the trend of the data is predicted well. Many phenomena can be the cause for the too low predictions of the sodium retention. At high fluxes the model variation with experiment increases, the same trend that is observed for the binary NaCl predictions at pH=6.0 (see Figure 3). This observation might point to some inaccuracy in the combination of adsorption parameters determined for sodium chloride.

Reviewing all the presented experimental retention data, it will be clear that the pH and the type of electrolyte strongly influence the retention of electrolyte solutions. It is therefore imperative that ion-material interactions should be properly incorporated in any transport model that is developed for predictive purposes. In our opinion, electrophoretic mobility experiments (Vacassy *et al.*, 1997; Palmeri *et al.*, 2000; chapter 6) are the most appropriate choice to obtain this information (i.e., zeta-potential data). Our analysis shows that the adsorption parameters can be insensitive at some experimental (retention) conditions (e.g., $\log(K_{Ca})$ at pH≤6.1). Unless this effect is taken into consideration, obtaining the adsorption parameters by a fit of retention data (Bowen and Mukthar, 1996; Hall, Starov and Lloyd, 1997; Hall, Lloyd and Starov, 1997; Bowen and Welfoot, 2002) will not result in physically realistic parameters. This is especially true for the fitting of adsorption parameters since they are highly correlated (Johnson jr., 1984).

### 3.3 Additional membrane information

In order to make a valid comparison between the model and experimental retention results presented above, two criteria have to be met. First, the membrane separation properties should not change during a retention experiment and secondly the assumptions applied in the transport model should be valid.

Therefore, the influence of the most important operating condition, that is, the pH, on the material properties of the membrane was investigated before any retention experiments were performed. Apart from the pH effect, the retention of the support was studied, since an important assumption in the transport model is that the support is non-separating (chapter 7).

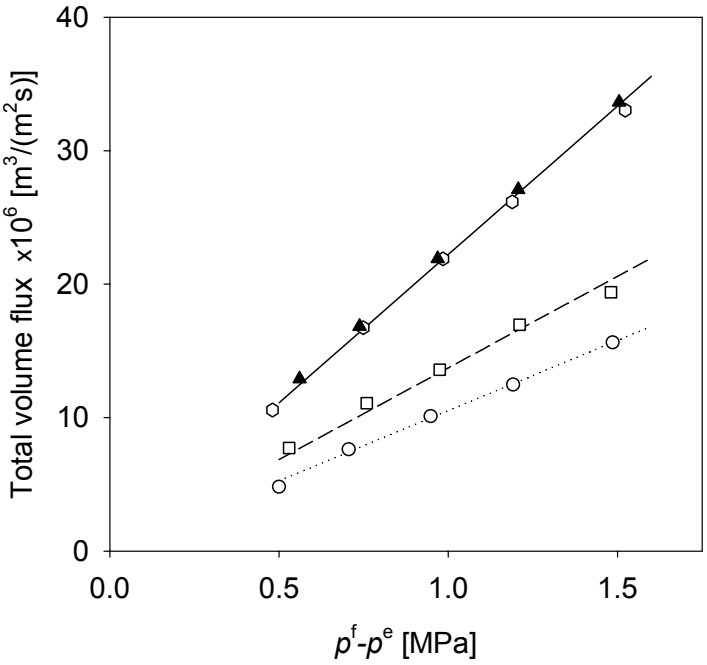


Figure 8: Volume flux for membrane sample #3 as function of pressure difference during retention experiments of 1 mol/m$^3$ $Na_2SO_4$ at $pH^f$=5.8 (open circles), $pH^f$=10.1 (open squares), $pH^f$=3.5 (open hexagons), and $pH^f$=9.3 (closed triangles). Lines are best fits according to Eq. [3].

### 3.3.1 Membrane pH stability

In previous work on unsupported material (chapter 6), a stable pH region for γ-alumina between pH=3 and pH=10 was reported. To test the stability for a supported alumina membrane, retention experiments for 1 mol/m$^3$ $Na_2SO_4$ were performed as function of pH for a single membrane on an AKP30

support (sample no. 3). The measurements were performed at feed pH ($pH^f$) values of 5.8, 10.1, 3.5 and 9.3, respectively, in this order. At $pH^f$=5.8 the membrane is considered chemically stable.

The observed volume flux as a function of pH during these retention experiments is shown in Figure 8. Clearly the pH has a significant influence on the membrane flux, which increases by a maximum of 60% for $pH^f$=10.1 and approximately by another 40% for $pH^f$=3.5 (both compared to the flux at $pH^f$=5.8). As the flux remains unchanged going from $pH^f$=3.5 to $pH^f$=9.3, the membrane is considered chemically stable at the latter pH.

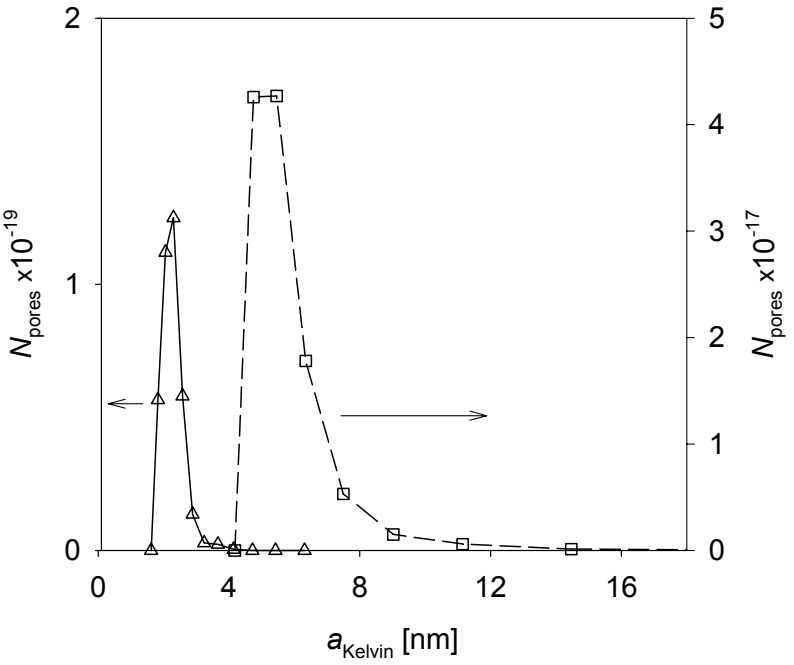


Figure 9: Typical shift in the pore-size distribution as a result of pH retention experiments. Initial (triangles) and final (squares) Kelvin radius $a_{Kelvin}$ as a function of the number of pores $N_{pores}$ as determined from permporometry. The pore shape is assumed cylindrical. Lines indicate the trend of the data points.

The cause of the membrane flux increase can be twofold, either the pore size of the top layer has increased or its thickness has decreased. An increase in pore size is likely to have the largest influence since it scales by the power 2 with the flux (assuming cylindrical pores). A typical change in the top-layer pore-size distribution (obtained from permporometry) before and after a series of retention measurements at extreme pH is displayed in Figure 9. Clearly the average Kelvin radius has increased significantly (from $a_{Kelvin}$≈2 nm to $a_{Kelvin}$≈6 nm) by the pH treatments.

Apparently, the influence of the pH on the membrane stability for supported material is more pronounced than for unsupported material. Further experimental studies indicated that the supported membranes were stable in a pH window between pH=4 and pH=10, corresponding well to literature stability data on γ-alumina (Hofman-Züter, 1995; Horst and Höll, 1997; Schaep *et al.*, 1999). Consequently, to facilitate a proper comparison of the model predictions with experimental data, the previously discussed retention experiments were performed within this stable pH range.

### 3.3.2 pH-dependent flux behaviour for NaCl and $CaCl_2$ retention experiments

Having ascertained the membrane's stable pH window, it is important to address a pH-dependent effect on the flux that was observed for the retention experiments of NaCl and $CaCl_2$.

During the NaCl and $CaCl_2$ retention experiments, the permeability of the γ-layer varied as a function of pH (see Table 3). For NaCl this variation with pH is shown in Figure 10. The trans-membrane flux is highest at $pH^{avg}$=4.6 and then decreases. For NaCl, the maximum variation in $B_0^{\gamma}$ is 33%, which is well above the measurement error. A somewhat different pH-dependent effect on the permeability was observed for the $CaCl_2$ experiments (see Table 3).

Though the pH characteristic in Figure 10 bears a strong resemblance to the pH leaching effect in Figure 8 discussed above, in our opinion a different phenomenon is responsible for the behaviour in Figure 10. To illustrate this, the permporometry pore-size distribution of the membrane before and after the NaCl experiments is shown in Figure 11. The distribution seems to be shifted to slightly higher pore sizes, but the change in the average pore size ($\overline{a}_{\text{Kelvin}}$ from 2.4 to 2.5 nm) and the width of the curve ($\sigma_{\text{Kelvin}}$ from 0.9 to 1.0 nm) is well within the experimental error. Furthermore, the permporometry data are in good agreement with the data of Nijmeijer *et al.* (2001), who measured a Kelvin radius of 2.0 nm on the same type of membranes.

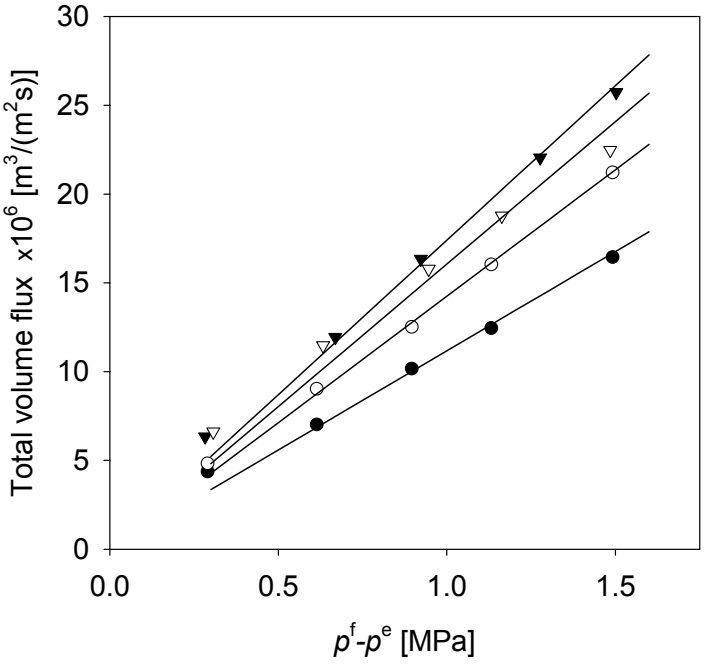


Figure 10: Total volume flux of sample #5 as function of the pressure difference for 1 mol/m$^3$ NaCl at pH$^{avg}$=6.0 (open circles), pH$^{avg}$=7.9 (closed triangles), pH$^{avg}$=4.6 (closed circles), and pH$^{avg}$=9.3 (open triangles). Lines are best fits according to Eq. [3].

It can therefore be concluded that the membrane pore radius did not change as a result of the different pH conditions in the NaCl experiment. The permporometry results for membrane samples 6 and 7 (not shown) also indicated that the pore radius was unchanged after the series of pH retention experiments. To date it is not clear what the cause is for the observed pH-dependent flux effect. It may be due to a reversible pH-dependent fouling mechanism but no evidence to support this hypothesis exists.

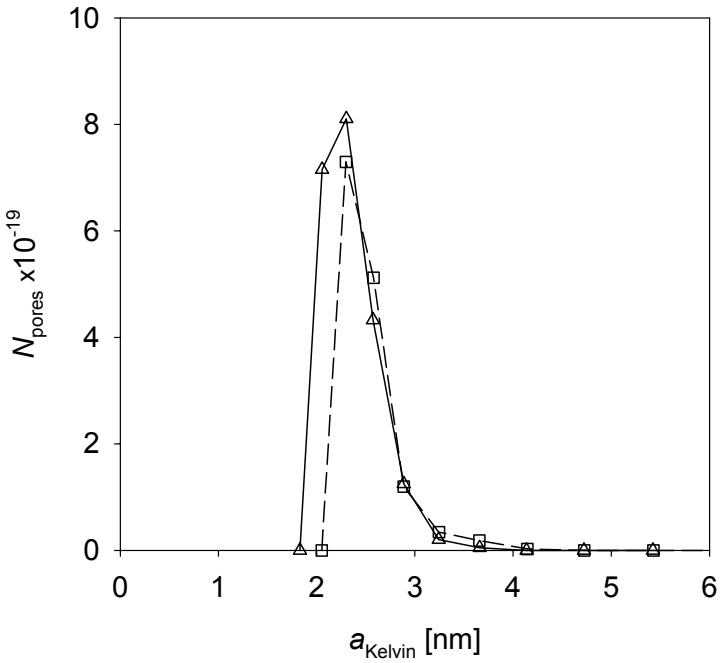


Figure 11: Initial (triangles) and final (squares) Kelvin radius $a_{Kelvin}$ as a function of the number of pores $N_{pores}$ as determined from permporometry for sample #5. The pore shape is assumed cylindrical. Lines indicate the trend of the data points.

Although the permporometry data suggests that the membrane pore radius $a$, and hence the top-layer permeability, are constant, it is clear that the flux during the retention experiments varied with pH. For a proper model prediction of the retention, this flux variation has to be taken into account.

For the model simulations in this work it was therefore decided to let $B_0^{\gamma}$ and $a$ vary as a function of the pH (see Table 3).

### 3.3.3 Influence of the support

Preferably a support should provide mechanical strength to the separating top layer while exhibiting a limited resistance (i.e., low pressure drop or high flux). The large required thickness of our inorganic support (≈2 mm), coupled to a relatively small pore size ($a$≈124 nm for an AKP30 support), strongly decreases the trans-membrane flux, which reduces the retention of the top layer. Apart from this effect, the support may exhibit retention (Takagi *et al.*, 2000; Szymczyck *et al.*, 2001).

| | $B_0^s \cdot 10^{17}$ [m²] $N_2$ permeation | $B_0^s \cdot 10^{17}$ [m²] Ultra-pure water permeation | $2a$ [μm] |
|---|---|---|---|
| Sample 1 | 4.55 | 4.63 | 0.20 |
| Sample 2 | 15.9 | 15.7 | 0.12 |

Table 4: Permeability of AKP30 and AKP15 support from $N_2$ and water permeation. The displayed pore size is calculated from the gas permeability data assuming cylindrical pores (see Eqs. [3.4] and [3.6] in Benes, 2000).

A decrease of the support resistance will therefore have two beneficial effects; both the overall membrane retention and flux are increased. In Figure 12 and Figure 13 the flux through two supports, samples 1 and 2 in Table 1, is compared. In our lab, generally AKP30 powder is used to prepare the support. By replacing AKP30 with the more coarse AKP15 powder (for material data see Experimental section), supports with a 3 to 4 times increased flux ($B_0 \sim a^2$) are obtained (see Figure 12 and Figure 13). By this substitution, the support contribution to the total pressure drop over the membrane (see Eq. [4]) decreased from ≈60% to 20%.

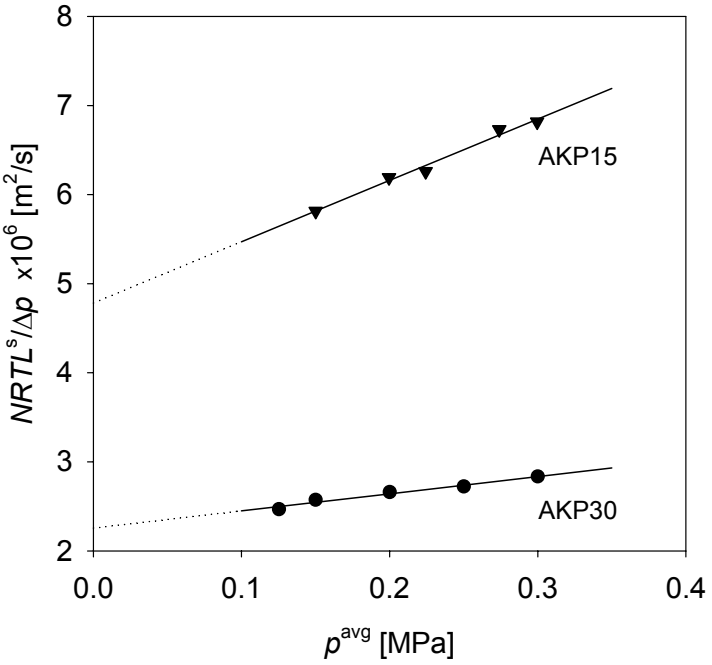


Figure 12: $N_2$ gas flux for sample no. 1 (circles) and sample no. 2 (triangles) as function of the average pressure difference. Lines are best fit according to Eq. [2].

The support permeability was measured by using both $N_2$ gas and ultra-pure water permeation. It is very interesting to note that the permeabilities obtained with both techniques are very similar (Table 4), though the contributions of convection and diffusion to mass transport are quite different for both techniques. Water permeation transport is completely convective, while gas permeation is governed by both convection and diffusion. Table 4 shows that the pores of the AKP15 support are 67% larger than those of the AKP30 support.

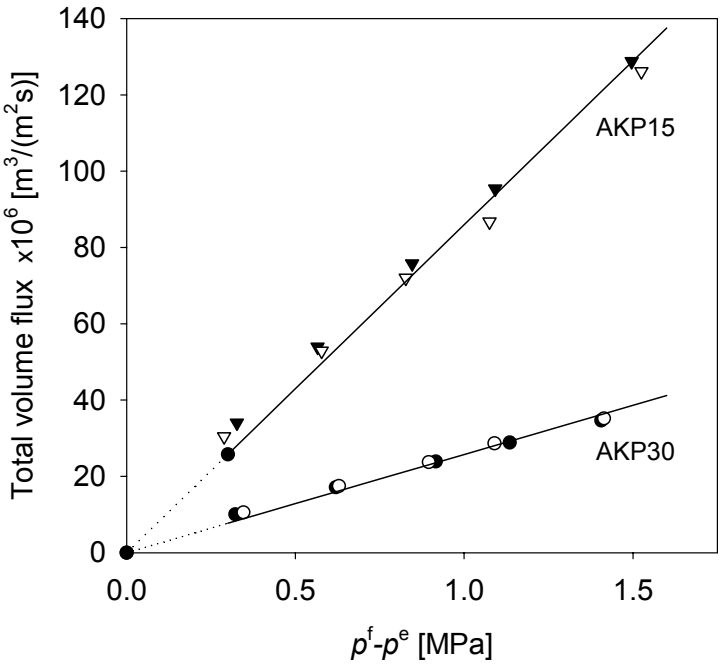


Figure 13: Volume flux for sample no. 1 (circles) and sample no. 2 (triangles) as function of pressure difference for ultra-pure water (filled symbols) and 1 mol/m$^3$ NaCl (open symbols) at pH$^f$=5.8 (AKP30) and pH$^f$=5.6 (AKP15), respectively. Lines are best fit according to Eq. [3].

Because of the flux increase, a decrease in the AKP15-support retention is expected. In Figure 14 the retention of both support types for 1 mol/m$^3$ NaCl is shown. Indeed the retention of the AKP15 support is almost zero (<2%), where it is ≈17% for the AKP30 support. Our transport model assumes a non-separating support. Clearly by using an AKP15 support this requirement is best satisfied. Therefore AKP15 supports were used for the comparison between the measured and the predicted model retentions (*viz.* membrane samples 5 to 7 in Table 1). Obviously more important than the decreased support retention with increased support flux is the increased overall membrane retention (chapter 7). Experimentally (data not shown), the increase in retention for a membrane with an AKP15 instead of an AKP30 support was 30%.

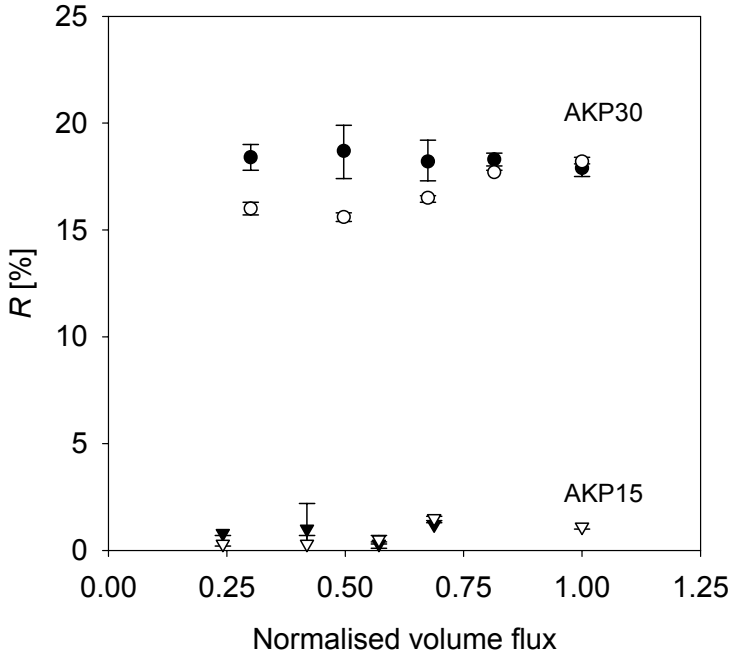


Figure 14: Cation retention (filled symbols) and anion retention (open symbols) for a sample 1 (circles) and sample 2 (triangles) of as function of normalised volume flux for 1 mol/m$^3$ NaCl at pH$^f$=5.8 (AKP30) and pH$^f$=5.6 (AKP15).

## 4. Conclusions

The retention behaviour of an asymmetric α-alumina supported γ-alumina membrane for both binary electrolytes as well as a ternary electrolyte mixture is predicted using a transport model without adjustable parameters. For the electrolyte solutions considered, the model predictions are in good agreement with the experimental retention data.

The measurements show that at a constant pH the trans-membrane volume-flux does not exhibit osmotic pressure effects. The flux remains constant up to electrolyte concentrations of 100 mol/m$^3$. Furthermore, the pH stability window of the selective γ-alumina top layer for supported

membranes is different than for unsupported material and lies between pH=4 and pH=10.

The large required thickness of the α-alumina support can lead to a considerable mechanical resistance, resulting in electrolyte separation by the support and a decrease of the overall membrane flux and retention. A support with a pore size of 0.20 μm increases the overall membrane flux and retention by ≈40% and 30%, respectively, compared to a support with a pore size of 0.12 μm.

## References


1. Abbasi M.H., Evans J.W., and Abramson I.S., "Diffusion of Gases in Porous Solids: Monte Carlo Simulations in the Knudsen and Ordinary Diffusion Regime," *AIChE J.*, **29**, 617 (1983).
2. Afonso M.D., and De Pinho M.N., "Transport of $MgSO_4$, $MgCl_2$ and $Na_2SO_4$ across an Amphoteric Nanofiltration Membrane," *J. Membrane Sci.*, **179**, 137 (2000).
3. Atkins P.W., "Physical Chemistry," 4th edition, Oxford University Press, Oxford, 1990, p. 155.
4. Baticle P., Kiefer C., Lakhchaf N., Larbot A., Leclerc O., Persin M., and Sarrazin J., "Salt Filtration on Gamma Alumina Nanofiltration Membranes Fired at Two Different Temperatures," *J. Membrane Sci.*, **135**, 1 (1997).
5. Benes N.E., "Mass Transport in Thin Supported Silica Membranes," Ph.D. Thesis, University of Twente, The Netherlands, 2000, chapter 3.
6. Benes N.E., Spijksma G., Verweij H., Wormeester H., and Poelsema B., "CO2 Sorption of a Thin Silica Layer determined by Spectroscopic Ellipsometry," *AIChE J.*, **47**, 1212 (2001).
7. Bontha J.R., and Pintauro P.N., "Water Orientation and Ion Solvation Effects During Multicomponent Salt Partitioning in a Nafion Cation Exchange Membrane," *Chem. Eng. Sci.*, **49**, 3835 (1994).
8. Bowen W.R., and Mukthar H., "Characterisation and Prediction of Separation Performance of Nanofiltration Membranes," *J. Membrane Sci.*, **112**, 263 (1996).
9. Bowen W.R., and Welfoot J.S., "Modelling Performance of Membrane Nanofiltration – Critical Assessment and Model Development," *Chem. Eng. Sci.*, **57**, 1121 (2002).
10. Bowen W.R., Welfoot J.S., and Williams P.M., "Linearized Transport Model for Nanofiltration: Development and Assessment," *AIChE J.*, **48**, 760 (2002).
11. Combe C., Guizard C., Aimar P., and Sanchez V., "Experimental Determination of Four Characteristics used to predict the Retention of a Ceramic Nanofiltration Membrane," *J. Membrane Sci.*, **129**, 147 (1997).
12. Cussler E.L., "Diffusion. Mass Transfer in Fluid Systems," Cambridge University Press, New York, 1984, p. 147.
13. Guzmán-Garcia A.G., Pintauro P.N., Verbrugge M.W., and Hill R.F., "Development of a Space-Charge Transport Model for Ion-Exchange Membranes," *AIChE J.*, **36**, 1061 (1990).
14. Hagmeyer G., and Gimbel R., "Modelling the Salt Rejection of Nanofiltration Membranes for Ternary Ion Mixtures and for Single Salts at Different pH Values," *Desalination*, **117**, 247 (1998).

15. Hall M.S., Starov V.M., and Lloyd D.R., "Reverse Osmosis of Multicomponent Electrolyte Solutions. Part I. Theoretical Development," *J. Membrane Sci.*, **128**, 23 (1997).
16. Hall M.S., Lloyd D.R., and Starov V.M., "Reverse Osmosis of Multicomponent Electrolyte Solutions. Part II. Experimental Verification," *J. Membrane Sci.*, **128**, 39 (1997).
17. Hofman-Züter J.M., "Chemical and Thermal Stability of (Modified) Mesoporous Ceramic Membranes," Ph.D. Thesis, 1995, University of Twente, The Netherlands, chapters 3 and 4.
18. Horst J., and Höll W.H., "Application of the Surface Complex Formation Model to Ion Exchange Equilibria. Part IV: Amphoteric Sorption onto γ-Aluminum Oxide," *J. Colloid Interface Sci.*, **195**, 250 (1997).
19. Horvath A.L., "Handbook of Aqueous Electrolyte Solutions. Physical Properties, Estimation and Correlation Methods, " Ellis Horwood, Chichester, 1985, p. 132.
20. Johnson jr. R.E., "A Thermodynamic Description of the Double Layer Surrounding Hydrous Oxides," *J. Colloid Interface Sci.*, **100**, 540 (1984).
21. Labbez C., Fievet P., Szymczyk A., Vidone A., Foissy A., and Pagetti J., "Analysis of the Salt Retention of a Titania Membrane using the "DSPM" model: Effect of pH, Salt Concentration and Nature," *J. Membrane Sci.*, **208**, 315 (2002).
22. Leenaars A.F.M., Keizer K., and Burggraaf A.J., "The Preparation and Characterization of Alumina Membranes with Ultra-Fine Pores. Part 1. Microstructural Investigations on Non-Supported Membranes," *J. Mater. Sci.*, **19**, 1077-1088 (1984).
23. Leenaars A.F.M., and Burggraaf A.J., "The Preparation and Characterization of Alumina Membranes with Ultrafine Pores. 2. The Formation of Supported Membranes," *J. Colloid Interface Sci.*, **1985**, *105*, 27.
24. Leenaars A.F.M., and Burggraaf A.J., "The Preparation and Characterization of Alumina Membranes with Ultra-Fine Pores. Part 3. The Permeability for Pure Liquids," *J. Membrane Sci.*, **24**, 245 (1985).
25. Lide D.L. (ed.), "CRC Handbook of Chemistry and Physics," 79th edition, CRC Press, New York, 1999, p. 5.90.
26. Nijmeijer A., Kruidhof H., Bredesen R., and Verweij H., "Preparation and Properties of Hydrothermally Stable γ-Alumina Membranes," *J. Am. Ceram. Soc.*, **84**, 136 (2001).
27. Palmeri J., Blanc P., Larbot A., and David P., "Theory of Pressure-Driven Transport of Neutral Solutes and Ions in Porous Ceramic Nanofiltration Membranes," *J. Membrane Sci.*, **160**, 141 (1999).
28. Palmeri J., Blanc P., Larbot A., and David P., "Hafnia Ceramic Nanofiltration Membranes. Part II. Modeling of Pressure-Driven Transport of Neutral Solutes and Ions," *J. Membrane Sci.*, **179**, 243 (2000).

29. Schaep J., Vandecasteele C., Mohammad A.W., and Bowen W.R., "Analysis of the Salt Retention of Nanofiltration Membranes Using the Donnan-Steric Partitioning Pore Model," *Sep. Sci. Technol.*, **34**, 3009 (1999).
30. Schaep J., Vandecasteele C., Peeters B., Luyten J., Dotremont C., and Roels D., "Characteristics and Retention Properties of a Mesoporous γ-$Al_2O_3$ Membrane for Nanofiltration," *J. Membrane Sci.*, **163**, 229 (1999).
31. Shenase A., Staude E., and Yaroshchuk A.E., "Separation of Counterions during Pressure-Driven Transport of Electrolyte Mixtures across Charge Porous Membranes," *Sep. Purif. Technol.*, **30**, 2865 (1995).
32. Szymczyck A., Labbez C., Fievet P., Aoubiza B., and Simon C., "Streaming Potential through Multi-Layer Membranes," *AIChE J.*, **47**, 2349 (2001).
33. Takagi R., Larbot A., Cot L., and Nakagaki M., "Effect of $Al_2O_3$ Support on Electrical Properties of $TiO_2/Al_2O_3$ Membrane formed by Sol-Gel Method," *J. Membrane Sci.*, **177**, 33 (2000).
34. Tompkins H.G., and McGahan W.A., "Spectroscopic Ellipsometry and Reflectometry: A User's Guide," Wiley, New York, 1999.
35. Tsuru T., Urairi M., Nakao S-I, and Kimura S., "Negative Rejection of Anions in the Loose Reverse Osmosis Separation of Mono- and Divalent Ion Mixtures," *Desalination*, **81**, 219 (1991).
36. Uhlhorn R.J.R., Huis in't Veld M.H.B.J., Keizer K., and Burggraaf A.J., "Synthesis of Ceramic Membranes. Part I. Synthesis of Non-Supported and Supported γ-Alumina Membranes without Defects," *J. Mater. Sci.*, **27**, 527 (1992).
37. Vacassy R., Guizard C., Thoraval V., and Cot L., "Synthesis and Characterization of Microporous Zirconia Powders: Application in Nanofilters and Nanofiltration Characteristics," *J. Membrane Sci.*, **132**, 109 (1997).
38. Van Gestel T., Vandecasteele C., Buekenhoudt A., Dotremont C., Luyten J., Leysen R., Van der Bruggen B., and Maes G., "Salt Retention in Nanofiltration with Multilayer Ceramic $TiO_2$ Membranes," *J. Membrane Sci.*, **209**, 379 (2002).
39. Yang Y., and Pintauro P.N., "Multicomponent Space-Charge Transport Model for Ion-Exchange Membranes," *AIChE J.*, **46**, 1177 (2000).

The greatest virtues are those
which are most useful to other persons.
*Aristotle (384 BC-322 BC)*

# Chapter 9

## Integration of Results and Recommendations for Future Work


### Abstract

The principle goal in this thesis was to develop a transport description for nanofiltration (NF) that could predict the separation of multi-component electrolyte solutions without any adjustable parameters. This objective has been met, as chapter 8 shows that the retention behaviour of an alumina NF membrane can indeed be predicted for both binary electrolytes as well as a ternary electrolyte mixture using no adjustable parameters.

This chapter integrates the main results of the thesis and proposes additional studies to more extensively validate these results.

## 1. Evaluation of results

The investigations of the charge regulation approach in chapters 3 and 4 made it clear that membrane charging is the key parameter that governs NF separation. The equilibrium model in chapter 3 shows that charge regulation is a concept that in a straightforward and intuitive manner incorporates all characteristics that are important in membrane charging, such as the iso-electric point, the pore size, as well as solution properties such as pH, concentration and ion valencies. For a monovalent salt the equilibrium calculations already describe commonly observed NF separation trends like a minimum ion retention at the iso-electric point and a decrease in retention with increasing salt concentration and pore size.

In chapter 4 the equilibrium approach was replaced by the Nernst-Planck flux expressions using the uniform potential (UF) approach. For a pore size of 4 nm, the deviation from the uniform potential assumption was 11.6% for the cation concentration and 3.8% for the electrostatic potential. Because in this approach protons and hydroxyl ions are taken into account, different retentions for anions and cations are predicted at pH values below 4 and above 10. Again the model results are compared qualitatively with literature data for NF membranes. It is found that the change of ion retention with pore radius, ion concentrations and pressure for a binary electrolyte as well as for multi-component mixtures with cations of different mobility and/or charge is in agreement with experimental evidence from literature.

Having tested the general applicability of the CR approach, it was necessary to derive the adsorption parameters for a NF membrane. These parameters could then be incorporated in a transport model and the predicted model retentions could be compared to experimental data on the same membrane. The adsorption parameters have to be obtained from experimental charging data assuming a model of the surface chemistry and the electrostatic double layer. Although such models are already abundantly investigated in colloid

science, they are less familiar in the field of NF. Therefore it was important to examine the applicability of these models for the charging behaviour of an NF membrane.

In chapter 5 a 1-pK adsorption model was combined with a Basic Stern electrolyte double layer model to describe adsorption of ions on an oxide material and derive the adsorption parameters. First the dependence of the surface charge, and the 1-plane potential, on the model parameters was investigated. Next the model was applied to extract adsorption parameters from an experimental study of NaCl adsorption on γ-alumina.

The deviation between the ion adsorption constants and the Helmholtz capacity obtained from a fit of the experimental zeta potential ($\log(K_C)$=-8.7, $\log(K_A)$=-2.2, $C_1$=0.12 C/(V·m$^2$)) and surface charge ($\log(K_C)$=-1.0, $\log(K_A)$=-2.5, $C_1$=1.6 C/(V·m$^2$)) data was significant. It was difficult to accurately fit the ζ data and furthermore multiple parameter solutions could be obtained that described the data equally well. The same model fits could be obtained with the parameters $\log(K_C)$=-10.6 and $\log(K_A)$=-2.5 (all other parameters remained constant).

Using the adsorption parameters obtained from the surface charge data fit to calculate the zeta potential and vice versa proofed to be difficult. Using the parameters for the surface charge, the ζ predictions were significantly lower than the experimental data. For the reverse procedure, the calculated surface charge was up to 5x as low as the titration measurement results.

The results in chapter 5 indicated that it is not straightforward to describe the charging behaviour of an oxide material in a consistent manner. Not only should the adsorption model be able to describe variation of both the zeta potential and the surface charge, but also care must be taken to avoid the occurrence of multiple solutions. This knowledge was used in chapter 6, where electrophoretic mobility measurements on γ-alumina NF membrane

particle suspensions were performed in electrolyte solutions of NaCl, $CaCl_2$ and $Na_2SO_4$ at different concentrations. The particle mobility was related to the zeta potential and a 1-pK triple-layer adsorption model was applied to extract the ion-material adsorption parameters from the mobility measurements.

Specific adsorption of calcium and sulphate was observed on the membrane particles, resulting in continuously positive zeta potential values for $CaCl_2$ and a strong shift of the isoelectric point to lower pH values for $Na_2SO_4$. Apart from the highest calcium chloride concentrations, the adsorption model predictions were in good agreement with the experimental data. Generally, the obtained adsorption parameters were in reasonable agreement with literature values.

The available adsorption parameters and the corresponding adsorption model could be implemented in a transport description, for which the full Maxwell-Stefan relations were used. This new model was an extension of the approaches described in chapters 3 and 4, and also contained no adjustable parameters. Apart from the adsorption parameters, experimental literature data was used to fix the structural material parameters in the model. The applicability of this transport concept to qualitatively predict the retention, flux and charging properties of an α-alumina supported γ-alumina NF membrane was studied in chapter 7. The trend in the modelling results were in accordance with theoretical and experimental evidence for NF systems presented in literature for a binary electrolyte as well as for mixtures with a common anion.

The culmination of the thesis is chapter 8, where the retention predictions of the model developed in chapter 7 was compared to the experimental retention behaviour of an asymmetric alumina membrane for both binary electrolytes as well as a ternary electrolyte mixture. The promising conclusion of chapter 8 was that for the electrolyte solutions considered, the

model predictions are in good agreement with the experimental retention data. Hence, the primary objective of the research project has been achieved; it is indeed possible to develop a predictive transport description for NF separation of multi-component electrolyte solutions.

## 2. Recommendations for future work

In this thesis the route to a predictive NF transport model for ceramic oxide membranes is discussed using a γ-alumina as reference material. To test the validity of the model and make it generally applicable for all kinds of NF membranes some issues still need to be resolved further. Basically there are three points that need further attention, and they will be briefly discussed below.

### 2.1 Testing of the current model

The particular strength of the transport models proposed in this work is that they can use adsorption data from binary electrolytes to describe multi-component separation. Only a flavour of this model feature has been given in chapter 8. It is therefore important to further test the model's capabilities by comparing its predictions against experimental retention data, particularly for more different multi-component electrolyte solutions. Such an investigation is currently conducted for a quaternary $CaCl_2$-$Na_2SO_4$ mixture.

Secondly, the applicability of the model to predict the retention of other ceramic oxides like titania and zirconia should be tested. Labbez et al. (2002) analysed the retention of a tubular titania membrane as a function of pH, type of electrolyte and concentration. Currently work is underway to apply the models described in this thesis to this type of membrane and compare

the predicted and experimentally observed retention for binary monovalent and divalent electrolyte solutions.

## 2.2 Model parameter improvement

The third important step in the testing of the transport model is to acquire further information on the required input parameters. With the current state-of-the-art analysis techniques, three type of model parameters can be determined in more detail.

- Ion-material adsorption parameters
- Diffusion coefficients
- Solvent dielectric constant

In the surface chemistry study presented in chapter 6 only electrophoretic mobility studies were performed on the alumina NF membrane. Instead a combination of surface analysis techniques will lead to a more consistent prediction of a membrane's charging behaviour. In chapter 6 literature titration data for NaCl adsorption on a γ-alumina were used to help determine the adsorption parameters. Useable titration data for divalent ions was however missing. Instead of using literature titration data, it is obviously preferable to perform titration studies on the actual NF material. The adsorption parameters can then be predicted more accurately. Additionally, surface analysis techniques like liquid infrared spectroscopy should be used to analyse the types of surface complexes formed at the material surface. Rietra, Hiemstra and Van Riemsdijk (1999) have shown that spectroscopic analyses can lead to a more consistent description of the surface adsorption chemistry, and hence more accurate adsorption parameters.

The diffusion coefficients of electrolytes in confined geometries can be significantly different from those in a bulk solution. In our transport model, the diffusion coefficients in the porous matrix are corrected for structural effects (porosity and tortuosity) and radial ordering of the solutes as a result of affinity with the pore wall according to the relations of Bungay and Brenner. However, Yaroshchuk and co-workers (2000a, b) have shown that that non-steady-state characterisation techniques can be used to measure the diffusion coefficients in a membrane. It is therefore very interesting to compare the results of these characterisation techniques with the model predictions for the diffusion coefficients.

In the NF transport descriptions throughout this thesis it is assumed that separation by dielectric exclusion (DE) is of negligible importance. Though there is strong evidence supporting this assumption (e.g., section 2.1.4 in chapter 7; Senapati and Chandra, 2001), it is important to experimentally quantify the DE effect. The magnitude of DE is directly determined by the change in the relative dielectric constant of the solvent in a membrane pore compared to that in a free solution. By measurement of the solvent permittivity variation the degree in which DE contributes to the overall separation in an NF membrane can be assessed. Optical analysis techniques like ellipsometry may be a good means to determine the solvent permittivity in a confined geometry (Timlin and Pachepsky, 1996). It should be noted that in chapters 6 and 7 the variation of the solvent dielectric constant near the pore wall is implicitly accounted for by the Helmholtz capacities in the triple-layer model. It is therefore of primary importance to determine the solvent dielectric constant in the diffuse double layer part of a pore.

## References

1. Labbez C., Fievet P., Szymczyk A., Vidone A., Foissy A., and Pagetti J., "Analysis of the Salt Retention of a Titania Membrane using the "DSPM" model: Effect of pH, Salt Concentration and Nature," *J. Membrane Sci.*, **208**, 315 (2002).
2. Rietra R.P.J.J., Hiemstra T., and Van Riemsdijk W.H., "Sulfate Adsorption on Goethite," *J. Colloid and Interface Sci.*, **218**, 511 (1999).
3. Senapati S., and Chandra A., "Dielectric Constant of Water confined in a Nanocavity," *J. Phys. Chem. B.*, **105**, 5106 (2001).
4. Timlin D.J., and Pachepsky Ya. A., "Comparison of Three Methods to Obtain the Apparent Dielectric Constant from Time Domain Reflectometry Wave Traces," *Soil Sci. Soc. Am. J.*, **60**, 970 (1996).
5. Yaroshchuk A.E., Makovetskiy A.L., Boiko Y.P., and Galinker E.W., "Non-Steady-State Membrane Potential: Theory and Measurements by a Novel Technique to Determine the Ion Transport Numbers in Active Layers of Nanofiltration Membranes," *J. Membrane Sci.*, **172**, 203 (2000).
6. Yaroshchuk A.E., and Ribitsch V., "The Uses of Non-Steady-State Membrane Characterisation Techniques for the Study of Transport Properties of Active Layers of Nanofiltration Membranes: Theory with Experimental Examples," *Chem. Eng. J.*, **80**, 203 (2000).

# Summary


## Abstract

Nanofiltration (NF) has become an increasingly important unit in separation processes, bridging the gap between ultrafiltration and reverse osmosis. Though NF applications are growing rapidly, the separation characteristics are still a matter of intensive scientific investigation. Therefore the objective of the work described in this thesis was to improve the understanding on NF separation and to develop a transport description without adjustable parameters that is able to predict the separation characteristics of NF membranes.

Two central themes can be distinguished in this thesis. First the appropriateness of the charge regulation (CR) approach to describe the charging characteristics of NF membranes is investigated. Secondly the applicability of the Maxwell-Stefan theory to describe mass transport through NF membranes is critically assessed.

## 1. Overview of the thesis

The Maxwell-Stefan relations originate from the theory of irreversible processes (TIP). Therefore, in *chapter 2* a discussion is presented on the TIP, and the assumptions involved in its application to multi-component transport of simple electrolytes in NF membranes are explained. Furthermore, since in this thesis the MS or the simpler Nernst-Planck (NP) relations are used to study mass transport, *chapter 2* describes the derivation of these expressions from the TIP.

In *chapter 3* the charge regulation (CR) approach is used to describe the separation of ions from aqueous solutions by the use of hydrophilic membranes. The CR model is employed to calculate the ion concentrations across the radius of a cylindrical pore slice assuming thermodynamic equilibrium. An expression for the cation retention is used that is based on the equilibrium ion profiles in that slice. For a monovalent salt this expression qualitatively describes the change of ion retention with pore radius, ion concentrations and pH.

The calculation in *chapter 3* does not yet incorporate ion transport expressions and hence, it cannot account for the influence of pressure and flux on retention or describe the retention for mixtures of salts.

*Chapter 4* discusses a combination of the CR concept with the Navier-Stokes and NP transport equations to describe the ion retention of nanofiltration membranes consisting of narrow cylindrical pores. Like in chapter 3 the model contains no adjustable parameters. In the model in *chapter 4* radial concentration and potential gradients are considered to be negligibly small (uniform potential approach), resulting in a one-dimensional transport description.

The model describes typical experimental data for nanofiltration membranes, such as the change of ion retention with pore radius, ion concentration, pH

and pressure both for monovalent and multivalent ions. For a constant pressure difference, the model in some cases predicts an optimum pore size for retention. Non-equal retentions for anions and cations are predicted at low and high pH values, as well as a minimum solvent velocity for very low salt concentrations. For higher salt concentrations, and at a fixed pressure difference, an increase in solvent velocity with increasing ion concentrations is predicted, in agreement with other one-dimensional transport descriptions found in literature, but in contrast to some experimental data.

In *chapter 5* a 1-pK adsorption model with a Basic Stern (BS) electrostatic double layer model is used to describe ion adsorption, and the sensitivity of the charge and potential in the double layer for various adsorption parameters is discussed. From a non-linear regression analysis of literature data for the surface charge and the zeta potential, adsorption parameters for the 1-pK model are obtained for NaCl on a γ-alumina.

The 1-pK BS model can describe the surface charge well, except for the highest concentration of 1000 mol/m$^3$. Reasonable agreement is found between the zeta potential data from literature and the model predictions.

Adsorption parameters are obtained in *chapter 6*, using electrophoretic mobility (EM) measurements on a ceramic γ–alumina NF membrane material in aqueous solutions of NaCl, $CaCl_2$ and $Na_2SO_4$, and literature potentiometric titration data on another γ–alumina. Various adsorption reaction models and descriptions of the electrostatic double layer are tested. A 1-pK triple-layer (TL) description is able to describe the adsorption data most satisfactory, and consequently the adsorption parameters are obtained with this model.

The zeta potential (ζ) data, calculated from the EM measurements, indicate that NaCl acts as an indifferent electrolyte on the NF γ-alumina, resulting in an iso-electric point (IEP) at pH=8.3. The ζ data can be accurately described

with the 1-pK TL model. Furthermore, the model predictions for the surface charge are in good agreement with literature titration data for this 1:1 electrolyte. Strong adsorption of $Ca^{2+}$ ions leads to positive zeta potentials for all investigated electrolyte concentrations and pH values. The model is capable to fit the potential data reasonably well. Strong adsorption of sulphate ions causes a shift of the iso-electric point to lower pH values. For a bulk concentration of 100 mol/$m^3$ $Na_2SO_4$ only negative zeta potentials are observed.

*Chapter 7* combines the CR concept with the Maxwell-Stefan theory to predict multi-component electrolyte transport in NF membranes. A predictive model is presented, which is an elaboration of the approach presented in chapter 4. Similarly, the model in *chapter 7* requires no adjustable parameters. Charging of the membrane surface is described using a 1-pK site-binding model with a triple-layer electrostatic description and mass transport is based on the uniform potential approach (i.e., a one-dimensional transport model). Input data is obtained from independent measurements, e.g., electrophoretic mobility data. The model predictions for the retention and flux of NaCl and a mixture of NaCl with $CaCl_2$ are discussed for an asymmetric γ-alumina nanofiltration membrane.

The transport model results show that double layer overlap in the pores, leading to charge regulation, appears to have a marked influence on the potential ($\Delta\phi$=59-88% for 4 nm pores), and thus on separation. Furthermore, the membrane surface charge varies significantly over the pore length, rendering the assumption of a constant charge generally applied in literature questionable. Additionally, the model predicts typical nanofiltration behaviour, including non-equal cation and anion retention at extreme pH values (binary electrolyte), dependencies of retention and flux on the permeability and thickness of the membrane top-layer and the support, and the influence of an additional external mass transport resistance.

In *chapter 8* the separation behaviour of asymmetric alumina nanofiltration membranes is determined experimentally for binary NaCl and $CaCl_2$ electrolyte solutions and a ternary NaCl-$CaCl_2$ mixture as a function of pH and pressure. The measured separation behaviour is compared to the retention predictions of the charge regulation transport model presented in chapter 7.

The model predictions are in good agreement with the experimental data both for the binary as well as for the ternary solutions. At pH values below 6 the retention of $CaCl_2$ is relatively insensitive to the value of the adsorption constant of $Ca^{2+}$. Obtaining the membrane adsorption parameters by fitting a model to retention data, as is often done in nanofiltration literature, can therefore be delicate. Instead, the acquisition of parameters by independent measurement techniques is obviously preferential.

Supports with small pore sizes enhance the membrane's mechanical strength but they can exhibit retention, which is undesired, and reduce the overall flux, leading to a decrease of the membrane retention. In *chapter 8* two supports with different pore sizes are compared. The support with larger pores increases the trans-membrane flux by ≈40% and the membrane retention by ≈30%, compared to the support with smaller pores.

# Samenvatting

## Abstract

Nanofiltratie (NF) wordt steeds belangrijker als scheidingsproces. Het overbrugt het gat in poriegrootte tussen ultrafiltratie en omgekeerde osmose. Ondanks dat de toepassingen snel toenemen, wordt er nog steeds intensief onderzoek gedaan naar het ophelderen van de scheidendingsprincipes van NF. Het doel van het onderzoek beschreven in dit proefschrift is daarom om het begrip van scheiding door middel van NF te vergroten en om een transportmodel zonder aanpasbare parameters te ontwikkelen dat in staat is om de scheidende eigenschappen van NF membranen te voorspellen.

Binnen het proefschrift zijn twee centrale thema's te onderscheiden. Allereerst is de geschiktheid van het ladingsregulatie (LR) concept om de ladingskarakteristieken van NF membranen te beschrijven onderzocht. Ten tweede is de toepasbaarheid van de Maxwell-Stefan (MS) theorie om massa transport door NF membranen te beschrijven kritisch bekeken.

## 1. Overzicht van het proefschrift

De Maxwell-Stefan (MS) relaties kunnen worden afgeleid door gebruik te maken van de theorie van irreversibele processen (TIP). Om die reden wordt in *hoofdstuk 2* de TIP besproken en wordt een uitleg gegeven van de aannames die gebruikt worden om deze theorie te gebruiken voor de beschrijving van het transport van zouten door NF membranen. Aangezien in dit proefschrift de MS of de simpelere Nernst-Planck (NP) vergelijkingen gebruikt worden om massatransport te bestuderen, wordt in *hoofdstuk 2* ook uitgelegd hoe beide transportbeschrijvingen zijn af te leiden uit de TIP.

In *hoofdstuk 3* wordt de methode van ladingsregulatie (LR) gebruikt om de scheiding van ionen in waterige oplossing met hydrofiele membranen te beschrijven. Het LR model wordt toegepast om de radiale ionconcentraties van een cilindrisch stukje porie te berekenen onder de aanname van thermodynamisch evenwicht.

Het eindresultaat van het model in dit hoofdstuk is een uitdrukking voor de kationretentie, gebaseerd op het evenwichtsconcentratieprofiel van het ion in het betreffende stukje porie. Voor een eenwaardig zout beschrijft deze vergelijking kwalitatief de verandering van de ionretentie als functie van de poriestraal, de ionconcentratie en de pH. De berekening in *hoofdstuk 3* beschouwt nog niet het transport van ionen. Daarom kunnen de druk- en fluxafhankelijkheid van de retentie alsmede de retentie van zoutmengsels met deze aanpak niet beschreven worden.

*Hoofdstuk 4* toont hoe een combinatie van het LR concept met de Navier-Stokes en NP transportrelaties gebruikt kan worden om het retentiegedrag van ionen in NF membranen bestaande uit nauwe cilindrische poriën te beschrijven. Net als in hoofdstuk 3 bevat dit transport model geen aanpasbare parameters. Een belangrijke aanname voor het model in *hoofdstuk 4* (en hoofdstuk 7) is dat radiale gradiënten in de concentratie en

de potentiaal verwaarloosbaar klein worden verondersteld. Deze zogenaamde uniforme potentiaal aanpak resulteert in een eendimensionale beschrijving voor transport.

Het model is in staat om kenmerkend experimenteel gedrag van NF membranen te beschrijven, zoals de ionretentie als functie van de poriestraal, de ionconcentratie, de pH, en de druk, zowel voor eenwaardige en tweewaardige ionen als voor mengsels. Bij een constant drukverschil wordt in sommige gevallen een optimale poriestraal voor de retentie verkregen. Verder wordt een ongelijke retentie voor anionen en kationen bij hoge en lage pH waarden voorspeld alsmede een minimale stroomsnelheid voor het oplosmiddel bij zeer lage zoutconcentraties. Voor hogere zoutconcentraties en een vast drukverschil, voorspeld het model een toename in de oplosmiddelsnelheid bij toenemende zoutconcentraties. Dit laatste gedrag is in overeenkomst met de resultaten van andere eendimensionale transportbeschrijvingen die aanwezig zijn in de literatuur, maar in tegenspraak met sommige experimentele gegevens.

In *hoofdstuk 5* wordt een 1-pK adsorptiemodel, gecombineerd met een Basic Stern (BS) beschrijving van de elektrostatische dubbellaag, gebruikt om adsorptie van ionen te bestuderen. De relatie tussen de lading en potentiaal in de dubbellaag en verschillende model adsorptieparameters wordt besproken. Tevens worden de 1-pK ionadsorptieparameters voor NaCl (keukenzout) op een γ-alumina materiaal bepaald door het toepassen van een niet-lineaire regressie-analyse op literatuurgegevens over de oppervlaktelading en de zetapotentiaal.

Het 1-pK BS model kan de oppervlaktelading data goed beschrijven, behalve voor de hoogste concentratie van 1000 mol/m$^3$. Redelijke overeenstemming is verkregen tussen de experimentele literatuurgegevens van de zetapotentiaal en de model beschrijving.

Door gebruik te maken van elektroforetische mobiliteitsmetingen (EM) op een keramisch γ–alumina NF membraan materiaal in waterige oplossingen van NaCl, $CaCl_2$ en $Na_2SO_4$, en potentiometrische titratiedata van γ–alumina uit de literatuur, worden in *hoofdstuk 6* adsorptieparameters bepaald. Tevens worden verschillende beschrijvingen voor de oppervlakte-adsorptie reacties en de elektrostatische dubbellaag getest.

Dit hoofdstuk toont dat een 1-pK drie-lagen model het beste in staat is om de adsorptiegegevens (EM en titratiedata) te beschrijven en daarom wordt dit model gebruikt om de adsorptieparameters te bepalen. De gegevens voor de zetapotentiaal, bepaald uit de EM metingen, tonen aan dat NaCl zich gedraagt als een indifferent elektrolyt op dit NF γ-alumina, wat resulteert in een iso-elektrisch punt bij pH=8.3. De NaCl zetapotentiaal gegevens kunnen nauwkeurig beschreven worden met het 1-pK drie-lagen model. Verder komen de model voorspellingen van de oppervlaktelading goed overeen met de titratie data uit de literatuur voor dit 1:1 elektrolyt. De sterke adsorptie van $Ca^{2+}$ ionen resulteert in positieve zetapotentialen voor alle onderzochte zoutconcentraties en pH waarden. Het model kan de zetapotentiaal gegevens redelijk beschrijven. Sterke adsorptie van sulfaat ionen veroorzaakt een verschuiving van het iso-elektrische punt naar lagere pH waarden. Voor een bulk concentratie van 100 mol/$m^3$ $Na_2SO_4$ worden zelfs enkel negatieve zetapotentialen gemeten.

*Hoofdstuk 7* combineert het LR concept met de MS theorie om elektrolyt transport in NF membranen te beschrijven. Een voorspellend model wordt ontwikkeld dat een uitbreiding is van de aanpak die beschreven is in hoofdstuk 4. Net als in dit hoofdstuk bevat het transport model in *hoofdstuk 7* geen aanpasbare parameters. Oplading van het membraan oppervlak wordt beschreven door gebruik te maken van een 1-pK model gekoppeld aan een drie-lagen beschrijving van de elektrostatische dubbellaag. Massatransport is gebaseerd op de uniforme potentiaal aanpak

(dus eendimensionaal transport model). De benodigde gegevens voor het model worden verkregen uit onafhankelijke metingen, zoals elektroforetische mobiliteitsexperimenten. De resultaten van het model voor een asymmetrisch γ-alumina nanofiltratie membraan worden beschreven aan de hand van de retentie voor NaCl en een mengsel van NaCl met $CaCl_2$.

De model resultaten tonen dat overlap van de dubbellagen, wat leidt tot ladinsregulatie, een sterke invloed heeft op de potentiaal ($\Delta\phi$=59-88% in 4 nm poriën) en dientengevolge op de scheidende eigenschappen van het membraan. Bovendien blijkt de oppervlaktelading van het membraan aanzienlijk te variëren over de lengte van een porie, waardoor de juistheid van de aanname van een constante oppervlaktelading, die veel gebruikt wordt in de NF literatuur, onzeker wordt. Naast deze interessante resultaten is het model ook in staat om bekende NF trends te voorspellen, zoals ongelijke retentie voor an- en kationen bij extreme pH waarden, de afhankelijkheid van de retentie en flux van de permeabiliteit, dikte van de membraan toplaag en drager, en de invloed van additionele externe massa transport weerstanden.

In *hoofdstuk 8* worden de scheidende eigenschappen van een asymmetrisch alumina NF membraan experimenteel bepaald voor binaire elektrolytoplossingen van NaCl en $CaCl_2$ en een ternair NaCl-$CaCl_2$ mengsel als functie van de pH en de druk. Het gemeten scheidingsgedrag wordt vergeleken met de voorspellingen van het transportmodel dat besproken is in hoofdstuk 7.

De modelbeschrijvingen komen goed overeen met de experimentele meetgegevens voor zowel de binaire als de ternaire oplossingen. Voor pH waarden beneden de 6 is de retentie van $CaCl_2$ relatief ongevoelig voor de waarde van de adsorptieconstante van $Ca^{2+}$. Het verkrijgen van de adsorptieparameters voor een membraan door middel van het fitten van een transport model aan retentie data, zoals vaak wordt gedaan in de NF

literatuur, moet daarom met veel voorzichtigheid gedaan worden. Het moge vanzelf spreken dat in plaats van de laatste methodiek het beter zou zijn om deze parameters uit onafhankelijke metingen te verkrijgen.

Het gebruik van een drager met kleine poriën verbetert de mechanische sterkte van een membraan. Echter, deze kleine poriën reduceren de flux door het membraan en kunnen tot gevolg hebben dat de drager retentie vertoont. Aangezien een fluxreductie de retentie van het membraan vermindert, is dit duidelijk ongewenst. Twee dragers met een verschillende poriegrootte zijn in *hoofdstuk 8* vergeleken. Het blijkt dat bij gebruik van de drager met de grootste poriën de flux door het membraan toeneemt met ≈40% en de membraan retentie stijgt met ≈30% in vergelijking tot de drager met de kleinere poriën.

Humanity practically *was* things that didn't have a position in time and space, such as imagination, pity, hope, history and belief. Take those away and all you had was an ape that fell out of a tree a lot.

*Terry Pratchett: Thief of Time*

# Dankwoord

Toen ik in januari 1999 begon aan mijn promotie waren Enschede en de Universiteit Twente volslagen onbekend voor mij. Nu na vier jaar kan ik zeggen dat ik het hier uitstekend naar mijn zin gehad heb. Niet alleen verdwaal ik nu niet meer in het centrum van Enschede of in de Bastille op de campus, maar ik heb veel mensen leren kennen die er allemaal op hun eigen manier aan hebben bijgedragen dat ik me hier thuis ben gaan voelen.

Op wetenschappelijk gebied zijn er in deze tijd veel deuren voor mij open gegaan. In eerste instantie is Henk Verweij daarbij erg belangrijk geweest. Henk, als professor bij anorganische materiaalkunde (AMK) heb je mij niet alleen in '99 aangenomen, maar je was ook mijn directe begeleider. Als we mijn vorderingen bespraken dwong jij me altijd de grote lijnen in de gaten te houden. Dat heeft er mede toe geleid dat ik nu netjes naar vier jaar mijn werk heb afgerond.

Naast Henk zijn er drie mensen uitermate belangrijk geweest voor mijn wetenschappelijke ontwikkeling: Nieck, Maarten en Arnoud. Nieckje, voor mij is het erg mooi geweest dat je na een korte afwezigheid weer teruggekeerd bent als mijn begeleider bij AMK. Jij hebt me met name geleerd om kort en bondig te schrijven omdat, zoals je zei, "de mensen je artikelen dan tenminste nog lezen." Samenwerken met jou was heel inspirerend. Niet in de laatste plaats omdat je tijdens een discussie het ineens kon hebben over het lekkere flesje rode wijn van gisteren, of een ander onderwerp dat helemaal niets te maken had met wetenschap. Maar, als we het dan wel over een wetenschappelijk probleem hadden, wat toch ook vaak voorkwam, dan begreep jij vaak veel sneller dan ik waar het om ging. Nog wel een ding, onthoud wel goed dat je voortaan niet meer je ontdekking van mooie tweedehands boxen toevertrouwt aan andere muziekfreaks.

Maarten, je hulpvaardige houding bij AMK heeft me erg geholpen om me daar thuis te gaan voelen. Maar, vooral ook daarna, toen je terug kwam uit Santa Barbara, hebben we menige, soms stevige, wetenschappelijke discussies gevoerd. Jou kennis over het ladingsgedrag van oxides is voor mij de springplank geweest voor mijn promotie. Veel dank daarvoor.

Arnie, alias Mr. Schwarzenegger, ik leerde je al kennen in Amsterdam, en toen kwam je ineens ook naar Twente. Je hebt me ontelbare keren uit de brand geholpen als ik weer eens een Maple probleempje had, maar ook je goede adviezen over massatransport waren buitengewoon waardevol. Tijdens het squashen konden we elkaar redelijk bijhouden, maar bij het hardlopen sjokte ik vaak hijgend achter je aan. Nee, ik heb Red Dwarf nog steeds niet gelezen.

Als enigszins theoretische AiO in het lab, kun je niet zonder goede hulp. Natascha, Cindy, Mieke en Wika, als jullie mij niet regelmatig voorzien hadden van verse membranen dan was mijn promotie nooit zo succesvol geweest. Door jullie niet-praten-maar-gewoon-doen mentaliteit kon ik ook in de spannende laatste fase op jullie praktische ondersteuning rekenen. Allee, zeker en vast. Atilla, als mijn “Atilla, vraagje…” weer door het lab klonk dan wist jij al wel weer voldoende. Desondanks bleef je me keer op keer weer helpen. Gerrit, jij hebt me veel geholpen bij het ontwerpen en bouwen van de waterpermeatie-opstelling die mij zo veel mooie meetresultaten heeft gebracht. Op een paar kleine opstartproblemen na heeft het apparaat als een zonnetje gewerkt. Veel van de eerste permeatie metingen zijn uitgevoerd door Gerald en Jurian. Heren, jullie ervaringen hebben mij veel geleerd over hoe ik de permeatie experimenten het beste kon uitvoeren.

Ook buiten AMK kon ik altijd op veel hulp rekenen bij mijn werkzaamheden. Met name de samenwerking met Hans Lyklema van de fysische chemie en colloidkunde groep in Wageningen is me bijgebleven. Hans, je stond altijd voor me klaar om vragen te beantwoorden over de oplading van oxiden en de

theoretische beschrijvingen en interpretatie daarvan. Mijn laatste hoofdstukken van het proefschrift dragen dan ook in sterke mate jou stempel. Het doet me een groot genoegen dat je ook zitting zal nemen in mijn promotiecommissie.

Op deze plek wil ik ook graag Matthias bedanken. Het was voor mij erg belangrijk dat jij in de onzekere situatie na het wegvallen van Henk als mijn promotor deze rol op je wilde nemen. Ondanks dat we elkaar maar weinig spraken was je altijd geïnteresseerd in mijn werk en probeerde je me waar mogelijk adviezen te geven. Veel dank hiervoor.

Als je zoveel van je werk achter de computer doorbrengt zijn kamergenoten erg belangrijk; met name als je even niet met wetenschap bezig wilt zijn. In mijn laatste twee jaar waren Mercedes en Riaan erg prettig gezelschap op mijn kamer. Meestal hadden we het over de diepere zin van het leven, over het verschil tussen Nederlanders, Spanjaarden en Zuidafrikanen, of reageerden we onze frustraties rond de promotie lekker op elkaar af. ¡Muchas gracias! en baie dankie!

Het is jammer dat het hier niet mogelijk is om iedereen binnen en rond AMK die ik heb leren kennen persoonlijk te bedanken. Monse (bedankt voor je gastvrijheid en hulp bij de voorkant van mijn proefschrift), Freddy (Le Boss), Jelena en Boris (geweldige vakantie in Nice), Mai en Shankho (ik zal jullie volledige naam blijven oefenen), Jurgen (gaan we nog squashen?), Tijana, Manon, Xavi en Belen (fuerza Catalunya), Henny (de Guru), Bernard, André, Louis, Klaas, José, Cis, Regina, Werner, Herman en alle anderen die ik nog vergeten ben, ik zal ik jullie allemaal erg missen.

In de eerste twee jaar van mijn promotie leefde ik me regelmatig uit bij volleybal en op klarinet. Bij beide was improvisatie mijn sterkste kant. Agnes, tijdens menig studie-uur hebben we gediscussieerd over wat nu de beste manier was om een bepaalde passage te spelen. Vaak hadden we totaal

verschillende inzichten, maar meestal wist je me wel te overtuigen, ook al was ik erg hardleers. De laatste anderhalf jaren heb ik die lessen erg gemist.

Ondanks dat ik meestal de oudste was in de teams bij Harambee, bleek in het veld dat inzicht lang niet altijd met de jaren komt. Toch veranderde ik mede door het volleybal wel van echte individualist in een teamspeler. Tobias, Renze, Thijs, Link, Szwanz, Matthijs, Arjen, Frank, Kelly, Teun, Jean-Michel, Schoemie, Ramon, Jeroen, Sven, Vijver, Paul, Heino, Joost, Robbert, en iedereen die ik vergeten ben, bedankt voor de gezelligheid.

Op woensdag middag bij een partijtje volleybal met de UT-kring kon ik alle volleybal aanwijzingen even vergeten en echt alle remmen los gooien. Liever een hele harde goede smash dan tien gescoorde plaatsballen. Dat ik in slimheid nog veel tekort kwam bleek regelmatig als ik weer eens gealexd of gerobd werd. Mannen (en soms Helen en Beb), ik heb me geweldig vermaakt en de gesprekken in de kleedkamer daarna waren erg gezellig. Trouwens Wil, die bal was wel in!

Pele en Helen, ik leerde jullie kennen bij het volleybal, maar ook daaromheen kwamen we elkaar regelmatig tegen. Zo verschillend als we alledrie zijn, elke keer als we elkaar zien is het weer gezellig. Ik hoop dat we deze infrequente bezoekjes ook na mijn promotie kunnen vervolgen.

Ondanks dat Enschede zo'n twee uur van Amsterdam af ligt, is zomers beachvolleybal met Martin vaste prik gebleven. Martin, vrijwel elke week struinden we dan de toernooien aan zee af. Voor de lol, maar ook wel om te winnen. Wat mij betreft houden we deze gewoonte er nog lang in.

Remko, Martijn, Dennis en Joost. Sinds de middelbare school trek ik al met jullie op, soms zelfs nog langer. Het is voor mij verbazend dat ondanks we allen zo verschillend zijn we toch zo goed met elkaar op kunnen schieten. Ieder heeft zijn eigen leven en we wonen ver van elkaar af, maar toch

proberen we elkaar regelmatig op te zoeken. Ik vind dit heel bijzonder en weet zeker dat we dit nog lang zullen blijven doen.

Het vertrek van Amsterdam naar Twente was voor mij het eerste moment waarop ik echt helemaal op eigen benen stond. En, Enschede is in de afgelopen vier jaar echt mijn thuis geworden. Desondanks bleef de band met het gezin onmisbaar; er was altijd een plek om naar terug te komen. Daarvoor ben ik Arie en Nelly en mijn zussen heel erg dankbaar. De liefde en onvoorwaardelijke steun die ik van jullie gekregen heb, heeft mij voor een belangrijk deel gemaakt tot wie ik nu ben. Het is daarom ook heel erg leuk dat jij Arie op de verdediging mijn paranimf zal zijn.

Enschede, 20 december, 2002

# Acknowledgement

When I started my Ph.D. in January 1999, Enschede and the University of Twente were completely unknown to me. Now, after four years I can say that I have really had a great time here. Not only can I find my way now in the centre of town or in the Bastille on campus, but I have met a lot of people who all in their own way contributed to making me feel at home during my stay here.

Scientifically, doors have opened for me. In the early period of my Ph.D. Henk Verweij played an important role in this. Henk, as the professor of the inorganic materials science (IMS) group you did not only hire me in '99, but you were also my direct supervisor. Each time we discussed my progress you forced me to stay focussed on the main issues and challenges in my work. Your persistence is partly the reason that I have finished my Ph.D. nicely in four years.

Apart from Henk, three people have been extremely important in my scientific development: Nieck, Maarten and Arnoud. Nieckje, it was really a great support for me that you returned to IMS and became my supervisor. You particularly taught me to write brief and concise because, as you often said, "people than at least still read your articles." Working together with you was always inspiring. Not in the least because during a discussion, quite suddenly, you could start talking about that nice bottle of red wine of yesterday or something else completely unconnected to science. And when we did discuss science, which was quite often, you generally understood the bottleneck of issues much quicker than I did. In the future, however, I would advise you not to trust other music freaks with your knowledge of great second-hand loudspeakers.

Maarten, your helpful attitude quickly made me feel at home within IMS. However, particularly after your promotion, when you came back from Santa Barabara, we shared many, sometimes firm, scientific discussions. Your knowledge with respect to the charging behaviour of oxides acted as a diving board for me to really start off my promotion. Many thanks for that.

Arnie, or shoud I say Mr. Schwarzenegger. We already met in Amsterdam, and then you suddenly also came to Twente. I cannot remember how many times you helped me out when I had some kind of Maple problem, but also your good advice in mass transport problems was invaluable. With squash we were quite evenly matched, but during the running I always followed you at some distance, puffing and choking. No, I still have not read Red Dwarf.

As a somewhat theoretical Ph.D. student, in the lab you cannot do without good assistance. Natascha, Cindy, Mieke en Wika, when you would not have presented me with new membranes once every wile, my Ph.D. would never have become such a success. Because of your 'no talking just act' approach I could always count on your pratical assistance, even in the stressy last period of my work. Atilla, when my "Ehh Atilla, question…" sounded through the lab you already knew what was going to happen. Still, each time you did your best to help me out. Gerrit, you helped me a lot to design and build the water permeation set-up, which brought me so much interesting data. Apart from an occasional hiccup here and there the device always worked perfectly. Gerald and Jurian performed many of the first permeation experiments. Guys, your experiences taught me a lot about how the permeation measurements could be performed best.

Also outside IMS I could count on much assistance with my work. In particular the collaboration with Hans Lyklema of the physical chemistry and colloid science group in Wageningen has stuck to my mind. Hans, you were always available to answer my questions about the charging of oxides and the theoretical description and interpretation thereof. The second half of

the chapters in my thesis strongly reflect your influence on my work. I consider it an honour that you are also a member of my Ph.D. committee.

Here I would also like to thank you, Matthias. For me it was very important that in the uncertain situation that arose when Henk Verweij left, you took the responsibility as my professor and promoter upon you. Despite the fact that it was not possible to discuss my work very often, you were always interested and tried to give me advice where possible. Many thanks for that.

When you spend most of your time behind your computer, officemates become very important. Even more so if for a while you do not want to occupy yourself with science. During my last two years, Mercedes and Riaan were excellent companions in my office. We often talked about the deeper meaning of life, about the differences between the Dutch, the Spanish and the South Africans, or just vented our frustrations concerning our Ph.D. ¡Muchas gracias! and baie dankie!

It is a pity that it is not possible here to thank everybody in and around IMS that I got to know personally through these years. Still, Monse (thanks for the hospitality and helping with the cover of my thesis), Freddy (Le Boss), Jelena en Boris (great holiday in Nice), Mai en Shankho (I will keep on practicing your full names), Jurgen (what about squash?), Tijana, Manon, Xavi en Belen (fuerza Catalunya), Henny (the Guru), Bernard, André, Louis, Klaas, José, Cis, Regina, Werner, Herman and all others that I forgot, I will all miss you very much.

During the first two years I indulged myself in volleyball and on the clarinet. In both improvising was my strongest point. Agnes, during many rehearsals we debated about what the best way was to play a certain part of a piece. Often our interpretations of the music were completely different, but although I was quite stubborn, you could generally convince me that your approach was best. The last one and half years I really missed these lessons.

Despite the fact that I often was the oldest person in the volleyball teams of Harambee, I was the perfect example that insight does not necessarily come with age. Still, volleyball did change me from an individualist into a team player. Tobias, Renze, Thijs, Link, Szwanz, Matthijs, Arjen, Frank, Kelly, Teun, Jean-Michel, Schoemie, Ramon, Jeroen, Sven, Vijver, Paul, Heino, Joost, Robbert, thanks for all the fun.

On Wednesday at a game of volleyball with the UT-circle I could for a minute forget about all the hints from my coach and just enjoy myself. One good hard smash was preferred over ten tactically scored points. That I was not one of the cleverest people on the court was shown several times when I got Alexed or Robbed. Gentlemen (and sometimes Helen and Beb), I had a great time and the talks in the change room afterward were good fun. By the way Wil, the ball was inside!

Pele and Helen, I got to know you at the volleyball, but also outside that circle we met regularly. Even though we are very different, I enjoy it every time we meet. I really hope that we can continue these infrequent visits after my graduation.

Although Enschede is about two hours travel from Amsterdam, beach volleyball with Martin remained a regularly returning event. Martin, in summer we visited the tournaments at the Dutch coast almost every week. For fun, but also to win. Hopefully we can continue this tradition for a long long time.

Remko, Martijn, Dennis en Joost. Since secondary school we are friends and it still is surprising for me that although we have very different characters, we can get along so well. Each of us has his own life and we live pretty far apart, but still we try to visit each other as often as possible. This is very special to me and I know for sure that we will continue to do this for many years to come.

My departure from Amsterdam to Twente was the first time that I was really on my own, and during these four years Enschede really became my home. There was, however, always a family tie, a place to come back to. For that Arie, Nelly and my sisters I am very grateful. The love and unconditional support that I always received from you has for a major part made me into the person that I am now. Therefore I also appreciate it very much that Arie will be my paranymph during my graduation.

Enschede, December 20, 2002